Localized Pattern Formation in Continuum Models of Urban Crime

by

Wang Hung Tse

A THESIS SUBMITTED IN PARTIAL FULFILLMENT
OF THE REQUIREMENTS FOR THE DEGREE OF

Doctor of Philosophy

in

THE FACULTY OF GRADUATE AND POSTDOCTORAL STUDIES
(Mathematics)

The University of British Columbia
(Vancouver)

April 2016

Abstract

In this thesis, the phenomenon of localized crime hotspots in models capturing the features of repeat and near-repeat victimization of urban crime was studied. Stability, insertion, slow movement of crime hotspots and the effect of police patrol modelled by an extra equation derived from biased random walk were studied by means of matched asymptotic expansions, nonlocal eigenvalue problem (NLEP) stability analysis, and numerical computations.

In the absence of police, we confirmed the linear stability of the far-from equilibrium steady-states with crime hotspots in the original parameters regimes as observed in [47]. The results hold for both the supercritical and subcritical regimes distinguished by a Turing bifurcation (cf. [48, 49]). Moreover, the phenomenon of peak insertion was characterized by a simple nonlinear equation computable by quadratures and a normal form equation identical to that of the self-replication of Mesa patterns [28] was derived. Slow dynamics of unevenly-spaced configurations of hotspots were described by a system of differential-algebraic systems (DAEs), which was derived from resolving an intricate triple-deck structure of boundary layers formed between the hotspots and their neighbouring regions.

In the presence of police, which was modelled by a simple interaction with criminals, single and multiple hotspots patterns were constructed in a near-shadow limit of criminal diffusivity. While a single hotspot was found to be unconditionally stable, the linear stability behaviour of multiple-hotspot patterns was found to depend on two thresholds, between which we also observe a novel Hopf bifurcation phenomenon leading to asynchronous oscillations. For one particular, but representative, parameter value in the model, the determination of the spectrum of the NLEP was found to reduce to the study of a quadratic equation for the eigenvalue. For more general parameter values, where this reduction does not apply, a winding number analysis on the NLEP was used to determine detailed stability properties associated with multiple hotspot steady-state solutions.

Preface

The research presented in this thesis was the result of independent and collaborative work by the author Wang Hung Tse, supervised by Prof. Michael J. Ward.

Chapter 1 was written independently by the author for the purpose of this dissertation. The derivation of the mathematical model presented in Sections 1.4 was an unpublished work by the author, based upon previous work referenced in the chapter. The specific case of the model that was studied Chapter 3 was first suggested by the thesis supervisor, who also attributed the current form to influence from the literature and his collaborators, and suggested a great portion of the literature reviewed in this chapter.

Chapter 2 was largely an expanded version of the paper by the author and the thesis supervisor: W.-H. Tse, M. J. Ward, *Hotspot Formation and Dynamics for a Continuum Model of Urban Crime*, European Journal of Applied Mathematics, accepted for publication. This chapter includes all results and figures of the paper with further editing, and also a significant amount of new and original mathematical details and numerical studies from the author's own work.

Chapter 3 was also the joint work of the author and the thesis supervisor Prof. Michael J. Ward. Most results are unpublished with an exception of the content of Section 3.6, which appears in a section of the paper: I. Moyles, W.-H. Tse, M. J. Ward (2015), *Explicitly Solvable Nonlocal Eigenvalue Problems and the Stability of Localized Stripes in Reaction-Diffusion Systems*, Studies in Appl. Math., to appear. Only the portion of the paper which were the joint work of the author and the thesis supervisor was included in Section 3.6 with further editing by the author.

All figures in this dissertation were independently produced by the author using publicly available data or numerical computations, and with references where necessary. The strategies of the numerical computations leading to the figures contain ideas from the thesis supervisor, who also assisted in the preparation of the manuscript and furnished suggestions in literature review and points for discussion.

Table of Contents

List of Tables

List of Figures

Chapter 1

Introduction to the Urban Crime Model

1.1 A Brief History of the Urban Crime Model

There has been an increasing interest in recent years on developing mathematical tools to understand and predict spatial patterns of urban crime (cf. [47, 48, 49] and the survey [17]). One main impetus underlying this effort is the increased availability of residential burglary data, partially due to improved mapping technology and digital record-keeping. Moreover, not only are the authorities releasing more data to the public, but also some commercial and non-profit organizations are starting to utilize such data to create publicly available visualizations of crime patterns. For example, Fig. 1.1 shows two crime density maps that illustrate the phenomenon of *crime hotspots*, where high levels of crime are often concentrated in certain spatial regions that may evolve slowly over time (cf. [4]). Many studies have hypothesized that such hotspots are due to a repeat or near-repeat victimization effect, which postulates that crime in a certain region induces more crime in that and nearby regions (cf. [21, 55]). Such theoretical descriptions of nonlinear feedback mechanisms that diffuses risk by proximity have resulted in various modelling efforts, that aim to quantify such mechanisms of criminology to provide an explanation for the emergence and persistence of crime hotspots.

In [47, 49], Short et al. introduced an agent-based model of urban crime that takes into

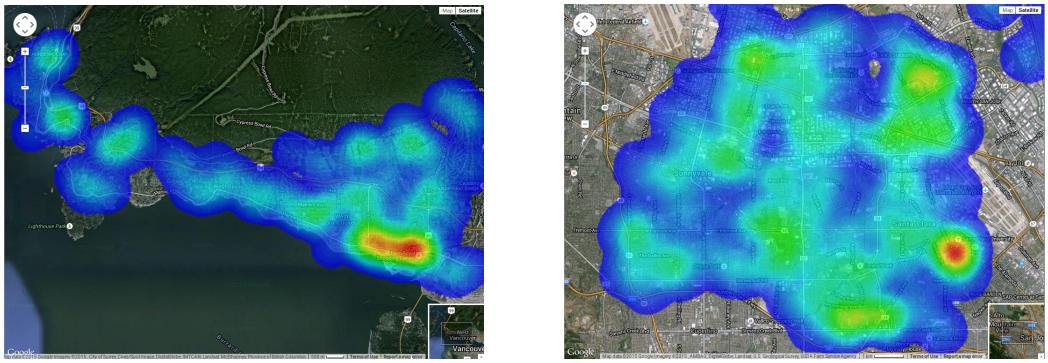

Figure 1.1: Burglary hotspots in West Vancouver, B.C., Canada (left) and Santa Clara-Sunnyville, California, US (right). Generated by raidsonline.com [44] using publicly available crime data for residential and commercial burglaries. Shown pictures are for a full year beginning August 2014.

account the features of repeat or near-repeat victimization of urban crime, and derived a continuum limit using methods similar to those used in analyzing biased random walk models in mathematical biology. In dimensionless form, the continuum limit of this agent-based model is the two-component reaction-diffusion (RD) system

$$A_t = \epsilon^2 \triangle A - A + \rho A + \alpha\,, \qquad \rho_t = D\nabla \cdot \left(\nabla \rho - \frac{2\rho}{A}\nabla A\right) - \rho A + \gamma - \alpha\,, \tag{1.1}$$

with no-flux boundary conditions.

Here, ρ represents the density of criminals, A measures the "attractiveness" of the environment to burglary, and the term $-D\nabla \cdot (2\rho\nabla A/A)$ models the tendency of criminals to move towards sites with a higher attractiveness. In addition, $\alpha > 0$ is the constant baseline attractiveness, while $\gamma - \alpha$, with $\gamma > \alpha$, models a constant rate of background re-introduction of criminals. The constant $0 < \epsilon \ll 1$ models the small diffusive spread of the attractiveness, which is relatively much slower compared to the movements of criminals, while the constant D, which represents the diffusivity of criminals, was not present in the form of the model originally proposed in [47]. It is added here for uniformity in the subsequent presentations of results of this dissertation, and the choice of the form presented in (1.1) will be justified in due course of our analysis. Further details of the model are given in [47] and in Section 1.4 as well, where we describe an agent-based model whose continuum limit is a three-component PDE extending (1.1).

We now turn to review briefly the history of the development of the model and the surrounding literature. In [47], the authors performed numerical simulations of the discrete agent-based model, and crime hotspots were clearly observed for some parameter choices. To study the range of parameters that would give rise to crime hotspots, they deduced the two-component PDE system (1.1) from the formal continuum limit of the agent-based model and performed Turing stability analysis from the constant equilibrium state. They were able to produce numerical simulations of the full deterministic PDE system to exhibit crime hotspots when the parameters predicts Turing instability. Furthermore, they observed that hotspots are formed *only* if areas of high criminal activity are separated far enough, and *only* when attractiveness diffuses over *shorter* distances. Otherwise, hotspots cannot be numerically observed. In other words, the diffusivity of the attractiveness, the parameter ϵ^2, is necessarily small for crime hotspot to exist numerically. This suggests that the system (1.1) possesses hotspots in the steady state only when it is singularly perturbed.

An admitted insufficiency in the initial work [47] was the lack of consideration of the impact of law enforcement on crime patterns. Thus, in a subsequent work [48], Short et al. studied the effect of suppression and investigated the conditions for dissipation of crime hotspots. Expounding on the finding that their model predicts hotspots only when the diffusion rate of risk is small, they performed weakly nonlinear analysis to determine that Turing bifurcation was subcritical and classified hotspots in the full numerics as being either subcritical or supercritical. By manually introducing large perturbations at the hotspots in their numerical simulations, they found that suppression of supercritical hotspots will cause risk to diffuse radially, forming a transient "ring-like structure", which subsequently disintegrated into multiple hotspots (see Fig. 10 of [48]). This phenomenon was referred to as "hotspot displacements". In contrast, when suppressing a subcritical hotspot, no such transient states were formed and the suppression effect was observed to persist without causing displacement or production of new hotspots. The intention of this numerical experiment was to distinguish the qualitative features of supercritical and subcritical hotspots, which have apparently similar localized structures in the solution profile, but differ markedly in their response to hotspot suppression. This is an interesting observation especially for criminologists, among which contains disagreeing groups, some doubting and some affirming the virtue of hotspot policing.

Shortly afterwards, Jones, Brantingham and Chayes, the latter two being co-authors of the initial work [47], published another work [22] which augments the initial work by considering possible models of police deployment strategies by means of introducing an extra component to the two-component PDE. They modelled it in two ways: firstly, by modifying crime-attractiveness perception by criminals when police are present; secondly, by the *deterrent* effect acting on the criminals directly when the police are located at the same place (they assumed the amount of immediate apprehension of lawbreakers was negligible). They focused more on discussing what deployment strategy could maximize the deterrent effect on the criminals, and they proposed three variants of police patrolling strategies: "random walkers", "cops on the dots" and "peripheral interdiction". By considering the continuum limits, both the former two models resulted in an extra PDE modelling the police movements, while the same effort proved difficult for the last model. This work has a strong influence on our work when we developed the form of our model (1.20) in the presence of police.

Meanwhile, the mathematical modelling of crime is gaining momentum in terms of public interest and recognition (cf. [11]). From within the mathematical community, an increasing amount of effort was invested to establish the theoretical validity of the models, and to extend the original model, or even to consider alternative mathematical basis of crime hotspots (cf. [17]).

For the continuous Short's model (1.1), there have been a few other previous studies, in addition to [47, 48, 49], on its pattern formation properties. For the parameter regime $D \gg 1$, hotspot equilibria and their stability properties were analyzed in [29] by a combination of formal asymptotic methods and results from the spectral theory of nonlocal eigenvalue problems (NLEP). In [2] the existence of these hotspot equilibria for the regime $D \gg 1$ was established rigorously using a Lyapunov-Schmidt reduction. In [46] the local existence of solutions to the crime model in multidimensional domains was established. In [7], the branching behaviour near the Turing point associated with the spatially homogeneous steady-state was characterized rigorously. Similar bifurcation theoretic results characterizing branching behaviour from the spatially homogeneous steady-state for some extensions of the basic crime model (1.1) are given in [18]. There are also new mathematical models that attempt to extend Short's model (1.1) by incorporating the action of the police (see [22, 41, 45] for such PDE models). Other

types of non-PDE mathematical models that attempt to reformulate the mathematical basis of crime hotspots, or introducing police deterrence in a different way also exist (cf. [1, 17, 56] and the references therein). In this dissertation, we introduce a three-component PDE model (3.3) that extends (1.1). The model is heavily influenced by the work in [22] and [45], where the police interaction introduced is a variant of hotspot policing that was discussed in [56].

As mentioned above, the key question that [49] attempts to address is whether crime hotspots can be eradicated by one-time suppression. They conclude that whether hotspot policing will be a successful strategy or not depends on the system parameters, and they classify crime hotspots as either supercritical or subcritical by the parameter regime that such solutions reside in. This will become one of the key themes in our analysis presented in Chapter 2 in that we work towards a more complete description of crime hotspots in both the supercritical and subcritical regimes, and at the same time shed light on the issue of crime hotspot displacement and annihilation. In Chapter 3, we use a continuous parameter that spans the spectrum between purely random policing to focused hotspot policing to seek an optimal policing strategy. The optimal policing strategy was measured by its efficacy in destabilizing preexisting crime hotspots. However, compared to Chapter 2, the results in this chapter are, in comparison, more preliminary in terms of application, and the central focus is to examine how much we could extend the tool-set used in the study of other reaction-diffusion (RD) system by dint of their structural similarities. For example, while the hotspot solution profile construction by means of matched asymptotic expansions are quite similar, the associated NLEP stability analysis is now rather intricate except for a particular parameter choice where it simplifies considerably.

For the methodology of this dissertation, the closest predecessor is the article by Kolokolnikov *et al.* in [29], which contains the first attempt of studying the stability of crime hotspots for the model by Short et al. in [47] in the far-from equilibrium regime. Realizing that the PDE system is fundamentally singularly perturbed, they constructed steady-states with hotspots directly using matched asymptotic expansions and then studied their stability with respect to key model parameters. Their far-from equilibrium results also connect with those found by linearity stability and weakly nonlinear analysis in [47, 48], by means of a numerically computed bifurcation diagram (cf. Fig. 7 of [29]). Our new work follows the approach in [29] and extends the analysis by solving the conjectures concerning the dynamics of hotspots, and augmenting

the equations by deriving a police PDE equation from scratch, and then studying the equilibrium and stability problems. As a result of the research in the course of the development of this dissertation, a large portion of Chapter 2 and the Section 3.6 of Chapter 3 have been published respectively in [51] and [37], and with further work being organized into new papers to be submitted in the future.

1.2 Comparisons to Other Systems of Reaction-Diffusion Type

The urban crime model with a new police component, given in (1.20), is also interesting mathematically because it possesses various properties that are not observed in similar systems of reaction-diffusion (RD) type. There are sufficient similarities between (1.20) and the RD models that exhibits localized patterns, for e.g. the Gierer-Meinhardt, Gray-Scott, Brusselator and the Schnakenburg models, to name a few (cf. [36, 54] and the references therein), so that the tools developed for such models are also applicable to a large extent. For example, in this dissertation, the study of the existence and the linear stability (in $O(1)$ time-scales) of multiple crime hotspots has drawn much influence from the corresponding study of multiple-spike solutions (cf. [13], [20], [24], [52], [53], [54] and also the references therein), and the methodology extends quite naturally from previous work. However, there are various novelties both in terms of the mathematical techniques developed and the results, which we describe briefly in this section.

Firstly, in terms of the asymptotic construction of a steady state pattern with localized structures of high amplitude, which are usually located in an "inner region" in a matched asymptotic expansion procedure, the interaction with the corresponding "outer region" is crucial in determining various properties of the localized structure, and notably the amplitude of the structure. In the references cited above, the background states in the "outer region" are usually quite simple, e.g. constant or solutions of a linear differential equation. However, in Chapter 2, we see that the background state is highly nonlinear and such a nonlinearity in the "outer region" lends to the possibility of "peak insertion" governed by thresholds, which explains the emergence to further localized crime hotspots. Such a threshold phenomenon cannot be described by elementary functions, which was the case when the shadow limit or a weaker coupling (cf. [29]) is considered.

Secondly, the interaction between the inner and outer regions is also considerably more complex in technical terms. In particular, to construct an approximation of a quasi-steady state that evolves slowly in time, new nested boundary layers in between the inner and outer regions are required and switchback terms were necessary to complete the matching procedure. The use of switchback terms also arise in the singular perturbation analysis of some other problems, including model problems of low Reynolds number flows (cf. [31], [32], [42]), and the analysis in [33] of singular solutions to a PDE model for the deflection of a micro-plate capacitor. The increasing technical effort that is required to produce a satisfactory correction to the leading order theory also prompted us to consider alternatives. In particular, we devised an algebraically simpler procedure, which was somewhat inspired by the renormalization approach in [8]. This approach is presented in this dissertation in Section 2.5 and the result was that the key effects from the switchback correction terms could be effectively incorporated in a relatively simple way.

The resolution of the nested boundary layers between the inner and outer regions also led to a novel form of equations governing slow dynamics of crime hotspots. For the dynamics of a single spike in standard singularly perturbed RD systems, such as the Gierer-Meinhardt, Schnakenberg, and Gray-Scott systems, studied in [9], [14], [15], [19], [43], [50] (see also the references therein), the governing equations were ODEs. In contrast, for the slow movement of crime hotspots studied in Section 2.7, the dynamics of a single hotspot is found to be governed by a system of differential algebraic equations (DAEs). For the case of multiple hotspots, a coupled system of DAEs was derived, and these asymptotic results were found to agree favourably with full numerical simulations of the PDEs.

With regards to the problem of studying the linear stability on $O(1)$ time scales of a multi-hotspot steady-state, the results in both Chapter 2 and 3 are also quite novel. In Section 2.3 for the $D = O(1)$ regime for the basic crime model with no police, we found unconditional stability for any number of crime hotpots (as long as they exist as steady states). This stands in sharp contrast to many other RD systems defined on a finite domain, and also with regards to the stability analysis of [29] for the near-shadow (large diffusivity) regime $D \gg 1$, where explicit stability thresholds in D were obtained. In terms of instability, the results in Chapter 3 for the urban crime model with police intervention also point to new possibilities not seen, to

the best of our knowledge, in other RD systems. For instance, in Section 3.4, at a particular choice of system parameter for the three-component system with the police component, a novel oscillatory instability that is asynchronous was found and characterized explicitly. We believe asynchronous oscillatory instability is a general trait exhibited by this system, though a full characterization is currently lacking due to the complexity of the NLEP in the general case. In contrast, for the case of Gray-Scott and Gierer-Meinhardt model studied in [9, 52, 50], where a similar analysis was performed, the dominant oscillatory instabilities of the spike amplitudes were all found to be synchronous.

The difficulty of the stability problem for the urban crime model with police is also exemplified by the fact that the NLEP studied in Section 3.2 has two nonlocal terms, while most of the RD systems studied in the past have only one nonlocal term. The novelty in the structure of the NLEP problem requests that new techniques be developed to analyze them, and also points to potentially richer behaviours that were not observed in previous studies of other RD systems.

Another feature of the rich structure of the systems studied in this dissertation is their rather intricate bifurcation diagrams of steady-state solutions. By using well established numerical continuation and evolution software (cf. [12, 3]), we were able to compute global bifurcation diagrams for the "far-from equilibrium" steady states and determine their stability. The structure we observed is rather intricate, yet possessing symmetry. In particular, we performed path-following numerical study of the steady states, similar to what is done in [35], but for a finite domain instead of a (truncated) infinite domain. Our conclusions were quite different from that in [35], which we believe to be caused by the nature of the domain topology. In an infinite domain, the phenomenon of homoclinic snaking is well-studied in many other RD systems, such as the Swift-Hohenberg model (see [5] and the references therein). In [35], the authors demonstrated numerically the existence of wave-packet type localized solutions which leads to a pattern of well-separated hotspots. However, in a finite domain with other parameters in the same regime as in [35], we observed a closed homotopy of localized equilibria with a single hotspot bifurcating out of a subcritical Turing point. We remark that it has been shown recently in [6] that homoclinic snaking behavior is a rather generic feature of solutions to certain types of RD systems near a subcritical Turing bifurcation point.

1.3 The Structure of This Dissertation

To provide a more thorough introduction to the model we study in this dissertation, in Section 1.4, we relate principles in criminology to the definition of a new agent-based model which extends that of [47] to include police interactions with the criminals. A key feature of this section is the idea to use a new form of biased random walk to model police patrol with different degrees of focus, modelled by a parameter k, to sites attractive to criminals. Then, in Section 1.5, we derive the continuum limit of this agent-based model to arrive at a three-component system which will become the centre of the study of this dissertation.

The remainder of the dissertation is divided into two chapters.

In Chapter 2, we study the case when police are absent, i.e. the same PDE that is derived in [47] but defined on a bounded 1-D domain. Unlike the analysis in [29], we study the regime $\epsilon \ll 1$, $D = O(1)$ where there is stronger interaction between the two components in the RD system. The key results are that the far-from equilibrium existence and stability theory do not depend on whether the criminal reintroduction rate is in the Turing stable or unstable regime. However, a peak insertion phenomenon was found to occur precisely when the crime reintroduction rate is higher than half the baseline attractiveness (which is the Turing unstable regime). Moreover, applicable to both regimes, we derived an asymptotic description of the slow dynamics of crime hotspots where the hotspots undergo mutual repulsion.

In Chapter 3, we study the case when policemen are present, who interact with the criminals via a simple interaction dynamics. We also study the problem on a bounded 1-D domain but in the weaker interaction asymptotic regime $\epsilon \ll 1$ and $D = O(\epsilon^{-2})$ as considered in [29] for the basic urban crime model. The key results are the construction of multiple crime hotspots using matched asymptotic expansions, the unconditional linear stability of a single hotspot, lower and upper thresholds for stability and instability, respectively, of multiple hotspots, and finally the existence of a Hopf bifurcation for multiple hotspots for parameters between the lower and upper thresholds. This instability is shown to lead to asynchronous oscillations in the amplitudes of the hotspots.

In both chapters, the key results from, for instance, formal asymptotic expansions, were also stated as propositions. However, the results may be formal and we do not imply a level

of mathematical rigour usually expected for proofs from a careful consideration of function spaces. Instead, we give evidence to the validity of our principal results by performing numerical simulations at appropriately chosen model parameters.

1.4 An Agent-Based Model of Urban Crime with Police Patrol

This section follows the approach in the original work in by Short et al. in [47], a result of the UC MaSC Project group located at University of California, Los Angeles, which includes both mathematicians and criminologists. Following [47], we will also formally derive the continuum limit of the discrete model, which leads to a coupled PDE system of reaction-diffusion type.

In [47], the authors drew support from both evidence from field data and well-established criminological theories of urban crimes to devise a model that aimed at reproducing the emergence, dynamics and steady-state properties of spatio-temporal clusters of crime, which is known as *crime hotspots*.

They chose household burglary as the prototypical crime to model due to the relative simplicity arising from the fact that sites of criminal activity are basically immobile. Their discrete model was based on three key ideas:

Firstly, two agents were assumed on a lattice which represents possible sites of burglary. The first "agent" was an intangible one called the *attractiveness*, measuring the crime susceptibility of each site, and it is perceptible by the second agent, the criminals, who were assumed to be random walkers, but with bias in that they are more likely to burglarize and roam towards sites with higher attractiveness. This results in a nonlinear drift term in the diffusion of criminals.

Secondly, a burglary event triggers a positive feedback via the increase of attractiveness of the same site or nearby-sites which is to model the criminological theory of repeat or near-repeat victimization. This results in a nonlinear coupled dynamics between the attractiveness and criminals. Moreover, criminals were assumed to be removed from the system after a successful burglary, but a constant background rate of introduction replenishes the number of criminal agents that roam on the lattice.

Lastly, corresponding to the observation of a slow proliferation of illegal activities towards neighbourhoods of crime hotspots, possibly due to various environmental cues and known pop-

ularly as the "broken windows" effect, the attractiveness agent is also assumed to diffuse, but in a much slower rate compared to the criminals. It is by this assumption that the eventual continuum model is naturally singularly perturbed by the diffusivity of attractiveness ($\epsilon^2 \ll 1$ in our subsequent model parameters).

Our work begins with a similar agent-based model which extends Short's model in [47] described above by incorporating a police agent. The model was modified from previous attempts to model police influence to criminal behaviours by deterrence but not direct apprehension. The closest model is particular case by Jones *et al.* in [22], where they model the criminal-police interaction by "behaviour modification", while the police movement was modelled to be of the "cops on the dot" type. The "cops on the dot" terminology also appeared in [56] where instead of deriving a PDE as a continuum limit, they assumed the police effect to be centred at the locations of crime hotspots, and look for solutions to a constrained minimization problem defined on an appropriately chosen function space. See also [41] for another method of incorporating police by means of an extra PDE.

The model in [22] is a natural extension of the initial model by Short *et al.*, and the key idea that we are interested in this work is that we can consider patrolling policemen as random walkers biased towards sites with higher attractiveness, like criminals, for which Jones *et al.* termed "cops on the dot" in [22]. We attempt to generalize this idea to accommodate different degrees of focused patrolling strategy using a degree parameter k on top of the attractiveness field, which we found flexible to accommodate the whole spectrum of police patrolling behaviour from pure random walk, to a more containment approach, and to very focused patrolling that deploys most of the policemen towards the centres of vulnerable sites.

Similar to [22], we will derive in Section 1.5 a continuum limit of the agent-based model we define in this section. The result will be an extra PDE for the police term coupled to the original continuous Short's model (1.1) by the PDE for the criminals only. It is the subject of the subsequent chapters by which we answer questions concerning the emergence, dynamics and stability of crime hotspots and the effects of police patrol.

Finally, we make a few remarks that compares our model to other related models in the literature. Our model and the variants in [22], do not make the assumption that the presence of police would alter the movements of criminals, in contrast to the models presented in [41].

Moreover, we also take a more conservative approach in the efficacy of police deployment. Unlike the identically named, but mathematically different version of "cops on the dots" by Zipkin in [55], who emphasized the advantage of police over criminals due to a more centralized planning and higher degree of collaboration, we do not envision the action of the police to be necessarily minimizing the the crime at each crime hotspots. Instead, we begin with the assumption that police agents are essentially a type of biased random walkers not unlike the criminals in their movement, both of which may bias their movements due to the perception of attractiveness (or, "risk", in police's perspective). Moreover, we mention in passing that according to our leading order steady-state theory in Section 3.1, such a conservative model can already predict a critical value of police deployment that would preclude the existence of steady-state crime hotspots.

We now give the details of our agent-based model by both summarizing the work in [47, 22] and augmenting it with our new modelling efforts for the police term.

1.4.1 A City with a Boundary Modelled by a Lattice

We describe the targets of burglary in an urban area using a square lattice $\underline{x} = (i, j)$, where $0 \leq i \leq M$ and $0 \leq j \leq N$, upon which we define moving "agents" with numerical values evolving with a discrete time variable t. The distance between two lattice point is fixed to be l and the time-step of the simulation is fixed to be δt. Note that by nature of this spatial configuration, no agent can leave or enter the lattice. This will be connected to the type of boundary condition we assume for the final PDE that we derive as a continuum limit of the following model.

At each point $\underline{x}$ and time instant t we associate four discretely evolving values: attractiveness $A(\underline{x}, t)$, number of crimes $E(\underline{x}, t)$, criminals $N(\underline{x}, t)$ and policemen $R(\underline{x}, t)$. Here, we begin by a overall sketch of the ideas that define our understanding of the relationships between these four numbers.

The attractiveness at the site is defined as the sum of a static term A_0 and a dynamic term B, i.e.

$$A(\underline{x}, t) = A_0(\underline{x}) + B(\underline{x}, t).$$

The static term can represent the sum of a variety of factors including the security design of urban homes etc., while the dynamic term refers to how the average burglar perceives of the desirability of the site. This dynamic term can change over time and is significantly affected by the number of crimes that occur close in time and space.

The number of crimes $E(\underline{x}, t)$ is incremented when the criminals, with number recorded by $N(\underline{x}, t)$, decide to burglarize. This is assumed to happen with higher probability depending on the attractiveness $A(\underline{x}, t)$ at the same site. The increase in the number of crimes $E(\underline{x}, t)$ will in turn contribute to the increase of the dynamic portion of attractiveness, i.e. $B(\underline{x}, t)$.

After committing a burglary, the criminals involved will return home, leading to a decrease of the number $N(\underline{x}, t)$. Unlike the discrete model in [47], this is not the only mechanism through which the number of criminals is decreased in our model. Instead, we introduce the new agent $R(\underline{x}, t)$, which records the number of policemen located at a particular site. The number of criminal $N(\underline{x}, t)$ will be decreased at a rate that increase with the number of police $R(\underline{x}, t)$ that is present at the same site.

While the number of criminals $N(\underline{x}, t)$ will be replenished uniformly on the lattice at a constant rate, we do not assume any mechanisms for either the increase or decrease of policemen $R(\underline{x}, t)$, i.e. the total number of policemen is conserved throughout.

In the next subsections, we describe in more detail the working mechanisms of this agent-based model and relate them to the criminology being modelled.

1.4.2 Key Probabilities that Determines the Actions of the Criminals and the Policemen

There are two key human agents: the criminal and the policeman. The probabilities that govern their actions is central to the formulation of this agent-based model.

We describe first the probabilities that determine the actions of the criminal which we call "windows-breaking" and "roaming". More precisely, each criminal is allowed to actively perform one of these two actions at every time step, i.e. burglarize the site or leave for a neighbouring site.

Windows-breaking

The probability for which a certain criminal located at $\underline{x}$ will burglarize the site is defined by the Poisson process

$$p_v(\underline{x}, t) = 1 - e^{-A(\underline{x},t)\delta t}. \tag{1.2}$$

Note that as A and δt vanish, p_v vanish as well. Also, as $A \to \infty$, we have $p_v \to 1^-$ as stipulated by the meaning of attractiveness. Moreover, after each burglary, we assume that the burglar does not commit another crime, but instead return home so we increase the count of crimes $E(\underline{x}, t)$ by 1 but reduce the count of criminal $N(\underline{x}, t)$ by 1. Finally, the number of burglars are maintained by a uniform background re-introduction rate Γ.

Roaming

Since the lattice is square, there are four neighbouring sites for the criminal to move to. We define the probability of moving to one of the neighbouring sites $\underline{x}'$ from $\underline{x}$ at discrete time instant t by

$$p_m(\underline{x}', t; \underline{x}) = \frac{A(\underline{x}', t)}{\sum_{\underline{x}'' \sim \underline{x}} A(\underline{x}'', t)}, \tag{1.3}$$

where $\underline{x}'' \sim \underline{x}$ denotes the four neighbouring sites to $\underline{x}$ and includes $\underline{x}'$. The form above means that the random movement towards the four immediate neighbours is biased in favour of higher attractiveness A. More precisely, for a particular neighbour $\underline{x}'$, $p_m(\underline{x}', t; \underline{x})$ is larger when $A(\underline{x}', t)$ is larger.

Next, we describe the probabilities that determine the actions of the policemen, which we call "deterring" and "patrolling". The reason for modeling deterrence as the only positive effect of police presence is that, according to [22] and the references there-in, it is documented that the vast majority of residential burglaries go unsolved. Therefore, we make the same assumption as in [22] that the main effect of police modelled is not intercepting but deterring crime. In terms of our variables, that means we do not assume any direct effect on the number of crimes, $E(\underline{x}, t)$. It is reasonable to posit that the presence of policemen may decrease the attractiveness of the site, and in particular the dynamic component $B(\underline{x}, t)$. However, as in [22], we focus our modelling effort on the deterrence effect *and* the way policemen patrol on the grid, which

effectively means we disregard any coupling effect that could exist between the attractiveness $A(\underline{x}, t)$ and police presence $R(\underline{x}, t)$, but focus on the coupling between the criminals $N(\underline{x}, t)$ and the policemen $R(\underline{x}, t)$.

In conclusion, we will only consider the effect of the number of policemen present, $R(\underline{x}, t)$, on the number of criminals present, $N(\underline{x}, t)$. Together with a biased random walk of the police that mimics the mentality of the criminals, the two major actions of the police term $R(\underline{x}, t)$ are summarized as follows.

Deterring

There are many possible ways to model the interaction of the policemen $R(\underline{x}, t)$ and criminals $N(\underline{x}, t)$. We present two of the most intuitive and simple interaction mechanisms.

The arguably simplest way is to assume that the deterrence effect is directly proportional to the number of policemen present, with no stochastic elements. This implies the number of criminals $N(\underline{x}, t)$ is decremented by a term proportional to $R(\underline{x}, t)$ at every time instant, which we simply express as

$$-\nu R(\underline{x}, t), \tag{1.4}$$

where ν is the constant of proportionality describing the deterrent effect of the policemen.

Another possibly more realistic way to model the deterrence effect is to imitate the classical predator-prey dynamics of Lotka–Volterra type and to regard the police as the "predator" and criminals as the "prey". Therefore, the deterrence effect is assumed to be directly proportional to the product of the number of criminals and the number of policemen. However, we would like to draw a key distinction here that we do not assume the totality of criminals either at a particular site or on the whole lattice to be actually visible to policemen. Instead, potential criminals (who have yet to commit a burglary), at their random encounter with policemen at the same site will return home by the deterrence effect of the police, which is directly proportional to the number of policemen present. However, we assume that the policemen can perceive the same environmental cues of crime attractiveness as the criminals do. In other words, whilst the criminals (predator) are foraging for vulnerable sites and moving towards attractive sites (prey), the police (predator) also moves towards attractive sites (but not the criminals themselves) to

deter away criminals (prey).

Therefore, we model the probability that criminals will decide to go home upon contact with police also as a Poisson process with probability

$$p_u(\underline{\mathrm{x}}, t) = 1 - e^{-\mu R(\underline{\mathrm{x}}, t)}, \tag{1.5}$$

where μ is measures the strength of the deterrence in such close contact events. We remark here that in both events if a criminal burglarizes, i.e. "meets its prey", or encounters a policeman, i.e. "meet its predator", the criminal is removed from the system.

Patrolling

Here, we model another significant action of the police, which draws inspiration from former models, and in particular, we consider the following as a generalization of the "cops on the dots" policing strategy devised by Jones et al. in [22].

Since policemen are assumed to detect the attractiveness of the sites in the same way as criminals, we assume that their patrolling behaviour is also directed towards neighbouring sites in favour of sites with higher risk of crime. However, the police may act in a more (or less) aggressive manner in focusing their patrolling efforts to more vulnerable sites. In the two extreme ends, a policeman can wander aimlessly like a random walker, or move always to the most vulnerable site in the neighbourhood.

To model this variation of patrolling behaviour, we introduce a simple degree parameter k on top of A to define the probability that the police will move from $\underline{\mathrm{x}}$ to a neighbouring site $\underline{\mathrm{x}}'$ by

$$p_k(\underline{\mathrm{x}}', t; \underline{\mathrm{x}}) = \frac{A^k(\underline{\mathrm{x}}', t)}{\sum_{\underline{\mathrm{x}}'' \sim \underline{\mathrm{x}}} A^k(\underline{\mathrm{x}}'', t)} \tag{1.6}$$

(cf. the paragraph immediately above formula (2.7) in [22]).

When $k = 1$, this coincide exactly with the "cops on the dots" strategy, which we also call *mimicry* patrolling, and the police is roaming in a biased random walk in the exact same fashion as criminals. Next, we observe that, in particular, as $k \to 0^+$, the probabilities will result in a pure random walk, which was mentioned as the less favourable strategy in [22]. On the other

hand, if $k \to \infty$, clearly we have

$$p_k(\underline{\mathrm{x}}', t; \underline{\mathrm{x}}) = \begin{cases} 1 & \text{if } \underline{\mathrm{x}}' = \max\{A(\underline{\mathrm{x}}'', t) : \ \underline{\mathrm{x}}'' \sim \underline{\mathrm{x}}\} \\ 0 & \text{otherwise}\,. \end{cases}$$

This means that the policeman has both the perfect competence to understand the attractiveness of the neighbourhood and the total willingness to patrol there.

We will not study both of these extreme cases in isolation, but instead allow the parameter k to range from 0 to ∞, so that we may study how the degree of focus may affect both police movement and the resulting deterring effect on the criminals, and ultimately the existence and stability of crime hotspots. We also remark that this is rather different from the assumptions made by Zipkin *et al.* concerning their version of "cops on the dot" strategy in [56]. The authors' main assumption about the policemen is that they are able to move in a highly coordinated way to actively suppress crime hotspots. In contrast, we do not assume any coordination among the members of the police force, but instead consider them as completely independent individuals.

Finally, note that if neighbouring sites are burglarized, thus raising the dynamic attractiveness, the possibility that nearby police agents also move towards those sites is increased in a manner similar to criminals. In other words, the "broken windows effect" also acts upon the police.

1.4.3 Discrete Evolution of Agents' State and the Localized Spread of the Risk of Crime

Having defined the key probabilities that determine the active and passive actions of the criminals and police, we turn to calculate the values of each of the agents at the next time step. Most importantly, the criminological theory of repeat or near-repeat victimization is introduced in this subsection.

Fading memory of criminal events

As in [47], we assume that the dynamic attractiveness decays with time exponentially as memory of crime fades, which is a feature of many social and ecological phenomena. Thus, for a site

without crime for a long time the dynamic attractiveness B should decay to zero as well, and the total attractiveness A should return to the baseline value A_0. This is modelled by

$$B(\underline{x}, t+\delta) = B(\underline{x}, t)(1-\omega\delta t), \tag{1.7}$$

where $\omega > 0$ controls the rate of memory fade.

Repeat and near-repeat victimization

Another crucial feature of the discrete model by Short et al. in [47] is that the burglary event raises the perception of all criminals in terms of the dynamic attractiveness of the very same site. Moreover, it is theorized that the increased risk also diffuses to the neighborhood as well. This is modelled by the update

$$B(\underline{x}, t+\delta t) \quad = \quad \left[(1-\eta)\, B(\underline{x}, t) + \frac{\eta}{4} \sum_{\underline{x}'' \sim \underline{x}} B(\underline{x}'', t)\right](1-\omega\delta t) + \theta E(\underline{x}, t). \tag{1.8}$$

The parameter $\theta > 0$ measures the effect of each crime on the dynamic attractiveness of the very site. In other words, the $\theta E(\underline{x}, t)$ term models the repeat victimization effect resulting from each burglary. On the other hand, the parameter $0 \leq \eta \leq 1$ measures the amount of perceived attractiveness that is transferred to the immediate neighbours. This models the near-repeat victimization phenomenon, where a site with high attractiveness is thought to also cause more crimes in the neighbourhood.

We believe that very often a small $\eta > 0$ is reasonable, which will subsequently lead to our PDE in the continuum limit to be *singularly perturbed*. In particular, a value higher than $\eta = \frac{1}{2}$ is rather counter-intuitive because location drifts of crime hotspots were documented to be rather slow in time, which effectively means the diffusivity-like constant η should also be low. In [47, 48], the authors also used a relatively small value of η.

Biased random walk and the dynamics of criminal movement

Since at each site, we assumed that the criminals would either burglarize or roam to a nearby site, the new criminal count $N(\underline{x}, t+\delta t)$ is the sum of criminals coming in from all the neighbour-

ing site $\underline{x}' \sim \underline{x}$. These criminals are those who did not commit a burglary (with the probability $1 - p_v$) and have chosen to move to this site $\underline{x}$ from their original site $\underline{x}'$ by a biased random walk (with probability $p_m(\underline{x}; t, \underline{x}')$). In this way, we get

$$N(\underline{x}, t + \delta t) \quad = \quad \sum_{\underline{x}' \sim \underline{x}} N(\underline{x}', t) \left(1 - p_v(\underline{x}', t)\right) p_m(\underline{x}; t, \underline{x}') + \Gamma \delta t \, .$$

Deterrent effect and mimicry movement of police agents

In Short et al's discrete model in [47], they stopped at the formula above for $N(\underline{x}, t)$. Now, we must include the presence of the police agents $R(\underline{x}, t)$. As mentioned in the previous subsection, we will discuss two cases of the effect of police.

For the simple interaction case (1.4), we assume that the number of criminals that go home is directly proportional to the number of police present at the same site, and thus the number of criminals at the next time-step is given by:

$$N(\underline{x}, t + \delta t) = \sum_{\underline{x}' \sim \underline{x}} N(\underline{x}', t) \left(1 - p_v(\underline{x}', t)\right) p_m(\underline{x}; t, \underline{x}') - \nu R(\underline{x}', t) + \Gamma \delta t \, . \tag{1.9}$$

For the predator-prey type interaction (1.5), we assume that each criminal located at $\underline{x}$ will go home with the probability $p_u(\underline{x}, t)$ upon encountering each patrolling police officers, and so we arrive at

$$N(\underline{x}, t + \delta t) = \sum_{\underline{x}' \sim \underline{x}} \left[N(\underline{x}', t) \left(1 - p_v(\underline{x}', t)\right) p_m(\underline{x}; t, \underline{x}')\right] \left(1 - p_u(\underline{x}, t)\right) + \Gamma \delta t, \tag{1.10}$$

where we note that the number of police $R(\underline{x}', t)$ is implicit in the definition of $p_u(\underline{x}, t)$.

As for police officers, since they are patrolling, we also assume that each officer at site $\underline{x}$ will proceed to patrol the neighbouring site, while the police at any neighbouring site $\underline{x}'$ will come to the site $\underline{x}$ also by the focused patrolling mechanism described above. Therefore, we deduce that

$$R(\underline{x}, t + \tau \delta t) = \sum_{\underline{x}' \sim \underline{x}} R(\underline{x}', t) p_k(\underline{x}; t, \underline{x}'), \tag{1.11}$$

where we also multiplied δt by τ to reflect the relative speed of police to the criminals. Recall

also that we do not assume any mechanisms for removing and introducing police so that the total number of police should be conserved.

1.5 Deriving the Continuum Limit as a System of PDEs

In what follows, we formally derive a continuum limit of this agent-based model to motivate the form of the specific PDEs considered in this work. We remark that the derivation is formal (referred to as "naÃ¯ve continuum limit" in [22]) and we will assume certain correlations between certain terms to be negligible, as mentioned in Remark (1.1) below.

Before we proceed, let us define the "discrete Laplacian", which we will need to apply several times to simplify algebra and the presentation:

$$\triangle F(\underline{x},t) = \frac{1}{l^2}\sum_{\underline{x}'\sim\underline{x}}\left(F(\underline{x}',t)-F(\underline{x},t)\right) = \frac{1}{l^2}\left(\sum_{\underline{x}'\sim\underline{x}}F(\underline{x}',t)-4F(\underline{x},t)\right),$$

where $F(\underline{x},t)$ is some agent that evolves on the grid. Therefore, we have

$$\sum_{\underline{x}'\sim\underline{x}}F(\underline{x}',t) = l^2\triangle F(\underline{x},t)+4F(\underline{x},t)\,. \tag{1.12}$$

This will allow us to write our formulas entirely in terms of the variables $\underline{x}$ and t.

We will derive a formal continuum limit from the discrete model, with attractiveness given by (1.8), the criminals given by (1.9) or (1.10) (simple interaction and predator-prey type interaction respectively), and the police given by (1.11).

1.5.1 Derivation of the Individual PDEs

For (1.8), we apply (1.12) to $B(\underline{x}',t)$ and replace $E(\underline{x},t)=N(\underline{x},t)p_v(\underline{x},t)$ to get

$$B(\underline{x},t+\delta t) = \left(B(\underline{x},t)+\frac{\eta l^2}{4}\triangle B(\underline{x},t)\right)(1-\omega\delta t)+\theta N(\underline{x},t)p_v(\underline{x},t)\,.$$

Remark 1.1. As pointed in [22], and also quoted in [56], the assumption that the random variables N and p_v are independent may not hold. However, as in [22], we assume that the correlation does not contribute a leading-order effect on the total number of crimes, which is

eventually represented by ρA in the continuum limit. The same point is also relevant to our subsequent derivation of the police deterrent effect in the predator-prey type interaction case. We also assume that the random variables N and p_u are essentially independent, so that the effect of criminal deterrence is represented eventually by ρU.

Note that the argument of each function is $(\underline{\mathrm{x}}, t)$, so we now subtract $B(\underline{\mathrm{x}}, t)$ from both sides and divide by δt to find, (dropping the arguments for notational simplicity)

$$\frac{\partial B}{\partial t} \sim \frac{\eta}{4}\frac{l^2}{\delta t}\triangle B - \omega B + \frac{l^2}{\delta t}\left(\frac{N}{l^2}\right)\theta A \delta t\,,$$

using $p_v = 1 - e^{-A\delta t} \sim A\delta t$.

Since $\delta t \to 0$, we maintain the the ratios of parameters that depend on the length and time scales of the model to be constants and make the following replacement:

$$\frac{l^2}{\delta t} \to D, \qquad \theta \delta t \to e, \qquad \frac{N}{l^2} \to \rho\,.$$

In this way, we arrive at the following PDE:

$$B_t = \eta\frac{D}{4}\triangle B - \omega B + e\rho A\,.$$

In terms of the total attractiveness $A = A_0 + B$, and assuming A_0 to be uniform in space also, then we can write

$$A_t = \eta\frac{D}{4}\triangle A - \omega A + e\rho A + \omega A_0$$

For the probability p_m associated with the biased random walk of criminals, which appears in both (1.9) and (1.10), we obtain that

$$p_m\left(\underline{\mathrm{x}}, t; \underline{\mathrm{x}}'\right) = \frac{A(\underline{\mathrm{x}}, t)}{\sum_{\underline{\mathrm{X}}'' \sim \underline{\mathrm{X}}'} A(\underline{\mathrm{x}}'', t)} = \frac{A(\underline{\mathrm{x}}, t)}{l^2 \triangle A(\underline{\mathrm{x}}', t) + 4A(\underline{\mathrm{x}}', t)}\,, \tag{1.13}$$

upon using the discrete Laplacian formula (1.12).

For the simple interaction case (1.9), we then have

$$N(\underline{x}', t+\delta t) = A(\underline{x}, t) \sum_{\underline{x}' \sim \underline{x}} \frac{N(\underline{x}', t)\,(1 - p_v(\underline{x}', t))}{l^2 \triangle A(\underline{x}', t) + 4A(\underline{x}', t)} - \nu R(\underline{x}', t) + \Gamma \delta t. \tag{1.14}$$

In contrast, for the predator-prey interaction case (1.10), we have instead that

$$\begin{aligned} N(\underline{x}', t+\delta t) &= A(\underline{x}, t) \sum_{\underline{x}' \sim \underline{x}} \frac{N(\underline{x}', t)\,(1 - p_v(\underline{x}', t))\,(1 - p_u(\underline{x}, t))}{l^2 \triangle A(\underline{x}', t) + 4A(\underline{x}', t)} + \Gamma \delta t\,, \\ &\triangleq A(\underline{x}, t) \sum_{\underline{x}' \sim \underline{x}} S(\underline{x}', t) + \Gamma \delta t\,, \end{aligned}$$

where we defined $S(\underline{x}, t)$ in the second equality.

Therefore, we have

$$A(\underline{x}, t) \left(l^2 \triangle S(\underline{x}, t) + 4S(\underline{x}, t) \right) + \Gamma \delta t\,. \tag{1.15}$$

We first focus on the more complicated case (1.15). We subtract $N(\underline{x}, t)$ from both sides of (1.15), and divide by l^2, applying $\frac{N}{l^2} \to \rho$, and then by δt to find that (dropping common arguments again):

$$\frac{\partial \rho}{\partial t} \sim \frac{1}{\delta t} \left(A \triangle S + \frac{4A}{l^2} S - \rho \right) + \gamma\,. \tag{1.16}$$

Here we made the replacement $\Gamma / l^2 \to \gamma$ for the parameter Γ which depends on the length-scale.

Now recall that $p_v \sim A \delta t$ as well as for $p_u = 1 - e^{-\mu R}$, since R is small when $l \to 0$. We then apply the replacement $\frac{R}{l^2} \to U$ to find

$$p_u \sim \mu R = \mu U l^2\,.$$

By using this relation, we can simply the key term S in (1.16) as follows:

$$\begin{aligned} S &= \frac{N\,(1 - p_v)\,(1 - p_u)}{l^2 \triangle A + 4A}\,, \\ &\sim \frac{l^2}{4A} \frac{\rho\,(1 - A\delta t)\,(1 - \mu U l^2)}{1 + \frac{l^2}{4A} \triangle A}\,, \\ &\sim \frac{l^2}{4A} \rho\,(1 - A\delta t) \left(1 - \mu U l^2\right) \left(1 - \frac{l^2}{4A} \triangle A\right)\,. \end{aligned}$$

This yields that

$$\frac{S}{\delta t} \sim \frac{l^2}{4\delta t} \frac{\rho}{A} = \frac{D}{4} \frac{\rho}{A}\,,$$

and consequently

$$\frac{A\triangle S}{\delta t} \sim \frac{D}{4} A\triangle\left(\frac{\rho}{A}\right),$$

which gives the first term in (1.16).

Next, observe that

$$\begin{aligned}\frac{4AS}{l^2} - \rho &\sim \rho\,(1 - A\delta t)\left(1 - \mu U l^2\right)\left(1 - \frac{l^2}{4A}\triangle A\right) - \rho\,,\\ &\sim -\rho A\delta t - l^2\mu\rho U - \frac{l^2}{4}\frac{\rho}{A}\triangle A,\end{aligned}$$

which implies to

$$\frac{1}{\delta t}\left(\frac{4AS}{l^2} - \rho\right) \sim -\rho A - D\mu\rho U - \frac{D}{4}\frac{\rho}{A}\triangle A.$$

Thus, by combining with the previous term, we arrive at the PDE

$$\begin{aligned}\frac{\partial\rho}{\partial t} &= \frac{D}{4} A\triangle\left(\frac{\rho}{A}\right) - \rho A - D\mu\rho U - \frac{D}{4}\frac{\rho}{A}\triangle A\\ &= \frac{D}{4}\left(A\triangle\left(\frac{\rho}{A}\right) - \frac{\rho}{A}\triangle A\right) - \rho A - D\mu\rho U. \qquad (1.17)\end{aligned}$$

Similarly, for the easier case (1.9) when simple interaction is assumed, we have instead that

$$\frac{\partial\rho}{\partial t} = \frac{D}{4}\left(A\triangle\left(\frac{\rho}{A}\right) - \frac{\rho}{A}\triangle A\right) - \rho A - D\nu U. \qquad (1.18)$$

We pause to remark that there is an applicable identity $A\triangle\left(\frac{\rho}{A}\right) - \frac{\rho}{A}\triangle A = \nabla\cdot\left(\nabla\rho - \frac{2\rho}{A}\nabla A\right)$, for which a more general case that also applies to an analogous term in the police equation will be derived in the next subsection.

Next, we turn to (1.11), where we rewrite the expression as

$$p_k(\underline{\mathrm{x}}; t, \underline{\mathrm{x}}') = \frac{A^k(\underline{\mathrm{x}}', t)}{\sum_{\underline{\mathrm{x}}''\sim\underline{\mathrm{x}}} A^k(\underline{\mathrm{x}}'', t)} = \frac{A^k(\underline{\mathrm{x}}, t)}{l^2\triangle A^k(\underline{\mathrm{x}}', t) + 4A^k(\underline{\mathrm{x}}', t)},$$

upon using the discrete Laplacian (1.12). Then, we calculate that

$$\begin{aligned} R(\underline{\mathrm{x}}, t+\tau\delta t) &= A^k(\underline{\mathrm{x}}, t) \sum_{\underline{\mathrm{x}}' \sim \underline{\mathrm{x}}} \frac{R(\underline{\mathrm{x}}', t)}{l^2 \triangle A^k(\underline{\mathrm{x}}', t) + 4A^k(\underline{\mathrm{x}}', t)}\,, \\ &\triangleq A^k(\underline{\mathrm{x}}, t) \sum_{\underline{\mathrm{x}}' \sim \underline{\mathrm{x}}} T(\underline{\mathrm{x}}', t)\,, \\ &= A^k(\underline{\mathrm{x}}, t) \Big(l^2 \triangle T(\underline{\mathrm{x}}, t) + 4T(\underline{\mathrm{x}}, t) \Big)\,. \end{aligned}$$

Similar to the criminal equation, after subtracting both sides by $R(\underline{\mathrm{x}}, t)$, dividing by $l^2\delta t$ and replacing $\frac{R}{l^2} \to U$, we find

$$\tau \frac{\partial U}{\partial t} \sim \frac{1}{\delta t} \left(A^k \triangle T + \frac{4A^k}{l^2} T - U \right),$$

where there is an extra τ on the time derivative due to chain rule.

Next, we observe that

$$T = \frac{R}{l^2 \triangle A^k + 4A^k} = \frac{l^2}{4A^k} \frac{U}{1 + \frac{l^2}{4A^k} \triangle A^k} \sim \frac{l^2}{4A^k} U \left(1 - \frac{l^2}{4A^k} \triangle A^k \right),$$

which gives $\frac{T}{\delta t} \sim \frac{D}{4} \frac{U}{A^k}$. In this way, we get

$$\frac{A^k \triangle T}{\delta t} \sim \frac{D}{4} \left(A^k \triangle \left(\frac{U}{A^k} \right) \right).$$

Next, observe that

$$\frac{1}{\delta t} \left(\frac{4A^k}{l^2} T - U \right) \sim \frac{1}{\delta t} \left[U \left(1 - \frac{l^2}{4A^k} \triangle A^k \right) - U \right] \sim -\frac{D}{4} \frac{U}{A^k} \triangle A^k.$$

This leads to the PDE for the police

$$\tau \frac{\partial U}{\partial t} = \frac{D}{4} \left(A^k \triangle \left(\frac{U}{A^k} \right) - \frac{U}{A^k} \triangle A^k \right).$$

1.5.2 The Final Form of the PDE system and a Special Identity for the Nonlinear Diffusion

Having converted the discrete models to their corresponding continuum limits, we now establish the following identity that converts the PDEs to our final form:

$$A^k \triangle \left(\frac{U}{A^k} \right) - \frac{U}{A^k} \triangle A^k \equiv \nabla \cdot \left(\nabla U - \frac{2kU}{A} \nabla A \right) . \tag{1.19}$$

To derive this identity, we proceed directly by using the Leibniz rule: $\nabla^2 (fg) = f\nabla^2 g + 2\nabla f \cdot \nabla g + g\nabla^2 f$. We obtain that

$$\begin{aligned}
A^k \triangle \left(\frac{U}{A^k} \right) &= A^k \left(\frac{\triangle U}{A^k} + 2\nabla U \cdot \nabla \left(\frac{1}{A^k} \right) + U \triangle \left(\frac{1}{A^k} \right) \right) , \\
&= A^k \left(\frac{\triangle U}{A^k} - \frac{2k}{A^{k+1}} \nabla U \cdot \nabla A + \frac{k(k+1)}{A^{k+2}} U |\nabla A|^2 - \frac{k}{A^{k+1}} U \triangle A \right) \\
&= \triangle U - \frac{2k}{A} \nabla U \cdot \nabla A + \frac{k(k+1)}{A^2} |\nabla A|^2 - \frac{k}{A} \triangle A , \\
\frac{U}{A^k} \triangle A^k &= \frac{U}{A^k} \nabla \cdot \left(k A^{k-1} \nabla A \right) , \\
&= \frac{U}{A^k} \left(A^{k-2} |\nabla A|^2 + k A^{k-1} \triangle A \right) , \\
&= \frac{k(k-1)}{A^2} U |\nabla A|^2 + \frac{k}{A} \triangle A .
\end{aligned}$$

By combining these results together we obtain that

$$\begin{aligned}
A^k \triangle \left(\frac{U}{A^k} \right) - \frac{U}{A^k} \triangle A^k &= \triangle U - \frac{2k}{A} \nabla U \cdot \nabla A + \frac{2k}{A^2} U |\nabla A|^2 - \frac{2k}{A} U \triangle A , \\
&= \triangle U - 2k \left(\nabla \left(\frac{U}{A} \right) \cdot \nabla A + \frac{U}{A} \triangle A \right) , \\
&= \triangle U - 2k \nabla \cdot \left(\frac{U}{A} \nabla A \right) \\
&= \nabla \cdot \left(\nabla U - \frac{2kU}{A} \nabla A \right) ,
\end{aligned}$$

as desired.

Finally, for notational convenience, we let $q = 2k$ and after nondimensionalization and

renaming of constants, we arrive at the following three-component RD system:

$$A_t = \epsilon^2 A_{xx} - A + \rho A + \alpha, \tag{1.20a}$$

$$\rho_t = D\left(\rho_x - 2\rho A_x/A\right)_x - \rho A + \gamma - \alpha - I(\rho, U), \tag{1.20b}$$

$$\tau_u U_t = = D\left(U_x - qU A_x/A\right)_x, \tag{1.20c}$$

where two cases of $I(\rho, U)$ were given by:

(i) Simple interaction case (corresponding to (1.18))

$$I(\rho, U) = U, \text{ and}$$

(ii) Predator-prey type interaction case (corresponding to (1.17))

$$I(\rho, U) = \rho U.$$

There are two further remarks concerning the form of (1.20) before we present various results about (1.20).

Firstly, we remark that due to a slightly different way of nondimensionalization, we obtained a model with an extra parameter D as compared to the model in [22, 47], where $D = 1$. A non-unit value of D can also be derived from the case $D = 1$ using a simple domain scaling argument. We will retain the diffusivity parameter D for ease in our subsequent analysis. Concerning the criminal-police interaction term $I(\rho, U)$, we also remark that the predator-prey type interaction is to be preferred over the simple interaction case for purposes of application. However, due to the difficulty in the NLEP stability analysis with multiple nonlocal terms (see the introductory paragraphs to Chapter 3 on page 95). The simple interaction case is favoured for mathematical feasibility to begin our research in our study of police-criminal interaction and its effect on crime hotspots.

Chapter 2

Crime Hotspot Formation and Long-time Behaviours

In this chapter, we consider (1.20) when $U \equiv 0$, i.e. with no police involvement in the crime dynamics and consider the finite one-dimensional domain $-\ell < x < \ell$. This reduces to the two-component reaction-diffusion (RD) system originally introduced by Short *et al.* in [47], which we express in the following form

$$A_t = \epsilon^2 A_{xx} - A + \rho A + \alpha\,, \qquad \rho_t = D\left(\rho_x - \frac{2\rho}{A}A_x\right)_x - \rho A + \gamma - \alpha\,, \tag{2.1}$$

with no-flux boundary conditions $\rho_x = A_x = 0$ at $x = \pm\ell$. Note that $\epsilon^2 \ll 1$ is a singular perturbation parameter, and we assume $D = O(1)$.

We remark that by the simple rescaling $\tilde{x} = x/\sqrt{D}$, (2.1) can be recast to the interval $(-\ell/\sqrt{D}, \ell/\sqrt{D})$, with the new diffusivities $\tilde{\epsilon} = \epsilon/\sqrt{D}$ and $\tilde{D} = 1$. This recovers the exact same form given in [47] and at (1.1) without the factor D. However, in our analysis, rather than using the domain length as a bifurcation parameter, we will consider (2.1) on a fixed domain, but allow the criminal diffusivity $D = O(1)$ to vary while treating the diffusivity ϵ^2 of the attractiveness field as an asymptotically small quantity. This has an advantage both in the notational simplicity in the asymptotic analysis of multiple crime hotspots, and also the numerical computations, where our formulation avoids problems arising out of domain rescaling in scenarios where the numerically computable range in terms of ϵ is too restrictive.

The study of (2.1) in this chapter is directly related to that of [29], where $D = O(\epsilon^{-2})$ was assumed and a similar tool-set of matched asymptotic expansions, supplemented by numerical computations were used in [29] as well. The work in this chapter is a variation of what is studied in [29] when the coupling of the two PDEs in (2.1) is stronger, which will lead to a couple of novel phenomena.

In addition to [29], the previous work that is most relevant to our study is that of [35]. For $D = 1$, in [35] the bifurcation software `AUTO-07p` (cf. [12]) was used to numerically show that there is an intricate homoclinic snaking bifurcation structure for the steady-states of (2.1) on the infinite line when the parameter γ is below the Turing bifurcation threshold γ_c, for which $\gamma_c \sim 3\alpha/2$ as $\epsilon \to 0$. At finite ϵ, the localized states for A that were computed in [35] are wave-packet type solutions consisting of closely spaced pulses. In the singular limit $\epsilon \to 0$, and with $\alpha < \gamma < \gamma_c \sim 3\alpha/2$, these wave-packet localized solutions were found in [35] to lead to a pattern of well-separated hotspots. An asymptotic analysis, based on geometric singular perturbation theory, was given in [35] for the construction of a solitary hotspot solution on the infinite line in the subcritical case $\alpha < \gamma < 3\alpha/2$. However, as remarked in [35], there were some issues in the asymptotic matching procedure in this construction that were left unresolved. Homoclinic snaking behaviour has been well-studied in other systems, such as the Swift-Hohenberg model (see [5] and the references therein). Moreover, it has been shown recently in [6] that homoclinic snaking behaviour is a rather generic feature of solutions to certain types of RD systems near a subcritical Turing bifurcation point.

In contrast to [35], our study of hotspot equilibria and the stability in the singular limit $\epsilon \to 0$ will focus on the *finite* domain problem, and our method of matched asymptotic expansion and NLEP stability analysis work equally well for both the supercritical regime $\gamma > 3\alpha/2$ and the subcritical regime, for which the spatially homogeneous steady-state is linearly unstable and stable respectively. Moreover, our numerical studies in Section (2.4.2), which is an extension of Fig. 7 in [29], show that the crime hotspot solutions follow a *closed-loop* which both begins and ends at the Turing bifurcation point from the subcritical side, instead of a snaking path in the infinite domain case of [35].

The outline of this chapter is as follows. In §2.2, we provide a leading-order construction of a single hotspot steady-state solution in the limit $\epsilon \to 0$ for $D = O(1)$. By reflecting and gluing

this single hotspot solution, equilibria with multiple hotspots are obtained. We emphasize a distinction between the supercritical and subcritical regime by a formula of the outer problem (2.23). In §2.3 we show that steady-state patterns with K interior hotspots are linearly stable on an $O(1)$ time-scale regardless of $D = O(1)$. In §2.4 we present numerical bifurcation results for hotspot equilibria computed using the bifurcation software `AUTO-07p` (cf. [12]). For the supercritical regime, we present results that exhibit a saddle-node bifurcation structure of hotspot equilibria and a peak insertion behaviour near the saddle-node bifurcation point. For the subcritical regime, we present a closed homotopy of homoclinic in a three-dimensional diagram and show the existence of a new type of unstable hotspot that connects the weakly nonlinear regime to the far-from equilibrium regime through a saddle-node bifurcation. In §2.5 we present a higher-order asymptotic theory to construct a steady-state hotspot solution, and in §2.6 we study analytically the onset of peak insertion behaviour near the saddle-node bifurcation point. In §2.7 we derive a system of differential-algebraic equations (DAE) characterizing the slow dynamics of a collection of hotspots for (2.10). Finally, in §2.8, we briefly discuss a few open problems that warrant further study.

2.1 Linear, Weakly Nonlinear and Far-from Equilibrium Regimes

In this section, we review results from linear stability analysis of [49, 29] and recall conclusions from the weakly nonlinear analysis in [48] that lead to the classification of the parameter regime into supercritical ($\gamma > 3\alpha/2$) and subcritical ($\gamma < 3\alpha/2$) regimes. Finally, we motivate our study in the far-from equilibrium regime by a few numerical computations to highlight the existence of crime hotspots away from the Turing bifurcation point. This will be the subject of the remainder of this chapter.

The system (2.1) has the unique spatially homogeneous steady-state solution given by

$$A_e = \gamma \text{ and } \rho_e = 1 - \alpha/\gamma > 0. \tag{2.2}$$

The linear stability analysis of [49] showed that this solution is linearly unstable in the limit

$\epsilon \to 0$ when

$$\gamma > \frac{3}{2}\alpha\,, \tag{2.3}$$

and that a spatially heterogeneous solution bifurcates from the spatially homogeneous steady-state at the bifurcation point $\gamma \sim \frac{3}{2}\alpha$ when $\epsilon \to 0$.

Here, reproduce some details about the Turing bifurcation that has been done in [49, 29]. First, we linearizing (2.1) around the steady-state by introducing the perturbation

$$A = A_e + a_0 e^{imx+\lambda t}, \qquad \rho = \rho_e + \rho_0 e^{imx+\lambda t}\,.$$

This leads to the dispersion relation

$$\left(\lambda + A_e + Dm^2\right)\left(\lambda + \epsilon^2 m^2 + (1-\rho_e)\right) + A_e\left(\rho_e - \frac{2D}{A_e}\rho_e m^2\right) = 0\,. \tag{2.4}$$

To calculate the instability band, we set $\lambda = 0$ to (2.4) and let $\epsilon \ll 1$, with $m = O(1)$, which yields the lower threshold

$$Dm_{\text{lower}}^2 = \frac{A_e}{3\rho_e - 1}, \qquad m_{\text{lower}} = \frac{\gamma}{\sqrt{D}\sqrt{2\gamma - 3\alpha}}\,. \tag{2.5}$$

To obtain the upper edge of the band we let $m \gg 1$ with $\epsilon^2 m^2 = O(1)$ to find

$$\epsilon^2 m_{\text{upper}}^2 + (1-\rho_e) = 2\rho_e, \qquad m_{\text{upper}} = \frac{1}{\epsilon}\frac{\sqrt{2\gamma - 3\alpha}}{\sqrt{\gamma}}\,. \tag{2.6}$$

To find the most unstable mode, we differentiate (2.4) with respect to m and set $d\lambda/dm = 0$ to find

$$\lambda\left(1 + \frac{\epsilon^2}{D}\right) = 3\rho_e - \frac{A_e}{D}\epsilon^2 - 2\epsilon^2 m^2\,.$$

In this way, we obtain that the dominant growth rate

$$\lambda_{\text{dom}} \sim 3\rho_e - 1 = 2 - 3\alpha/\gamma\,, \tag{2.7}$$

and that the most unstable mode is

$$m_{\rm dom} \sim \epsilon^{-1/2} \left[\left(\frac{2\rho_e}{D} \right) \left(\frac{3}{2} A_e + \lambda_{dom} \right) \right]^{1/4} = \epsilon^{-1/2} \left[2 \left(\frac{1-\alpha/\gamma}{D} \right) \left(\frac{3}{2}\gamma + \lambda_{dom} \right) \right]^{1/4} . \quad (2.8)$$

In other words, for an initial condition condition consisting of a random perturbation of a spatially uniform steady-state, we can calculate the characteristic half length of the pattern from the Turing instability to be

$$\ell_{\rm Turing} \sim \frac{\pi}{m_{\rm dom}} = \epsilon^{1/2} \pi \left[2 \left(\frac{1-\alpha/\gamma}{D} \right) \left(\frac{3}{2}\gamma + \lambda_{dom} \right) \right]^{-1/4} .$$

For $\alpha = 1$, $\gamma = 2$, $D = 2$, $\epsilon = 0.05$, we calculate $\ell_{\rm Turing} \approx 0.59$. We observe from the full numerical results computed from the PDE shown in Fig. 2.1 and 2.2 that this Turing instability can lead to the creation of either a single or a double hotspot pattern on the domain $(-1, 1)$.

Moreover, the weakly nonlinear analysis of [48] showed that this Turing bifurcation is *subcritical* when $\epsilon \ll 1$ (see also Fig. 7 of [29]). The theory in [48], based on a normal form equation derived from a multiple-scales approximation, is able to characterize the development of spatial patterns near the Turing bifurcation point. However, it is not capable of describing the highly localized spatial patterns observed in full numerical simulations of (2.1) when the parameter values are not near the Turing point. More specifically, an initial random perturbation close to an unstable spatially homogeneous steady-state typically leads to highly localized spatial patterns, consisting of the concentration of criminal activity in localized spatial regions. We refer to such patterns as hotspot patterns. A localized hotspot solution, not amenable to an analytical description by a weakly nonlinear analysis, was observed in the numerical solutions of [48].

To illustrate these hotspot patterns, we perform full numerical simulations of (2.1) using the software `PDEPE` in `MATLAB R2013b`. For $\epsilon = 0.05$, $D = 2$, $\gamma = 2$, and $\alpha = 1$, in the right panel of Fig. 2.1 we plot A and ρ at some large time when the initial condition is a small random perturbation of the unstable spatially uniform state as shown in the left panel of Fig. 2.1. In the supercritical regime, $\gamma > 3\alpha/2$, the spatially uniform state is unstable and we observe, for large time, that the solution approaches a steady-state pattern with one interior hotspot. For the

same parameter set, but where the initial condition for A has two localized bumps, in Fig. 2.2 we show the initial formation of a two-hotpot pattern on an $O(1)$ time-scale, followed by a very slow dynamics of the two-hotspot pattern towards its steady-state limit. One of the main goals of this chapter is to give an explicit analytical characterization of the slow dynamics of such quasi-steady state hotspot patterns.

For the subcritical regime $\alpha < \gamma < 3\alpha/2$, we also observe from (2.7) that a crime hotspot born in the supercritical regime persists into subcritical regime without dissipating, even though the spatially homogeneous equilibrium (2.2) is stable in this regime. The leading order theory in the next section will show that asymptotic structures of crime hotspot in both the supercritical and subcritical regimes are largely rather similar, which also lead to identical linear stability predictions.

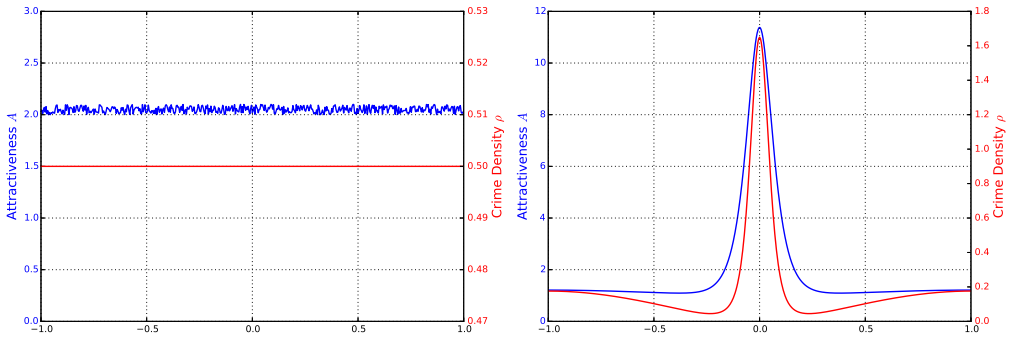

Figure 2.1: A Turing instability leading to a localized steady-state solution. Parameter values are $\epsilon = 0.05$, $D = 2$, $\ell = 1$, $\gamma = 2$, $\alpha = 1$, so that $\gamma > 3\alpha/2$. The initial condition (left panel) for the numerical solution of (2.1) is a small random perturbation of the spatially uniform state given by $A(x,0) = A_e + \text{rand} * 0.1$, $\rho(x,0) = \rho_e$, where $A_e = \gamma = 2$ and $\rho_e = 1 - \alpha/\gamma = 0.5$. The right panel shows the hotspot solution at the final time $t = 10^5$ with A (solid curve) and ρ (dotted curve). Notice that the range of A and ρ are on different scales.

2.2 Super- and Sub-critical Crime Hotspots: Leading-Order Steady-State Theory

In our analysis of (2.1) it is convenient to introduce the new variable V, as first introduced in [29], defined by

$$V \equiv \rho/A^2 \,. \tag{2.9}$$

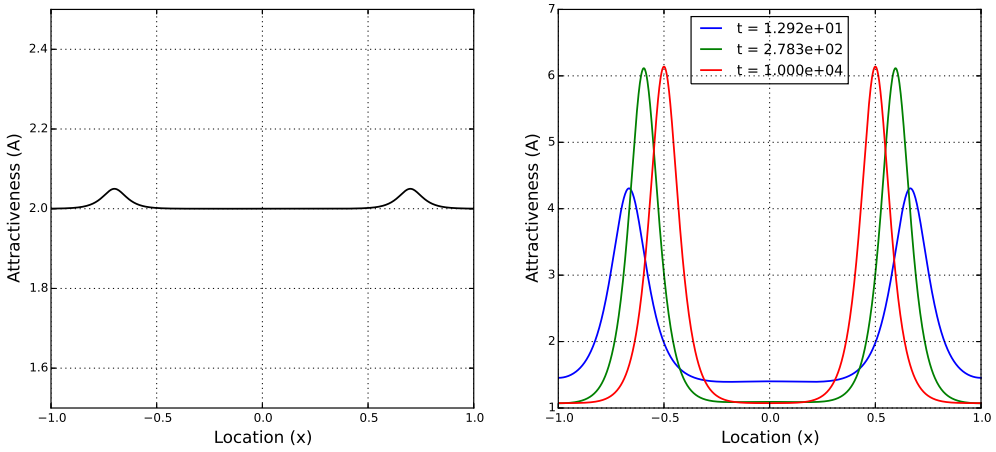

Figure 2.2: Small initial bumps in A quickly evolve into hotspots, which then move slowly to their steady-state locations. Parameter values are $\epsilon = 0.05$, $D = 2$, $\ell = 1$, $\gamma = 2$, $\alpha = 1$, so that $\gamma > 3\alpha/2$. The initial condition (left panel) for the numerical solution of (2.1) is $A(x,0) = A_e + \epsilon \sum_{i=1}^{2} \operatorname{sech}(\frac{x-x_{0,i}}{\epsilon})$ and $\rho(x,0) = \rho_e$, where $x_{0,1} = -0.7$, $x_{0,2} = -.7$, $A_e = \gamma = 2$, and $\rho_e = 1 - \alpha/\gamma = 0.5$. We only plot A.

In terms of A and V, (2.1) transforms to the PDE system

$$A_t = \epsilon^2 A_{xx} - A + VA^3 + \alpha\,, \qquad \left(A^2 V\right)_t = D\left(A^2 V_x\right)_x - VA^3 + \gamma - \alpha\,, \tag{2.10}$$

on $-\ell < x < \ell$, with $A_x = V_x = 0$ at $x = \pm\ell$. The corresponding steady-state problem for (2.10) is

$$\epsilon^2 A_{xx} - A + VA^3 + \alpha = 0\,, \qquad D\left(A^2 V_x\right)_x - VA^3 + \gamma - \alpha = 0\,. \tag{2.11}$$

We use the method of matched asymptotic expansions in the limit $\epsilon \to 0$ to construct a leading-order approximation of a steady-state solution with a single hotspot, or spike, for (2.11) on a domain of length 2ℓ. For a fixed D, we will show that such a solution exists for any ℓ regardless of whether $\alpha < \gamma < 3\alpha/2$ (subcritical) or $\gamma > 3\alpha/2$. We emphasize that the construction does *not* depend on whether γ is in the subcritical or supercritical case, but only on the positivity of $\gamma - \alpha$, i.e. nonzero crime reintroduction rate.

Moreover, we characterize a threshold phenomenon that occurs if and only if $\gamma > 3\alpha/2$, so that a critical length $\ell_{\max}$ exists so that $\ell < \ell_{\max}$ is required for a solution to exist. The hotspot solution for (2.11) is an even solution with a spike in the profile of A centred at the

midpoint of the interval $-\ell < x < \ell$, and the solution satisfies the no-flux boundary condition: $A_x = V_x = 0$ at $x = \pm\ell$.

By reflecting and gluing copies of this single hotspot solution defined on $(-\tilde{\ell}, \tilde{\ell})$ and $\tilde{\ell} = \ell/K$, we can readily obtain a Khotspot solution on the original interval $(-\ell, \ell)$. The key difference between our analysis and that in [29] is that here we consider the $D = O(1)$ regime, which leads below to a nonlinear ODE characterizing the outer solution. In [29], the limit $D \gg O(1)$ was considered, which leads to a linear outer problem and, consequently, a more elementary construction of the hotspot solution than for the case $D = O(1)$.

As in [29], a hotspot is characterized by a localized region of width $O(\epsilon)$ near $x = 0$ where $A \gg 1$ and $V \ll 1$. In the outer region, where $|x| \gg O(\epsilon)$, we have from (2.11) that both A and V are $O(1)$ when $D = O(1)$.

To determine the scaling for the inner region, we introduce the inner variable $y = \epsilon^{-1}x$ so that (2.11) becomes

$$A_{yy} - A + VA^3 - \alpha = 0\,, \qquad D\epsilon^{-2}\left(A^2 V_y\right)_y - VA^3 + \gamma - \alpha = 0\,. \tag{2.12}$$

In this inner region, we pose $A = O(\epsilon^{-p})$, with $p > 0$, and $V = O(\epsilon^q)$. In order to obtain a homoclinic solution solution characterizing the hotspot core, we must balance $O(A) = O(VA^3)$ in the first equation of (2.12), which yields $q = 2p$. To determine the second scaling relation, we integrate the second equation in (2.11) over $|x| \le \ell$ to obtain that $\int_{-\ell}^{\ell} VA^3\,dx = O(1)$. In order that the inner region makes an $O(1)$ contribution to this integral, we require that $1+q-3p = 0$. With $q = 2p$, this yields that $p = 1$ and $q = 2$.

One of the key differences between the analysis for our $D = O(1)$ regime and that in [29] for $D \gg O(1)$, is that here V is characterized by a rapid transition of scale from $V = O(\epsilon^2)$ in the inner region to $V = O(1)$ in the outer region. In the analysis of [29] for the $D \gg 1$ case, it was found that $V \ll 1$ *uniformly* across $-\ell < x < \ell$. A detailed analysis of this rapid transition of scale for V, which requires introducing an intermediate layer between the inner and outer scales, is essential for characterizing the slow dynamics of a collection of hotspots. This more refined analysis is given below in §2.5. In the remainder of this section we only construct a leading-order hotspot solution.

The simple scaling analysis above motivates the following inner expansion for (2.12):

$$A \sim \epsilon^{-1} A_0 + A_1 + \dots , \qquad V \sim \epsilon^2 V_0 + \epsilon^3 V_1 + \dots .$$

Upon substituting this expansion into (2.12) we obtain that V_0 is a constant independent of y and that A_0 satisfies $A_{0yy} - A_0 + V_0 A_0^3 = 0$. This yields that

$$A_0 = \frac{w(y)}{\sqrt{V_0}} , \tag{2.13}$$

where $w(y) = \sqrt{2}\,\mathrm{sech}\, y$ is the unique homoclinic solution to

$$w_{yy} - w + w^3 = 0 , \quad -\infty < y < \infty ; \qquad w(0) > 0 , \quad w_y(0) = 0 , \quad w \to 0 \quad \text{as} \quad y \to \pm\infty . \tag{2.14}$$

A remarkable fact is that the crime density ρ is a constant independent of all model parameters at the hotspot, and is given to leading order by

$$\rho = A^2 V \sim \left(\frac{A_0}{\epsilon}\right)^2 \left(\epsilon^2 V_0\right) = w^2(x/\epsilon) . \tag{2.15}$$

Moreover, the maximum crime density is at the centre of the hotspot

$$\max \rho \sim w^2(0) = 2 . \tag{2.16}$$

To determine V_0, we first need to construct an outer solution on the intervals $0^+ < x < \ell$ and $-\ell < x < 0^-$. Since the hotspot solution is even, we need only consider the range $0^+ < x < \ell$. On this range, we expand $A \sim a_0 + o(1)$ and $V \sim v_0 + o(1)$. Upon substituting this expansion into (2.11) we obtain

$$D\left(a_0^2 v_{0x}\right)_x - v_0 a_0^3 + \gamma - \alpha = 0 , \qquad v_0 = g(a_0) \equiv \frac{(a_0 - \alpha)}{a_0^3} . \tag{2.17}$$

In order that v_0 can match to the inner solution, we require that $v_0(0^+) = 0$, so that $a_0(0^+) = \alpha$. Then, upon combining the two equations in (2.17), it follows that in the outer region a_0 satisfies

the nonlinear BVP

$$D\left(f(a_0)a_{0x}\right)_x = a_0 - \gamma\,, \qquad 0^+ < x < \ell\,; \qquad a_0(0^+) = \alpha\,, \quad a_{0x}(\ell) = 0\,, \tag{2.18a}$$

where we have defined $f(a_0)$ by

$$f(a_0) \equiv \frac{(3\alpha - 2a_0)}{a_0^2} = a_0^2 g'(a_0)\,. \tag{2.18b}$$

2.2.1 Monotonicity of the Outer Problem

For the well-posedness of this outer problem (2.18a) we require that $f(a_0)$ is non-vanishing on $0^+ < x < \ell$. Since the only zero of $f(a_0)$ is at $3\alpha/2$ and $f(\alpha) = \alpha^{-1} > 0$, we shall consider the range $\alpha < a_0 < 3\alpha/2$. If one assumes $\gamma > 3\alpha/2$, which implies that we are in the Turing-unstable regime, it follows that the right-hand side of the differential equation in (2.18a) is always negative on the range $\alpha < a_0 < 3\alpha/2$. This yields that $a_{0x} > 0$ on $0^+ < x < \ell$ when $\alpha < a_0 < 3\alpha/2$. However this is not a necessary condition and we will show that $\gamma > \alpha$ is sufficient to guarantee that $a_{0x} > 0$ whenever a solution exists to (2.18a). This is a crucial property of the solution $a_0(x)$ that will enable us to reduce the problem (2.18a) to a quadrature.

Before solving the ODE, we first illustrate the structure of the leading-order outer solution from a phase plane viewpoint, which will lead naturally to an argument showing that $a_{0x} > 0$ whenever $\gamma > \alpha$. To do so, we introduce the temporary notation $u \equiv a_0$ and $v \equiv f(a_0)a_{0x} = f(u)u'$ to rewrite (2.18a) in the following usual form of a dynamical system:

$$u' = \frac{v}{f(u)}\,, \qquad v' = \frac{(u-\gamma)}{D}\,. \tag{2.19}$$

We seek to identify trajectories in the u, v phase-plane that satisfy $u(0) = \alpha$ and $v(\ell) = 0$, corresponding to the boundary conditions of (2.18a). From the two phase portraits shown in Fig. 2.3, corresponding to the supercritical case where $\gamma > 3\alpha/2$ and subcritical case where $\alpha < \gamma < 3\alpha/2$ respectively, we clearly observe two types of trajectories and a critical threshold v_c for $v(0)$. If $v(0) < v_c$, then the trajectory converges to $v(\ell) = 0$ for some finite positive ℓ.

However, if $v(0) > v_c$, then the solution develops a singularity as

$$u \to \left(\frac{3\alpha}{2}\right)^{-} \text{ where } u' \to +\infty\,,$$

according to (2.19).

For the supercritical case, near where this singularity occurs a new local boundary layer near $x = \ell$ must be constructed. As motivated by the numerical bifurcation results in §2.4, in §2.6 we analytically show that this singularity behaviour is associated with a fold-point bifurcation of equilibrium hotspot solutions, and it characterizes the onset of a hotspot insertion phenomena at $x = \ell$ when $\gamma > 3\alpha/2$, i.e. when we are in the Turing-unstable regime.

On the other hand, for the subcritical case, we observe that admissible trajectories that satisfies $v(\ell) = 0$ share a common characteristic that $u(\ell) < \gamma$, and so the values of u are away from the line of singularity $u = 3\alpha/2$. Therefore, for both cases, assuming only $\gamma > \alpha$, we see that the value of u never exceeds $\min\{\gamma, 3\alpha/2\}$. It turns out this can be proved rigorously which we will present as a lemma. This important observation implies that in particular a_{0x} (i.e. u') is always positive.

In other words, a nonzero crime reintroduction rate, i.e. $\gamma > \alpha$, which is a rather minimal assumption for the urban crime model, is sufficient to guarantee a monotonically increasing behaviour in the attractiveness field A away from the crime hotspot, and *regardless* of whether we are in the supercritical ($\gamma > 3\alpha/2$) or subcritical regime ($\alpha < \gamma < 3\alpha/2$).

We now state and prove the claim.

Lemma 2.1. *Any solution to* (2.19) *on the interval* $x \in [0, \ell]$ *subject to the conditions* $u(0) = \alpha$ *and* $v(\ell) = 0$ *must satisfy that* $u(x) < \gamma$ *for all* $x \in [0, \ell)$.

We also state an obvious corollary about the monotonicity of the solution which is essential for our subsequent calculations to reduce (2.18a) to a quadrature, which is valid for any $\gamma > \alpha$.

Corollary 2.2. $u(x)$ *is monotonically increasing and* $\alpha < u(x) < \gamma$ *for all* $x \in (0, \ell)$.

Proof: First, we claim that if $x_0 \in (0, \ell)$ is a point such that $u(x_0) < \gamma$, then we must also have $v(x_0) > 0$. We prove this by contradiction.

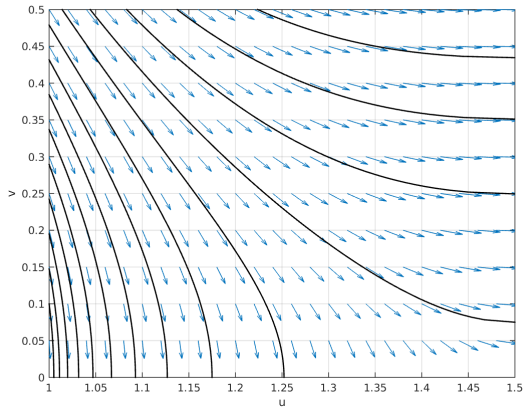

(a) Supercritical case: $\gamma > 3\alpha/2$

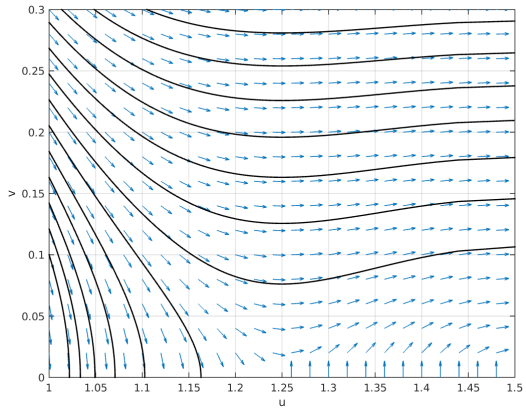

(b) Subcritical case: $\alpha < \gamma < 3\alpha/2$

Figure 2.3: Phase portraits of (2.19) with trajectories emanating from the line $u = \alpha$. There are two types of trajectories: (i) those that hit the $u-$axis are admissible solutions to (2.19) satisfying $v(\ell) = 0$ for some $\ell > 0$, (ii) those that do not, but goes to the line $u = 1.5$ develops singularity for finite values of x. The model parameters chosen were $D = 1$, $\alpha = 1$ for both plots and $\gamma = 2.0$ and $\gamma = 1.25$ respectively for the left and right plots.

Recall that for well-posedness of (2.18a), we required $f(u) > 0$ which holds only if $u(x) < 3\alpha/2$ for all $x \in (0, \ell)$ because $f(3\alpha/2) = 0$. Now, if a solution exists to (2.19), and $u(x_0) < \gamma$, then we must have $u(x_0) < \min\{\gamma, 3\alpha/2\}$ so that $f(u(x_0)) > 0$.

Then, if to the contrary $v(x_0) \leq 0$, then $u'(x_0) = v(x_0)/f(u(x_0)) \leq 0$ as well. However, since x_0 was chosen to give $u(x_0) < \gamma$, we have $v'(x_0) = (u(x_0) - \gamma)/D < 0$. Thus, by continuity, there is a number x_1 such that $v'(x) < 0$ for all x in $[x_0, x_1)$. Moreover, we can choose $x_1 \leq \ell$ to be the maximal one, so that i.e. $v'(x_1) = 0$.

If $x_1 < \ell$, then note that $v(x_0) \leq 0$ and $v'(x) < 0$ for $x \in [x_0, x_1)$ implies $v(x) < 0$ and thus $u'(x) < 0$ throughout the interval $[x_0, x_1)$. Therefore, $u(x_1) < u(x_0) < \gamma$. However, substituting $u(x_1) < \gamma$ to (2.19) gives $v'(x_1) = (u(x_1) - \gamma)/D < 0$ contradicting $v'(x_1) = 0$.

If $x_1 = \ell$, then $v'(x) < 0$ for all $x \in [x_0, \ell)$. This statement with $v(x_0) \leq 0$ in turn implies $v(\ell) < 0$ so that the shooting B.C. $v(\ell) = 0$ cannot be satisfied, another contradiction.

Therefore, such x_1 does not exist and we must have $v(x_0) > 0$ instead. In conclusion, for a solution to (2.19) exists, we must have $v(x_0) > 0$ whenever $u(x_0) < \gamma$.

Next, we substantiate the claim that $u(x) < \gamma$ for all $x < \ell$, which will imply $v(x) > 0$ as well by the above argument. We again prove this claim by contradiction.

Since $u(0) = \alpha < \gamma$, so suppose, to the contrary that $u(x) = \gamma$ does happen. Denote $x_2 \leq \ell$ to be the first such number so that $u(x_2) = \gamma$, which means we have $u(x) < \gamma$ for $x \in [0, x_2)$. Then, $v(x) > 0$ for $x < x_2$ by the previous claim. Moreover, $v(x_2) > 0$ as well because otherwise $v(x_2) = 0$ together with $u(x_2) = \gamma$ will coincide with the stationary solution $u(x) = \gamma$, $v(x) = 0$ to (2.19), which satisfies an incompatible initial condition $u(0) = \gamma$ and $v(0) = 0$. Therefore, this is a contradiction to the uniqueness of solutions to ODEs.

Now, since $v(x_2) > 0$ and $v(\ell) = 0$, we must have $x_2 < \ell$ and there exists at least one root to $v(x)$ in the interval $(x_2, \ell]$. Denote the first root a (if there is exactly one root, then $a = \ell$ obviously). Thus the number $a \in (x_2, \ell]$ satisfies this condition:

$$(*) \qquad v(a) = 0, \text{ but } v(x) > 0 \text{ for all } x_2 \leq x < a\,.$$

Now $v(x_2) > 0$ and $v(a) = 0$ implies that there exists another number b in (x_2, a) such that $v'(b) < 0$. But from the equation for $v'(x)$ in (2.19), we observe that

$$u(b) = v'(b)D + \gamma < \gamma\,.$$

Here, the strict inequality is essential. Now, from the assumption that $u(x_2) = \gamma$, this implies there must exist yet another number c in (x_2, b) such that $u'(c) < 0$. This in turn means that $v(c) < 0$ from the equation for $u'(x)$ in (2.19).

By arranging the new numbers in ascending order as $x_2 < c < b < a$, it follows that we have obtained a number $c < a$ with $v(c) < 0$, and so contradicting (*).

Therefore, the initial assumption that $u(x_2) = \gamma$ for some $x_2 < \ell$ must then be false, and we have thus proved that $u(x) < \gamma$ for all $x < \ell$. The first claim then implies $v(x) > 0$, and substituting these results into (2.19), we immediately obtain that $v'(x) < 0$ and $u'(x) > 0$, which proves Corollary (2.2) as well. ■

The results above tell us, in particular, that the solution a_0 to the nonlinear boundary value problem (2.18a) must be strictly increasing, i.e. $a_{0x} > 0$, and it never exceeds γ. Together with

the solvability restriction that $\alpha < a_0 < 3\alpha/2$, the solution to (2.18a) satisfies

$$a_0(x) < \min\{\gamma, 3\alpha/2\}\,,$$

which holds in the two cases $\alpha < \gamma < 3\alpha/2$ and $\gamma > 3\alpha/2$, corresponding to where the spatially uniform steady-state is Turing stable and unstable, respectively.

2.2.2 Reduction to a Quadrature and Existence of a Maximum Threshold

We may now proceed reduce to reduce the problem (2.18a) to a quadrature.

First, we multiply (2.18a) by $f(a_0)a_{0x}$ and integrate the resulting expression using $a_{0x}(\ell) = 0$ to get

$$\frac{D}{2}\left(f(a_0)a_{0x}\right)^2 = \int_\ell^x f(a_0)(a_0-\gamma)\frac{da_0}{d\eta}\,d\eta\,.$$

Since $a_{0x} > 0$, we have upon labelling $\mu \equiv a_0(\ell)$ that

$$\frac{D}{2}\left(f(a_0)a_{0x}\right)^2 = \int_\mu^{a_0} f(w)(w\gamma)\,dw = G(\mu) - G(a_0)\,, \tag{2.20a}$$

where $G(u)$, satisfying $G'(u) = f(u)(\gamma - u)$, is given explicitly by

$$G(u) \equiv 2u - (2\gamma + 3\alpha)\log u - \frac{3\alpha\gamma}{u}\,. \tag{2.20b}$$

Notice that $G'(u)$ is also positive on $\alpha < u < \min\{\gamma, 3\alpha/2\}$ and so the right-hand side of (2.20a) is positive for all $x \in (0, \ell)$. We remark that in [35], similar integration procedures and phase plane analysis were found for the slow system in the one-dimensional unbounded domain.

Next, we take the appropriate square root in (2.20a) and integrate from 0 to x to obtain

$$\sqrt{\frac{2}{D}}x = \int_\alpha^{a_0} \frac{f(w)\,dw}{\sqrt{G(\mu) - G(w)}}\,, \tag{2.21}$$

where we used $a_0(0) = \alpha$ and the change of variable $w = a_0(x)$, which is valid because $a_0'(x) > 0$.

Finally, upon setting $x = \ell$ and $a_0(\ell) = \mu$, we obtain an implicit equation for μ given by

$$\sqrt{\frac{2}{D}}\ell = \chi(\mu)\,, \qquad \chi(\mu) \equiv \int_\alpha^\mu \frac{f(w)\,dw}{\sqrt{G(\mu) - G(w)}}\,. \tag{2.22}$$

We now show that the function $\chi(\mu)$ is well-defined for $\alpha < \mu < \min\{\gamma, 3\alpha/2\}$.

Using $f(u) = G'(u)/(\gamma - u)$, together with integration by parts, we derive the key formula

$$\chi(\mu) = \int_\alpha^\mu \frac{G'(w)\,dw}{(\gamma - w)\sqrt{G(\mu) - G(w)}} = \frac{2\sqrt{G(\mu) - G(\alpha)}}{\gamma - \alpha} + 2\int_\alpha^\mu \frac{\sqrt{G(\mu) - G(w)}}{(\gamma - w)^2}\,dw\,. \tag{2.23}$$

This expression shows that $\chi(\mu)$ is a well-defined, positive and strictly increasing function on the range $(\alpha, \min\{\gamma, 3\alpha/2\})$. Remarkably, this last expression has important consequences that distinguishes the subcritical regime $\gamma < 3\alpha/2$ from the supercritical regime $\gamma > 3\alpha/2$.

For the subcritical regime, $\gamma < 3\alpha/2$, $\chi(\mu)$ diverges to $+\infty$ as $\mu \to \gamma^-$. Recall that $\alpha < u(x) < \min\{\gamma, 3\alpha/2\} = \gamma$ for this regime, the implicit relation (2.21) maps the range (α, μ) back to a domain $(0, \ell)$ of x with unbounded ℓ as $\mu \to \gamma^-$. Therefore, since the outer problem is always solvable, a single hotspot solution can be constructed regardless of the half-domain length $\ell > 0$. In Fig. 2.4b, we plot $\chi(\mu)$ on this range when $\alpha = 1$ and $\gamma = 1.25$.

shite

In contrast, for the supercritical regime where $\gamma > 3\alpha/2$, (2.23) shows that $\chi(\mu)$ attains its maximum value

$$\chi_{\max} \equiv \chi(3\alpha/2)\,, \tag{2.24}$$

as $\mu \to (3\alpha/2)^-$, where the upper bound of the range of u is $\min\{\gamma, 3\alpha/2\} = 3\alpha/2 < \gamma$. In view of (2.22), this translates to a maximum interval length

$$\ell_{\max} \equiv \sqrt{\frac{D}{2}}\chi_{\max}\,, \tag{2.25}$$

for the outer solution to exist. In Fig. 2.4a, we plot $\chi(\mu)$ on this range when $\alpha = 1$ and $\gamma = 2$.

2.2.3 Crime Hotspot Insertion - the One-Sixth Rule and Fold Bifurcation

We now proceed to investigate what is the significance of the following implicit relation in the supercritical regime $\gamma > 3\alpha/2$, especially near its criticality:

$$\chi(\mu) = \sqrt{\frac{2}{D}}\ell\,. \tag{2.26}$$

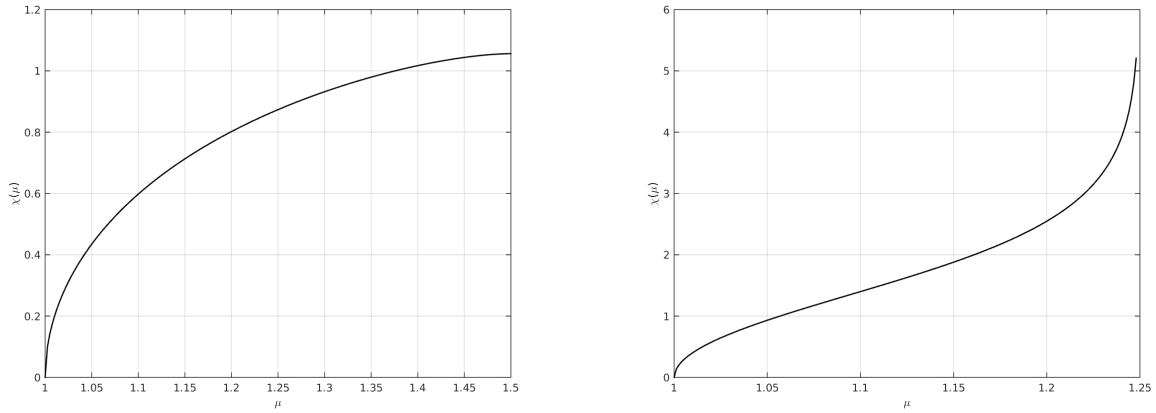

(a) $\chi(\mu)$ attains a maximum at $\mu = 3\alpha/2$ when $\gamma > 3\alpha/2$, $\gamma = 2$.

(b) $\chi(\mu)$ is unbounded on (α, γ) when $\alpha < \gamma < 3\alpha/2$, $\gamma = 1.25$.

Figure 2.4: The function $\chi(\mu)$, from (2.4a), that determines the outer solution for any $\mu \equiv a_0(\ell)$ on $\alpha < \mu < \min\{\gamma, 3\alpha/2\}$. Common parameter values are $D = 1$ and $\alpha = 1$.

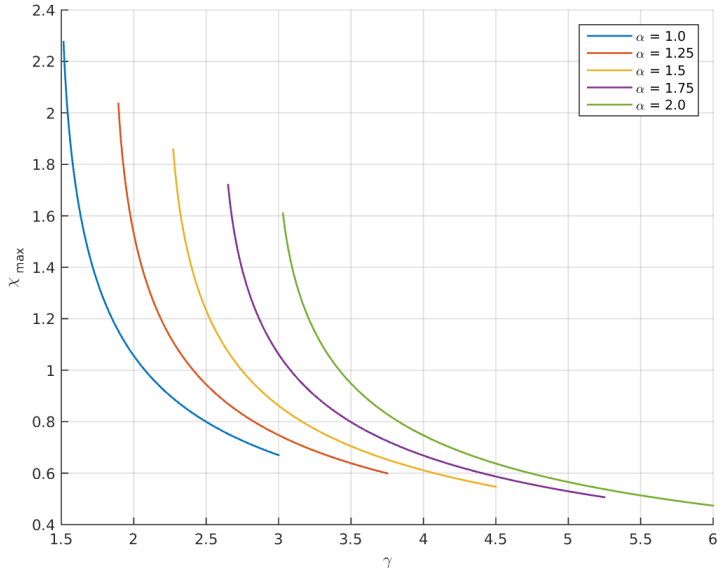

Figure 2.5: $\chi_{\max}$ against γ for five values of α (1.0, 1.25, 1.5, 1.75, 2.0), given by formulas (2.26) and (2.28). The curves were evaluated on the respective ranges of γ satisfying $((3\alpha/2) \cdot 1.01, (3\alpha/2) \cdot 2)$. It is evident from the plots that $\chi_{\max} \to +\infty$ as $\gamma \to (3\alpha/2)^+$.

Notice that the left-hand side of this expression depends on γ and α, appearing implicitly through $\chi(\mu)$, while the right-hand side depends on the ratio $\ell/\sqrt{D}$. Thus, this relation compares the spatial parameters to those that concerns criminology in a nonlinear fashion.

Next, since $\chi(\mu)$ is monotone, we can invert the one-to-one function $\chi(\mu)$ to compute $a_0(\ell) = \mu = \chi^{-1}(\sqrt{\frac{2}{D}}\ell)$ for any $\ell \in (0, \ell_{max}]$. In this way, we identify $v_0(\ell) = g\left(a_0(\ell)\right)$ from (2.17). In particular, at $\ell = \ell_{\max}$, this gives a maximal criminal density at the endpoint of the interval $(0, \ell)$ other than which the crime hotspot exists. The value is given simply by substituting $\mu = 3\alpha/2$ for the values of a and v in $\rho = a^2 v$ at $x = \ell$:

$$\lim_{x\to\ell} \rho = \mu^2 g(\mu) = \frac{\mu - \alpha}{\mu} = \frac{1}{3}\,, \tag{2.27}$$

which is a surprisingly simple number independent of all model parameters.

Combining (2.27) with (2.16), we observe that

$$\frac{\rho(\ell)}{\rho(0)} \sim \frac{1/3}{2} = \frac{1}{6}\,.$$

This simple observation gives an interesting *one-sixth rule* for determining whether a crime hotspot is being born in supercritical regime*:*

One-sixth Rule The ratio of crime density at a nascent hotspot to a preexisting neighbouring hotspot is approximately 1/6.

This is the level of criminal density where the outer problem begins to break down and a possibly new boundary layer emerges at this end of the domain, as was suggested earlier by the phase portrait description of the system (2.19).

To more accurately determine what actually happens when such a criminal density is reached at edge of the outer region, we investigate how the solution depends on the parameter D. This will turn out to be an equivalent but more convenient parameter for bifurcation analysis near the vicinity where (2.26) begins to break down.

For $\gamma = 2$ and $\alpha = 1$, we calculate numerically from (2.23) (see Fig. 2.4a) that

$$\chi\text{max} \equiv \chi\left(\frac{3\alpha}{2}\right) \approx 1.0561\,. \tag{2.28}$$

Correspondingly, if we fix ℓ, we can then use $\chi_{\max}$ to characterize the minimum value D_{crit} of D for which the outer solution exists as

$$D_{\text{crit}} \equiv \frac{2\ell^2}{\chi^2_{\max}}\,. \tag{2.29}$$

In most of our numerical simulations below, we consider the domain $(-1,1)$ containing K interior hot-spots. To determine the minimum value of D for this pattern, we simply put $\ell = 1/K$ to obtain the critical thresholds

$$D_{\text{crit},K} = \frac{2}{K^2\chi^2_{max}}\,. \tag{2.30}$$

To compare with our full numerical results in §2.4, we calculate for $\alpha = 1$ and $\gamma = 2$ that

$$D_{\text{crit},1} \approx 1.7930\,, \qquad D_{\text{crit},2} \approx 0.4483\,, \qquad D_{\text{crit},4} \approx 0.1121\,. \tag{2.31}$$

2.2.4 Determination of Attractiveness Amplitude at the Hotspot

To complete the leading-order theory, we must determine the leading-order constant V_0 in the inner expansion. By using the outer expansion, we obtain the following limiting behaviour from (2.17) and (2.21):

$$A \sim a_0(0^+) = \alpha\,, \qquad v_{0x}(0^+) \sim g'(\alpha)a_{0x}(0^+) = \frac{1}{\alpha^2}\sqrt{\frac{2}{D}}\sqrt{G(\mu) - G(\alpha)}\,. \tag{2.32}$$

To determine V_0, we integrate the V-equation of (2.11) over an intermediate region $(-\delta, \delta)$, with $\epsilon \ll \delta \ll 1$, to obtain

$$D\left(A^2V_x\right)|_{x=-\delta}^{x=\delta} = \int_{-\delta}^{\delta} VA^3\,dx + O(\delta)\,. \tag{2.33}$$

Since $\delta \gg \epsilon$, the outer expansion (2.32) is used to evaluate the left-hand side of (2.33), upon noting the symmetry condition $v_{0x}(0^+) = -v_{0x}(0^-)$. In contrast, since $VA^3 = O(\epsilon^{-1})$ in the inner region, the integral in (2.33) is dominated by contributions from the inner region where

$A \sim w/\sqrt{V_0}$ and $V \sim \epsilon^2 V_0$. In this way, using $\delta \gg \epsilon$ and $w(y) = \sqrt{2}\,\mathrm{sech}\, y$, we calculate that

$$D\alpha^2 \left(v_{0x}(0^+) - v_{0x}(0^-) \right) = 2D\alpha^2 v_{0x}(0^+) \sim \frac{1}{\sqrt{V_0}} \int_{-\infty}^{\infty} w^3 \, dy = \frac{\sqrt{2}\pi}{\sqrt{V_0}} \,. \tag{2.34}$$

Finally, upon using (2.32) for $v_{0x}(0^+)$, we obtain

$$V_0 = \frac{\pi^2}{4D} \left[G(\mu) - G(\alpha) \right]^{-1} \,. \tag{2.35}$$

Here $\mu = a_0(\ell)$ is a root of (2.26) and $G(u)$ is defined in (2.20b).

As ϵ is decreased, and for $\alpha = 1$, $\gamma = 2$ and $D = 2$, in Fig. 2.6 we compare our leading-order asymptotic results for $\epsilon A(0)$ (left panel) and for $\epsilon^{-2} V(0)$ (right panel) with corresponding full numerical results computed from (2.11) using the continuation software `AUTO-07p` (cf. [12]). The leading-order asymptotic results are $\epsilon A(0) \sim \sqrt{2}/\sqrt{V_0}$ and $\epsilon^{-2} V(0) \sim V_0$, where V_0 is defined in (2.35). These comparisons show that the leading-order asymptotic theory only agrees well with the full numerical results when ϵ is very small. As such, in order to obtain decent agreement between the asymptotic theory and full numerical results when ϵ is only moderately small, we must provide a higher-order asymptotic theory. This more refined asymptotic theory, done in §2.5, shows that the error in the leading-order prediction is in fact $O(-\epsilon \log \epsilon)$, which explains why the leading-order theory is rather inaccurate unless ϵ is very small. The asymptotic results from this improved theory are shown by the thin dotted curves in Fig. 2.6.

2.3 NLEP Stability Analysis

In this section we analyze the stability of steady-state hotspot solutions to (2.10) in the regime where $D = O(1)$. We show that all eigenvalues λ, with $\lambda = O(1)$, of the militarization satisfy $\mathrm{Re}(\lambda) < 0$ so that steady-state hotspot solutions are stable on an $O(1)$ time-scale.

We let $a_e(x)$, $v_e(x)$ be a hotspot solution to the steady-state problem (2.11). Recall that in the inner region near the core of the hotspot, we have $a_e = O(\epsilon^{-1})$ and $v_e = O(\epsilon^2)$, while both a_e and v_e are $O(1)$ in the outer region. Upon introducing the perturbation

$$A = a_e + e^{\lambda t} \phi \,, \qquad V = v_e + e^{\lambda t} \epsilon^3 \psi \,,$$

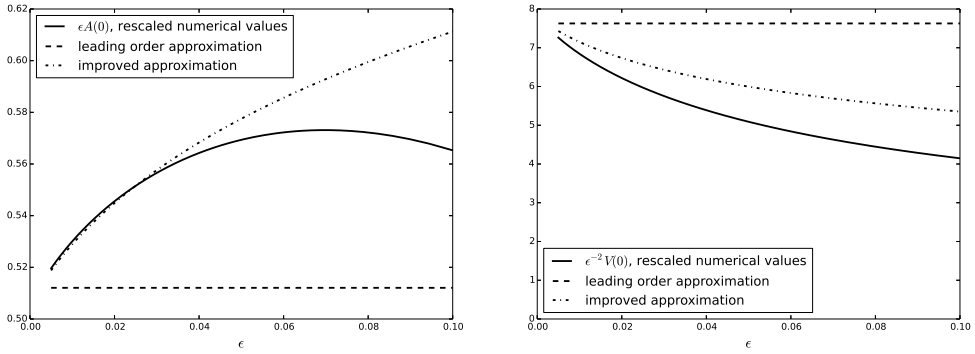

Figure 2.6: Comparison of numerical and asymptotic results for $\epsilon A(0)$ (left panel) and for $\epsilon^{-2}V(0)$ (right panel) as ϵ is decreased for a single hotspot centred at the origin. The parameter values are $\alpha = 1$, $\gamma = 2$, $\ell = 1$, and $D = 2$. The dashed horizontal lines are the leading-order prediction of $\epsilon A(0) \approx \sqrt{2}/\sqrt{V_0}$ and $\epsilon^{-2}V(0) \approx V_0$, where V_0 is given in (2.35). The thin dotted curves are from the improved asymptotic theory with V_0 now given by (2.81).

into (2.10), we obtain the following singularly perturbed eigenvalue problem on $|x| < \ell$:

$$\epsilon^2\phi_{xx} - \phi + 3v_e a_e^2\phi + \epsilon^3 a_e^3\psi = \lambda\phi\,, \tag{2.36a}$$

$$D\left(a_e^2\epsilon^3\psi_x + 2a_e v_{ex}\phi\right)_x = 3a_e^2 v_e\phi + \epsilon^3 a_e^3\psi + \lambda\left(\epsilon^3 a_e^2\psi + 2a_e v_e\phi\right)\,. \tag{2.36b}$$

We remark that our choice of $O(1)$ and $O(\epsilon^3)$ perturbations for A and V produce a distinguished balance for all terms in the equation for ϕ in the inner region, where the length scale is $O(\epsilon)$.

To examine the stability of a single hotspot solution or a multiple hotspot solution we impose either homogeneous Neumann or Floquet-type boundary conditions, respectively, on $x = \pm\ell$, as was done in [29]. However, as we show below, in the regime $\epsilon \ll 1$ and $D = O(1)$, the leading-order stability problem is independent of the specific choice of boundary condition, and this leading-order problem predicts that hotspot equilibria are unconditionally linearly stable to $O(1)$ time-scale perturbations.

We begin by deriving the leading-order stability problem for a hotspot solution centred at the origin in the domain $|x| \le \ell$. The eigenfunction component ϕ is singularly perturbed. It has rapid spatial variation near $x = 0$, but varies on an $O(1)$ scale away from the hotspot core. The leading-order stability problem will consist of a nonlocal eigenvalue problem (NLEP) for ϕ on the inner-scale centred at $x = 0$. Alternatively, the eigenfunction component ψ is not singularly perturbed and varies on an $O(1)$ scale across the entire domain $|x| \le \ell$.

In the inner region near the core of the hotspot at $x = 0$ we introduce the local variables $y = x/\epsilon$, $\phi = \Phi(y)$, and $\psi = \Psi(y)$. Then, from (2.36b), we observe that the leading-order equation is $\left(w^2\Psi_y\right)_y = 0$. The bounded solution to this equation is the constant solution $\Psi = \psi(0)$, which must be determined in the ensuing analysis. With regards to Φ, we recall from §2.2 that $a_e \sim \epsilon^{-1}w/\sqrt{V_0}$ and $v_e \sim \epsilon^2 V_0$. Upon substituting these expressions into (2.36a), we obtain the leading-order inner problem for $\Phi(y)$ on $-\infty < y < \infty$, given by

$$L_0\Phi + \frac{1}{V_0^{3/2}}w^3\psi(0) = \lambda\Phi\,, \qquad L_0\Phi \equiv \Phi_{yy} - \Phi + 3w^2\Phi\,, \tag{2.37}$$

where $\Phi \to 0$ as $|y| \to \infty$.

2.3.1 Derivation of Jump Conditions

Next, we integrate (2.36b) over $-\delta < x < \delta$ to derive a "jump condition" for ψ, valid as $\epsilon \to 0$. Here we let δ denote any intermediate scale satisfying $\epsilon \ll \delta \ll 1$. This integration yields

$$\epsilon^3 D\left[a_e^2\psi_x\right]_0 + 2D\left[a_e v_{ex}\phi\right]_0 \sim 3\epsilon\int_{-\delta/\epsilon}^{\delta/\epsilon} w^2\Phi\,dy + \frac{\epsilon\psi(0)}{V_0^{3/2}}\int_{-\delta/\epsilon}^{\delta/\epsilon} w^3\,dy \\ + \lambda\left[2\epsilon^2\sqrt{V_0}\int_{-\delta/\epsilon}^{\delta/\epsilon} w\Phi\,dy + \frac{\epsilon^2\psi(0)}{V_0}\int_{-\delta/\epsilon}^{\delta/\epsilon} w^2\,dy\right].$$

Here we have defined $[f]_0 \equiv \lim_{x\to 0^+} f(x) - \lim_{x\to 0^-} f(x)$. For $\epsilon \to 0$, we can then neglect the terms in the square brackets in the expression above, let $\delta/\epsilon \to +\infty$, and use $a_e \sim \alpha$ as $x \to 0^{\pm}$ from the outer solution. In this way, we obtain the following asymptotic approximation of the jump condition:

$$\epsilon^3 D\alpha^2\left[\psi_x\right]_0 + 2D\alpha\left[v_{ex}\phi\right]_0 \sim 3\epsilon\int_{-\infty}^{\infty} w^2\Phi\,dy + \frac{\epsilon\psi(0)}{V_0^{3/2}}\int_{-\infty}^{\infty} w^3\,dy\,. \tag{2.38}$$

Next, we examine the outer expansion for ϕ and ψ in order to estimate the left-hand side of (2.38). From the outer approximation of (2.36a), we use $v_\epsilon \sim v_0$ and $a_\epsilon \sim a_0$ to obtain that

$$\left(3v_0a_0^2 - 1\right)\phi + \epsilon^3 a_0^3\psi \sim \lambda\phi\,.$$

Then, since $v_0 = g(a_0)$, where $g(a_0)$ is defined in (2.17), we solve for ϕ_0 to obtain

$$\phi = \epsilon^3 \tilde{\phi}\,, \qquad \tilde{\phi} \equiv \left(\frac{a_0^3}{\lambda - 2 + 3\alpha/a_0} \right) \psi\,. \tag{2.39}$$

Since $\alpha \le a_0 < \min\{\gamma, 3\alpha/2\}$ for $|x| \le \ell$, we conclude by examining the denominator in (2.39) that $\tilde{\phi}$ is analytic in $\mathrm{Re}(\lambda) \ge 0$. We then let $x \to 0^{\pm}$ in (2.39) to get

$$\phi(0^{\pm}) = \epsilon^3 \left(\frac{\alpha^3}{\lambda + 1} \right) \psi(0)\,. \tag{2.40}$$

We then use (2.40), together with $v_{ex}(0^{\pm}) \sim g'(\alpha) a_{0x}(0^{\pm})$ and $g'(\alpha) = 1/\alpha^3$, to estimate the second term on the left-hand side of (2.38) as

$$2D\alpha \left[v_{ex}\phi \right]_0 \sim \left(\frac{2D\alpha}{\lambda + 1} \right) \epsilon^3 \psi(0) \left[a_{0x} \right]_0\,.$$

In this way, we obtain that the asymptotic jump condition (2.38) for $\psi(x)$ becomes

$$\epsilon^2 D \left(\alpha^2 \left[\psi_x \right]_0 + \frac{2\alpha}{\lambda + 1} \psi(0) \left[a_{0x} \right]_0 \right) \sim 3 \int_{-\infty}^{\infty} w^2 \Phi \, dy + \frac{\psi(0)}{V_0^{3/2}} \int_{-\infty}^{\infty} w^3 \, dy\,, \tag{2.41}$$

where $a_0(x)$ satisfies the nonlinear BVP (2.18a) in the outer region.

2.3.2 The Outer Problem and Analyticity of Coefficients

Next, we derive the outer problem for $\psi(x)$ on $-\ell < x < 0^-$ and on $0^+ < x < \ell$ by considering the outer limit for (2.36b), where we have $a_\epsilon \sim a_0$, $v_\epsilon \sim v_0$, and $\phi \sim \epsilon^3 \tilde{\phi}$. This outer problem is

$$D \left(a_0^2 \psi_x + 2 a_0 v_{0x} \tilde{\phi} \right)_x = 3 a_0^2 v_0 \tilde{\phi} + a_0^3 \psi + \lambda \left(2 a_0 v_0 \tilde{\phi} + a_0^2 \psi \right)\,, \tag{2.42}$$

where $\tilde{\phi}$ depends linearly on ψ from (2.39). We then substitute (2.39), $v_0 = g(a_0)$, and $v_{0x} = g'(a_0) a_{0x}$ into (2.42), where $g(a_0)$ is defined in (2.17). After some algebra, we obtain that (2.42) reduces on $0 < |x| < \ell$ to

$$\left(a_0^2 \psi_x + \left(\frac{3\alpha - 2a_0}{3\alpha + a_0(\lambda - 2)} \right) \left(a_0^2 \right)_x \psi \right)_x = \left(\frac{(\lambda + 1) a_0^3 + \lambda a_0 (\alpha + a_0 \lambda)}{\lambda - 2 + 3\alpha/a_0} \right) \psi\,. \tag{2.43}$$

The problem for ψ is to solve (2.43) on the intervals $0 < x < \ell$ and $-\ell < x < 0$, together with the continuity of ψ across $x = 0$, the jump condition (2.41), and subject to either homogeneous Neumann or Floquet-type boundary conditions imposed at $x = \pm\ell$ depending on whether we are considering single or multiple hotspot solutions, respectively. From the solution to this problem we can determine $\psi(0)$, which is needed for the inner problem (2.37).

The differential equation (2.43) can be written in the general form

$$(b(x)\psi_x + b_1(x,\lambda)\psi)_x = b_2(x,\lambda)\psi\,. \tag{2.44}$$

where $b(x) > 0$ on $0 < |x| \le \ell$. Since $\alpha \le a_0 < \min\{\gamma, 3\alpha/2\}$ for $|x| \le \ell$, we conclude from (2.43) that $b_1(x,\lambda)$ and $b_2(x,\lambda)$ are analytic in $\mathrm{Re}(\lambda) \ge 0$. Since ψ satisfies a linear ODE with analytic coefficients in $\mathrm{Re}(\lambda) \ge 0$, any solution to (2.43) must be analytic in $\mathrm{Re}(\lambda) \ge 0$ by classical ODE theory.

Although it is intractable to determine a closed-form for $\psi(x)$, what is essential in this context is that we are still able to determine $\psi(0)$ as $\epsilon \to 0$ simply from the leading-order approximation (2.41) of the jump condition. Since the outer solution satisfying (2.43) is smooth, we have that $\psi_x(0^{\pm})$ is finite and independent of ϵ. Letting $\epsilon \to 0$ in the jump condition (2.41) we identify that

$$\psi(0) \sim -3V_0^{3/2}\left(\frac{\int_{-\infty}^{\infty} w^2\Phi\,dy}{\int_{-\infty}^{\infty} w^3\,dy}\right)\,. \tag{2.45}$$

Finally, upon substituting (2.45) into (2.37), we obtain the nonlocal eigenvalue problem (NLEP)

$$L_0\Phi - 3w^3\left(\frac{\int_{-\infty}^{\infty} w^2\Phi\,dy}{\int_{-\infty}^{\infty} w^3\,dy}\right) = \lambda\Phi\,, \quad -\infty < y < \infty\,; \qquad \Phi \to 0 \quad \text{as} \quad |y| \to \infty\,. \tag{2.46}$$

As shown in Lemma 3.2 of [29], the NLEP (2.46) is explicitly solvable in the sense that its discrete spectrum can be found analytically. Lemma 3.2 of [29] shows that any nonzero eigenvalue of (2.46) must satisfy $\mathrm{Re}(\lambda) < 0$.

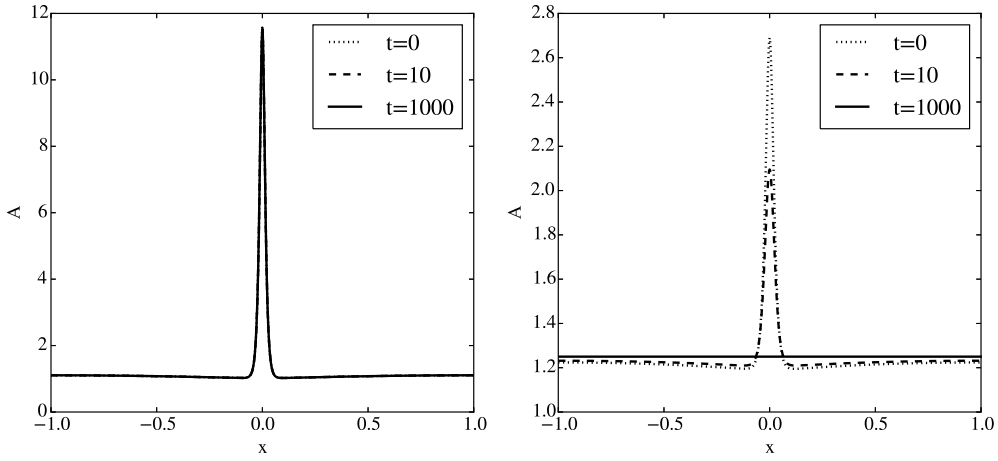

Figure 2.7: Stability of $\mathcal{O}(\epsilon^{-1})$-amplitude and $\mathcal{O}(1)$-amplitude hotspots. Parameter values are $\epsilon = 0.01$, $D = 1$, $\alpha = 1$, $\gamma = 1.25$. Left plot: the $\mathcal{O}(\epsilon^{-1})$-amplitude hotspot persists in this subcritical regime. Right plot: the $O(1)$-amplitude hotspot is transient and dissipates into the Turing-stable homogeneous state.

2.3.3 Conclusions on Stability for Various Patterns

Since this NLEP is independent of the boundary conditions for ψ on $x = \pm\ell$, it applies to both single and multiple hotspot solutions. It is also independent of whether $\gamma > 3\alpha/2$ or $\alpha < \gamma < 3\alpha/2$ because the outer solution and its derivatives are the same near $x = 0$. In other words, crime hotspots in both supercritical and subcritical regimes are both stable to linear perturbations.

In Fig. 2.7, we confirm numerically the stability of a single hotspot solution and plot the profile of the attractiveness profile A. We also show a different type of hotspot that is found from numerical computations of the bifurcation diagram. This kind of hotspot has an $O(1)$ amplitude for the attractiveness A, but is unstable. It is an open problem to both construct and show analytically the instability of this kind of hotspot, which we do not consider in Section 2.2.

Finally, we recall for comparison that, for the regime $D = O(\epsilon^{-2})$ studied in [29], the NLEP problem for $O(1)$ eigenvalues of a $K-$hotspot solution on an interval of length S is given by:

$$L_0\Phi - \chi_j w^3 \left(\frac{\int_{-\infty}^{\infty} w^2\Phi\, dy}{\int_{-\infty}^{\infty} w^3\, dy} \right) = \lambda\Phi\,, \quad -\infty < y < \infty\,; \qquad \Phi \to 0 \quad \text{as} \quad |y| \to \infty\,. \tag{2.47}$$

The multiplier

$$\chi_j = 3\left[1 + \frac{D_0\alpha^2\pi^2K^4}{4(\gamma-\alpha)^3}\left(\frac{2}{S}\right)^4(1-\cos\pi j/K)\right]^{-1}, \quad j = 0,\ldots,K-1\,,$$

where $D_0 \equiv D\epsilon^2$ corresponds to different "modes" of instability. For a single hotspot solution, i.e. $K = 1$, we have $\chi_0 = \chi_1 = 3$ which gives exactly the same NLEP (2.46) and, thus, the solution is stable for all D_0. For a multiple hotspot solution, stability is governed by the smallest multiplier χ_{K-1}. This gives a stability threshold

$$D_{0K}^L \equiv \frac{2(\gamma-\alpha)^3(S/2)^4}{K^4\alpha^2\pi^2\left[1+\cos(\pi/K)\right]}\,, \tag{2.48}$$

so that a $K-$hotspot pattern is stable only when $D_0 < D_{0K}^L$. In contrast, there is no such thresholds when $D = O(1)$ and multiple hotspot patterns are stable whenever they exist.

2.4 Bifurcation Diagrams of Hotspot Equilibria: Numerical Continuation Computations

2.4.1 Supercritical Regime - Fold Points for Spike Insertion

In this section we show full numerical bifurcation results for hotspot equilibria of (2.11) computed using the continuation software `AUTO-07p` (cf. [12]). These computations show that new hotspots are created near the endpoints $x = \pm l$ or at the midpoint between two hotspots when D approaches a saddle-node bifurcation value, which we denote by $D_{\rm fold}$. We call this phenomena *hotspot or spike insertion*. Our numerical results show clearly that the fold-point value $D_{\rm fold}$ tends, as $\epsilon \to 0$, to the critical value $D_{\rm crit}$, as derived from the leading-order asymptotic theory of §2.2. However, unless ϵ is very small, our results show that the leading-order theory for the critical value of D is quantitatively rather inaccurate. This motivates the need for a higher-order asymptotic theory in §2.5.

By using `AUTO-07p` we compute from (2.11) the bifurcation diagrams of branches of steady-state solutions starting with either $K = 1$, $K = 2$, or $K = 4$, interior hotspots. Instead of using the L^2 norm, it is more convenient to use the boundary value $A(\ell)$ as the vertical axis on

the bifurcation diagram, as this prevents the overlapping of solution branches with boundary hotspots. The horizontal axis on the bifurcation diagram is D. Our computational results for the parameter set $\gamma = 2$, $\alpha = 1$, $\ell = 1$, and $\epsilon = 0.01$, displayed in Fig. 2.8(a) show that as D is varied, the steady-state solution branch with one interior hotspot is connected to a solution that has an interior hotspot together with a hotspot at each boundary. Boundary hotspots are created at the endpoints $x = \pm\ell$ near the fold point associated with the small norm branch for $A(\ell)$ versus D.

Similar bifurcation results starting from either two or four interior hotspots on the small norm $A(\ell)$ versus D branch are shown in Fig. 2.8(b) and Fig. 2.8(c) to be path-connected to solutions with mixed boundary and interior hotspots. We observe that new hotspots are nucleated at the endpoints $x = \pm\ell$ and at the midpoint of the interval between adjacent hotspots at the fold point associated with the small norm solution branch.

In each set of the four solution profiles in Fig. 2.8 we observe, as expected by symmetry, that the right top and bottom figures have the same value of D at the two fold points where D is smallest. In each case, as we follow the small norm solution branch of $A(\ell)$ versus D towards the fold-point value, we observe a decrease in the amplitude of the hotspot and a gradual bulging up of the solution at the midpoint between hotspots or at the domain boundaries (i.e. at the boundary of the outer regions). This leads to a large amplitude pattern of hotspots when the boundary value $A(\ell)$ exceeds a certain value close to $3\alpha/2 = 1.5$.

As compared to the large $O(\epsilon^{-1})$ scale of the hotspot amplitude, the nucleation or formation of hotspots near the boundary, or at the midpoint between hotspots, is not so conspicuous in our plots, especially when ϵ is small. However, the implication of hotspot nucleation is interesting qualitatively. It predicts that a new crime hotspot can emerge from an essentially quiescent background state when the parameters are close to a fold-point value in D.

Next, we show how the criminal density changes at the onset of spot insertion. In Fig. 2.10 we give various plots of $\rho = A^2V$ for values of D at and close to the fold point. We remark that since $\rho = O(1)$ in both the inner and outer regions, i.e. globally, the spot insertion phenomenon can be observed quite clearly in these plots.

We now discuss whether the solution branches in Fig. 2.10 corresponding to parameter values immediately above the fold point, consisting of "small" hotspots between the large am-

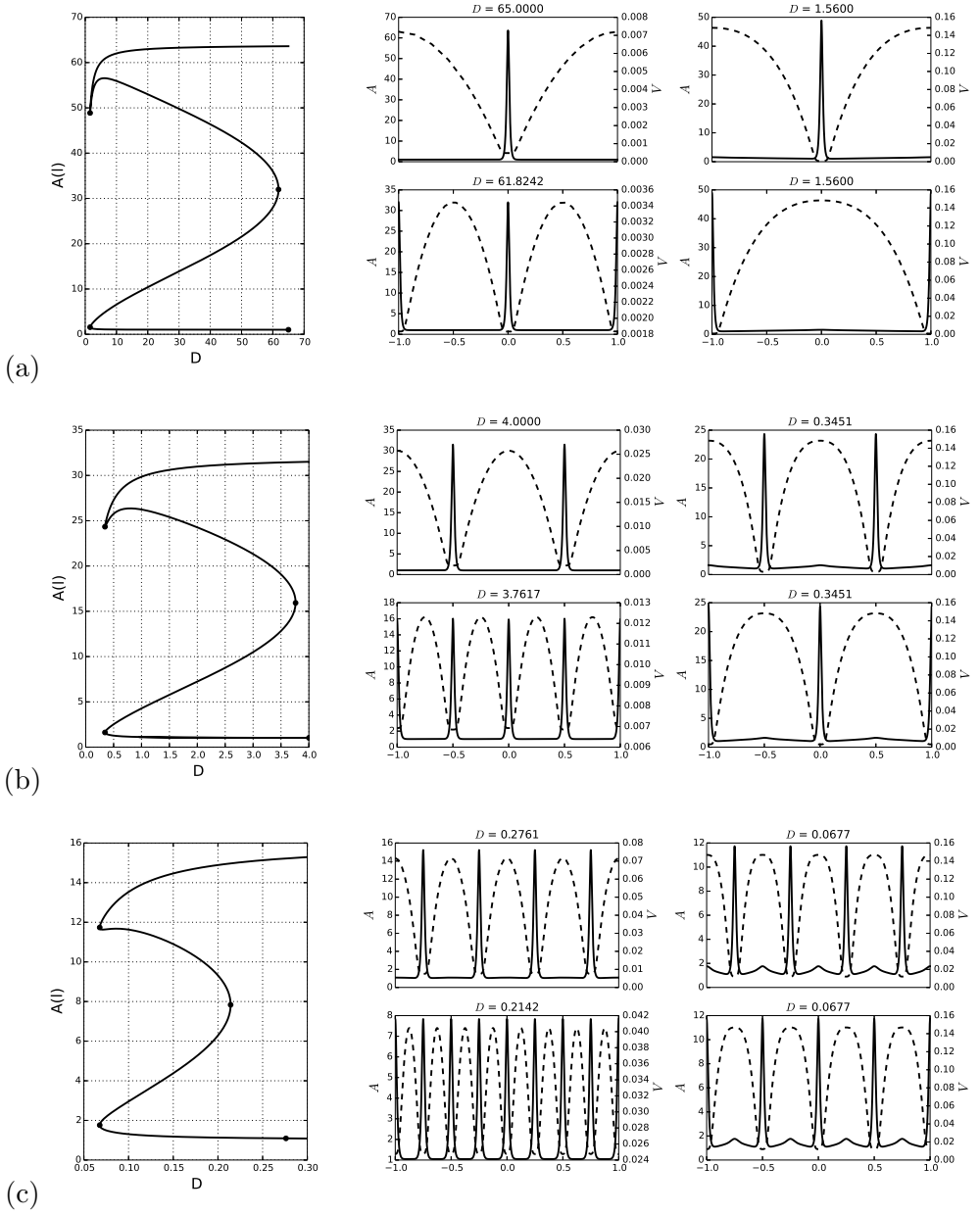

Figure 2.8: The plots (a), (b) and (c) show the continuation of steady states starting with either one, two, or four, interior hotspots, respectively, for $\epsilon = 0.01$. The other parameters are $\gamma = 2$, $\alpha = 1$, and $\ell = 1$. The solid and dashed curves in the subplots show the profiles of A and V, respectively, at various values of D specified on top of the plots. These values of D correspond to the marked points on the bifurcation diagram as shown on the left. Notice that the range of A and V are on different scales.

plitude hotspots, are linearly stable or not. An analytical stability theory of the solution branch beyond the fold point would first require an asymptotic construction of such an alternating pattern with new boundary layers for these "small" hotspots (since the previous outer solution is no longer valid), and would be rather difficult to undertake. Some directions are outlined in Section 2.8. Although we do not pursue the analysis here, we conjecture that all such patterns are unstable. Indeed, from a number of numerical experiments, we observe that a solution on the "upper" branch evolves quickly to its counterpart directly below on the lower branch, i.e. with the same value of D in the bifurcation diagrams (and all other parameters as well) shown in Fig. 2.9. In Fig. 2.11, we show the evolutionary dynamics computed by PDEPE using the "upper" branch solutions computed in AUTO-07p as initial conditions. In all cases shown, the dynamics stabilizes to exactly the pattern of the solution on the corresponding "lower" branch, with no visible difference.

Our numerical bifurcation results for the fold-point bifurcation along the small norm solution branch for $\gamma = 2$, $\alpha = 1$, $\ell = 1$, and $\epsilon = 0.01$ are

$$D_{\text{fold},1} = 1.5600\,, \qquad D_{\text{fold},2} = 0.3451\,, \qquad D_{\text{fold},4} = 0.0677\,. \tag{2.49}$$

Observe, as expected by symmetry, that these values are quartered as the number of hotspots doubles. However, we observe that the quantitative agreement of these fold-point values with the critical values $D_{\text{crit},K}$ of (2.31), as computed from the leading-order theory of Section 2.2, is suggestive, but is not particularly close even when $\epsilon = 0.01$.

As a result of this rather poor quantitative agreement at finite ϵ, we used `AUTO-07p` (cf. [12]) to perform a codimension-two path-following of the fold point as ϵ is decreased. The computations were done for the case of $K = 1$, $K = 2$, or $K = 4$, interior hotspots. The goal of performing this codimension-two continuation to trace the curves $D_{\text{fold},K}(\epsilon)$ was to establish evidence for the conjecture that $\lim_{\epsilon\to 0} D_{\text{fold},K}(\epsilon) = D_{\text{crit},K}$, and to find a range of small ϵ where the agreement between $D_{\text{fold},K}$ and $D_{\text{crit},K}$ is close.

The results of this codimension-two computation are shown in Fig. 2.9. From this figure, we observe that the "almost" straight solid curves for the numerically computed values of $D_{\text{fold},K}(\epsilon)$ versus ϵ does seem to extrapolate as $\epsilon \to 0$ to the leading-order limiting critical value

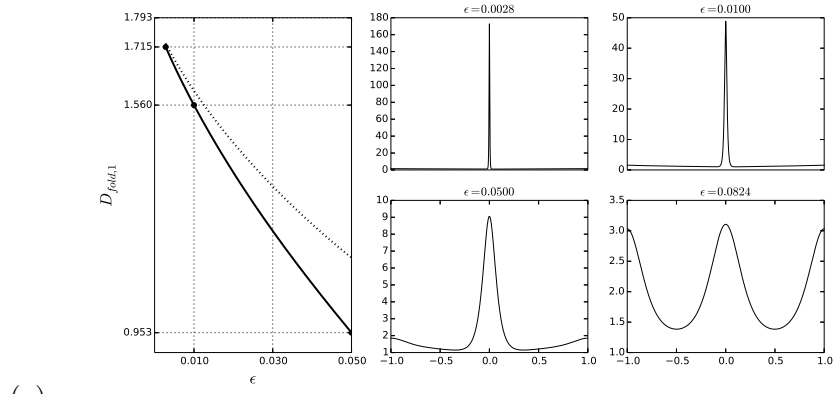

(a)

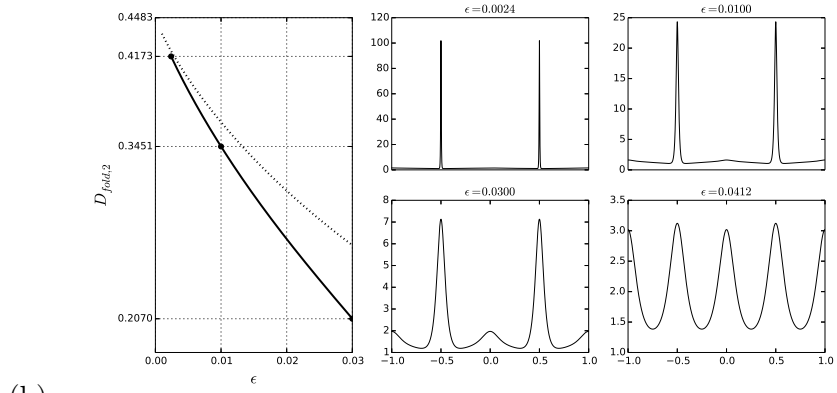

(b)

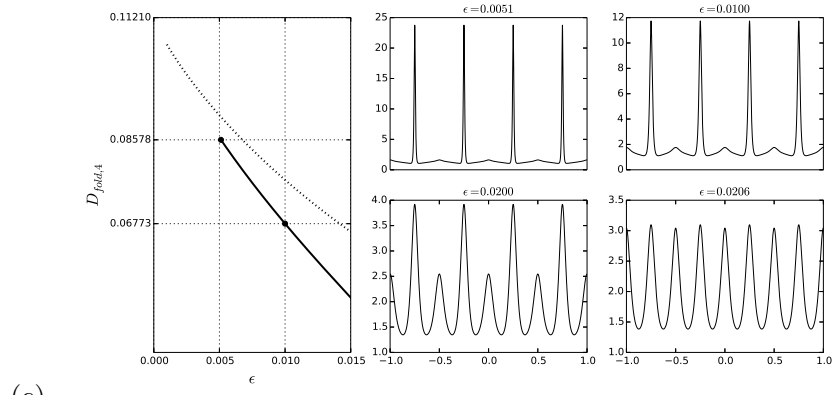

(c)

Figure 2.9: For the parameter set $\gamma = 2$, $\alpha = 1$, and $\ell = 1$, the solid curves on the left of each of (a), (b), and (c), for $K = 1$, $K = 2$, and $K = 4$, interior hotspots, respectively, show the fold point values $D_{\text{fold},K}(\epsilon)$ associated with the small norm solution branch of $A(\ell)$ versus D. The top tick-mark on the vertical axes in these plots are the approximate values $D_{\text{crit},1} \approx 1.793$, $D_{\text{crit},2} \approx 0.448$, and $D_{\text{crit},4} \approx 0.112$ from the leading-order theory of §2.2. The dashed curves in each of (a), (b), and (c), are the asymptotic results (2.82) for the fold point value for D, as predicted by the higher-order asymptotic theory of §2.5. For each of the three sets, the numerically computed A versus x is plotted on $|x| \leq 1$ at four values of ϵ. At the larger values of ϵ the pattern is essentially sinusoidal.

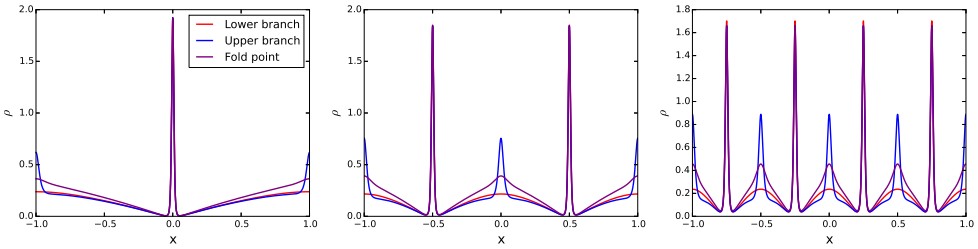

Figure 2.10: Plots of criminal density ρ near the onset of spot insertion as indicated in Fig. 2.9. The parameter values are the same, i.e. $\epsilon = 0.01, \gamma = 2, \alpha = 1, \ell = 1$. The purple curves correspond to ρ at the numerically computed fold point, while the red and blue curves correspond to the upper and lower branch solutions at some identical values of D close to, but respectively above and below the fold points shown in Fig. 2.9. Such chosen values of D are 2.0, 0.5 and 0.1 respectively for one, two and four interior spikes (before the insertion event), corresponding to the sub-figures on the left, centre, and right, respectively. The fold point values of D are given in (2.49).

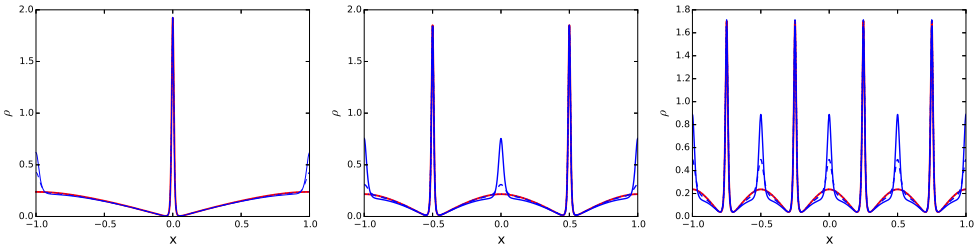

Figure 2.11: Time evolution of criminal density ρ for spatial patterns found by continuation beyond the fold point. Parameter values are the same as in Fig. (2.9), i.e. $\epsilon = 0.01, \gamma = 2, \alpha = 1, \ell = 1$. Also, $D = 2.0, 0.5, 0.1$ for the left, centre and right sub-figures, respectively. The dotted, dashed and solid blue curves shows the evolution of the upper solution at $t = 0, 15, 100$, respectively, while the heavy solid red curves shows the lower branch solution. We find that the plots at $t = 100$ all overlap exactly with those of the lower branch counterparts, which are the linearly stable patterns proved in Section 2.3.

of §2.2. Due to numerical resolution difficulties, we were not able to perform computations for smaller values of ϵ than shown in Fig. 2.9. However, these computational results do give clear numerical evidence for the conjecture that $\lim_{\epsilon\to 0} D_{\text{fold},K}(\epsilon) = D_{\text{crit},K}$ for $K = 1, 2, 4$. An analytical justification that $D_{\text{crit},K}$ does in fact correspond to a fold point is given in the analysis of hotspot insertion phenomena in § 2.6 below. In Fig. 2.9, we also plot the improved approximation for $D_{\text{crit},K}$ versus ϵ (dashed curves), as given in (2.82), that will be derived from the higher-order asymptotic theory of §2.5.

Finally, from the plots of A versus x in Fig. 2.9 at selected values of ϵ, we observe that when ϵ is only moderately small the steady-state solution more closely resembles a sinusoidal pattern

than a pattern of localized hotspots.

2.4.2 Subcritical Regime - Fold Points for Spike Type Switching

Here, we present the results of analogous studies of the bifurcation diagrams for the case $\alpha < \gamma < 3\alpha/2$. As discussed previously, this is the subcritical regime studied in [35] on the infinite line where homoclinic snaking behaviour observed. In Fig. 2.12, we instead observe an interesting closed-loop structure, containing crime hotspots solutions of two different order of amplitude: $O(1)$ and $O(\epsilon^{-1})$, with the latter type comprehensively developed in this chapter. The fold points II and III belong to the supercritical regime $\gamma > 3\alpha/2$ and is in agreement with the Fig. 2.8 as a reduction in γ leads to an increase of $\chi_{\max}$ as shown in Fig. 2.5 in the supercritical regime. Moreover, the same hotspot centre mirroring phenomenon is also observed as we follow the path from point II to point III, analogous to the first plot in Fig. 2.8.

In contrast, the fold points I and IV are novel in that they occur for a solution branch with $A = O(1)$. We conjecture that this is the same fold point as shown in Fig. 7 of [29], and thus they connect the weakly nonlinear regime born from the subcritical Turing bifurcation to the far-from equilibrium theory in this chapter valid for the solution branch beyond fold points I and IV. In Fig. 2.7, we took precisely a solution at $\gamma = 1.25$ in the branch before reaching point I from the Turing bifurcation to perform the full numerics. The result was that this solution is unstable as expected.

The development of an asymptotic theory for the solution branch with $A = O(1)$ hotspots is an interesting open problem. However, these solutions are likely all linearly unstable.

2.5 Refinements of the Steady State Solution: Higher-Order Theory

In this section we present a more refined asymptotic theory than that given in §2.2 to construct a steady-state hotspot solution centred at the origin on the interval $|x| \leq \ell$. The results from this higher-order theory provide a rather close asymptotic prediction of the saddle-node bifurcation point observed in §2.4, as well as providing the error terms associated with the leading-order theory. In addition, this more refined asymptotic analysis is essential for the analysis in §2.7,

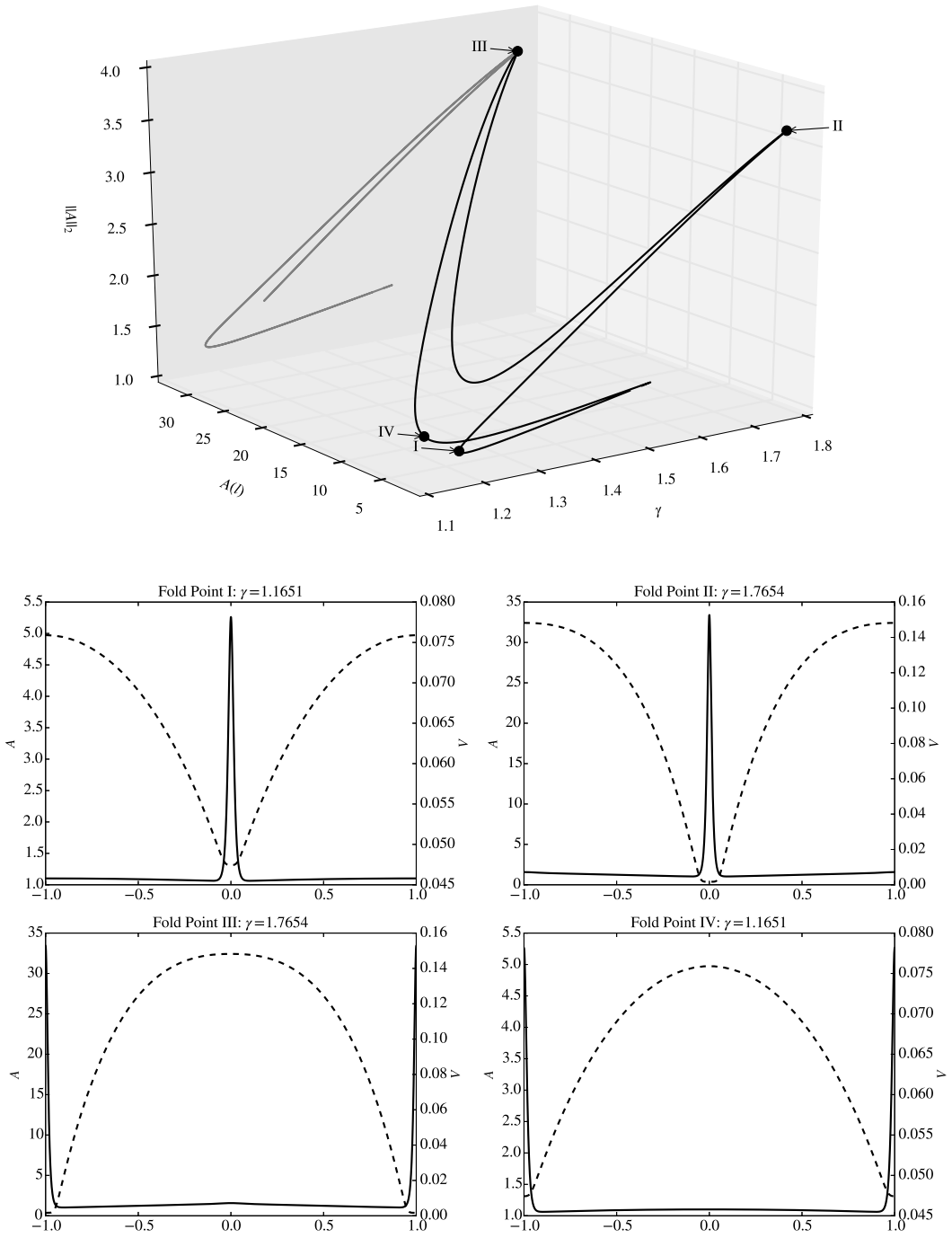

Figure 2.12: A closed homotopy of equilibria with a single hotspot (or two boundary hotspots) from the continuation in γ from the subcritical Turing bifurcation. Model parameters are: $\epsilon = 0.01$, $D = 1$, $\alpha = 1$. Observe that the amplitude of A at Point I and IV are $O(1)$ and equal but different to that of Point II and III, which are of $O(\epsilon^{-1})$.

where a DAE system for the slow time evolution of a collection of hotspots is derived.

In the inner region, where $y = \epsilon^{-1}x$ and $y = O(1)$, we pose a two-term expansion for A as

$$A \sim A_0/\epsilon + A_1 + \dots\,, \qquad V \sim \epsilon^2 V_\epsilon\,.$$

Upon substituting this expansion into (2.11), and retaining the dominant correction terms we obtain

$$\left(A_{0yy} - A_0 + V_\epsilon A_0^3\right) + \epsilon\left(A_{1yy} - A_1 + 3V_\epsilon A_0^2 A_1 + \alpha\right) + \cdots = 0\,, \tag{2.50a}$$

$$D\left[\left(A_0^2 + 2\epsilon A_0 A_1\right)V_{\epsilon y}\right]_y - \epsilon V_\epsilon\left(A_0^3 + 3A_0^2 A_1\epsilon\right) + \epsilon^2(\gamma - \alpha) + \cdots = 0\,. \tag{2.50b}$$

This suggests that we expand $V_\epsilon = V_0 + \epsilon V_1 + \cdots$. Upon substituting this expansion into (2.50), and collecting powers of ϵ, we obtain our leading-order result that V_0 is an unknown constant and $A_0 = w/\sqrt{V_0}$, where $w(y) = \sqrt{2}\,\mathrm{sech}\, y$ is the homoclinic solution of (2.14). At next order, we obtain that $A_1(y)$ and $V_1(y)$ on $-\infty < y < \infty$ satisfy

$$A_{1yy} - A_1 + 3A_0^2 A_1 V_0 = -\alpha - V_1 A_0^3\,, \qquad D\left[A_0^2 V_{1y}\right]_y = V_0 A_0^3\,. \tag{2.51}$$

Then, upon substituting $A_0 = w/\sqrt{V_0}$ into (2.51), we conclude that

$$L_0 A_1 \equiv A_{1yy} - A_1 + 3w^2 A_1 = -\alpha - \frac{V_1}{V_0^{3/2}}w^3\,, \qquad \left[w^2 V_{1y}\right]_y = \frac{\sqrt{V_0}}{D}w^3\,. \tag{2.52}$$

A key step in analyzing the inner region is to determine the far-field asymptotic behaviour as $y \to +\infty$ for the solution to (2.52). Since $w(y) \sim 2\sqrt{2}e^{-y}$ as $y \to \infty$, it readily follows upon integrating the V_1-equation that $V_1 = O(e^{2y})$ as $y \to \infty$. Then, since $w^3 V_1 \to 0$ as $y \to \infty$, it follows from the A_1-equation in (2.52) that $A_1 \to \alpha$ as $y \to \infty$. These simple results show that the V_ϵ-expansion $V_\epsilon = V_0 + \epsilon V_1 + \cdots$ becomes disordered when $y = O(-(1/2)\log\epsilon)$, while the far-field as $y \to \infty$ of the A-expansion $A = w/\left[\epsilon\sqrt{V_0}\right] + A_1 \sim \epsilon^{-1}2\sqrt{2}e^{-y} + \alpha$ becomes disordered when $y = O(-\log\epsilon)$.

As a result, for $y > 0$, we will need to introduce two additional inner layers before we are finally able to match to the outer solution. For $\epsilon \to 0$, we define the *mid-inner layer* by

$y = -(1/2)\log\epsilon + O(1)$ and the *knee layer* by $y = -\log\epsilon + O(1)$. The asymptotic solution in the knee layer can then be matched to the outer solution valid on $0 < x < \ell$. By symmetry, a similar construction can be done for $y < 0$. In Fig. 2.13 we plot the full numerical steady-state solution for V, as computed from (2.11), showing the knee behaviour of V for $\gamma = 2$, $\alpha = 1$, $D = 2$, $\epsilon = 0.01$, and $\ell = 1$.

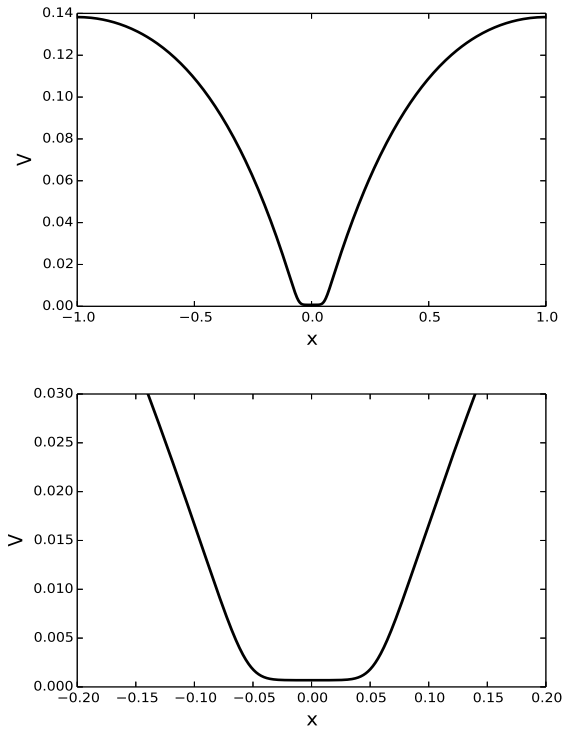

Figure 2.13: Plot of the full numerical solution to the steady-state problem (2.11) showing the knee behaviour of V for $\gamma = 2$, $\alpha = 1$, $D = 2$, $\epsilon = 0.01$, and $\ell = 1$. The figure on the right is a zoom of the one on the left.

The asymptotic matching of the expansions of the solution across the mid-inner and knee layers will specify the appropriate far field behaviour for the solution V_1 to (2.52) in the form

$$V_1 \sim b_+ e^{2|y|}\,, \quad \text{as} \quad |y| \to \infty\,, \tag{2.53}$$

for a certain constant b_+ that is, ultimately, determined by the outer solution. In this way, we can decompose the inner correction term V_1, satisfying (2.52), as $V_1(y) = V_{10} + V_{1p}(y)$, where

V_{10} is a constant to be determined and where $V_{1p}(y)$ satisfies

$$\left[w^2 V_{1py}\right]_y = \frac{\sqrt{V_0}}{D} w^3\,, \qquad -\infty < y < \infty\,; \qquad V_{1p} \sim b_+ e^{2|y|} \quad \text{as} \quad |y| \to \infty\,; \quad V_{1p}(0) = 0\,. \tag{2.54}$$

Upon integrating (2.54) on $-\infty < y < \infty$, we conclude that a solution to (2.54) exists if and only if

$$\frac{\sqrt{V_0}}{D} \int_{-\infty}^{\infty} w^3\, dy = \lim_{y\to+\infty} \left(w^2 V_{1py}\right) - \lim_{y\to-\infty} \left(w^2 V_{1py}\right)\,. \tag{2.55}$$

By using the limiting behaviours of w and V_{1p} as $|y| \to \infty$, together with $\int_{-\infty}^{\infty} w^3\, dy = \sqrt{2}\pi$, we obtain that

$$\frac{\sqrt{V_0}}{D} = \frac{16\sqrt{2}}{\pi} b_+\,. \tag{2.56}$$

Thus, the value of V_0 can be found when b_+ is known, which is be determined by a far-field matching with the outer solution.

Next, we show how to readily determine V_{1p} explicitly. Upon integrating (2.54) from $-\infty$ to y and using (2.56), we get

$$w^2 V_{1py} = \frac{\sqrt{V_0}}{D} \int_{-\infty}^{y} w^3 ds - 16 b_+ = \frac{\sqrt{V_0}}{D} \left(\int_{-\infty}^{y} w^3 ds - \frac{\pi}{\sqrt{2}} \right)\,. \tag{2.57}$$

Observe that

$$\int_{-\infty}^{y} w^3 ds - \frac{\pi}{\sqrt{2}} = \frac{1}{2} \int_{-\infty}^{\infty} w^3 ds - \frac{\pi}{\sqrt{2}} + \int_0^y w^3 ds = \int_0^y w^3 ds\,,$$

while integrating (2.14) from 0 to y yields

$$\int_0^y w^3\, ds = \int_0^y w\, ds - w'(y)\,.$$

Therefore, (2.57) implies that

$$V_{1py}(y) = \frac{\sqrt{V_0}}{D} \left(\frac{\int_0^y w\, ds - w'(y)}{w^2(y)} \right)\,. \tag{2.58}$$

Then, upon integrating (2.58) from 0 to y, and using $V_{1p}(0) = 0$ from (2.54), we finally obtain

that

$$V_{1p}(y) = \frac{\sqrt{V_0}}{D}\left(\int_0^y w^{-2}(s)W(s)ds + \frac{1}{w(y)} - \frac{1}{w(0)}\right), \qquad W(s) \equiv \int_0^s w(y)\,dy\,. \tag{2.59}$$

Note that $V_{1p}(y)$, like $w(y)$, is even in y as well. Also, one can use the explicit formula $w(y) = \sqrt{2}\,\mathrm{sech}\,y$ to compute

$$V_{1p} = \frac{\sqrt{V_0}}{D}\left(\sqrt{2}\int_0^y \cosh^2(s)\tan^{-1}\left[\tanh\left(\frac{s}{2}\right)\right]\,ds + \frac{1}{\sqrt{2}}\left(\cosh y - 1\right)\right). \tag{2.60}$$

To determine b_+, we now proceed by analyzing the two additional inner layers. We begin with the knee-layer, defined by $y = -\log\epsilon + O(1)$, which can be matched to the limiting behaviour as $x \to 0^+$ of the outer solution. In the knee-layer, we introduce the new variables $\hat{A}$, $\hat{V}$, and z by

$$A = \hat{A}(z)\,, \qquad V = \epsilon\hat{V}(z)\,, \qquad y = -\log\epsilon + z\,,$$

with $z = O(1)$, so that $x = -\epsilon\log\epsilon + \epsilon z$. In terms of these new variables, (2.11) becomes

$$\hat{A}_{zz} - \hat{A} + \epsilon\hat{V}\hat{A}^3 + \alpha = 0\,, \qquad D\left(\hat{A}^2\hat{V}_z\right)_z - \epsilon^2\hat{V}\hat{A}^3 + \epsilon(\gamma - \alpha) = 0\,. \tag{2.61}$$

We substitute the expansion $\hat{A} = \hat{A}_0 + \cdots$ and $\hat{V} = \hat{V}_0 + \cdots$ into (2.61) to obtain that $\hat{A}_{0zz} - \hat{A}_0 = -\alpha$. The solution for $\hat{A}_0$ that agrees with the far-field behaviour of the inner solution for A is

$$\hat{A}_0 = ce^{-z} + \alpha\,, \qquad c \equiv \frac{2\sqrt{2}}{\sqrt{V_0}}\,. \tag{2.62}$$

In contrast, $\hat{V}_0(z)$ satisfies

$$\left[\hat{A}_0^2\hat{V}_{0z}\right]_z = 0\,, \qquad -\infty < z < \infty\,. \tag{2.63}$$

To determine the appropriate far-field behaviour as $z \to +\infty$ for (2.63), we expand the leading-order outer solution $v_0(x)$ of §2.2 as $x \to 0$, and then rewrite the expression in terms of z to

obtain the matching condition

$$\epsilon\hat{V} \sim \epsilon v_{0x}(0^+)z + (-\epsilon\log\epsilon)v_{0x}(0^+) + \cdots . \tag{2.64}$$

The dominant constant term of order $O(-\epsilon\log\epsilon)$ in (2.64) cannot be accounted for by the knee solution. Instead, we must introduce a switchback term of order $O(-\epsilon\log\epsilon)$ into the outer expansion. More specifically, the outer expansion on $0 < x < \ell$ must have the form

$$A \sim a_0 + (-\epsilon\log\epsilon)\, a_1 + \epsilon a_2 + \cdots , \qquad V \sim v_0 + (-\epsilon\log\epsilon)\, v_1 + \epsilon v_2 + \cdots , \tag{2.65}$$

with $v_1(0^+) = -v_{0x}(0^+)$, chosen to eliminate the constant term in (2.64)

Therefore, to match the knee solution $\hat{V}_0$ to the near-field behaviour (2.64) of the outer solution we require that $\hat{V}_{0z} \sim v_{0x}(0^+)$ as $z \to \infty$. In contrast, to match the knee solution $\hat{V}_0$ to the mid-inner solution where $V = O(\epsilon^2)$, we need that $\hat{V}_0 \to 0$ as $z \to -\infty$. Thus, we must solve (2.63) subject to

$$\hat{V}_{0z} \sim v_{0x}(0^+)\,, \quad \text{as} \quad z \to +\infty\,; \qquad \hat{V}_0 \to 0\,, \quad \text{as} \quad z \to -\infty\,. \tag{2.66}$$

Given the decay as $z \to -\infty$ and linear ramp as $z \to +\infty$, it is now clear why we refer to $\hat{V}_0$ as the *knee solution*. Upon using (2.62) for $\hat{A}_0$, a first integral of (2.63), which satisfies $\hat{V}_{0z} \sim v_{0x}(0^+)$ as $z \to +\infty$, is

$$\hat{V}_{0z} = \frac{\alpha^2 v_{0x}(0^+)}{(ce^{-z} + \alpha)^2}\,. \tag{2.67}$$

Integrating (2.67) and imposing the condition that $\hat{V}_0 \to 0$ as $z \to -\infty$, we find

$$\hat{V}_0 = v_{0x}(0^+)F(z), \qquad F(z) \equiv \int_{-\infty}^{z} \left(1 + ce^{-s}/\alpha\right)^{-2} ds \tag{2.68}$$

This special nonlinear function $F(z)$ furnishes the required knee-shape which allows the transition of scales from the outer to the inner region.

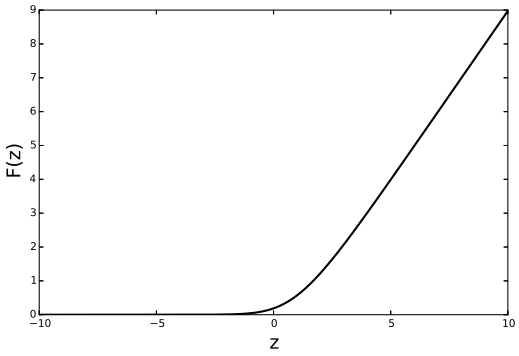

Figure 2.14: The knee-shaped function $F(z)$ defined at (2.68). Parameter choices are the same as in Fig. 2.13 which showed the numerical solution of V.

Lemma 2.3. *The knee-shaped function $F(z)$ is given explicitly by*

$$F(z) = \log\left(c + \alpha e^z\right) + \frac{c}{c + \alpha e^z} + \kappa, \qquad \kappa = -\log c - 1\,, \tag{2.69}$$

and it has the following asymptotic behaviours as $z \to \pm\infty$:

$$F(z) \sim \begin{cases} \frac{\alpha^2}{2c^2} e^{2z} & \text{as } z \to -\infty \\ z + \left(\log \frac{\alpha}{c} - 1\right) & \text{as } z \to \infty\,. \end{cases}$$

Proof: An indefinite integral to $\left(1 + ce^{-z}/\alpha\right)^{-2}$ is given by

$$\log\left(c + \alpha e^z\right) + \frac{c}{c + \alpha e^z} + \kappa\,,$$

where κ is a constant to be determined.

Now, we let $\delta = \alpha e^z/c$ and rewrite $F(z)$ to

$$F(z) = \log(c + \alpha e^z) + \frac{c}{c + \alpha e^z} + \kappa = \log c + \log(1 + \delta) + \frac{1}{1 + \delta} + \kappa\,.$$

As $z \to -\infty$, we observe $\delta \to 0$ and so we expand to estimate

$$F(z) \sim \log c + \left(\delta - \frac{\delta^2}{2} + \dots\right) + \left(1 - \delta + \delta^2 + \dots\right) + \kappa \sim \log c + 1 + \kappa + \frac{\delta^2}{2} + \dots\,,$$

thus we choose $\kappa = -\log c - 1$ to satisfy $\lim_{z\to-\infty} F(z) = 0$.

As $z \to \infty$, we observe $\delta \to \infty$, and we rewrite $F(z)$ in terms of δ as

$$F(z) = \log\delta + \log(1+\delta^{-1}) + (1+\delta)^{-1} + \log c + \kappa\,,$$

and then substitute in $\kappa = -\log c - 1$, $\delta = \alpha e^z/c$ to find the asymptotic behaviour

$$F(z) = \log(\alpha e^z/c) - 1 + O(e^{-z}) \sim z + \log\frac{\alpha}{c} - 1\,.$$

■

We conclude from Lemma 2.3 that the knee solution can be given explicitly as

$$\hat{V}_0 = v_{0x}(0^+)\left(\log(c+\alpha e^z) + \frac{c}{(c+\alpha e^z)} - \log c - 1\right). \tag{2.70}$$

and that, as $z \to +\infty$, we have the asymptotic behaviour

$$\hat{V}_0 \sim v_{0x}(0^+)z + \left[\log\left(\frac{\alpha}{c}\right) - 1\right] v_{0x}(0^+)\,. \tag{2.71}$$

This second term in (2.71) provides a matching condition for the outer correction v_2 in (2.65) of the form

$$v_2(0^+) = \left[\log\left(\frac{\alpha}{c}\right) - 1\right] v_{0x}(0^+)\,. \tag{2.72}$$

Alternatively, as $z \to -\infty$, we conclude from Lemma 2.3 that

$$\hat{V}_0 \sim \frac{\alpha^2 v_{0x}(0^+)}{2c^2} e^{2z}\,, \quad \text{as} \quad z \to -\infty\,. \tag{2.73}$$

Equation (2.73) yields the far-field behaviour of the mid-inner solution for V, which we now construct.

To analyze the mid-inner layer, which is between the inner and knee-layer regions, we introduce the new variables $\tilde{A}$, $\tilde{V}$, and η by

$$A = \tilde{A}(\eta)\,, \qquad V = \epsilon^2\tilde{V}(\eta)\,, \qquad y = -\frac{1}{2}\log\epsilon + \eta\,,$$

with $\eta = O(1)$, so that $x = -(\epsilon/2)\log\epsilon + \epsilon\eta$. In this layer, where $V = O(\epsilon^2)$, the asymptotic order of V is the same as that in the inner layer. Therefore, it is the knee layer that has allowed for the fast transition in V from an $O(\epsilon^2)$ scale to an $O(\epsilon)$ scale, which is then matchable to the outer solution. Upon substituting these new variables into (2.11), we obtain to leading-order that $\tilde{A} \sim \tilde{A}_0 + \cdots$ where

$$\tilde{A}_0 = \frac{c}{\sqrt{\epsilon}} e^{-\eta} + \alpha\,, \qquad c \equiv \frac{2\sqrt{2}}{\sqrt{V_0}}\,,$$

and that $\tilde{V} = \tilde{V}_0 + \cdots$, where $\tilde{V}_0$ satisfies

$$\left[e^{-2\eta}\tilde{V}_{0\eta}\right]_\eta = 0\,, \qquad -\infty < \eta < \infty\,. \tag{2.74}$$

The solution to (2.74) that matches as $\eta \to +\infty$ to the asymptotics (2.73) of the knee solution, and that satisfies $\tilde{V}_0 \sim V_0$ as $\eta \to -\infty$ in order to match to inner layer solution, is simply

$$\tilde{V}_0 = \frac{\alpha^2 v_{0x}(0^+)}{2c^2} e^{2\eta} + V_0\,. \tag{2.75}$$

Finally, we write (2.75) in terms of the inner variable y as $\eta = y + (1/2)\log\epsilon$ to obtain the following matching condition as $y \to +\infty$ for the inner solution:

$$V \sim \epsilon^2 \tilde{V}_0 \sim \epsilon^2 V_0 + \epsilon^3 \left(\frac{\alpha^2 v_{0x}(0^+)}{2c^2}\right) e^{2y}\,.$$

In this way, we conclude that the solution $V_{1p}(y)$ to (2.54) must satisfy

$$V_{1p} \sim b_+ e^{2y}\,, \quad \text{as} \quad y \to +\infty\,, \qquad b_+ \equiv \frac{\alpha^2 v_{0x}(0^+)}{2c^2}\,, \qquad c \equiv \frac{2\sqrt{2}}{\sqrt{V_0}}\,. \tag{2.76}$$

This rather intricate asymptotic construction has served to identify the constant b_+ in (2.54), which can then be used in (2.56) to determine the leading-order constant V_0. In fact, upon substituting (2.76) into (2.56), and solving for V_0, we obtain

$$\sqrt{V_0} = \frac{\pi}{\sqrt{2}\alpha^2 D v_{0x}(0^+)}\,. \tag{2.77}$$

Then, by using (2.32) for $v_{0x}(0^+)$ in (2.77), we recover the leading order result (2.35) for V_0,

as derived previously in §2.2. A higher order approximation for $V(0)$, based on analyzing correction terms to V_0, is derived in (2.81) below.

We remark that although the leading-order theory of §2.2 was also able to determine V_0 by simply integrating the V-equation in (2.11) over an intermediate, but otherwise unspecified, length-scale δ with $\epsilon \ll \delta \ll 1$, as was done in (2.33), the more refined asymptotic approach in this section provides the gradient information in V that is essential in §2.7 for deriving a DAE system for the slow dynamics of a hotspot. Moreover, this asymptotic construction has shown how the knee-layer solution allows V to make a fast transition between $O(\epsilon^2)$ and $O(\epsilon)$ scales.

Next, we proceed to analyze the correction terms in the outer region of the form (2.65). Upon substituting the A-expansion of (2.65) into (2.11), we obtain that $V = g(A)$ to both $O(-\epsilon \log \epsilon)$ and $O(\epsilon)$ terms, where $g(A)$ is defined in (2.17). Therefore, $v_j = g'(a_0)a_j$ for $j = 1, 2$, and hence the problems for a_1 and a_2 can be obtained by replacing a_0 in (2.18a) with $a_0 + (-\epsilon \log \epsilon)a_1 + \epsilon a_2$, and then performing a simple Taylor series expansion. To determine the boundary conditions for a_1 and a_2, we use $a_0(0^+) = \alpha$, $g'(\alpha) = \alpha^{-3}$, and $v_j = g'(a_0)a_j$ for $j = 1, 2$, together with the matching conditions $v_1(0^+) = -v_{0x}(0^+)$ and $v_2(0^+) = \left[\log\left(\frac{\alpha}{c}\right) - 1\right] v_{0x}(0^+)$, to identify conditions for a_1 and a_2 at $x = 0^+$. In this way, we obtain that $a_0(x)$ satisfies (2.18a), while $a_1(x)$ and $a_2(x)$ satisfy

$$D\left[f(a_0)a_1\right]_{xx} = a_1\,, \qquad 0 < x < \ell\,; \qquad a_1(0^+) = -a_{0x}(0^+)\,, \quad a_{1x}(\ell) = 0\,, \tag{2.78a}$$

$$D\left[f(a_0)a_2\right]_{xx} = a_2\,, \qquad 0 < x < \ell\,; \qquad a_2(0^+) = \left[\log\left(\frac{\alpha}{c}\right) - 1\right] a_{0x}(0^+)\,, \quad a_{2x}(\ell) = 0\,. \tag{2.78b}$$

Our key observation is that instead of solving (2.18a) and (2.78) recursively for a_0, a_1, and a_2, these outer approximations are contained in the solution to a *renormalized outer problem* for $a_\epsilon(x)$, formulated as

$$D\left[f(a_\epsilon)a_{\epsilon x}\right]_x = a_\epsilon - \gamma\,, \qquad x_\epsilon < x < \ell\,; \qquad a_\epsilon(x_\epsilon) = \alpha\,, \quad a_{\epsilon x}(\ell) = 0\,, \tag{2.79a}$$

where $x_\epsilon > 0$ is defined by

$$x_\epsilon = (-\epsilon \log \epsilon)\, x_1 + \epsilon x_2\,; \qquad x_1 = 1\,, \quad x_2 \equiv 1 - \log\left(\frac{\alpha}{c}\right)\,, \quad c \equiv \frac{2\sqrt{2}}{\sqrt{V_0}}\,. \tag{2.79b}$$

The fact that the solutions to (2.79) corresponds correctly to those of (2.78) can be verified easily.

First, observe the key nonlinear term in the equation can be formally expanded as follows:

$$D\left[f(a_\epsilon)a_{\epsilon x}\right]_x = D\left[\left(f(a_0) + (-\epsilon\log\epsilon)f'(a_0)a_1 + \epsilon f'(a_0)a_2\right)\cdot\left(a_{0x} + (-\epsilon\log\epsilon)a_{1x} + \epsilon a_{2x}\right)\right]_x\,,$$

so the $O(1)$, $O(-\epsilon\log\epsilon)$ and $O(\epsilon)$ terms are respectively

$$\begin{aligned} D\left[f(a_0)a_{0x}\right]_x & \\ D\left[f'(a_0)a_{0x}a_1 + f(a_0)a_{1x}\right]_x &= D\left[f(a_0)a_1\right]_{xx} \\ D\left[f'(a_0)a_{0x}a_2 + f(a_0)a_{2x}\right]_x &= D\left[f(a_0)a_2\right]_{xx} \end{aligned}$$

which gives the L.H.S. of equations in (2.18a) and (2.78).

Second, the nonzero matching condition $a_\epsilon(x_\epsilon) = \alpha$ can be formally expanded as:

$$\alpha = a_\epsilon(x_\epsilon) = a_0(0^+) + a_{0x}(0^+)\left((-\epsilon\log\epsilon)x_1 + \epsilon x_2\right) + (-\epsilon\log\epsilon)a_1(0^+) + \epsilon a_2(0^+) + \dots\,,$$

so the $O(1)$, $O(-\epsilon\log\epsilon)$ and $O(\epsilon)$ terms are respectively

$$\begin{aligned} \alpha &= a_0(0^+) \\ a_1(0^+) &= -a_{0x}(0^+) \\ a_2(0^+) = a_{0x}(0^+)x_2 &= \left(\log(\frac{\alpha}{c}) - 1\right)a_{0x}(0^+) \end{aligned}$$

which recovers the matching conditions stated in (2.18a) and (2.78) for a_0, a_1, and a_2.

Therefore, the effect on the outer solution of the knee layer is that one needs to account for an inner region that is $O(-\epsilon\log\epsilon)$ thick. The expression (2.79b) also shows that the outer solution has a weak dependence on the amplitude of the hotspot, mediated by V_0. One key advantage of using the renormalized problem (2.79) is that the leading-order theory of §2.2 can

still be used provided that we simply replace ℓ with $\ell - x_\epsilon$. This idea of renormalizing the outer solution to account for the switchback term is vaguely similar to the renormalization method proposed in [8] for analyzing weakly nonlinear oscillators.

Next, we use the renormalized problem (2.79) to determine an improved approximation $V_{0\epsilon}$ for $\epsilon^{-2}V(0)$. This new approximation consists of two weakly coupled nonlinear algebraic equations for $\mu_\epsilon \equiv a_\epsilon(\ell)$ and $V_{0\epsilon}$. To determine the first relation between μ_ϵ and $V_{0\epsilon}$ we integrate the V-equation in (2.11) from $-x_\epsilon < x < x_\epsilon$ to obtain, in place of (2.33), that

$$2D\alpha^2 v_{\epsilon x}(x_\epsilon) = 2\sqrt{2D}\sqrt{G(\mu_\epsilon) - G(\alpha)} \sim \frac{1}{\sqrt{V_{0\epsilon}}}\int_{-\infty}^{\infty} w^3\,dy - 2x_\epsilon(\gamma - \alpha)\,. \tag{2.80}$$

Here we have used $v_{\epsilon x}(x_\epsilon) = g'(\alpha)a_{\epsilon x}(x_\epsilon)$, where $g'(\alpha) = \alpha^{-3}$ and $a_{\epsilon x}(x_\epsilon)$ is obtained from a first integral of the renormalized problem (2.79). By solving the expression above for $V_{0\epsilon}$, we obtain our first relation

$$V_{0\epsilon} = \frac{\pi^2}{2\left[\sqrt{2D}\left(\sqrt{G(\mu_\epsilon) - G(\alpha)}\right) + (\gamma - \alpha)x_\epsilon\right]^2}\,. \tag{2.81a}$$

The second relation is obtained by replacing μ and ℓ in (2.26) with μ_ϵ and $\ell - x_\epsilon$, where x_ϵ is defined in (2.79b). This yields

$$\chi(\mu_\epsilon) = \sqrt{\frac{2}{D}}\,(\ell - x_\epsilon)\,, \qquad x_\epsilon = (-\epsilon\log\epsilon) + \epsilon\left(1 + \log\left(\frac{2\sqrt{2}}{\alpha}\right) - \log\sqrt{V_{0\epsilon}}\right)\,, \tag{2.81b}$$

where $\chi(\mu)$ is defined in (2.23).

The system (2.81) is a weakly coupled nonlinear algebraic system for $V_{0\epsilon}$ and $\mu_\epsilon \equiv a_\epsilon(\ell)$, where the coupling arises through the fact that x_ϵ depends weakly on $V_{0\epsilon}$. By solving this weakly coupled system using Newton's method for $\gamma = 2$, $\alpha = 1$, $D = 2$, and $\ell = 1$, in the right panel of Fig. 2.6 (thin dotted curve) we showed that $V_{0\epsilon}$ compares more favourably with the full numerical result than does the leading-order result V_0. Similarly, as was shown in the left panel of Fig. 2.6, the renormalized approximation $\sqrt{2}/\sqrt{V_{0\epsilon}}$ for $\epsilon A(0)$ compares rather well with full numerics when ϵ is small.

2.5.1 Improved Approximation of the Fold Point for the Supercritical Regime

For the supercritical regime $\gamma > 3\alpha/2$, (2.81b) implies same maximum threshold $\chi_{\max} = \lim_{\mu_\epsilon \to (3\alpha/2)^-} \chi(\mu_\epsilon)$ as in (2.24) which converges due to the formula (2.23) given in Section 2.2. However, the improvement of (2.81b) over (2.26) allows us to determine a more accurate minimum value of D for which a steady-state hotspot solution on $|x| \leq \ell$ exists, which we denote as $D_{\text{crit},\epsilon}$.

We simply set $\mu_\epsilon = 3\alpha/2$ in (2.81) and solve the resulting system for $D = D_{\text{crit},\epsilon}$ and $V_{0\epsilon}$. In particular, for a single hotspot solution on $|x| \leq \ell$ we have

$$D_{\text{crit},\epsilon} \equiv \frac{2(\ell - x_\epsilon)^2}{\chi^2_{\max}}\,, \tag{2.82a}$$

where $\chi_{\max} \equiv \chi\,(3\alpha/2)$, and $\chi(\mu)$ is defined in (2.23). In addition, the minimum value of D for a pattern of K interior hotspots on the domain $|x| \leq 1$, is obtained by setting $\ell = 1/K$ into (2.82a). This yields the critical thresholds

$$D_{\text{crit},\epsilon,K} = \frac{2(K^{-1} - x_\epsilon)^2}{\chi^2_{\max}}\ . \tag{2.82b}$$

In Fig. 2.9 of §2.4 we showed that the improved approximation $D_{\text{crit},\epsilon,K}$ for the minimum value of D for a steady-state pattern of K-interior hotspots on the domain $|x| \leq 1$ compares rather well with the full numerical results as ϵ is decreased. In comparison with the ϵ-independent results of (2.31) of §2.2 for the minimum value of D as obtained from the leading-order theory, our improved theory on $|x| \leq 1$ when $\gamma = 2$, $\alpha = 1$, and $\epsilon = 0.01$, yields

$$D_{\text{crit},\epsilon,1} \approx 1.5985\,, \qquad D_{\text{crit},\epsilon,2} \approx 0.3646\,, \qquad D_{\text{crit},\epsilon,4} \approx 0.0771\,. \tag{2.83}$$

As seen from Fig. 2.9 and (2.49), these improved approximations for the minimum value of D compare rather favourably with full numerical results. Moreover, in comparing (2.83) with the results (2.31) from the leading-order theory of §2.2, it is evident that the effect of the ϵ-dependent correction terms is rather significant even at $\epsilon = 0.01$.

For a one-hotspot solution, in §2.6 below we construct a new boundary layer near $x = \ell$ when $D \approx D_{\text{crit},\epsilon}$. For this analysis, we need to determine the local behaviour near $x = \ell$ of the solution to (2.79) when $D = D_{\text{crit},\epsilon}$, corresponding to when $a_\epsilon(\ell) = a_{0c} \equiv 3\alpha/2$. Near $x = l$, we put $a_\epsilon = a_{0c} + \bar{a}(x)$, where $\bar{a} \ll 1$ and $\bar{a}(\ell) = 0$. Upon substituting into (2.79), we obtain near $x = \ell$ that $[f'(a_{0c})\bar{a}\bar{a}_x]_x \sim (a_{0c} - \gamma)/D_{\text{crit},\epsilon}$, where $f'(a_{0c}) = -2/a_{0c}^2$. Therefore, near $x = \ell$, we have

$$(\bar{a}\bar{a}_x)_x \sim \frac{a_{0c}^2(\gamma - a_{0c})}{2D_{\text{crit},\epsilon}}\,.$$

Upon integrating this equation and imposing $\bar{a}(\ell) = 0$, we get for x near ℓ that

$$\left(\frac{1}{2}\bar{a}^2\right)_x \sim \beta a_{0c}^2(x - \ell)\,, \qquad \beta \equiv \frac{(\gamma - a_{0c})}{2D_{\text{crit},\epsilon}}\,.$$

Integrating once more, and imposing $\bar{a}(\ell) = 0$, we obtain that $\bar{a} \sim \sqrt{\beta} a_{0c}(x - \ell)$ as $x \to \ell^-$. We conclude that as $x \to \ell^-$, the local behaviour of the solution to (2.79) when $D = D_{\text{crit},\epsilon}$ is

$$a_\epsilon(x) \sim a_{0c} + \beta^{1/2} a_{0c}(x - \ell)\,, \quad \text{as} \quad x \to \ell^-\,, \qquad \text{where} \qquad a_{0c} \equiv \frac{3\alpha}{2}\,, \qquad \beta \equiv \frac{(\gamma - a_{0c})}{2D_{\text{crit},\epsilon}}\,. \tag{2.84}$$

Since, when $a_\epsilon(\ell) = 3\alpha/2$, the solution $a_\epsilon(x)$ no longer satisfies the no-flux condition $a_{\epsilon,x}(\ell) = 0$, we need to construct a new boundary layer near $x = \ell$. This is done in the next section.

2.6 A Normal Form for Hotspot Insertion

The full numerical computations in §2.4.1 for the supercritical regime, and the local analysis in (2.84) of §2.5, motivate the need for constructing a new boundary layer solution near the endpoints $x = \pm\ell$ when D is near the critical value $D_{\text{crit},\epsilon}$. This boundary layer analysis, which is shown below to generate multiple solutions in the boundary layer region, characterizes the onset of the peak insertion phenomena at the edges of the domain. We show that the overall mechanism for the creation of new hotspots is markedly similar to the analysis of [28] for the onset of self-replication behaviour of mesa patterns. Indeed, we derive a normal form equation, characterizing the local behaviour of the peak insertion process, that has the same structure as that derived in [28]. However, as an extension of the analysis of [28], we derive a formula,

valid near the critical threshold $D_{\mathrm{crit},\epsilon}$, that shows analytically how the solution multiplicity associated with the boundary layer solution near $x = \ell$ leads to a fold-point behaviour in the bifurcation diagram of $A(\ell)$ versus D.

Throughout this section, we assume $\gamma > 3\alpha/2$ so that $\alpha < a_0(x) < 3\alpha/2$ holds for all $x_\epsilon < x < \ell$ and the maximum value $\chi_{\max} = \chi(3\alpha/2)$ exists.

To analyze the onset of the peak insertion process, we first write the outer problem for the steady-state problem (2.11) in the form

$$\epsilon^2 A_{xx} + A^3\left[V - g(A)\right] = 0\,, \qquad D\left[A^2 V_x\right]_x - A + \gamma - A^3\left[V - g(A)\right] = 0\,, \tag{2.85}$$

on $x_\epsilon < x < \ell$, where $g(A)$ is defined in (2.17). We let $a_\epsilon(x)$ and $D_{\mathrm{crit},\epsilon}$ denote the solution to the renormalized outer problem (2.79) at the critical value where $a_\epsilon(\ell) = 3\alpha/2$. In terms of $a_\epsilon(x)$, $v_\epsilon(x)$ is given by $v_\epsilon(x) = g(a_\epsilon(x))$, where $g(A)$ is defined in (2.17). In the outer region, away from both the hotspot core and a thin boundary layer to be constructed near $x = \ell$, we expand the outer solution to (2.85), together with $\Lambda \equiv 1/D$, as

$$A = a_\epsilon + \nu a_{\epsilon,1} + \cdots\,, \qquad V = v_\epsilon + \nu v_{\epsilon,1} + \cdots\,, \qquad \Lambda \equiv \frac{1}{D} = \Lambda_\epsilon + \nu\Lambda_{\epsilon,1} + \cdots\,, \tag{2.86}$$

where the gauge function $\nu \ll 1$ and the constant $\Lambda_{\epsilon,1}$ are to be determined. By expanding $D = D_{\mathrm{crit},\epsilon} + \nu D_{\epsilon,1} + \cdots$, and then comparing with the expansion of Λ in (2.86), we identify that

$$D_{\mathrm{crit},\epsilon} = \frac{1}{\Lambda_\epsilon}\,, \qquad D_{\epsilon,1} = -\frac{\Lambda_{\epsilon,1}}{\Lambda_\epsilon^2}\,. \tag{2.87}$$

We substitute (2.86) into (2.85) and collect powers of ν. Assuming that $\nu \gg O(\epsilon^2)$, we obtain that a_ϵ satisfies the renormalized problem (2.79) with $a_\epsilon(\ell) = 3\alpha/2$, and that $a_{\epsilon,1}$ satisfies

$$\left[f(a_\epsilon)a_{\epsilon,1}\right]_{xx} - \Lambda_\epsilon a_{\epsilon,1} = \Lambda_{\epsilon,1} a_\epsilon\,, \qquad x_\epsilon < x < \ell\,; \qquad a_{\epsilon,1}(x_\epsilon) = 0\,. \tag{2.88}$$

The asymptotic boundary condition for $a_{\epsilon,1}$ as $x \to \ell^-$ will be derived below upon matching to the boundary layer solution to be constructed near $x = \ell$.

To construct the thin boundary layer near $x = \ell$, we begin by introducing the new variables

$\mathcal{A}_1$, $\mathcal{V}_1$, and z, by

$$A = a_{0c} + \delta \mathcal{A}_1(z) + \cdots , \qquad V = v_{0c} + \delta^2 \mathcal{V}_1(z) + \cdots , \qquad z \equiv \sigma^{-1}[\ell - x] , \tag{2.89}$$

where $a_{0c} \equiv 3\alpha/2$ and $v_{0c} \equiv g(a_{0c}) = 4/(27\alpha^2)$. Here the gauge functions $\sigma \ll 1$ and $\delta \ll 1$ are to be determined. The choice of different scales for A and V is motivated by the fact that $g'(a_{0c}) = 0$. We substitute (2.89) into (2.85), and after a Taylor expansion of $g(A)$, we obtain that

$$\frac{\epsilon^2 \delta}{\sigma^2} \mathcal{A}_{1zz} + \delta^2 a_{0c}^3 \left[\mathcal{V}_1 - \frac{1}{2} g''(a_{0c}) \mathcal{A}_1^2 \right] + \cdots = 0 , \qquad \frac{a_{0c}^2}{\sigma^2} \delta^2 \mathcal{V}_{1zz} = \Lambda_\epsilon \left(a_{0c} - \gamma \right) + \cdots , \tag{2.90}$$

where from (2.17) we calculate that

$$g''(a_{0c}) = -2 a_{0c}^{-4} , \qquad a_{0c} \equiv \frac{3\alpha}{2} . \tag{2.91}$$

To balance the terms in (2.90) we must relate σ and δ to ϵ by $\delta = \sigma$ and $\delta \sigma^2 = \epsilon^2$, which yields that

$$\delta = \epsilon^{2/3} , \qquad \sigma = \epsilon^{2/3} . \tag{2.92}$$

With this choice, (2.90) reduces to leading order on $0 < z < \infty$ to

$$\mathcal{A}_{1zz} + a_{0c}^3 \left(\mathcal{V}_1 + \frac{\mathcal{A}_1^2}{a_{0c}^4} \right) = 0 , \qquad \mathcal{V}_{1zz} = -\frac{2\beta}{a_{0c}^2} , \qquad \beta \equiv \frac{\Delta_\epsilon}{2} \left(\gamma - a_{0c} \right) > 0 . \tag{2.93}$$

In order to satisfy the no-flux boundary conditions for A and V on $x = \ell$ we must impose that $\mathcal{A}_{1z}(0) = \mathcal{V}_{1z}(0) = 0$.

Upon integrating the $\mathcal{V}_1$-equation, and imposing $\mathcal{V}_{1z}(0) = 0$, we get that $\mathcal{V}_1 = \mathcal{V}_{10} - \beta z^2 / a_{0c}^2$. Then, from the $\mathcal{A}_1$-equation in (2.93), we obtain

$$\mathcal{A}_{1zz} + a_{0c}^3 \left(-\frac{\beta}{a_{0c}^2} z^2 + \mathcal{V}_{10} + \frac{\mathcal{A}_1^2}{a_{0c}^4} \right) = 0 , \qquad 0 < z < \infty , \tag{2.94}$$

where $\mathcal{V}_{10}$ is an arbitrary constant. To obtain our normal form equation we eliminate as many

parameters as possible in (2.94) by rescaling z and $\mathcal{A}_1$ by

$$\mathcal{A}_1 = bU\,, \qquad z = \xi y\,. \tag{2.95a}$$

By choosing

$$\xi = \beta^{-1/6}\,, \qquad b = a_{0c}\beta^{1/3}\,, \tag{2.95b}$$

we obtain that (2.94) transforms to the normal form equation

$$U_{yy} + U^2 - y^2 + \kappa = 0\,, \qquad 0 < y < \infty\,; \qquad U_y(0) = 0\,, \tag{2.96a}$$

where the parameter κ is defined

$$\kappa \equiv a_{0c}^2\beta^{-2/3}\mathcal{V}_{10}\,. \tag{2.96b}$$

In order to match solutions to (2.96) with those in the outer region, we need that $U_y \to -1$ as $y \to +\infty$, which is consistent with the condition that $A_x > 0$ as $x \to \ell^-$.

Finally, in terms of the original variables, we obtain from (2.89), (2.92), and (2.95), that the boundary layer solution near $x = \ell$ is characterized by

$$A \sim a_{0c} + \epsilon^{2/3}a_{0c}\beta^{1/3}U(y)\,, \qquad V \sim v_{0c} + \epsilon^{4/3}\frac{\beta^{2/3}}{a_{0c}^2}\left(\kappa - y^2\right)\,, \qquad y \equiv \beta^{1/6}\epsilon^{-2/3}(\ell - x)\,, \tag{2.97}$$

where $a_{0c} \equiv 3\alpha/2$, $v_{0c} \equiv g(a_{0c}) = 4/(27\alpha^2)$, and β is defined in (2.93).

We observe that $-U$ satisfies exactly the equation (2.26) in [28]. The properties of solutions to (2.96) were established in Theorem 2 of [28], and we simply restate this result here for the convenience of the reader.

Theorem 1 (From [28])**.** *In the limit $\kappa \to -\infty$, (2.96) admits exactly two solutions $U = U^{\pm}(y)$ with $U' < 0$ for $y > 0$, with the following uniform expansions:*

$$U^+ \sim -\sqrt{y^2 - \kappa}\,, \qquad U^+(0) \sim -\sqrt{-\kappa}\,, \tag{2.98a}$$

$$U^- \sim -\sqrt{y^2 - \kappa}\left(1 - 3\,\mathrm{sech}^{\,2}\left(\frac{\sqrt{-\kappa}y}{\sqrt{2}}\right)\right)\,, \qquad U^-(0) \sim +\sqrt{-\kappa}\,. \tag{2.98b}$$

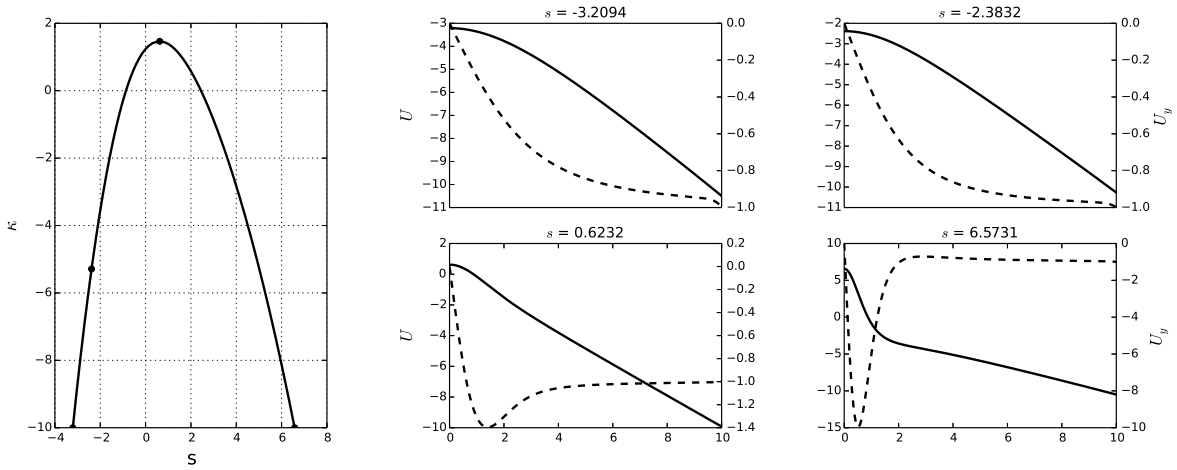

Figure 2.15: Left: Plot of the bifurcation diagram of κ versus $s = U(0)$ for solutions to the normal form equation (2.96). Right: the solution $U(y)$ (solid curves) and the derivative $U'(y)$ (dashed curves) versus y at four values of s on the bifurcation diagram.

These two solutions are connected. For any such solution, define s by $s \equiv U(0)$ and consider the solution branch $\kappa = \kappa(s)$. Then, $\kappa(s)$ has a unique (maximum) critical point at $s = s_{max}$ and $\kappa = \kappa_{max}$. Numerical computations yield that $\kappa_{max} \approx 1.46638$ and $s_{max} \approx 0.61512$.

A bifurcation diagram of κ versus $s \equiv U(0)$ for solutions to the normal form equation (2.96) is shown in the left panel of Fig. 2.15. In the right panel of Fig. 2.15 we plot the numerically computed solution $U(y)$ (solid curve), and the derivative $U'(y)$ (dashed curve), at a few selected values of $s = U(0)$.

We now proceed to analyze how the solution multiplicity in this boundary layer solution leads to a fold-point behaviour in the bifurcation diagram of $A(\ell)$ versus D. This analysis is new and was not done in [28]. To do so, we first need to determine the far-field behaviour as $y \to \infty$ for any solution of (2.96). We let $U = -\sqrt{y^2 - \kappa} + \bar{U}$ in (2.96), where $\bar{U} \ll 1$, to obtain that

$$\bar{U}_{yy} - \left(2\sqrt{y^2 - \kappa}\right)\bar{U} \sim -\frac{\kappa}{y^3}\,, \quad \text{as} \quad y \to \infty\,. \tag{2.99}$$

A homogeneous solution $\bar{U}_h$ to this equation has decay $\bar{U}_h = O(e^{-2\sqrt{2}|y|^{3/2}/3})$ as $y \to \infty$, whereas the particular solution $\bar{U}_p$ satisfies $\bar{U}_p = O(y^{-4})$ as $y \to \infty$. This shows that any solution to

(2.96) with $U_y \to -1$ as $y \to \infty$, has asymptotics

$$U \sim -\sqrt{y^2 - \kappa} + O(y^{-4}) \sim -y + \frac{\kappa}{2y} + O(y^{-2}), \qquad \text{as} \quad y \to \infty. \tag{2.100}$$

We then substitute (2.100) into (2.97) for A to obtain the following far-field behaviour of the boundary-layer solution:

$$A \sim a_{0c} + \epsilon^{2/3} a_{0c} \beta^{1/2} \left(-y + \frac{\kappa}{2y} \right).$$

Upon recalling that $y = \epsilon^{-2/3} \beta^{1/6} (\ell - x)$, the equation above yields the following matching condition for the outer solution:

$$A \sim a_{0c} + a_{0c} \beta^{1/2} (x - \ell) + \epsilon^{4/3} \left(\frac{a_{0c} \kappa \beta^{1/6}}{2} \right) \frac{1}{\ell - x}, \qquad \text{as} \quad x \to \ell^-. \tag{2.101}$$

Since the first two terms in (2.101) agree with the local behaviour (2.84) as $x \to \ell^-$ of the renormalized outer solution $a_\epsilon(x)$, we obtain upon comparing (2.86) with (2.101) that

$$\nu \equiv \epsilon^{4/3}, \tag{2.102}$$

and that $a_{\epsilon,1}$ satisfies (2.88) subject to the singular behaviour

$$a_{\epsilon,1} \sim \left(\frac{a_{0c} \kappa \beta^{1/6}}{2} \right) \frac{1}{\ell - x}, \qquad \text{as} \quad x \to \ell^-. \tag{2.103}$$

To solve (2.88) subject to (2.103) it is convenient to introduce the new variable $\tilde{a}_{\epsilon,1}$ defined by

$$\tilde{a}_{\epsilon,1} \equiv f(a_\epsilon) a_{\epsilon,1}.$$

Then, we calculate using (2.84), (2.103), and $f'(a_{0c}) = -2/a_{0c}^2$ that

$$\tilde{a}_{\epsilon,1} \sim f'(a_{0c}) a_{0c} \beta^{1/2} (x - \ell) \left(\frac{a_{0c} \kappa \beta^{1/6}}{2} \right) \frac{1}{\ell - x} = \beta^{2/3} \kappa, \qquad \text{as} \quad x \to \ell^-.$$

Therefore, from this limiting behaviour and (2.88), we conclude that $\tilde{a}_{\epsilon,1}$ satisfies

$$(\tilde{a}_{\epsilon,1})_{xx} - \frac{\Lambda_\epsilon}{f(a_\epsilon)}\tilde{a}_{\epsilon,1} = \Lambda_{\epsilon,1} a_\epsilon \,, \qquad x_\epsilon < x < \ell \,, \tag{2.104a}$$

$$\tilde{a}_{\epsilon,1}(x_\epsilon) = 0 \,; \qquad \tilde{a}_{\epsilon,1} \to \beta^{2/3}\kappa \,, \quad \text{as} \quad x \to \ell^- \,. \tag{2.104b}$$

We observe that since $f(a_\epsilon) = 0$ has a simple zero at $x = \ell$, then $x = \ell$ is a regular singular point for the differential operator in (2.104a). In (2.104) the condition at $x = \ell$ is over-determined in the sense that we are specifying that $\tilde{a}_{\epsilon,1}$ is bounded as $x \to \ell^-$ and that the limiting behaviour of $\tilde{a}_{\epsilon,1}$ as $x \to \ell^-$ is a per-specified constant. This extra implicit condition in the boundary condition at $x = \ell$ is the condition that determines $\Lambda_{\epsilon,1}$.

To determine $\Lambda_{\epsilon,1}$ it is convenient to reformulate (2.104) by introducing the new variable H by $\tilde{a}_{\epsilon,1} \equiv \Lambda_{\epsilon,1} H$, so that H satisfies

$$H_{xx} - \frac{\Lambda_\epsilon}{f(a_\epsilon)}H = a_\epsilon \,, \qquad x_\epsilon < x < \ell \,; \qquad H(x_\epsilon) = 0 \,, \quad H \ \text{bounded as} \ x \to \ell^- \,. \tag{2.105}$$

In terms of the solution to (2.105) we identify the constant H_ℓ from $H_\ell \equiv \lim_{x\to\ell^-} H(x)$. With H_ℓ now known, we obtain upon comparing (2.105) with (2.104) that

$$\Lambda_{\epsilon,1} = \frac{\beta^{2/3}\kappa}{H_\ell} \,. \tag{2.106}$$

Our numerical computations below show that $H_\ell > 0$.

Finally, from (2.87) and (2.97), and the expression for β in (2.93), we obtain a local parametric description of the bifurcation diagram of $A(\ell)$ and D in the form

$$D \sim D_{\text{crit},\epsilon} - \epsilon^{4/3} D_{\text{crit},\epsilon}^{4/3} \left(\frac{(\gamma-\alpha)^{2/3}\kappa}{2^{2/3} H_\ell} \right) , \qquad A(\ell) \sim a_{0c} \left(1 + \epsilon^{2/3}\beta^{1/3} U(0) \right) , \tag{2.107}$$

where $a_{0c} = 3\alpha/2$. Since the graph of κ versus $U(0)$ is multivalued from Fig. 2.15, we conclude from (2.107) that the graph of $A(\ell)$ versus D has a fold-point behaviour near $D_{\text{crit},\epsilon}$. When $H_\ell > 0$, we observe from (2.107) and Fig. 2.15 that D attains its minimum value $D_{\min,\epsilon}$ when $\kappa = \kappa_{\max} \approx 1.466$, corresponding to $U(0) \approx 0.615$.

To numerically compute the constant H_ℓ, we use a shooting method after first formulating

an asymptotic boundary condition to hold as $x \to \ell^-$. Near $x = \ell$, we calculate from (2.84) that

$$\frac{\Lambda_\epsilon}{f(a_\epsilon)} \sim \frac{r}{\eta}\,, \qquad r \equiv \frac{\Lambda_\epsilon a_{0c}}{2\beta^{1/2}}\,, \qquad \eta = \ell - x\,,$$

so that near $x = \ell$, (2.105) becomes

$$H_{\eta\eta} - \frac{r}{\eta} H = a_{0c} - \beta^{1/2} a_{0c}\eta + \cdots\,.$$

The local behaviour of the solution is readily calculated as

$$H(\eta) \sim H_\ell \left[1 + r\eta \log\eta + O(\eta)\right]\,, \qquad \text{as} \quad \eta \to 0^+\,, \tag{2.108}$$

which, after eliminating H_ℓ, yields the asymptotic boundary condition

$$H_x \sim -rH \log(\ell - x)\,, \qquad \text{as} \quad x \to \ell^-\,. \tag{2.109}$$

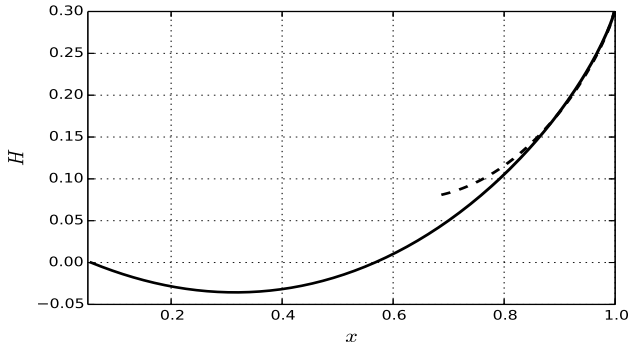

Figure 2.16: Numerically computed solution (solid curve) to (2.105) with asymptotic boundary condition (2.109) imposed at $x = \ell - \delta$, with $\delta = 0.000001$, and with parameter values $\gamma = 2$, $\alpha = 1$, $\ell = 1$, and $\epsilon = 0.01$. We obtain $H_\ell = \lim_{x\to\ell^-} H(x) \approx 0.303$. The dashed curve is the local Frobenius series approximation for H, valid near $x = \ell$, with leading terms given in (2.108).

To determine the constant H_ℓ we use a shooting method on (2.105), which consists of iterating on the constant H_0 in $H_x(x_\epsilon) = H_0$, and then imposing (2.109) at $x = \ell - \delta$, where δ with $0 < \delta \ll 1$ is a regularization parameter. The function $a_\epsilon(x)$ in (2.105) is determined by calculating $a_{\epsilon,x}$ from a first integral of (2.79). For $\gamma = 2$, $\alpha = 1$, and $\epsilon = 0.01$, our computations

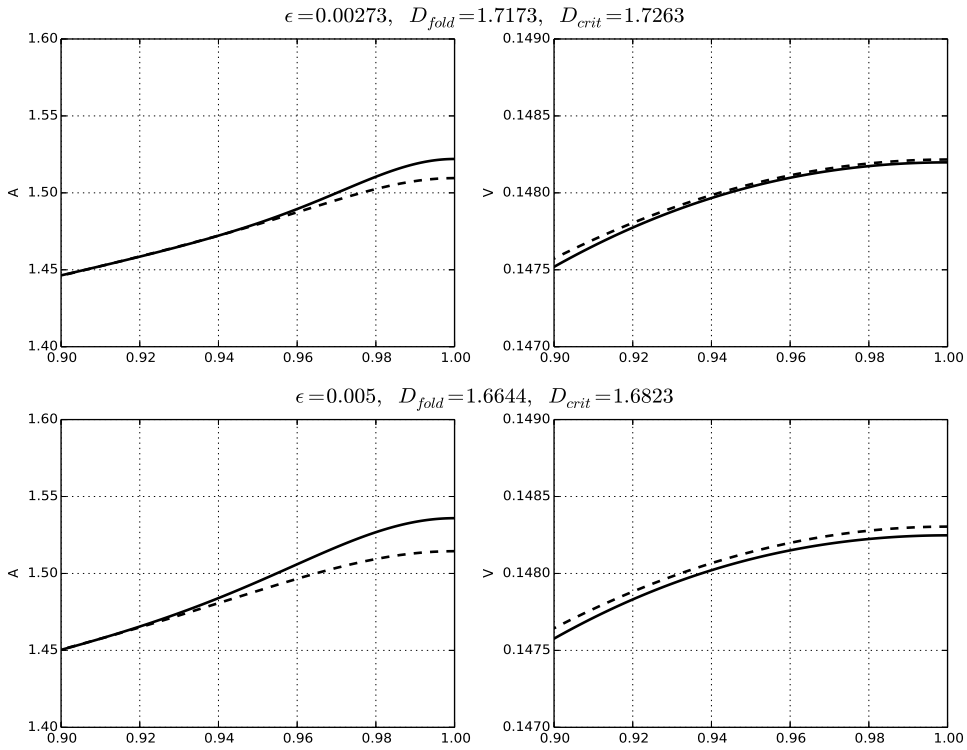

Figure 2.17: The asymptotic results (dashed curves) for A (left) and V (right) in the boundary layer region near $x = \ell$ at the fold point value for D are compared with corresponding full numerical results (solid curves). The asymptotic fold point value is given by (2.107). The top row is for $\epsilon = 0.00273$ and the bottom row is for $\epsilon = 0.005$. The other parameter values are $\gamma = 2$, $\alpha = 1$, and $\ell = 1$.

yield $H_\ell \approx 0.303$ when $\delta = 0.000001$, which yields $D_{\min,\epsilon} \approx 1.598$ from (2.107). In Fig. 2.16 we plot the numerically computed $H(x)$ versus x when $\gamma = 2$, $\alpha = 1$, $\ell = 1$, $\epsilon = 0.01$, and $H_\ell = 0.303$. The dashed curve in this plot is a local Frobenius series approximation valid near $x = \ell$, with leading terms given in (2.108).

For two values of ϵ, in Fig. 2.17 we show a favorable comparison between the asymptotic and full numerical results for A and V in the boundary layer region at the fold point value. The full numerical results are computed using `AUTO-07p`. Finally, in Fig. 2.18 we compare the asymptotic result (2.107) for $A(\ell)$ versus D, with $H_\ell \approx 0.303$, near the fold point with the corresponding full numerical result computed using `AUTO-07p`. The plot is a zoom of the region near the fold point.

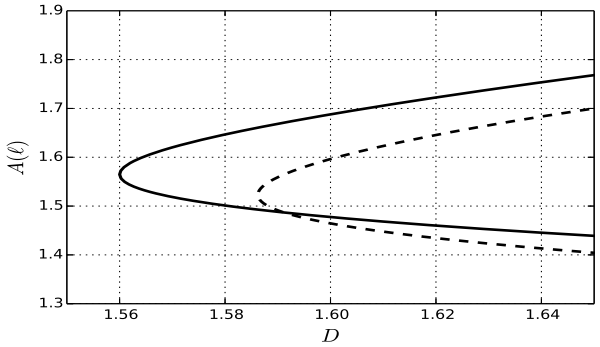

Figure 2.18: The asymptotic result (dashed curve) for $A(\ell)$ versus D in a narrow interval near the fold point, as obtained from (2.107) with $H_\ell \approx 0.303$, is compared with the corresponding full numerical result (solid curve) computed using `AUTO-07p`. The parameter values are $\gamma = 2$, $\alpha = 1$, $\ell = 1$, and $\epsilon = 0.01$.

2.7 Slow Dynamics of Crime Hotspots

In this section we derive a DAE system for the slow dynamics of a collection of hotspots. In our analysis we assume that a quasi-steady pattern of localized hotspots has emerged from initial data by way of some transient process for (2.10). As such, we assume that we have "prepared" initial data consisting of a quasi steady-state hotspot pattern. The analysis below characterizing the slow evolution of the quasi steady-state hotspot pattern relies heavily on the refined asymptotic theory of §2.5. We first consider the dynamics of a single hotspot centered at x_0 in the domain $|x| \le \ell$. In §2.7.2 we extend the analysis to study the dynamics of a multi-hotspot pattern. In §2.7.3 we compare results from the asymptotic theory of slow hotspot dynamics with corresponding full numerical results.

2.7.1 The Slow Dynamics of One Hotspot

To characterize the slow dynamics of a single hotspot we proceed by adapting the analysis of §2.5. A dominant balance argument shows that the speed of the hotspot is $O(\epsilon^2)$. In the inner region, where $y = \epsilon^{-1}(x - x_0(\sigma))$, with $\sigma = \epsilon^2 t$, we pose a two-term expansion for A as

$$A \sim A_0/\epsilon + A_1 + \dots , \qquad V \sim \epsilon^2 V_\epsilon \, .$$

Upon substituting this expansion into (2.10), and after retaining the dominant correction terms, we obtain that

$$\left(A_{0yy} - A_0 + V_\epsilon A_0^3\right) + \epsilon\left(A_{1yy} - A_1 + 3V_\epsilon A_0^2 A_1 + \alpha\right) + \cdots = -\epsilon \dot{x}_0 A_{0y}\,, \tag{2.110a}$$

$$D\left[\left(A_0^2 + 2\epsilon A_0 A_1\right) V_{\epsilon y}\right]_y - \epsilon V_\epsilon\left(A_0^3 + 3A_0^2 A_1 \epsilon\right) + \epsilon^2(\gamma - \alpha) + \cdots = -\epsilon^3\left(A_0^2 V_\epsilon\right)_y \dot{x}_0\,. \tag{2.110b}$$

As in §2.5, we expand $V_\epsilon = V_0 + \epsilon V_1 + \cdots$ and substitute this expansion into (2.50) and collect powers of ϵ. This yields the leading-order result that V_0 is an unknown constant and that $A_0 = w/\sqrt{V_0}$, where $w(y) = \sqrt{2}\,\mathrm{sech}\, y$. At next order, in place of (2.52), we obtain on $-\infty < y < \infty$ that

$$L_0 A_1 \equiv A_{1yy} - A_1 + 3w^2 A_1 = -\alpha - \frac{V_1}{V_0^{3/2}} w^3 - \frac{w_y}{\sqrt{V}_0}\dot{x}_0\,, \qquad \left[w^2 V_{1y}\right]_y = \frac{\sqrt{V_0}}{D} w^3\,. \tag{2.111}$$

Since L_0 has a one-dimensional nullspace with $L_0 w_y = 0$, the solvability condition for the A_1-equation in (2.111) provides

$$\int_{-\infty}^{\infty}\left(\alpha w_y + \frac{V_1}{V_0^{3/2}} w^3 w_y + \frac{w_y^2}{\sqrt{V_0}}\dot{x}_0\right) dy = 0\,.$$

Since w is odd with $w(\pm\infty) = 0$, this condition reduces to

$$\dot{x}_0 \int_{-\infty}^{\infty} w_y^2\, dy = -\frac{1}{4V_0}\int_{-\infty}^{\infty} V_1\left(w^4\right)_y\, dy\,.$$

We integrate this expression by parts and use the fact that $w = O(e^{-|y|})$ as $|y| \to \infty$, together with $V_1 = O(e^{2|y|})$ as $|y| \to \infty$ (see the discussion below equation (2.52)), to eliminate the boundary term and obtain that

$$\dot{x}_0 \int_{-\infty}^{\infty} w_y^2\, dy = \frac{1}{4V_0}\int_{-\infty}^{\infty}\left(w^2 V_{1y}\right) w^2\, dy\,.$$

We then integrate this expression once more by parts to get

$$\dot{x}_0 \int_{-\infty}^{\infty} w_y^2\, dy = \frac{1}{4V_0}\left[\left(w^2 V_{1y}\right) I(y)\big|_{-\infty}^{\infty} - \int_{-\infty}^{\infty}\left(w^2 V_{1y}\right)_y I(y)\, dy\right], \tag{2.112}$$

where $I(y) \equiv \int_0^y w^2\,ds$. Since $I(y)$ is odd, and $\left(w^2 V_{1y}\right)_y$ is even in y from (2.111), it follows that the integral on the right-hand side of (2.112) vanishes identically. In addition, upon using $w = \sqrt{2}\,\mathrm{sech}\, y$, we can evaluate the integral ratio $\int_{-\infty}^{\infty} w^2\,dy / \int_{-\infty}^{\infty} w_y^2\,dy = 3$. In this way, (2.112) reduces to

$$\dot{x}_0 = \frac{3}{8V_0}\left[\lim_{y\to\infty}\left(w^2 V_{1y}\right) + \lim_{y\to-\infty}\left(w^2 V_{1y}\right)\right]. \tag{2.113}$$

The last step in the analysis is to evaluate the two limits in (2.113) by using the gradient information on V provided by the knee solution. The analysis of the mid-inner, knee, and outer solutions for A and V proceeds analogously as in §2.5, since these solutions are quasi-steady on the time-scale of the slow dynamics. As such, in our discussion below, we only highlight the results of the analysis.

In place of (2.79), the renormalized outer problem is now formulated as

$$D\left[f(a_\epsilon)a_{\epsilon x}\right]_x = a_\epsilon - \gamma\,, \qquad \text{on} \quad x_{0+\epsilon} < x < \ell\,, \quad -\ell < x < x_{0-\epsilon}\,, \tag{2.114a}$$

$$a_\epsilon(x_{0+\epsilon}) = \alpha\,, \quad a_\epsilon(x_{0-\epsilon}) = \alpha\,, \quad a_{\epsilon x}(\pm\ell) = 0\,, \tag{2.114b}$$

where $x_{0\pm\epsilon} > 0$ is defined by in terms of the hotspot location x_0 by

$$x_{0\pm\epsilon} \equiv x_0 \pm x_\epsilon \qquad x_\epsilon \equiv (-\epsilon\log\epsilon) + \epsilon\left(1 + \log\left(\frac{2\sqrt{2}}{\alpha}\right) - \log\sqrt{V_0}\right). \tag{2.114c}$$

In terms of $a_\epsilon(x)$, the renormalized outer solution $v_\epsilon(x)$ is

$$v_\epsilon(x) = g\left(a_\epsilon(x)\right), \tag{2.115}$$

where $g(a)$ is defined in (2.17).

By matching the renormalized outer solution across the knee and mid-inner solutions one can obtain, as in §2.5, the gradient information for V_1 as $y \to \pm\infty$. More specifically, in place of (2.76), we obtain that

$$V_1 \sim b_\pm e^{2\pm y}\,, \quad \text{as} \quad y \to \pm\infty\,, \qquad b_\pm \equiv \pm\left(\frac{\alpha^2}{2c^2}\right) v_{\epsilon x}(x_{0\pm\epsilon})\,, \qquad c \equiv \frac{2\sqrt{2}}{\sqrt{V_0}}\,. \tag{2.116}$$

By using this limiting behaviour, together with the asymptotics $w \sim 2\sqrt{2}e^{\pm y}$ as $y \to \pm\infty$, we can evaluate the two limits in (2.113) as

$$\lim_{y\to\pm\infty}\left(w^2 V_{1y}\right) = 8\lim_{y\to\pm\infty}\left(e^{\mp 2y}V_{1y}\right) = \alpha^2 V_0 v_{\epsilon x}(x_{0\pm\epsilon})\,. \tag{2.117}$$

Then, from (2.115) we calculate $v_{\epsilon x}(x_{0\pm\epsilon}) = \alpha^{-3}a_{\epsilon x}(x_{0\pm\epsilon})$, where we used $g'(\alpha) = \alpha^{-3}$. In this way, (2.113) reduces to an ODE determined in terms of the renormalized outer solution $a_\epsilon(x)$, satisfying (2.114), given by

$$\dot{x}_0 = \frac{3}{8\alpha}\left[a_{\epsilon x}(x_{0+\epsilon}) + a_{\epsilon x}(x_{0-\epsilon})\right]\,. \tag{2.118}$$

By calculating a first integral of (2.114), as similar to that in (2.21), we readily derive that

$$a_{\epsilon x}(x_{0+\epsilon}) = \sqrt{\frac{2}{D}}\alpha\sqrt{G(\mu_+) - G(\alpha)}\,, \qquad a_{\epsilon x}(x_{0-\epsilon}) = -\sqrt{\frac{2}{D}}\alpha\sqrt{G(\mu_-) - G(\alpha)}\,, \tag{2.119}$$

so that (2.118) becomes

$$\frac{dx_0}{d\sigma} = \frac{3}{8}\sqrt{\frac{2}{D}}\left[\sqrt{G(\mu_+) - G(\alpha)} - \sqrt{G(\mu_-) - G(\alpha)}\right]\,, \qquad \sigma \equiv \epsilon^2 t\,. \tag{2.120a}$$

Here $G(u)$ is defined in (2.20b), and $\mu_\pm \equiv a_\epsilon(\pm l)$ are determined in terms of the hotspot location x_0 and the constant V_0 from the implicit relations

$$\chi(\mu_+) = \sqrt{\frac{2}{D}}\left(\ell - x_{0+\epsilon}\right)\,, \qquad \chi(\mu_-) = \sqrt{\frac{2}{D}}\left(\ell + x_{0-\epsilon}\right)\,, \tag{2.120b}$$

where $\chi(\mu)$ is defined in (2.23). Finally, to derive the renormalized equation for V_0 we proceed as in (2.80) of §2.5, to obtain

$$D\alpha^2\left[v_{\epsilon x}(x_{0+\epsilon}) - v_{\epsilon x}(x_{0-\epsilon})\right] \sim \frac{1}{\sqrt{V_0}}\int_{-\infty}^{\infty} w^3\,dy - 2x_\epsilon(\gamma - \alpha)\,.$$

By substituting $v_{\epsilon x}(x_{0\pm\epsilon}) = \alpha^{-3}a_{\epsilon x}(x_{0\pm\epsilon})$, and using (2.119), we solve the resulting expression

for V_0 to get the approximate equation

$$V_0 = \frac{2\pi^2}{\left[\sqrt{2D}\left(\sqrt{G(\mu_+) - G(\alpha)} - \sqrt{G(\mu_-) - G(\alpha)}\right) + 2x_\epsilon(\gamma - \alpha)\right]^2} \,. \tag{2.120c}$$

For a given x_0, (2.120b) and (2.120c) are a weakly nonlinear algebraic system for $\mu_\pm$ and V_0, where the coupling arises through the weak dependence of x_ϵ on V_0. With $\mu_\pm$ determined in this way for a given x_0, the speed of the hotspot when at location x_0 is given by (2.120a). In this sense, the system (2.120) is a differential-algebraic ODE system for the evolution of a single hotspot, starting from some initial value $x_0(0)$ with $|x_0(0)| < \ell$.

For the solvability of (2.120b) and (2.120c), corresponding to the existence of an outer solution, we require that the domain lengths for the two outer solutions on either side of x_0 not exceed a threshold. In particular, as similar to that in (2.25) of §2.2, we require that the following constraint, guaranteeing that no new hotspot is nucleated or created at the domain boundaries, is satisfied:

$$\max\{\ell + x_{0-\epsilon}, \ell - x_{0+\epsilon}\} \le \ell_{\max} \,, \qquad \ell_{\max} \equiv \sqrt{\frac{D}{2}}\chi_{\max} \,, \qquad \chi_{\max} \equiv \chi\left(3\alpha/2\right) \,. \tag{2.121}$$

We now discuss a key qualitative feature of the dynamics (2.120). Our main observation is that the dynamics of a single hotspot is symmetrizing in the sense that

$$\begin{cases} \dot{x}_0 < 0 & \text{if } x_0 > 0 \\ \dot{x}_0 > 0 & \text{if } x_0 < 0 \end{cases} , \tag{2.122}$$

so that the hotspot is repelled from the domain boundaries. To see this, we note that if $x_0 < 0$, then from (2.120b) and the fact that $\chi(\mu)$ is monotone increasing in μ, it follows that $\mu_- < \mu_+$. Then, since $G(u)$ is monotone increasing in u, we conclude that $G(\mu_-) < G(\mu_+)$, so that $\dot{x}_0 > 0$ from (2.120a). As a result of this symmetrizing property of the hotspot dynamics, it follows that if the constraint (2.121) is satisfied for the initial hotspot location $x_0(0)$, then this constraint will still hold for all time under the DAE evolution (2.120). This implies that no new hotspots can be nucleated at later times near the domain boundaries under the slow dynamics of a single

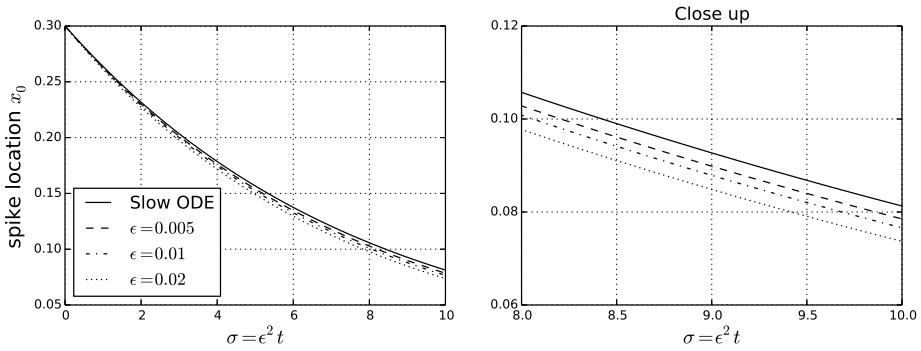

Figure 2.19: For parameter values $\gamma = 2$, $\alpha = 1$, $\ell = 1$, $D = 4$, and with initial state $x_0(0) = 0.3$, the asymptotic result (2.120) for slow hotspot dynamics is plotted for three values of ϵ. These results are compared with the corresponding result when the switchback term $-\epsilon \log \epsilon$ is neglected, so that $x_{0\pm\epsilon} = x_0$ in (2.120b). The plot on the right is a zoom of that on the left.

hotspot. Since $x_{0e} = 0$ is the only fixed point of the dynamics, we have that $x_0 \to 0$ as $\sigma \to \infty$ for any $x_0(0)$.

In Fig. 2.19 we show the quantitative effect on the slow hotspot dynamics of the switchback term $-\epsilon \log \epsilon$. Recall that in (2.120b), $x_{0\pm\epsilon}$ is defined in terms of this switchback term by (2.114c). With the initial value $x_0(0) = 0.3$, the asymptotic result for the slow dynamics of x_0 versus $\sigma = \epsilon^2 t$ is plotted for three values of ϵ, and is compared with the corresponding result when the switchback term is not included, so that $x_{0\pm\epsilon} = x_0$ in (2.120b).

We remark that although the DAE dynamics (2.120) for x_0 is highly nonlinear when $D = O(1)$, it simplifies considerably in the limit $D \gg 1$. For $D \gg 1$, we can approximate the solution to the renormalized problem (2.114) by

$$a_\epsilon = \alpha + \frac{1}{D}\tilde{a}_\epsilon + \cdots ,$$

where $\tilde{a}_\epsilon$ satisfies

$$\tilde{a}_{\epsilon xx} = \frac{(\alpha-\gamma)}{f(\alpha)} = \alpha(\alpha-\gamma)\,, \qquad x_{0+\epsilon} < x < \ell\,, \quad -\ell < x < x_{0-\epsilon}\,,$$

$$\tilde{a}_\epsilon(x_{0\pm\epsilon}) = 0\,, \quad \tilde{a}_{\epsilon x}(\pm\ell) = 0\,.$$

From the simple solution to this limiting problem, we calculate for $D \gg 1$ that

$$a_{\epsilon x}(x_{0+\epsilon}) \sim \frac{1}{D}\alpha(\alpha-\gamma)(x_{0+\epsilon}-\ell)\,, \qquad a_{\epsilon x}(x_{0-\epsilon}) \sim \frac{1}{D}\alpha(\alpha-\gamma)(x_{0-\epsilon}+\ell)\,. \tag{2.123}$$

By substituting (2.123) into (2.118), we obtain the following simple linear ODE dynamics, with flow towards the origin, for a one-hotspot solution when $D \gg 1$:

$$\dot{x}_0 \sim -\frac{3}{4D}(\gamma-\alpha)x_0\,, \tag{2.124}$$

with only exponentially decaying solutions:

$$x_0 = C\exp\left(-\frac{3}{4D}\left(\gamma-\alpha\right)\tau\right) \to 0 \qquad \text{as } \tau \to \infty.$$

2.7.2 A DAE System for Repulsive Hotspot Dynamics

In this section we generalize the results for the dynamics of a single hotspot to the case where there are $N \geq 1$ hotspots on the domain $|x| \leq \ell$. We label the centers of the hotspots by x_j for $j = 1, \ldots, N$, and assume the ordering $-\ell < x_1 < x_2 < \cdots < x_N < \ell$. In order to simplify our analysis, we will use the leading-order result that the spatial extent of the hotspot centered at x_j is $x_j - x_\epsilon < x < x_j + \epsilon$, where $x_\epsilon = -\epsilon\log\epsilon + O(\epsilon)$. By neglecting the $O(\epsilon)$ term in x_ϵ and using $x_\epsilon \sim -\epsilon\log\epsilon$ the slow hotspot dynamics becomes uncoupled from the heights of the hotspots. With this simplification, the adjacent outer problems for the hotspots centered x_j and x_{j+1} must agree at a common vanishing Neumann boundary point at the midpoint $(x_j + x_{j+1})/2$. With this observation, and by using translation invariance of (2.10), it is clear that the one-hotspot results derived above can be readily adapted to determine the dynamics of a collection of hotspots.

More precisely, let ℓ_{j+} and ℓ_{j-} denote the half-lengths of the outer problems on either side of the hotspot centered at x_j for $j = 2, \ldots, N-1$. In contrast, for the hotspot adjacent to $x = -\ell$, we let ℓ_{1-} be the distance from x_1 to $x = -\ell$, whereas ℓ_{N+} is the distance from x_N to

$x = \ell$. In terms of x_j, this yields

$$\begin{aligned} &\ell_{j+} \equiv \frac{(x_{j+1} - x_j)}{2}\,, \quad j = 1, \ldots, N-1\,; \quad \ell_{j-} \equiv \frac{(x_j - x_{j-1})}{2}\,, \quad j = 2, \ldots, N\,, \\ &\ell_{N+} = \ell - x_N\,, \quad \ell_{1-} = l + x_1\,. \end{aligned} \tag{2.125a}$$

We then define the constants μ_{j+} and μ_{j-} for $j = 1, \ldots, N$ by the implicit equations

$$\chi(\mu_{j+}) = \sqrt{\frac{2}{D}}\left[\ell_{j+} - (-\epsilon \log \epsilon)\right]\,, \qquad \chi(\mu_{j-}) = \sqrt{\frac{2}{D}}\left[\ell_{j-} - (-\epsilon \log \epsilon)\right]\,. \tag{2.125b}$$

In terms of the $\mu_{j\pm}$, which depend on the instantaneous locations of the hotspots, the centers of the N hotspots satisfies the slow dynamics

$$\dot{x}_j \sim \frac{3}{8}\sqrt{\frac{2}{D}}\left(\sqrt{G(\mu_{j+}) - G(\alpha)} - \sqrt{G(\mu_{j-}) - G(\alpha)}\right)\,, \qquad j = 1, \ldots, N. \tag{2.125c}$$

The DAE system (2.125) for the slow evolution of a collection of hotspots is valid provided that the lengths of the outer regions between adjacent hotspots is below a threshold, i. e. provided that

$$\max_{j=1,\ldots,N}\{\ell_{j-}, \ell_{j+}\} \leq \ell_{\max}\,, \qquad \ell_{\max} \equiv \sqrt{\frac{D}{2}}\chi_{\max}\,, \qquad \chi_{\max} \equiv \chi\left(3\alpha/2\right)\,. \tag{2.126}$$

A steady-state configuration for the $N-$hotspot pattern is the equally-spaced solution whereby

$$x_j = -\ell + \frac{(2j-1)}{N}\ell\,, \qquad j = 1, \ldots, N\,.$$

2.7.3 Comparison of Asymptotic and Full Numerical Results for Slow Hotspot Dynamics

Finally, we compare the asymptotic results (2.120) and (2.125) for slow hotspot dynamics with corresponding full numerical results computed using the software `PDEPE` in `MATLAB R2013b`. For the full numerical computations, we take $10/\epsilon + 1$ evenly-spaced spatial mesh points in order to adequately resolve the narrow cores of the hotspots. Initial conditions for the quasi

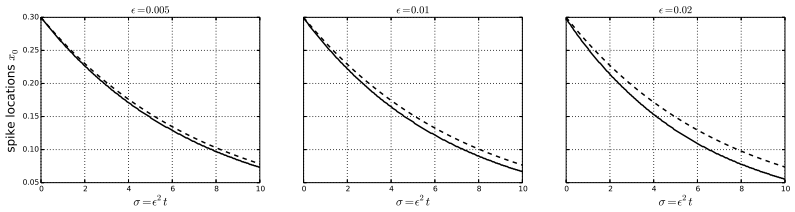

Figure 2.20: The slow dynamics of a single hotspot on the slow time-scale σ, as predicted by the asymptotic theory (2.120) (dashed curves), are compared with corresponding full numerical results of the PDE system (2.10) (solid curves) computed using `PDEPE` of `MATLAB R2013b`. The domain is $|x| \leq 1$ and the parameter values are $\gamma = 2$, $\alpha = 1$, and $D = 4$. Left: $\epsilon = 0.005$. Middle: $\epsilon = 0.01$. Right: $\epsilon = 0.02$.

steady-state hotspot patterns are generated by evolving the PDE (2.10) from small initial bump perturbations, such as shown in the left panel of Fig. 2.2. The resulting transient evolution leads to the formation of a pattern of hotspots that is essentially stationary on $O(1)$ time intervals. The locations of the maxima of A for this pattern are then identified numerically. We re-initialize the full numerical computations by using this computed hotspot pattern as the initial condition for (2.10). Then, the subsequent slow evolution of the maxima of A are tracked numerically over very long time intervals, and compared with corresponding results from the asymptotic theory.

In Fig. 2.20 we compare the asymptotic results for the slow dynamics of a single hotspot, as predicted by (2.120), with corresponding full numerical results. The comparisons are done for three values of ϵ. The agreement between the asymptotic and numerical results is very close when $\epsilon = 0.005$, but is still decent even when $\epsilon = 0.02$.

For the case of multiple hotspots, and with $\epsilon = 0.01$, in Fig. 2.21 we show a very favorable comparison between the slow dynamics predicted from the asymptotic theory (2.125) and that computed numerically from the full PDE system (2.10) for either a two or four hotspot evolution.

2.8 Discussion

2.8.1 Summary

In this chapter, we used the method of matched asymptotic expansions, together with the numerical bifurcation software `AUTO-07p` to analyze the bifurcation properties of steady-state hotspot solutions of (2.11) in the limit $\epsilon \to 0$ for the regime $D = O(1)$ for any $\gamma > \alpha$. It

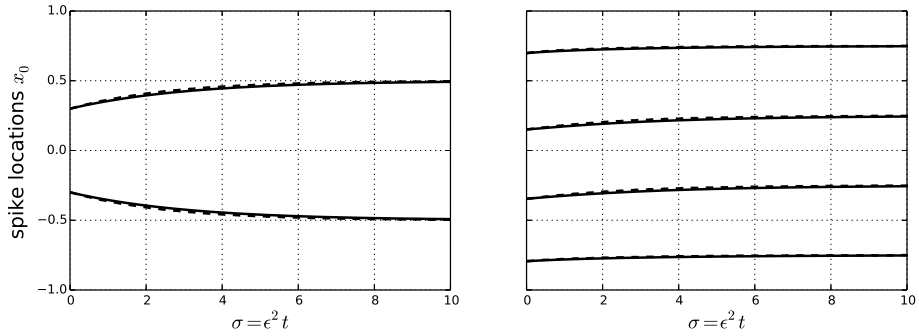

Figure 2.21: Comparison of slow dynamics predicted from the asymptotic theory (2.125) (dashed curves) and from full numerical simulations (solid curves) of the PDE system (2.10). The domain is $|x| \leq 1$ and the parameter values are $\gamma = 2$, $\alpha = 1$, and $\epsilon = 0.01$. Left: a two-hotspot evolution with $D = 2$, with initial locations $x_0 \approx -0.300, 0.299$. Right: a four-hotspot evolution with $D = 0.3$, with initial locations are $x_0 \approx -0.794, -0.346, 0.151, 0.698$.

was shown, both analytically and numerically, that new hotspots of criminal activity can be nucleated at the domain boundary or in the middle of two adjacent hotspots, and that such events are characterized by a saddle-node bifurcation point of the corresponding bifurcation diagram. Such nucleations are also known as "peak insertion" events, and they occur whenever the distance between neighbouring hotspots, or between a hotspot and the domain boundary, increases beyond a critical threshold. This "peak insertion" behaviour effectively determines the minimum number of steady-state hotspots that will occur for a given domain length. Furthermore, the peak insertion behaviour for (2.11) is very similar to the mechanism characterizing the onset of the rupture, and ultimately self-replication, of mesa patterns in RD systems (cf. [28]), and the breakup of droplets for a diffusive interface surface tension model under compressible flow (cf. [34]).

Our leading-order-in-ϵ asymptotic theory in Section 2.2 features a nonlinear but strictly monotone outer problem which is at the crux of the distinction of the supercritical and subcritical behaviours of crime hotspots as observed in [48]. Moreover, the asymptotic theory predicts a simple *one-sixth* rule for the prediction of the insertion of hotspots on page 43. The leading order theory was also sufficient for the NLEP theory in Section 2.3 to prove that multi-hotspot steady-state solutions are unconditionally linearly stable on an $O(1)$ time-scale when $D = O(1)$, regardless of the number of hotspots and the value of D, and as long as the pattern exists as a steady state.

The previous study [29] of the stability of hotspot equilibria for the regime $D = O(\epsilon^{-2})$ showed that K-hotspot equilibria with $K \geq 2$ are linearly stable on an $O(1)$ time-scale only when $D < D_{0K}/\epsilon^{-2}$ for some constant D_{0K}. For other RD activator-inhibitor systems, without the chemotactic term, nonlocal eigenvalue problems characterizing the stability of multi-spike patterns in 1-D on $O(1)$ time-scales have been derived and analyzed in [13], [20], [24], [52], [53], [54] (see also the references therein).

However, our leading-order-in-ϵ asymptotic theory in Section 2.2 for the construction of steady-state hotspot solutions was found to agree well with full numerical results for (2.11) only when ϵ is quite small. A more refined asymptotic theory in Section 2.5, based on a detailed analysis of a triple-deck structure near the core of the hotspot and the retention of a certain switchback term that is logarithmic in ϵ, was shown to provide a significantly better approximation of hotspot equilibria at moderately small values of ϵ. Switchback terms also arise in the singular perturbation analysis of some other problems, including model problems of low Reynolds number flows (cf. [31], [32], [42]), and the analysis in [33] of singular solutions to a PDE model for the deflection of a micro-plate capacitor. In order to include the effect of switchback correction terms, we used a novel procedure, somewhat similar to the renormalization approach in [8], whereby the leading-order-in-ϵ asymptotic theory can still be used upon re-defining a certain term with an ϵ-dependent quantity.

The refined asymptotic theory for the construction of hotspot equilibria was shown to be central for deriving a differential algebraic system (DAE) characterizing the slow dynamics of a collection of quasi-steady hotspots for the time-dependent problem (2.10) in Section 2.7. From this DAE system, it is shown that the dynamic interactions between neighbouring hotspots are repulsive. Therefore, due to the geometrical constraint of the 1-D domain, peak insertion events that are triggered dynamically as a result of the distance between two neighbouring hotspots exceeding some critical threshold are not typically possible in 1-D. This behaviour is qualitatively different than the merging-emerging dynamics of localized peaks for the chemotaxis-growth model of [39], whereby localized peaks experience attractive, rather than repulsive, dynamics. Peak insertion events, together with attractive dynamics between neighbouring peaks, was shown in [39] to lead to spatio-temporal chaotic behaviour of localized peaks for the chemotaxis-growth model.

We emphasize that our DAE system for the evolution of a single hotspot for the urban crime model (2.10) has a rather different form to that for the dynamics of a single localized spike for other singularly perturbed RD systems such as the Gierer-Meinhardt, Schnakenberg, and Gray-Scott systems, studied in [9], [14], [15], [19], [43], [50] (see also the references therein). In these previous studies, the outer problem away from a spike is linear and its solution for the inhibitor variable can be represented in terms of a Green's function. This leads to a single, explicit, ODE for the evolution of a spike. In contrast, in our analysis of (2.10), the outer problem is nonlinear and there is an intricate triple-deck inner layer structure near the hotspot core for the slow V variable that must be resolved. The resolution of this intricate inner layer structure leads to the generation of switchback terms characterizing the correction terms for the outer expansion away from the core of the hotspot. Overall, this analysis leads to a DAE system rather than a single ODE characterizing the slow motion of a single hotspot.

2.8.2 Open Problems

We conclude this chapter by briefly discussing a few possible directions for further research.

An open problem evident from the numerical studies in Section 2.4.2 is to construct the pattern observed with $O(1)$ amplitude in both A and V. Our preliminary results show that by expanding $A \sim A_0 + \ldots$, $V \sim V_0 + \ldots$ and substituting to (2.12) gives $V_0 = \text{const}$ while $A_0(y)$ solves the problem.

$$\begin{cases} A_{0yy} - A_0 + V_0 A_0^3 + \alpha = 0 \\ A_0(0) = \max A_0, \qquad A_{0y}(y) \to 0 \text{ as } y \to \pm\infty \end{cases} \tag{2.127}$$

is a homoclinic for V_0 in the range of $0 < V_0 < \frac{4}{27}$. This will present a potential solvability condition from the matching process. The fact that $A_0 = O(1)$ and $V_0 = O(1)$ is numerically verified by continuation of the solution in the limit of $\epsilon \to 0^+$ as shown in Fig. 2.22.

An immediately related question is whether these two types of hotspots can be glued together to form a new type of asymmetric pattern. We remark that such a pattern with spiky profiles of different asymptotic order is novel to the best of our knowledge. Fig. 2.23 shows that such a possibility exists. We also remark that this may be related to the interim states contained in

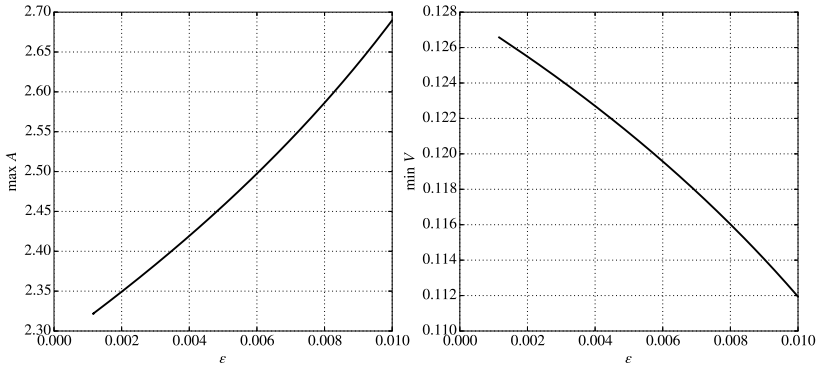

Figure 2.22: The continuation of the function values at the core of the unstable crime hotspot shown in Fig. 2.12. Other parameter values are $D = 1$, $\alpha = 1$, $\gamma = 1.25$. These show that $\max A = A(0)$ and $\min V = V(0) \sim V_0$ are indeed $O(1)$ as $\epsilon \to 0^+$. Note that $\min V < \frac{4}{27} = 0.\dot{1}4\dot{8}$.

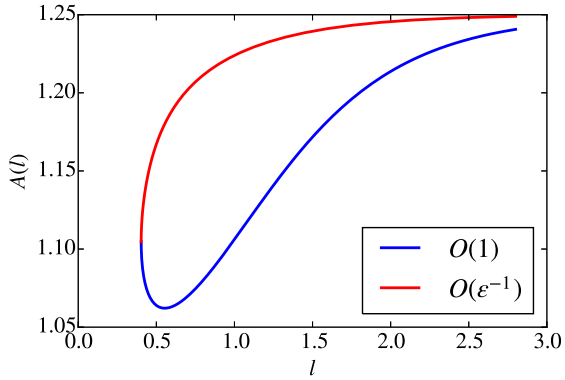

Figure 2.23: Continuation of $O(1)$ amplitude spike in the A component in domain length ℓ naturally connects to the $O(\epsilon^{-1})$-amplitude spike at a fold bifurcation. We plots the range of possible $A(\ell)$ and check possible overlapping in their range. This is to throw light on the possibility of asymmetric patterns with neighbouring $O(1)$ and $O(\epsilon^{-1})$ spikes. Model parameters are $\epsilon = 0.01$, $D = 1$, $\gamma = 1.25$, $\alpha = 1$.

Fig. 2.8 after the solution goes around the insertion fold point but before the hotspot doubling is complete. When a new spike is being born, it seem plausible that a transitional spike solution of amplitude $O(1)$ in A exists. However, an asymptotic theory for this kind of spike is currently lacking.

Other open directions include, first and foremost, to consider extensions of the basic 1-D model. For instance, one may analyze hotspot slow dynamics for some extensions of the basic 1-D model (2.10). Such possible extensions of the basic model include, allowing for spatial variability of the rate at which criminals are re-introduced, so that $\gamma - \alpha$ depends on x,

accounting for the effect of crime deterrence by police presence (cf. [41], [56]), or allowing for a nonlinear diffusivity of the attractiveness field (cf. [18]). These extensions have a potential to allow for both heterogeneous patterns and more complex spatio-temporal dynamics not observed in this chapter.

Another key open problem is to extend the preliminary analysis in [29] to analyze the existence, stability, and dynamics of 2-D localized hotspot patterns to (2.1) in the limit $\epsilon \to 0$ with $D = O(1)$ on bounded 2-D domains. For simpler RD systems, without the chemotactic term in the inhibitor variable as in (2.1), such as the Gierer-Meinhardt, Schnakenberg, and Gray-Scott systems, results in 2-D for the slow dynamics of localized solutions are given in [23], [27], and [10] (see also the references therein).

In Section 5 of [29], a formal asymptotic analysis was used in the limit $\epsilon \to 0$, and with $D \gg 1$, to construct quasi steady-state patterns of $K \geq 1$ well-separated hotspots for (2.1) in arbitrary, but bounded, 2-D domains. Through the derivation and analysis of a nonlocal eigenvalue problem, it was shown in [29] that, on the $D \gg O(1)$ regime, a one-hotspot pattern is linearly stable on an $O(1)$ time-scale. Additionally, it was shown that $K-$hotspot patterns with $K \geq 2$ are linearly stable on an $O(1)$ time-scale when $D < \epsilon^{-4} D_{0c}/K^3$, where D_{0c} depends on γ, α and the area of the domain. Therefore, for multi-hotspot patterns on the regime $D \gg O(1)$, the stability threshold occurs when $D = O(\epsilon^{-4})$. No study of the slow dynamics of 2-D hotspot patterns was made in [29].

The mathematical challenge with analyzing the $D = O(1)$ regime in 2-D is that, in contrast to the 1-D case studied herein, the outer problem for the attractiveness field will consist of a nonlinear elliptic PDE that cannot be reduced to a simple quadrature. However, we do expect that this nonlinear PDE has a saddle-node bifurcation structure and leads to a peak insertion phenomena, similar to that studied in 1-D. Furthermore, the characterization of the slow dynamics of a collection of hotspots should depend on the spatial gradient of the solution to the nonlinear outer problem at the hotspot locations. The goal would be to investigate whether it is possible in 2-D that new hotspots can be nucleated through peak-insertion events that are triggered, intermittently in time, from the overall collective dynamics of interacting hotspots.

Such a mechanism, if it exists, would give rise to highly complex spatio-temporal patterns

of dynamically interacting hotspots, similar to that found for the chemotaxis-growth model of [39] in one spatial dimension.

Chapter 3

Police Intervention - a Simple Interaction Model

In this chapter, we consider the simple interaction case for the police-criminal dynamics ($I(\rho, U) = U$) in the three-component reaction-diffusion model introduced in (1.20). The following model is included as a special case of a general form proposed in [45]. In particular, the simple interaction term $-U$ in the ρ-equation (criminal density) represents a criminal removal rate proportional to the number of police present at the same spatial location. The nonlinear police movement term corresponds to a choice of the function $v(A)$ not explicitly studied in [45], given by

$$v(A) = qD\nabla \log A\,.$$

We leave the predator-prey interaction case ($I(\rho, U) = \rho U$) for future study, except to mention that our preliminary results suggest that there are three nonlocal terms in the corresponding NLEP problem compared to two nonlocal terms for the current system, which we will derive in this chapter in Section 3.2.

We begin our study of the simple police interaction model on the finite one-dimensional

domain $-\ell < x < \ell$, formulated as

$$A_t = \epsilon^2 A_{xx} - A + \rho A^3 + \alpha\,, \tag{3.1a}$$

$$\rho_t = D\left(\rho_x - 2\rho A_x/A\right)_x - \rho A + \gamma - \alpha - U\,, \tag{3.1b}$$

$$\tau_u U_t = D\left(U_x - qUA_x/A\right)_x\,, \tag{3.1c}$$

subject to the no-flux boundary conditions

$$A_x = \rho_x = U_x = 0 \qquad \text{at} \quad x = \pm\ell\,.$$

We first observe that by integrating (3.1c) over the domain, we obtain that the total amount of police $\int_{-\ell}^{\ell} U(x,t)dx$ is conserved in time. The parameter $q > 0$ measures the degree of focus in the police patrol random walk, as was discussed in the paragraphs containing the formula (1.6). The choice of boundary conditions indicates we are studying a closed system, and this makes sense when the main crime and police deployment are localized in a city sufficiently isolated from its neighbors.

There are two important remarks regarding the police diffusion term $(U_x - qUA_x/A)_x$.

Firstly, we recall that choosing the factor $q = 2$ in front of UA_x/A in the third equation we are modeling a mimicry police deployment strategy whereby the police concentration diffuses in exactly the same way as the criminals. When q is above or below 2, the police force diffuses in a less or more focused manner, respectively, compared to the movement of the criminals.

Secondly, the diffusivity of the police can be regarded as D/τ_u, and so if $\tau_u < 1$, the police are more mobile than the criminals. Conversely, $\tau_u > 1$ can be interpreted as the police being comparatively more "sluggish" in their movements.

The key qualitative question we ask is the following. What should the optimum degree of focus be in patrolling? The common overarching question in virtually all the efforts in crime modeling is to seek strategies to reduce crime, by minimizing the number of crime hotspots in a given region. In our context, we will investigate whether there are optimal values of q and τ_u, so that the least number of hotspots can be stable. From a mathematical perspective, this is equivalent to optimizing the stability threshold of the diffusivity D by tuning q and τ_u.

3.1 Asymptotic Construction of a Multiple Hotspot Steady-State

We now construct steady-state solutions for (3.1) with multiple hotspots. First, we observe that the spatial differential operators on ρ and U are similar, and has the simpler flux form by reversing a product rule

$$\frac{\partial}{\partial x}\left[\left(\frac{\partial}{\partial x} - qA_x/A\right)(\cdots)\right] = \frac{\partial}{\partial x}\left[A^q \frac{\partial}{\partial x}\left(A^{-q}(\cdots)\right)\right].$$

This suggests that we make the change of variables analogous to (2.9)

$$\rho = VA^2\,, \qquad U = uA^q\,,$$

so that (3.1) transforms to

$$A_t = \epsilon^2 A_{xx} - A + VA^3 + \alpha\,, \tag{3.2a}$$

$$\left(VA^2\right)_t = D\left(A^2 V_x\right)_x - VA + \gamma - \alpha - uA^q\,, \tag{3.2b}$$

$$\tau_u \left(uA^q\right)_t = D\left(A^q u_x\right)_x\,. \tag{3.2c}$$

The key assumption is that the attractiveness field A is highly localized as compared to both the criminal and police densities, so that $\epsilon \ll 1$. Then, anticipating a homoclinic in A with hotspot amplitude of order $O(\epsilon^{-1})$, we will consider the large D regime where $D = O(\epsilon^{-2})$. Then, by choosing $V = O(\epsilon^2)$, we obtain a distinguished balance. This motivates the rescaling

$$V = \epsilon^2 v, \qquad D = D_0/\epsilon^2\,,$$

so that (3.2) transforms to

$$A_t = \epsilon^2 A_{xx} - A + \epsilon^2 v A^3 + \alpha\,, \tag{3.3a}$$

$$\epsilon^2 \left(A^2 v\right)_t = D_0 \left(A^2 v_x\right)_x - \epsilon^2 v A^3 + \gamma - \alpha - u A^q\,, \tag{3.3b}$$

$$\tau_u \epsilon^2 \left(A^q u\right)_t = D_0 \left(A^q u_x\right)_x\,, \tag{3.3c}$$

with $A_x = u_x = v_x = 0$ at $x = \pm\ell$.

Observe that, as compared to (2.10), our system will be coupled more weakly as some key nonlinear terms have a different order with respect to ϵ. This will facilitate our asymptotic analysis. The analysis of the stronger coupling regime where $D = O(1)$, as considered for the basic crime model in the previous chapter, would be the natural next step in future work. In this chapter we will focus our analysis on (3.3), pertaining to the $D = O(\epsilon^{-2})$ regime.

3.1.1 A Symmetric Pattern of Hotspots of Equal Amplitude

To construct a symmetric steady-state with K hotspots to (3.3), a simple way to do so is to consider a larger domain of length S, where $S = (2\ell)K$, and construct a single hotspot on $(-\ell, \ell)$. Owing to the translation-invariance of the equations (3.3), the single hotspot steady-state can be placed side-by-side to give a $K-$hotspot pattern on the large domain of length S, which we conveniently choose to be $(0, S)$. Consequently, the total number of police, given by

$$U_0 \equiv \int_0^S U(x,t)\,dx\,, \tag{3.4}$$

which is constant in time, can now be expressed as

$$U_0 = K \int_{-\ell}^{\ell} U\,dx\,, \tag{3.5}$$

if we integrate (3.1c) on $(0, S)$ and use translation-invariance. We now begin the matched asymptotic expansions procedure to construct a single hotspot solution on $(-\ell, \ell)$

First, we substitute $U = uA^q$ into (3.5) to readily obtain the steady-state solution to (3.3c)

as

$$u = \frac{U_0}{K \int_{-\ell}^{\ell} A^q \, dx} \,, \tag{3.6}$$

provided the steady-state solution A to (3.3a) is known. Therefore, the steady-state problem for the 3-component system (3.3) is equivalent to the following two-component system with an nonlocal integral term:

$$\epsilon^2 A_{xx} - A + \epsilon^2 v A^3 + \alpha = 0 \,, \tag{3.7a}$$

$$D_0 \left(A^2 v_x \right)_x - \epsilon^2 v A^3 + \gamma - \alpha - \frac{U_0}{K} \frac{A^q}{\int_{-\ell}^{\ell} A^q \, dx} = 0 \,. \tag{3.7b}$$

For the first component, we have $A \sim \alpha + O(\epsilon^2)$ in the outer region, while in the inner region, we put $y = \epsilon^{-1} x$ and $A \sim A_0/\epsilon$ to obtain

$$A_{0yy} - A_0 + v A_0^3 + \epsilon \alpha = 0 \,, \qquad D_0 \epsilon^{-4} \left(A_0^2 v_y \right)_y + O(\epsilon^{-1}) = 0 \,.$$

Therefore, to leading order it follows that $v \sim v_0$ is a constant, and that

$$A_0 = \frac{w(y)}{\sqrt{v_0}} \,, \tag{3.8}$$

where $w(y) = \sqrt{2} \operatorname{sech} y$ is the homoclinic solution of

$$w'' - w + w^3 = 0, \qquad -\infty < y < \infty \,,$$

$$w(0) > 0, \quad w'(0) = 0, \quad w \to 0 \quad \text{as} \quad y \to \pm\infty \,.$$

Some particular values of the integrals of $w(y)$ will be needed below. They are collected here as

$$\int_{-\infty}^{\infty} w(y) dy = \int_{-\infty}^{\infty} w^3(y) dy = \sqrt{2}\pi \,,$$

$$\int_{-\infty}^{\infty} w^2(y) dy = 4, \qquad \int_{-\infty}^{\infty} w^4(y) dy = 16/3 \,,$$

$$\int_{-\infty}^{\infty} w^5(y) dy \Big/ \int_{-\infty}^{\infty} w^3(y) dy = \frac{3}{2} \,.$$

In particular, a general formula for $I_q \equiv \int_{-\infty}^{\infty} w^q(y)dy$ is

$$I_q = \int_{-\infty}^{\infty} w^q(y)\, dy = 2^{3q/2-1}\frac{\Gamma^2(q/2)}{\Gamma(q)}\,, \tag{3.9}$$

where $\Gamma(z)$ is the usual Gamma function. This general formula, along with the analogous formula for a general class of homoclinic solutions is computed in the Appendix at (A.11) and (A.13).

We return to (3.6), which is valid uniformly on the whole domain, and estimate the key integral

$$\int_{-\ell}^{\ell} A^q\, dx \sim 2\ell\alpha + \epsilon^{1-q} v_0^{q/2} \int_{-\infty}^{\infty} w^q(y)\, dy = O(\epsilon^{1-q})\,,$$

so that $u = O(\epsilon^{q-1})$.

Remark 3.1. A key assumption we make is that $q > 1$ so that the integral $\int_{-\ell}^{\ell} A^q dx$, and thus u depend only on the inner region contribution from A^q, and is decoupled from the $O(1)$ term $2\ell\alpha$. With this assumption, the leading order solution to u is given by

$$u \sim \epsilon^{q-1}\tilde{u_e}, \qquad \text{where} \qquad \tilde{u_e} \equiv \frac{U_0}{K}\frac{v_0^{q/2}}{I_q}\,. \tag{3.10}$$

Next, we determine v_0 by integrating (3.7b) on $(-\ell, \ell)$ and imposing $v_x(\pm\ell) = 0$ to find

$$\epsilon^2 \int_{-\ell}^{\ell} vA^3 dx = 2\ell\,(\gamma - \alpha) - U_0/K\,.$$

Therefore, since $A \sim \alpha = O(1)$ in the outer region, while $A = O(\epsilon^{-1})$ in the inner region, it follows that the dominant contribution to the integral arises from the inner region. In this way, we estimate

$$\frac{1}{\sqrt{v_0}\int w^3} = 2\ell\,(\gamma - \alpha) - U_0/K\,, \tag{3.11}$$

which determines v_0 as

$$v_0 = 2\pi^2\,(2\ell\,(\gamma - \alpha) - U_0/K)^{-2}\,. \tag{3.12}$$

We observe that v_0, and thus the amplitude of the hotspot, as determined by A_0, is independent of the parameter q.

Remark 3.2. In Chapter 2, the value V_0 given in (2.35), which has a role analogous to v_0 given above at 3.12, are both a limit of the outer solution $v(x)$ at hotspot the spot location, and in both cases $2/\sqrt{V_0}$ and $1/\sqrt{v_0}$ give the leading order approximations of the amplitudes of the corresponding attractiveness hotspots. However, the strengths of interaction between the inner and outer solutions are significantly different for the $D = O(\epsilon^{-2})$ regime, versus the $D = O(1)$ regime studied in Chapter 2), with the stronger interaction case $D = O(1)$ being asymptotically more intricate to analyze. Therefore, unlike the leading order approximation for A, which we use A_0 for both, we are distinguishing V_0 from v_0 by the capitalization.

Also, we observe from (3.11) that a necessary condition for a hotspot solution with $A = O(\epsilon^{-1})$ to exist is that

$$U_0 < U_{0,\max} \equiv 2\ell K\,(\gamma - \alpha)\;, \tag{3.13}$$

so that the total police deployment must be below some threshold. We will assume such a condition for U_0 throughout this section.

In the outer region, we expand $v \sim v_e(x) + \dots$ and recalling that $A \sim \alpha + O(\epsilon^2)$ we find that $v_e(x)$ solves the simple ODE problem on $0 < x < \ell$ given by

$$D_0 v_{exx} = -\frac{(\gamma - \alpha)}{D_0 \alpha^2} \equiv -\zeta\,, \quad 0 < x < \ell\,; \qquad v_e(0) = v_0,\; v_{ex}(\ell) = 0\,, \tag{3.14}$$

which has the solution

$$v_e(x) = \frac{\zeta}{2}\left[(\ell - |x|)^2 - \ell^2\right] + v_0, \qquad 0 < |x| \le \ell\,, \tag{3.15}$$

with v_0 as given in (3.12). Notice that this is a uniformly valid leading order solution for v.

We summarize the results for the leading order approximation of a steady-state with a single hotspot on $(-\ell, \ell)$ as follows.

Theorem 3.3. *For the system (3.3), there exists a symmetric steady-state solution on $(0, S)$ with K hotspots. On each sub-domain with length $2\ell = S/K$, and translated to $(-\ell, \ell)$ to contain*

exactly one hotspot at $x = 0$, the steady-state solution, to leading order, is given by

$$A \sim \frac{w(x/\epsilon)}{\sqrt{v_0}}\,, \quad \textit{if} \quad x = O(\epsilon), \qquad A \sim \alpha \quad \textit{if} \quad x = O(1)\,,$$

$$v \sim v_e = \frac{\zeta}{2}\left[(\ell - |x|)^2 - \ell^2\right] + v_0\,,$$

$$u \sim \epsilon^{q-1}\tilde{u}_e, \qquad \tilde{u}_e \equiv \frac{U_0}{K}\frac{v_0^{q/2}}{I_q}\,,$$

where $v_0 = 2\pi^2\left(2\ell\left(\gamma - \alpha\right) - U_0/K\right)^{-2}$ *and* $I_q = 2^{3q/2-1}\frac{\Gamma^2(q/2)}{\Gamma(q)}$.

Remark 3.4. The leading order behavior is now seen to be entailed predominantly by the local behavior of the $O(\epsilon^{-1})$ spike in the A-component. In contrast, the only term that depends on the assumption that the the hotspot is located at $x = 0$ in $(-\ell, \ell)$ is v_e which has a simple explicit formula. Therefore, in the construction of an asymmetric pattern, i.e. with hotspot located at $0 \neq x_0 \in (-\ell, \ell)$, only the term v_e needs to be changed.

We now also summarize the above result in terms of the original variables to facilitate the interpretation of what it means to the original model (3.3).

Corollary 3.5. *For the system (3.3), the K-hotspot steady-state that corresponds to that stated in (3.3) is given by:*

$$A \sim \frac{w(x/\epsilon)}{\sqrt{v_0}}\,, \quad \textit{if} \quad x = O(\epsilon), \qquad A \sim \alpha\,, \quad \textit{if} \quad O(\epsilon) \ll |x| < \ell\,,$$

$$\rho \sim w^2(x/\epsilon)\,, \quad \textit{if} \quad x = O(\epsilon), \qquad \rho \sim \epsilon^2 v_e \alpha^2\,, \quad \textit{if} \quad O(\epsilon) \ll |x| < \ell\,,$$

$$U \sim \epsilon^{-1}\frac{U_0}{K} w^q / I_q\,, \quad \textit{if} \quad x = O(\epsilon), \quad U \sim \epsilon^{q-1}\frac{U_0}{K}\alpha^q v_0^{q/2}/I_q\,, \quad \textit{if} \quad O(\epsilon) \ll |x| < \ell\,.$$

3.2 NLEP Stability of Multiple Spike Steady-State for General Power $1 < q < \infty$

To analyze the linear stability of a K-hotspot steady-state solution, we will first derive the non-local eigenvalue problem (NLEP) by using the method of matched asymptotic expansions. We first derive the NLEP for a one-hotspot solution where the boundary conditions are of Floquet type. From this canonical problem we readily extract the corresponding NLEP corresponding to a multi-spike pattern with our desired Neumann boundary conditions by following the methodology described in the Appendix, Section A.1 on page 179). This approach to study the

stability of multi-spike steady-states is a relatively new technique first applied to spike-stability problems for a general class of reaction-diffusion systems [40], for the study of the stability of mesa patterns [36], and for a spike solution to a competition model with cross-diffusion [30].

Our approach is related to the recent work by Kolokolnikov *et al.* in [29] on the basic crime model, but here we extend this analysis to incorporate the third component representing the police density. The novelty of the analysis is that it leads to an NLEP that now has two distinct nonlocal terms. Nevertheless, we will show that the spectrum of this NLEP can be reduced to the study of a simple transcendental equation in the eigenvalue parameter for the case where $q = 3$. For this value of q, the equation for the discrete eigenvalue of the NLEP will be sufficiently simple so as to lead to an explicit characterization of an asynchronous, or anti-phase, oscillation in the hotspot amplitudes for a pattern of two hotspots in a certain parameter regime. This oscillation is due to a Hopf bifurcation, whose threshold can be determined analytically. The existence of robust asynchronous oscillations in the spike amplitudes is a new phenomena, which does not occur in the study of spike stability for other reaction-diffusion systems such as the Gierer-Meinhardt and Gray-Scott models, where synchronous oscillations typically occur.

We also mention in passing that such problems with two or more nonlocal terms are relatively novel in the literature for NLEP stability analysis. Active research is being conducted to investigate new ways to treat multiple nonlocal terms in an NLEP, and in this chapter we present some new results in this direction for the value $q = 3$ where the analysis is particularly simple, and for the more challenging case where $q \neq 3$.

3.2.1 Linearization with Floquet B.C.

To study the linear stability problem for a K-hotspot pattern we first introduce a linear perturbation of the form

$$A = A_e + e^{\lambda t}, \qquad v = v_e + e^{\lambda t}\epsilon\psi, \qquad u = u_e + e^{\lambda t}\epsilon^q\eta\,, \tag{3.16}$$

where (A_e, v_e, u_e) represents a steady-state with a single hotspot centered at the origin in $-\ell < x < \ell$. The orders of perturbations ($O(1)$, $O(\epsilon)$ and $O(\epsilon^q)$ for the A, v and u components relatively) were chosen such that ϕ, ψ, and η are all $O(1)$ in the inner region.

Then, we obtain from (3.3) that

$$\epsilon^2\phi_{xx} - \phi + 3\epsilon^2 v_e A_e^2\phi + \epsilon^3 A_e^3\psi = \lambda\phi\,, \tag{3.17a}$$

$$D_0\left(2A_e v_{ex}\phi + \epsilon A_e^2\psi_x\right)_x - 3\epsilon^2 A_e^2 v_e\phi - \epsilon^3 A_e^3\psi$$

$$-qu_e A_e^{q-1}\phi - \epsilon^q\eta A_e^q = \lambda\epsilon^2\left(2A_e v_e\phi + \epsilon A_e^2\psi\right)\,, \tag{3.17b}$$

$$D_0\left(qA_e^{q-1}\phi u_{ex} + \epsilon^q A_e^q\eta_x\right)_x = \epsilon^2\tau_u\lambda\left(qA_e^{q-1}u_e\phi + \epsilon^q A_e^q\eta\right)\,. \tag{3.17c}$$

For (3.17b),(3.17c), we impose the following Floquet boundary conditions on $x = \pm\ell$

$$\begin{pmatrix}\eta(\ell)\\ \psi(\ell)\end{pmatrix} = z\begin{pmatrix}\eta(-\ell)\\ \psi(-\ell)\end{pmatrix}\,, \qquad \begin{pmatrix}\eta(\ell)\\ \psi(\ell)\end{pmatrix} = z\begin{pmatrix}\eta_x(-\ell)\\ \psi_x(-\ell)\end{pmatrix}\,, \tag{3.18}$$

where z is a complex-valued parameter. In Section A.1 we discuss how to extract the spectrum for the Neumann problem for a multi-spike pattern from our initial imposition of Floquet boundary conditions.

For (3.17a), in the inner region, we use $A_e \sim w/\sqrt{\epsilon}$ and $\psi \sim \psi_0$ to obtain that

$$\Phi'' - \Phi + 3w^2\Phi + \frac{\psi(0)}{v_0^{3/2}}w^3 = \lambda\Phi\,, \tag{3.19}$$

where $\Phi(y) = \phi(x_j + \epsilon y)$ is the leading order inner expansion of ϕ. In contrast, in the outer region we obtain from (3.17) to leading-order that

$$\phi \sim \epsilon^3\alpha^3\psi/[\lambda + 1 - 3\epsilon^2\alpha^2 v_e] = O(\epsilon^3), \qquad \psi_{xx} = 0, \qquad \eta_{xx} = 0\,.$$

The main goal of the calculation below involves determining the values $\psi(0)$ and $\eta(0)$. We will find that $\psi(0)$ depends on $\eta(0)$.

3.2.2 The Jump Conditions

We first recall that $u_e = O(\epsilon^{q-1})$, as shown from our steady-state analysis. As such, we define $u_e = \epsilon^{q-1}\tilde{u}_e$ and integrate (3.17b) over an intermediate domain $(-\delta, \delta)$ with $1 \gg \delta \gg \epsilon$. We use

the facts that $A_e \sim w/\sqrt{v_0},\ \phi \sim \Phi(y)$ and $A_e(\pm\delta) \sim \alpha$, and we obtain, upon letting $\delta/\epsilon \to +\infty$, that

$$\begin{aligned}\epsilon D_0\alpha^2\left[\psi_x\right]_0 + 2D_0\alpha\left[v_{ex}\phi\right]_0 &= 3\epsilon\int_{-\infty}^{\infty} w^2\Phi dy + \frac{\epsilon\psi(0)}{v_0^{3/2}}\int_{-\infty}^{\infty} w^3 dy \\ &\quad + \frac{q\epsilon\tilde{u}_e}{v_0^{(q-1)/2}}\int_{-\infty}^{\infty} w^{q-1}\Phi dy + \frac{\epsilon\eta(0)}{v_0^{q/2}}\int_{-\infty}^{\infty} w^q dy + O(\epsilon^2\lambda)\,,\end{aligned}$$

where we used the notation $[a]_0 \equiv a(0^+) - a(0^-)$.

Since $\phi = O(\epsilon^3)$ in the outer region, we can neglect the second term on the left-hand side of this expression. For eigenvalues for which $\lambda \ll O(\epsilon^{-1})$, we obtain that

$$D_0\alpha^2[\psi_x]_0 = 3\int w^2\Phi + \frac{\psi(0)}{v_0^{3/2}}\int w^3 + \frac{q\tilde{u}_e}{v_0^{(q-1)/2}}\int w^{q-1}\Phi + \frac{\eta(0)}{v_0^{q/2}}\int w^q\,, \tag{3.20}$$

where we used the convenient shorthand notation that $\int(\dots) \equiv \int_{-\infty}^{\infty}(\dots)\,dy$.

Now from (3.17b), we use $\phi = O(\epsilon^3)$ in the outer region, together the fact with $q > 1$, so that the term $\epsilon^q\eta A_e^q$ is of lower order. In this way, we obtain the following BVP problem for ψ with jump condition across $x = 0$:

$$\begin{aligned}\psi_{xx} &= 0\,, \qquad |x| \le \ell\,, \\ e_0\left[\psi_x\right]_0 &= e_1\psi(0) + e_2\eta(0) + e_3\,, \\ \psi(\ell) &= z\psi(-\ell), \qquad \psi_x(\ell) = z\psi_x(-\ell)\,,\end{aligned} \tag{3.21}$$

where we have defined e_j for $j = 0, \dots, 3$ by

$$e_0 = D_0\alpha^2, \quad e_1 = \frac{1}{v_0^{3/2}}\int w^3, \quad e_2 = \frac{1}{v_0^{q/2}}\int w^q\,, \quad e_3 = 3\int w^2\Phi + \frac{q\tilde{u}_e}{v_0^{(q-1)/2}}\int w^{q-1}\Phi\,. \tag{3.22}$$

This BVP problem for ψ can be solved using the generic procedure outlined in Lemma A.1. This leads to the following expression for the central value of ψ:

$$\psi(0) = -\frac{e_2\eta(0) + e_3}{e_0\left(1 - \cos(\pi j/K)\right)/\ell + e_1}\,. \tag{3.23}$$

This expression shows that we need to calculate $\eta(0)$ as well. To determine this value we first

integrate (3.17c) over the region $|x| = O(\delta)$ to obtain

$$D_0\epsilon^q\alpha^q\left[\eta_x\right]_0 + D_0 q\alpha^{q-1}O(\epsilon^{q+2}) = \epsilon^2\tau_u\lambda\left[\frac{q\epsilon^{q-1}\tilde{u}_e}{\epsilon^{q-1}}\frac{\epsilon}{v_0^{(q-1)/2}}\int w^{q-1}\Phi + \frac{\epsilon}{v_0^{q/2}}\eta(0)\int w^q\right].$$

If we define $\hat{\tau_u}$ by

$$\hat{\tau_u} \equiv \epsilon^{q-3}\tau_u\,, \tag{3.24}$$

we can write the expression above as

$$D_0\alpha^q\left[\eta_x\right]_0 = \hat{\tau_u}\lambda\left[\frac{q\tilde{u}_e}{v_0^{(q-1)/2}}\int w^{q-1}\Phi + \frac{1}{v_0^{q/2}}\eta(0)\int w^q\right]. \tag{3.25}$$

We observe that $\hat{\tau}_u = O(1)$ when $q = 3$, and we will use this parameter below as a bifurcation parameter.

Now in the outer region we obtain from (3.17c) that

$$D_0\epsilon^q\alpha^q\eta_{xx} + O(\epsilon^{q+2}) = \epsilon^2\tau_u\lambda\left[O(\epsilon^{q+2}) + O(\epsilon^q)\right].$$

Therefore, if we assume

$$\tau_u \ll O(\epsilon^{-2})\,, \tag{3.26}$$

so that $\hat{\tau_u} \ll O(\epsilon^{q-5})$, then we obtain that $\eta_{xx} = 0$ to a first approximation. In this way, we obtain that the BVP problem for η, with jump condition across $x = 0$, is

$$\begin{aligned}
\eta_{xx} &= 0\,, \qquad |x| \le \ell\,,\\
d_0\left[\eta_x\right]_0 &= d_1\eta(0) + d_2\,,\\
\eta(\ell) &= z\eta(-\ell), \qquad \eta_x(\ell) = z\eta_x(-\ell)\,,
\end{aligned} \tag{3.27}$$

where the constants d_j for $j = 0, \ldots, 2$ are defined by

$$d_0 = D_0\alpha^q, \qquad d_1 = \frac{\hat{\tau}_u\lambda}{v_0^{q/2}}\int w^q, \qquad d_2 = \frac{\hat{\tau}_u\lambda q\tilde{u}_e}{v_0^{(q-1)/2}}\int w^{q-1}\Phi\,. \tag{3.28}$$

Then, by applying Lemma A.1 again, we determine $\eta(0)$ as

$$\eta(0) = -\frac{d_2}{d_0\left(1-\cos(\pi j/K)\right)/\ell + d_1}\,. \tag{3.29}$$

The final step in the analysis is to simplify $\psi(0)$ and express it explicitly in terms of the original parameters, so as to identify the key coefficient $\psi(0)/v_0^{3/2}$ in the NLEP (3.19).

First, since $d_0 = D_0\alpha^q$ and $e_0 = D_0\alpha^2$ have similar forms, this suggests that we define a key factor in the denominators of (3.23) and (3.29) as

$$D_{j,q} \equiv \frac{D_0\alpha^q}{\ell}\left(1-\cos(\pi j/K)\right) \equiv D_j\alpha^q\,, \tag{3.30}$$

where

$$D_j \equiv \frac{D_0}{\ell}\left(1-\cos(\pi j/K)\right)\,. \tag{3.31}$$

We observe that $D_{j,q} < D_{j+1,q}$ for any $j = 1, 2, \ldots, K-2$ and any q.

Then, we substitute (3.30) into both the expressions for $\psi(0)$ and $\eta(0)$, as given in (3.23) and (3.29), and in this way obtain that

$$\psi(0) \;=\; -\frac{1}{D_{j,2}+e_1}\left[e_3 - \frac{e_2 d_2}{D_{j,q}+d_1}\right]\,. \tag{3.32}$$

Before continuing, we use the formula for $\tilde{u}_e$ given in (3.10) to rewrite the expressions for e_1, e_2, e_3, d_1, and d_2 as

$$e_1 = \frac{\int w^3}{v_0^{3/2}}, \qquad e_2 = \frac{\int w^q}{v_0^{q/2}}, \qquad e_3 = 3\int w^2\Phi + \frac{U_0\sqrt{v_0}}{K}\frac{q\int w^{q-1}\Phi}{\int w^q}\,,$$
$$d_1 = \hat{\tau}_u\lambda\frac{\int w^q}{v_0^{q/2}}, \qquad d_2 = \hat{\tau}_u\lambda\left(\frac{U_0\sqrt{v_0}}{K}\frac{q\int w^{q-1}\Phi}{\int w^q}\right)\,.$$

With these expressions we can write $\psi(0)$ as

$$\begin{aligned}\psi(0) \;&=\; -\frac{1}{e_1}\frac{1}{1+D_{j,2}/e_1}\left[e_3 - \frac{(e_2/d_1)\,d_2}{1+D_{j,q}/d_1}\right]\\ &=\; -\frac{v_0^{3/2}}{\int w^3}\frac{1}{1+v_0^{3/2}D_{j,2}/\int w^3}\left[e_3 - \frac{d_2/\left(\hat{\tau}_u\lambda\right)}{1+v_0^{q/2}D_{j,q}/\int w^q/\left(\hat{\tau}_u\lambda\right)}\right]\,.\end{aligned}$$

We simplify the expression in the bracket by noting that $e_3 = 3\int w^2\Phi + d_2/\left(\hat{\tau}_u\lambda\right)$, which yields

$$e_3 - \frac{d_2/\left(\hat{\tau}_u\lambda\right)}{1+v_0^{q/2}D_{j,q}/\int w^q/\left(\hat{\tau}_u\lambda\right)}\cdot \\ = 3\int w^2\Phi + \left(1-\frac{\hat{\tau}_u\lambda}{\hat{\tau}_u\lambda + v_0^{q/2}D_{j,q}/\int w^q}\right)\left(\frac{U_0\sqrt{v_0}}{K}\frac{q\int w^{q-1}\Phi}{\int w^q}\right).$$

We then group terms together to define a key quantity χ as

$$\chi \equiv -\frac{\psi(0)}{v_0^{3/2}} = \frac{1}{1+v_0^{3/2}D_{j,2}/\int w^3}\left[\frac{3\int w^2\Phi}{\int w^3} + \right. \\ \left. \frac{v_0^{q/2}D_{j,q}/\int w^q}{\hat{\tau}_u\lambda + v_0^{q/2}D_{j,q}/\int w^q}\left(\frac{U_0\sqrt{v_0}}{K\int w^3}\cdot\frac{q\int w^{q-1}\Phi}{\int w^q}\right)\right]. \quad (3.33)$$

This expression motivates the introduction of a few new quantities

$$\chi_{0,j} \equiv \frac{1}{1+v_0^{3/2}D_{j,2}/\int w^3}, \qquad \chi_{1,j} \equiv \frac{U_0\sqrt{v_0}}{K\int w^3}\frac{\chi_{0,j}}{\mathcal{C}_q(\lambda)}, \qquad \mathcal{C}_q(\lambda) \equiv 1 + \frac{\hat{\tau}_u\lambda}{v_0^{q/2}D_{j,q}/\int w^q}, \quad (3.34)$$

so that χ can be written compactly as

$$\chi(\lambda) \equiv \chi_{0,j}\frac{3\int w^2\Phi}{\int w^3} + \chi_{1,j}(\lambda)\frac{q\int w^{q-1}\Phi}{\int w^q}. \quad (3.35)$$

We observe that $\mathcal{C}_q(0) = 1$ and $\chi_{1,j}(0) = \frac{U_0\sqrt{v_0}}{K\int w^3}\chi_{0,j}$.

Finally, we substitute these expression back into our NLEP (3.19), and in this way derive the main result of this section, which we summarize as follows:

Proposition 3.6. *(Principal Result) The linear stability of a symmetric $K-$hotspot state given by Theorem 3.3 is governed by the spectrum of the following NLEP:*

$$L_0\Phi - \chi(\lambda)w^3 = \lambda\Phi, \quad (3.36)$$

where the local operator is given by

$$L_0\Phi \equiv \Phi'' - \Phi + 3w^2\Phi, \quad (3.37)$$

and where the multiplier $\chi(\lambda)$ consists of two nonlocal terms of the form

$$\chi(\lambda) = \chi_{0,j}\frac{3\int w^2\Phi}{\int w^3} + \chi_{1,j}(\lambda)\frac{q\int w^{q-1}\Phi}{\int w^q}\,, \tag{3.38}$$

with coefficients defined in 3.34.

3.2.3 The Competition Instability Threshold

We now turn to determining the competition instability threshold value of the diffusivity D, which is characterized by the zero eigenvalue crossing of the NLEP. Before proceeding, we remind ourselves of the assumptions made on the model parameters during the construction of the steady-state solution and the derivation of the NLEP, which are that

$$q > 1, \qquad U_0 < U_{0,\max} \equiv S(\gamma-\alpha), \qquad \tau_u \ll O(\epsilon^{-2})\,.$$

We set $\lambda = 0$ in (3.36) together with $\Phi = w$. Then, since $L_0 w = 2w^3$, we have $(2-\chi(0))\,w^3 = 0$, so that $\chi(0) = 2$. We then calculate,

$$2 = \chi(0) = \chi_{0,j}\frac{3\int w^2\cdot w}{\int w^3} + \chi_{1,j}(0)\frac{q\int w^{q-1}\cdot w}{\int w^q} = 3\chi_{0,j} + q\left(\frac{U_0\sqrt{v_0}}{K\int w^3}\chi_{0,j}\right)\,,$$

which determines $\chi_{0,j}$ as

$$\chi_{0,j} = \frac{2}{3 + qU_0\sqrt{v_0}/K\int w^3}\,. \tag{3.39}$$

We then recall the definition of $\chi_{0,j}$ given in (3.34), which yields then algebraic equation for $D_{j,2}$ given by

$$\frac{1}{1+v_0^{3/2}D_{j,2}/\int w^3} = \frac{2}{3+qU_0\sqrt{v_0}/K\int w^3}$$

Upon solving for the critical value of $D_{j,2}$, we get

$$D^*_{j,2} = \frac{1}{2}\frac{\int w^3}{v_0^{3/2}}\left(1 + qU_0\sqrt{v_0}/K\int w^3\right)\,. \tag{3.40}$$

For convenience, we define ω by

$$\omega \equiv U_{0,\max} - U_0 = S(\gamma - \alpha) - U_0\,, \tag{3.41}$$

and rewrite $\sqrt{v_0}$ given in (3.12) in terms of ω as

$$\sqrt{v_0} = \frac{K\int w^3}{S(\gamma-\alpha)-U_0} = \frac{K}{\omega}\int w^3\,. \tag{3.42}$$

In this way, we can further rewrite (3.40) compactly as

$$D^*_{j,2} = \frac{1}{2\left(\int w^3\right)^2}\frac{\omega^3}{K^3}\left(1+\frac{qU_0}{\omega}\right) = \frac{\omega^3}{4\pi^2K^3}\left(1+\frac{qU_0}{\omega}\right)\,. \tag{3.43}$$

Finally, we recall that the outer domain width of a hotspot is given by $\ell = S/(2K)$, and so from the definition of $D_{j,2}$ given in (3.30), we have that the threshold value for the j-th mode is given by

$$D^*_{j,2} = \frac{D_0\alpha^2\,(2K)}{S}\left(1-\cos(\pi j/K)\right)\,. \tag{3.44}$$

Comparing (3.43) and (3.44) we see that there are $K-1$ zero eigenvalue crossings for the NLEP (3.36), which occur at the following critical values of D_0:

$$D^*_{0,j} \equiv \frac{S}{8\pi^2K^4\alpha^2}\frac{1}{\left[1-\cos(\pi j/K)\right]}\omega^3\left(1+\frac{qU_0}{\omega}\right), \qquad j=1,\ldots,K-1\,, \tag{3.45}$$

where $\omega = S(\gamma-\alpha)-U_0 > 0$.

Remark 3.7.

1. Note that $D_{0,j}$ is undefined for the $j=0$ synchronous mode. We will have to show separately below that no competition instability threshold, corresponding to a zero eigenvalue crossing of the NLEP, exists for a single spike steady-state solution.

2. The original model parameter in (3.2) is D, and so the zero eigenvalue crossings in terms of the diiffusivity D of criminals are at $D = \epsilon^{-2}D_{0,j}$.

We conjecture that when $D_0 < D_0^* \equiv \min_j(D_{0,j}) = D_{0,K-1}$, we will have linear stability for $\hat{\tau}_u$ small enough. However, when $D_0 > D_0^*$ we expect instability. This is studied in some detail

later in the chapter. We summarize our main result for the competition instability threshold derived above as

$$D_0^* \equiv \frac{S}{8\pi^2 K^4 \alpha^2} \frac{1}{[1+\cos(\pi/K)]} \omega^3 \left(1 + \frac{qU_0}{\omega}\right). \tag{3.46}$$

Next, we will analyze the behavior of the competition instability threshold D_0^* with respect to the degree of patrol focus q and the total number U_0 of police.

3.2.4 Interpretation of the Threshold

According to the results in Corollary (3.5), we can use (3.42) to obtain to leading order that

$$A_{\max} \sim \frac{\sqrt{2}}{\sqrt{v_0}} = \frac{\sqrt{2}\omega}{K \int w^3} = \frac{\omega}{K\pi}.$$

Therefore, the amplitude of the hotspot in the attractiveness field is directly proportional to ω, but inversely proportional to the number of hotspots K. However, the amplitude of the criminal density ρ at the hotspot locations is $\rho_{\max} = w^2(0) = 2$, which is independent of all model parameters. In addition, away from the hotspots in the outer region the criminal density is $O(\epsilon^2)$. Therefore, it is the number of hotspots that is the most important factor in reducing the total crime in the domain, and we seek to tune the police related parameters q and U_0 so that the range of diffusivity D_0 for which a K-hotspot pattern is linearly stable is smallest.

By examining (3.46), we observe that D_0^* increases with q in a linear fashion. This predicts that if the police become increasingly focused on patrolling the more crime-attractive areas, and under the assumption that the police-criminal interaction is of the simple type $-U$ which does not depend on criminal density, then paradoxically the range of D_0 where a K-hotspot steady-state exists and is stable increases. Therefore, for the goal of reducing crime hotspots, a police deployment with intense focus on crime-attractive areas does not offer an advantage over that of a less focused patrol. We remark that the lower limit of q is 1 for which the above theory is valid, while $q = 0$ and $q = 2$ corresponds to police exhibiting a pure random walk and a movement mimicking the criminals, respectively.

For a fixed $q > 1$, we next examine how the stability of a K-hotspot steady-state changes with respect to the total police deployment U_0. To this end, we substitute $U_0 = S(\gamma - \alpha) - \omega$

into (3.46) and write D_0^* as a function of ω as

$$D_0^* = \frac{S}{8\pi^2 K^4 \alpha^2} \frac{1}{[1+\cos(\pi/K)]} g(\omega)\,, \qquad \text{where} \qquad g(\omega) \equiv \omega^3(1-q) + qS(\gamma-\alpha)\omega^2\,. \quad (3.47)$$

We now analyze the critical points of $g(\omega)$.

We first observe that $d\omega/dU_0 = -1$ and that $U_0 \to U_{0,\max}$ as $\omega \to 0$. We then differentiate g with respect to U_0 to get

$$\frac{dg}{dU_0} = -3\omega^2(1-q) - 2qS(\gamma-\alpha)\omega = -\omega\left(3\omega(1-q) + 2qS(\gamma-\alpha)\right)\,,$$

which shows that $dg/dU_0 \sim -2\omega qS(\gamma-\alpha)$ as $\omega \to 0$. We conclude that g must have a critical point in $0 < U_0 < U_{0,\max}$, which must be necessarily be a maximum, if and only if

$$\omega_c = \frac{2qS(\gamma-\alpha)}{3(q-1)} < S(\gamma-\alpha)\,, \quad \text{which implies} \quad \frac{2q}{3(q-1)} < 1 \quad \text{so that} \quad q > 3\,.$$

On the range where $q \le 3$ we have $dg/dU_0 < 0$ for $0 < U_0 < U_{0,\max}$.

Our main conclusion from this simple calculus exercise is that if the degree of focus q satisfies $q \le 3$, then D_0^* is monotonically decreasing in U_0, and thus with increasing police deployment U_0 the parameter region where the crime hotspots are stable decreases. However, if $q > 3$, then initially as police deployment increases from zero, the stability of hotspots is paradoxically strengthened until the critical value

$$U_{0,c} \equiv S(\gamma-\alpha) - \omega_c = S(\gamma-\alpha)\frac{q-3}{3(q-1)}\,,$$

is reached. For $U_0 > U_{0,c}$, the hotspot pattern becomes less stable when more police deployment is added. We display these results graphically in Fig. 3.1.

3.2.5 Stability of a Single Spike

The NLEP (3.36) was derived by imposing Floquet boundary conditions to analyze the stability of $K-$hotspot equilibrium with $K > 1$. For the case of a single hotspot, we can impose the Neumann boundary conditions directly on $x = \pm\ell$, as the Floquet analysis is not needed. With

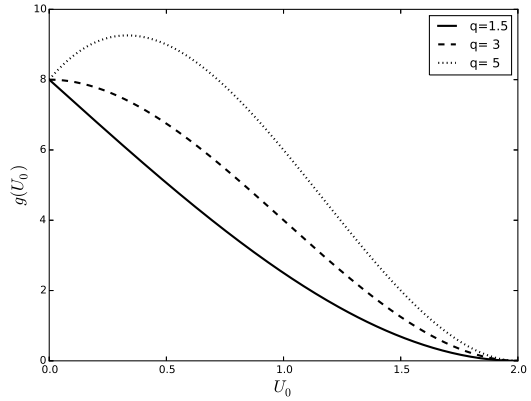

Figure 3.1: Competition instability threshold nonlinearity $g(U_0)$ against police deployment U_0 at various focus degrees q. Other model parameters are $S = 2$, $\gamma = 2$, $\alpha = 1$, so $U_{0,\max} = 2$ as shown in the right-most tick of the figure. The competition instability threshold D_0^* is simply a positive scaling of $g(U_0)$ according to (3.47).

the same procedure as that leading to (3.21) and (3.27) above, we now obtain that

$$\begin{aligned} \psi_{xx} &= 0\,, \qquad |x| \le \ell\,, \\ e_0\,[\psi_x]_0 &= e_1\psi(0) + e_2\eta(0) + e_3\,, \\ \psi_x(\pm\ell) &= 0\,, \end{aligned} \tag{3.48}$$

together with the BVP for $\eta(x)$, given by

$$\begin{aligned} \eta_{xx} &= 0\,, \qquad |x| \le \ell\,, \\ d_0\,[\eta_x]_0 &= d_1\eta(0) + d_2\,, \\ \eta_x(\pm\ell) &= 0\,. \end{aligned} \tag{3.49}$$

Here the coefficients e_0, e_1, e_2, e_3 and d_0, d_1 and d_2, are as defined in (3.22) and (3.28), respectively.

From these two problems it immediately follows that $\eta(x) = \eta(0)$ everywhere and that $\eta(0) = -d_2/d_1$. In addition, we find that $\psi(x) = \psi(0)$ everywhere, with $\psi(0)$ given by

$$\psi(0) = -\frac{1}{e_1}(e_2\eta(0) + e_3)/e_1 = -\frac{1}{e_1}(e_3 - \frac{e_2 d_2}{d_1})\,.$$

This is precisely the formula given in (3.32) with $D_{j,2}$ and $D_{j,q}$ set to zero.

Therefore, by proceeding in the same way as done in the Floquet analysis performed earlier, we simply set $D_{j,2}$ and $D_{j,q}$ to zero in the expression (3.33), and in this way determine χ as

$$\chi \equiv -\frac{\psi(0)}{v_0^{3/2}} = \frac{3\int w^2\Phi}{\int w^3}\,. \tag{3.50}$$

This leads to an NLEP for a single hotspot solution of the form

$$L_0\Phi - 3w^3\frac{\int w^2\Phi}{\int w^3} = \lambda\Phi\,,$$

which is independent of all model parameters. Moreover, it is identical to that given in (2.46) in Chapter 2. We conclude from Lemma 3.2 of [29] that any nonzero eigenvalue of (2.46) must satisfy $\mathrm{Re}(\lambda) < 0$. Therefore, we conclude that a single hotspot steady-state solution is unconditionally stable for any D_0 when $\tau_u \ll O(\epsilon^{-2})$.

3.3 Analysis of the NLEP - Competition Instability and Hopf Bifurcation

3.3.1 Combining the Nonlocal Terms

We now proceed to analyze the NLEP (3.36), which we first write in the following more explicit form by invoking (3.35):

$$\begin{aligned} &L_0\Phi - \chi_{0,j}w^3\frac{3\int w^2\Phi}{\int w^3} - \chi_{1,j}(\lambda)w^3\frac{q\int w^{q-1}\Phi}{\int w^q} = \lambda\Phi\,,\\ &\chi_{0,j} \equiv \frac{1}{1+v_0^{3/2}D_{j,2}/\int w^3}, \qquad \chi_{1,j} \equiv \frac{\chi_{0,j}}{\mathcal{C}_q(\lambda)}\frac{U_0\sqrt{v_0}}{K\int w^3}\,,\\ &\mathcal{C}_q(\lambda) \equiv 1 + \frac{\hat{\tau}_u\lambda}{v_0^{q/2}D_{j,q}/\int w^q}\,. \end{aligned} \tag{3.51}$$

We now use a special property of the local operator L_0, which has the eigenpair $L_0w^2 = 3w^2$ (see Appendix, Section A.2 for a discussion of how we can exploit properties of L_0 to help solve the NLEP). By applying Green's identity to w^2 and Φ, we get $\int\left(w^2L_0\Phi - \Phi L_0w^2\right) = 0$, which

yields

$$\int w^5 \left(\chi_{0,j} \frac{3\int w^2\Phi}{\int w^3} + \chi_{1,j} \frac{q\int w^{q-1}\Phi}{\int w^q} \right) + (\lambda - 3) \int w^2\Phi = 0\,.$$

We combine terms with $\int w^2\Phi$ to find

$$\left(\frac{3\int w^5}{\int w^3}\chi_{0,j} + \lambda - 3 \right) \int w^2\Phi = -\int w^5 \chi_{1,j} \frac{q\int w^{q-1}\Phi}{\int w^q}\,.$$

Since the integral ratio $\int w^5 / \int w^3$ is $3/2$, as seen by using formulas given in (A.12), we can write one nonlocal term in terms of the other as

$$\frac{3\int w^2\Phi}{\int w^3} = \frac{-9}{9\chi_{0,j} + 2(\lambda - 3)} \left(\chi_{1,j} \frac{q\int w^{q-1}\Phi}{\int w^q} \right)\,.$$

Therefore, we may combine the nonlocal terms in the multiplier as follows:

$$\begin{aligned}
\chi &= \chi_{0,j} \frac{3\int w^2\Phi}{\int w^3} + \chi_{1,j}(\lambda) \frac{q\int w^{q-1}\Phi}{\int w^q}\,, \\
&= \left(1 - \frac{9\chi_{0,j}}{9\chi_{0,j} + 2(\lambda - 3)} \right) \chi_{1,j} \frac{q\int w^{q-1}\Phi}{\int w^q}\,, \\
&= \left[\frac{2(\lambda - 3)}{9\chi_{0,j} + 2(\lambda - 3)} \chi_{1,j} \right] \frac{q\int w^{q-1}\Phi}{\int w^q}\,.
\end{aligned}$$

If we define

$$\mathcal{C}(\lambda) \equiv \frac{1}{q\chi_{1,j}} \left(1 + \frac{3}{2} \cdot \frac{3\chi_{0,j}}{\lambda - 3} \right)\,, \tag{3.52}$$

we conclude that 3.51 takes the form

$$L_0\Phi - \chi(\lambda) w^3 \frac{\int w^{q-1}\Phi}{\int w^q} = \lambda\Phi, \qquad \text{where} \qquad \chi = \frac{1}{\mathcal{C}(\lambda)}\,. \tag{3.53}$$

Finally, we write $\mathcal{C}(\lambda)$ in terms of the original model parameters and simplify the resulting expression. First, we substitute $\sqrt{v_0} = K\int w^3/\omega$ into the formula for $\chi_{1,j}$ to get

$$\chi_{1,j} = \frac{\chi_{0,j}}{\mathcal{C}_q(\lambda)} \frac{U_0\sqrt{v_0}}{K\int w^3} = \frac{\chi_{0,j}}{\mathcal{C}_q(\lambda)} \frac{U_0}{\omega}\,.$$

In this way, we obtain that

$$\mathcal{C}(\lambda) = \frac{\omega}{U_0}\frac{\mathcal{C}_q(\lambda)}{q\chi_{0,j}}\left(1+\left(\frac{3}{2}\right)\frac{3\chi_{0,j}}{\lambda-3}\right). \tag{3.54}$$

We eventually would like to express $\mathcal{C}(\lambda)$ in terms of the parameters q and ω. To this end, we first rewrite $\mathcal{C}_q(\lambda)$ and $\chi_{0,j}$, by using $\sqrt{v_0} = K\int w^3/\omega$, as

$$\mathcal{C}_q(\lambda) \equiv 1 + \tilde{\tau}_j\lambda\,, \tag{3.55}$$

where

$$\tilde{\tau}_j = \hat{\tau}_u/\left[\left(\sqrt{2}K\pi/\omega\right)^q D_{j,q}/\int w^q\right], \tag{3.56}$$

and

$$\chi_{0,j} \;=\; \left(1+2\pi^2(K/\omega)^3 D_{j,2}\right)^{-1}. \tag{3.57}$$

Here we have defined new intermediate parameter $\tilde{\tau}_j$ for subsequent notational convenience.

We then define

$$\kappa_q \equiv \left(\frac{\sqrt{2}\pi\alpha K}{\omega}\right)^q / \int w^q\,. \tag{3.58}$$

Upon recalling that $D_{j,q} = \alpha^q D_j$, we arrive at simpler expressions for $\tilde{\tau}_j$ and $\chi_{0,j}$ given by

$$\tilde{\tau}_j \;=\; \frac{\hat{\tau}_u}{\kappa_q D_j}\,, \tag{3.59}$$

$$\chi_{0,j}^{-1} \;=\; 1+\alpha\kappa_3 D_j\,. \tag{3.60}$$

In particular, for the special case where $q = 3$ we have

$$\kappa_3 = \frac{2\sqrt{2}\pi^3\alpha^3K^3}{\omega^3\left(\sqrt{2}\pi\right)} = \frac{2\pi^2\alpha^3K^3}{\omega^3}\,, \tag{3.61}$$

and so for this value of q we have that $\chi_{0,j}^{-1}$ is related to $\tilde{\tau}_j$ rather explicitly as

$$\chi_{0,j}^{-1} = 1+\alpha\hat{\tau}_u/\tilde{\tau}_j\,. \tag{3.62}$$

Remark 3.8. In the study of spikes for similar reaction diffusion systems, $\tilde{\tau}_j$ usually is the result of an "effective" time relaxation constant. Also note that $D_j = D_0 \left(1 - \cos(\pi j/K)\right)/\ell$ appearing in the formulas above is an important factor resulting from the Floquet boundary condition. It was found to be crucially related to the competition instability, corresponding to the zero eigenvalue crossing.

We keep here for a quick reference the form of $\mathcal{C}(\lambda)$ which will be central in a subsequent explicit calculation of eigenvalues:

$$\mathcal{C}(\lambda) = \frac{\omega}{qU_0}\left(1 + \tilde{\tau}_j\lambda\right)\left(\frac{1}{\chi_{0,j}} + \frac{9}{2(\lambda - 3)}\right). \tag{3.63}$$

Remark 3.9.

1. We observe that our current NLEP is of the form

$$L_0\Phi - \left(\frac{a_0 + a_1\lambda}{b_0 + b_1\lambda + b_2\lambda^2}\right) w^3 \frac{\int w^{q-1}\Phi}{\int w^q} = \lambda\Phi\,.$$

   i.e. the multiplier is a proper rational function of degree 2. There have been no prior studies to our knowledge of NLEP's arising from other reaction-diffusion systems with this type of multiplier.

2. The key model parameters we will use to analyze the NLEP will be q and ω. The latter being a complementary quantity defined in relation to the maximum police presence so that hotspots can exist, i.e. $\omega = U_{0,\max} - U_0$, where $U_{0,\max} = S(\gamma - \alpha)$ is defined by the model parameters.

3.3.2 The Zero Eigenvalue Crossing Revisited

We would like to recover our result for the competition instability threshold given in (3.46) to further ascertain that the new form of NLEP with one single nonlocal term is correct.

Upon setting $\lambda = 0$ in (3.63) we get

$$\mathcal{C}(0) = \frac{\omega}{qU_0}\left(\frac{1}{\chi_{0,j}} - \frac{3}{2}\right), \tag{3.64}$$

where we have used the fact that $\mathcal{C}_q(0) = 1$ as noted before. We further set $\Phi = w$ in the multiplier to get

$$\chi = \frac{1}{\mathcal{C}(0)} \frac{\int w^{q-1} \cdot w}{\int w^q} = \frac{1}{\mathcal{C}(0)} \,,$$

so that our NLEP at (3.53) becomes

$$L_0 w = w^3 / \mathcal{C}(0) \,.$$

Then, since $L_0 w = 2w^3$ implies $\mathcal{C}(0) = 1/2$, we arrive at the equation

$$\frac{\omega}{qU_0} \left(\frac{1}{\chi_{0,j}} - \frac{3}{2} \right) = \frac{1}{2} \tag{3.65}$$

Upon solving for $\chi_{0,j}$, we get

$$\frac{1}{\chi_{0,j}} = \left(\frac{3 + qU_0/\omega}{2} \right) \,,$$

which is equivalent to (3.39) since $\omega = \sqrt{v_0}/K \int w^3$ by (3.42). Therefore, the exact same calculations after (3.39) gives that $\mathcal{C}(0) = 1/2$ implies (3.65), which in turn implies that

$$D_{j,2} = D^*_{j,2} \equiv \frac{\omega^3}{4\pi^2 K^3} \left(1 + \frac{qU_0}{\omega} \right) \,. \tag{3.66}$$

Now, note that from the definition of $\chi_{0,j}$ at (3.57), we obtain that $\chi_{0,j}$, given by

$$\chi_{0,j}^{-1} = 1 + 2\pi^2 (K/\omega)^3 D_{j,2} \,,$$

is strictly increasing with $D_{j,2}$. Therefore, when $D_{j,2}$ is not exactly equal to the j-th mode instability threshold $D^*_{j,2}$, we have the following equivalence of inequalities:

$$D_{j,2} < D^*_{j,2} \quad \text{iff} \qquad \frac{\omega}{qU_0} \left(\frac{1}{\chi_{0,j}} - \frac{3}{2} \right) = \mathcal{C}(0) < \frac{1}{2} \,, \tag{3.67}$$

with a similar statement for $D_{j,2} > D^*_{j,2}$.

If we express using $D_j = D_{j,2}/\alpha^2$ instead, the statement $\mathcal{C}(0) = 1/2$ can be found to be

equivalent to the inequality

$$D_j < D_j^* \equiv \frac{\omega^3}{4\alpha^2\pi^2 K^3}\left(1+\frac{qU_0}{\omega}\right). \tag{3.68}$$

3.3.3 Solution to NLEP as Zeros of a Meromorphic Function

We now reformulate (3.53) so that we are seeking the eigenvalues λ as the zeros of some meromorphic function $\zeta(\lambda)$ in the complex plane. We first write (3.53) as

$$(L_0-\lambda)\,\Phi = \left(\frac{1}{\mathcal{C}(\lambda)}\frac{\int w^{q-1}\Phi}{\int w^q}\right) w^3\,,$$

so that

$$\Phi = \frac{1}{\mathcal{C}(\lambda)}\frac{\int w^{q-1}\Phi}{\int w^q}\,(L_0-\lambda)^{-1}\,w^3\,.$$

We then multiply both sides of this expression by w^{q-1} and integrate to get

$$\left(\int w^{q-1}\Phi\right)\left(1-\frac{\mathcal{F}(\lambda)}{\mathcal{C}(\lambda)}\right)=0, \qquad \mathcal{F}(\lambda)\equiv\frac{\int w^{q-1}\,(L_0-\lambda)^{-1}\,w^3}{\int w^q}\,. \tag{3.69}$$

Provided that the eigenfunction satisfies $\int w^{q-1}\Phi \neq 0$, the eigenvalue λ solves

$$\zeta(\lambda)\equiv\mathcal{C}(\lambda)-\mathcal{F}(\lambda)=0\,, \tag{3.70}$$

where $\mathcal{C}(\lambda)$ is a proper rational function of degree 2 defined in (3.54).

We will proceed to analyze the zeros of the meromorphic function at $\zeta(\lambda)=\mathcal{C}(\lambda)-\mathcal{F}(\lambda)$ in two cases: $q=3$ and $q>1$, with the former being explicitly solvable, and the latter requiring the Nyquist criterion to count the number of zeros in the right half plane. Moreover, we will also investigate the possibility of Hopf bifurcation, i.e. seeking solutions of the form $\lambda_\pm=\pm i\lambda_I$ to (3.70)with $\lambda_I>0$.

Remark 3.10. If $\int w^{q-1}\Phi=0$, then the NLEP becomes simply the local eigenvalue problem: $L_0\Phi=\lambda\Phi$ with an extra condition $\int w^{q-1}\Phi=0$. From Proposition 5.6 of [13], we know that there are exactly two discrete eigenvalues, and the only eigenpair with an odd eigenfunction is $\lambda=0$, $\Phi=w'$. This suggests that there should also be discrete spectra of the full problem

that are near zero as $\epsilon \to 0$. These are the "small" eigenvalues that are related to translational instabilities. A relevant treatment for the two-component system without police in the regime $\epsilon \ll 1$, $D = O(1)$ was found in Section 2.7. There we observed a mild instability in the slow dynamics of hotspots with an asymmetrical pattern (different outer region lengths). Our analysis of the NLEP characterizes only those eigenvalues that are $O(1)$ as $\epsilon \to 0$, which can lead to $O(1)$ time-scale instabilities.

3.4 Explicitly Solvable Case $q = 3$ and Asynchronous Oscillations

We now study the stability of a K-hotspot solution and also illustrate the possibility of a Hopf bifurcation for the explicitly solvable case $q = 3$, where $\mathcal{F}(\lambda)$ can be written in a closed form. Rather remarkably, we will be able to reduce the problem of determining unstable spectra of the NLEP to finding pure imaginary solutions to a quadratic equation in the eigenvalue parameter.

When $q = 3$, we can calculate $\mathcal{F}(\lambda)$ explicitly by using the principal eigenpair of L_0 given by $L_0 w^2 = 3w^2$. We consider the integral in the numerator of $\mathcal{F}(\lambda)$, and use integration by parts to get

$$I \equiv \int w^2 \left(L_0 - \lambda\right)^{-1} w^3 = \int w^3 \left(L_0 - \lambda\right)^{-1} w^2 \,.$$

Since $w^2 = \frac{1}{3} L_0 w^2 = \frac{1}{3}\left[(L_0 - \lambda) w^2 + \lambda w^2\right]$, we find that

$$I = \frac{1}{3}\left[\int w^5 + \lambda \int w^3 \left(L_0 - \lambda\right)^{-1} w^2\right] = \frac{1}{3}\left(\int w^5 + \lambda I\right) .$$

Upon solving for I we get $I = -\int w^5/(\lambda - 3)$, and so

$$\mathcal{F}(\lambda) = \frac{I}{\int w^3} = \frac{\int w^5}{\int w^3} \frac{1}{3 - \lambda} = -\left(\frac{3}{2}\right) \frac{1}{\lambda - 3} \,. \tag{3.71}$$

Upon substituting (3.63) and (3.71) into $\zeta(\lambda) = \mathcal{C}(\lambda) - \mathcal{F}(\lambda) = 0$, we get

$$\frac{\omega}{q U_0} \left(1 + \tilde{\tau}_j \lambda\right) \left(\frac{1}{\chi_{0,j}} + \left(\frac{3}{2}\right) \frac{3}{\lambda - 3}\right) = -\left(\frac{3}{2}\right) \frac{1}{\lambda - 3} \,.$$

The resulting equation for λ is simply a quadratic equation, which we write as

$$c_2\lambda^2 + c_1\lambda + c_0 = 0\,, \tag{3.72}$$

which has a positive leading coefficient $c_2 = \tilde{\tau}_j\chi_{0,j}^{-1}/3 > 0$. The other two coefficients in the quadratic are

$$c_1 = \tilde{\tau}_j\left(\frac{3}{2} - \frac{1}{\chi_{0,j}}\right) + \frac{1}{3\chi_{0,j}}, \qquad c_0 = \frac{qU_0}{2\omega} + \frac{3}{2} - \frac{1}{\chi_{0,j}}\,. \tag{3.73}$$

Remark 3.11. If we are only interested in the explicitly solvable case $q = 3$ where $\mathcal{F}(\lambda)$ has a closed-form formula, one could have observed that (3.53) takes the form

$$L_0[\phi] - \chi w^r \int_{-\infty}^{\infty} w^{(p+1)/2}\Phi dy = \lambda\Phi\,,$$

where $r = 3$ and $p = 3$ is the degree of the nonlinearity in the homoclinic equation (2.14). One can then apply the formula in Proposition (A.3) directly to obtain

$$\lambda = \nu_0 - \chi\int_{-\infty}^{\infty} w^{\frac{p+1}{2}+r}dy\,,$$

where $\nu_0 = 3$ is the principal eigenvalue of the local operator L_0. This provides an alternative derivation of (3.72) as well. The above treatment highlights how $\mathcal{F}(\lambda)$ in the general form reduces to a simple function when $q = 3$.

Next, we analyze the complex roots of the quadratic equation (3.72) to determine the location of eigenvalues. We have that $\mathrm{Re}(\lambda) < 0$ iff $c_1 > 0$ and $c_0 > 0$. Firstly, we check that $c_0 > 0$ holds if and only if

$$\frac{qU_0}{2\omega} > \frac{1}{\chi_{0,j}} - \frac{3}{2}$$

which is exactly the inequality (3.67) that in turn is equivalent to $D_{j,2} < D_{j,2}^*$. This confirms that the stability of K-hotspot occurs *only if* $D_{j,2}$ is *below* the competition instability threshold $D_{j,2}^*$. Secondly, we check that the condition $c_1 > 0$ holds if and only if

$$\frac{1}{3\chi_{0,j}} > \tilde{\tau}_j\left(\frac{1}{\chi_{0,j}} - \frac{3}{2}\right)\,, \tag{3.74}$$

which is always true if

$$\frac{1}{\chi_{0,j}} < \frac{3}{2}\,. \tag{3.75}$$

In other words, recalling (3.57), this is equivalent to $1 + 2\pi^2(K/\omega)^3 D_{j,2} < 3/2$, which yields that

$$D_{j,2} < \frac{\omega^3}{4\pi^2 K^3} \equiv D^*_{j,2,\min}\,. \tag{3.76}$$

Thus we have arrived at a threshold (3.76) below which we have stability.

Remark 3.12. We also note in passing that the same statement can also be expressed using D_j and κ_q from (3.58) and (3.31), which yields

$$D_j < D^*_{j,2,\min} \equiv \frac{\omega^3}{4\pi^2\alpha^2 K^3} = \frac{\alpha}{2\kappa_3}\,. \tag{3.77}$$

This suggests a possibility that $D^*_{j,2,\min}$ may not be a uniform bound for all $q \neq 3$ because it depends on κ_3, which can be the result from choosing $q = 3$. In contrast, $D^*_{j,2}$ was derived in (3.66) in a context when $q = 3$ was not assumed. This observation is related to an eventual difficulty we will encounter below for proving stability for the range $D_{j,2} < D^*_{j,2,\min}$ when $q \neq 3$ regardless of τ_u. This furnishes a possible route of investigation in the algebraic relationships between the stability thresholds and the problem parameters.

Finally, for the parameter range where $D^*_{j,2,\min} < D_{j,2} < D^*_{j,2}$, then we find from (3.74) that there is a Hopf bifurcation threshold where purely imaginary complex conjugate eigenvalues exist, given by

$$\tilde{\tau}_{j,\mathrm{Hopf}} \equiv \left(\frac{2}{3}\right)\frac{1}{2 - 3\chi_{0,j}}\,. \tag{3.78}$$

This threshold determines the sign of the coefficient c_1 in the quadratic in the following way:

$$0 < \tilde{\tau}_j < \tilde{\tau}_{j,\mathrm{Hopf}} \quad \text{iff} \quad c_1 > 0\,; \qquad \tilde{\tau}_j > \tilde{\tau}_{j,\mathrm{Hopf}} \quad \text{iff} \quad c_1 < 0\,. \tag{3.79}$$

Therefore, in this interval, instability is governed by an "effective" time relaxation constant $\tilde{\tau}_j$, which leads to the existence of a Hopf bifurcation.

In addition, if we compare the lower threshold $D^*_{j,2,\min}$ with the upper threshold $D^*_{j,2}$ given

in (3.67), we see that

$$\frac{D^*_{j,2}}{D^*_{j,2,\min}} = 1 + \frac{qU_0}{\omega}\,. \tag{3.80}$$

We observe that the case where $D_{j,2}$ lies between $D^*_{j,2}$ and $D^*_{j,2,\min}$ does not exist when $U_0 = 0$, i.e. the removal of the police equation. Conversely, if $U_0 \to U^-_{0,\max}$ so that $\omega = U_{0,\max} - U_0 \to 0^+$, then both $D^*_{j,2}$ and $D^*_{j,2,\min}$ vanish, but $D^*_{j,2}/D^*_{j,2,\min} \to +\infty$.

We now summarize the above findings. The location of the two zeros $\lambda_\pm$ of the meromorphic function $\zeta(\lambda) = \mathcal{C}(\lambda) - \mathcal{F}(\lambda)$, depend on the values of $D_{j,2}$ and $\tilde{\tau}_j$ in the following way:

Proposition 3.13. *Let λ_+, λ_-, with $\mathrm{Re}\lambda_+ \geq \mathrm{Re}\lambda_-$, denote the two solutions of the quadratic equation (3.72) in the complex plane. Then, their location in the complex plane depends on $D_{j,2} = D_0\alpha^2(1-\cos(\pi j/K)/\ell$ in the following way:*

1. If $D_{j,2} > D^*_{j,2} = \frac{\omega^3}{4\pi^2 K^3}\left(1 + \frac{qU_0}{\omega}\right)$, then we have a pair of opposite-signed real eigenvalues $\lambda_+ > 0 > \lambda_-$, and the K-hotspot steady-state is unstable.

2. If $D_{j,2} < D^*_{j,2,\min} = \frac{\omega^3}{4\pi^2 K^3}$, then $\mathrm{Re}\lambda_\pm < 0$, and we have stability.

3. If $D^*_{j,2,\min} < D_{j,2} < D^*_{j,2}$, then if

   (a) $\tilde{\tau}_j = \tilde{\tau}_{j,\mathrm{Hopf}} \equiv \frac{2}{3}\frac{1}{2-3\chi_{0,j}}$, we have $\mathrm{Re}\lambda_\pm = 0$ and a Hopf bifurcation occurs.

   (b) $\tilde{\tau}_j > \tilde{\tau}_{j,\mathrm{Hopf}}$, then $\mathrm{Re}\lambda_\pm > 0$,

   (c) $0 < \tilde{\tau}_j < \tilde{\tau}_{j,\mathrm{Hopf}}$, then $\mathrm{Re}\lambda_\pm < 0$.

Remark 3.14. The multiple hotspot steady-state exhibits an interesting novel phenomenon in the context of the study of the stability of spike patterns to reaction-diffusion systems. Firstly, the window of oscillatory instability, i.e. the interval $(D^*_{j,2,\min}, D^*_{j,2})$, where a Hopf bifurcation occurs can occur is the result of the addition of the police equation with a simple coupling term $-U$ in the ρ-equation (criminal density). In particular, for a two-hotspot equilibrium, then $j = 1$ is the only mode of oscillation, and our theory predicts the possibility of an *asynchronous* Hopf bifurcation so that the amplitudes of the two crime hotspots begin to exhibit temporal anti-phase oscillations. In terms of the urban crime model, this means that when police patrols with a certain specific diffusivity relative to the criminals (determined by $\tilde{\tau}_{j,\mathrm{Hopf}}$), one observes an

interesting picture that the police concentration is drifting to and fro from the hotspots without annihilating any of them. However, if the police patrol diffusivity exceeds such a threshold, then one of the hotspot will dissipate due to an oscillatory instability. Such a qualitative behavior in the possible types of detstabilization of localized spike patterns was not observed in other well-studied reaction-diffusion systems exhibiting similar concentration phenomena, such as the Gray-Scott, Gierer-Meinhardt and Schnakenburg models.

3.4.1 Explicit Determination of Hopf Bifurcation and Stability Region

In this section, we again consider the case $q = 3$, but we will determine stability thresholds for an arbitrary number $K \geq 2$ of hotspots. For $K > 2$, the number of modes j is $K - 1 > 1$. To analyze this more complicated situation, we first express our results above in terms of the original model parameters. We first observe that the expression

$$D_{j,2} = D_0 \alpha^2 \left(1 - \cos(\pi j/K)\right)/\ell \,,$$

implies the following ordering relation:

$$D_{1,2} < D_{2,2} < \cdots < D_{K-1,2} \,.$$

Therefore, for a pattern of K-symmetric hotspot on an interval of length $S = 2K\ell$ with $q = 3$, it is easy to define a sufficient condition for instability and stability, corresponding to Case 1 and 2 of Proposition 3.13 as follows.

We first conclude that we have an unstable real eigenvalue due to the $K-1$-mode whenever $D_{K-1,2} > D^*_{j,2}$. This motivates introducing $D_{0,\mathrm{upper}}$ by

$$\begin{aligned} D_{0,\mathrm{upper}} &\equiv D_0 \left(D^*_{j,2}/D_{K-1,2} \right) \\ &= \frac{S\omega^3}{8\pi^2\alpha^2 K^4 \left(1 + \cos(\pi/K)\right)} \left(1 + \frac{3U_0}{\omega}\right) , \end{aligned}$$

so that we have instability if $D_0 > D_{0,\mathrm{upper}}$.

Similarly, for the eigenvalues with respect to all $j = 1, 2, \ldots, K-1$ modes to be in the left

half-plane $\mathrm{Re}(\lambda) < 0$, we need that $D_{K-1,2} < D^*_{j,2,\min}$. This motivates the introduction of a second threshold $D_{0,\mathrm{lower}}$ by

$$\begin{aligned} D_{0,\mathrm{lower}} &\equiv D_0 \left(D^*_{j,2,\min}/D_{K-1,2} \right) , \\ &= \frac{S\omega^3}{8\pi^2\alpha^2 K^4 \left(1+\cos(\pi/K)\right)} . \end{aligned}$$

We conclude that the K-spike pattern is linearly stable if $D_0 < D_{0,\mathrm{lower}}$.

We observe that the ratio of these two thresholds, given by

$$\frac{D_{0,\mathrm{upper}}}{D_{0,\mathrm{lower}}} = \frac{D^*_{j,2}}{D^*_{j,2,\min}} = 1 + \frac{3U_0}{\omega} ,$$

holds regardless of the value of $\tilde{\tau}_j = \hat{\tau_u}/(\kappa_3 D_j)$. Therefore, this ratio is independent of the value of $\hat{\tau_u} = \tau_u$ as well (since $q = 3$, see (3.24)).

However, if $D_{0,\mathrm{lower}} < D_0 < D_{0,\mathrm{upper}}$, then we certainly have $D^*_{j,2,\min} < D_{K-1,2} < D^*_{j,2}$. As a result, there will be a Hopf bifurcation associated with the $K-1$-mode when $\tilde{\tau}_{K-1} = \tilde{\tau}_{K-1,\mathrm{Hopf}}$, as defined in Proposition 3.13, i.e. at $\tau_u = \kappa_3 D_{K-1} \tilde{\tau}_{K-1,\mathrm{Hopf}}$. Moreover, it can also happen that $D^*_{j,2,\min} < D_{j_0,2}$ for some minimal $1 \le j_0 < K-1$ as well.

This indicates that there can be multiple Hopf bifurcation curves of the form

$$\tau_u = \mathcal{H}_j(D_0) \quad \text{for} \quad j = j_0, j_0+1, \ldots, K-1 ,$$

whose domains may or may not overlap. If they do not overlap, then all the Hopf curves $\mathcal{H}_j$ for $j < K-1$ exist in domains to the right of $D_{0,\mathrm{upper}}$, and consequently do not affect stability since $D_0 > D_{0,\mathrm{upper}}$ is already sufficient to conclude instability due to a real unstable eigenvalue in the $K-1$ mode. However, if they do overlap, then one needs to determine if they have intersection points.

To analyze this more complicated case, we need to first discuss, the domain of $\mathcal{H}_j$, i.e. the range of D_0 so that Hopf bifurcation is possible for each mode j separately.

First, we define oscillatory instability thresholds $D_{0,j}^-$ and $D_{0,j}^+$ for the j-th mode as follows:

$$\begin{aligned} D_{0,j}^- &\equiv D_0\left(D_{j,2,\min}^*/D_{j,2}\right) = \frac{S\omega^3}{8\pi^2\alpha^2K^4\left(1-\cos\frac{j\pi}{K}\right)}\,, \\ D_{0,j}^+ &\equiv D_0\left(D_{j,2}^*/D_{j,2}\right) = D_{0,j}^-\left(1+\frac{3U_0}{\omega}\right) = \frac{S\omega^3}{8\pi^2\alpha^2K^4\left(1-\cos\frac{j\pi}{K}\right)}\left(1+\frac{3U_0}{\omega}\right)\,. \end{aligned}$$

Then, with respect to a specific mode j only, the steady-state is stable if $D_0 < D_{0,j}^-$, is unstable if $D_0 > D_{0,j}^+$, and a Hopf bifurcation occurs at some $\tau_u = \tau_{j,\text{Hopf}}$ when D_0 is on the interval $D_{0,j}^- < D_0 < D_{0,j}^+$.

Notice that $D_{0,\text{lower}} = D_{0,K-1}^-$ and $D_{0,\text{upper}} = D_{0,K-1}^+$. Moreover, we have the following ordering for the thresholds for each mode of oscillation:

$$D_{0,j}^- < D_{0,j}^+ \quad \text{for} \quad j = 1, 2, \ldots, K-1\,, \tag{3.81}$$

owing to the fact that $D_{0,j}^+/D_{0,j}^- = 1 + 3U_0/\omega > 1$. Moreover, if $K \geq 3$, we have

$$D_{0,j+1}^\pm < D_{0,j}^\pm \quad \text{for} \quad j = 1, 2, \ldots, K-2\,, \tag{3.82}$$

as a result of the fact that $D_{j+1,2} > D_{j,2}$ for $j = 1, 2, \ldots, K-2$.

An issue of interest is then to determine whether $D_{0,j+1}^+ \leq D_{0,j}^-$ for all j, so that the domains of the Hopf curves $\mathcal{H}_j$ do not overlap and a complete ordering is possible:

$$D_{0,K-1}^- < D_{0,K-1}^+ \leq D_{0,K-2}^- < D_{0,K-2}^+ \leq \cdots \leq D_{0,1}^- < D_{0,1}^+\,. \tag{3.83}$$

To investigate this issue, we first note that $1 \geq D_{0,j+1}^+/D_{0,j}^- = \left(D_{0,j+1}^-/D_{0,j}^-\right)(1+3U_0/\omega)$ gives the inequality

$$1 + \frac{3U_0}{\omega} \leq \frac{1-\cos\frac{j+1}{K}\pi}{1-\cos\frac{j}{K}\pi}\,,$$

which implies that

$$\omega U_0 \geq \frac{3\left(1-\cos\frac{j\pi}{K}\right)}{\cos\frac{j\pi}{K} - \cos\frac{j+1\pi}{K}}\,.$$

Next, recall that since $\omega = U_{0,\max} - U_0$, the expression above implies the following condition

on the ratio $U_0/U_{0,\max}$ depending on j and K:

$$\begin{aligned}\frac{U_0}{U_{0,\max}} &= \left(\frac{\omega}{U_0}+1\right)^{-1} \\ &\le \frac{\cos\frac{j\pi}{K}-\cos\frac{j+1\pi}{K}}{3-2\cos\frac{j\pi}{K}-\cos\frac{j+1\pi}{K}} \equiv r_{j,K}\,. \end{aligned} \tag{3.84}$$

To maintain a weaker ordering compared to (3.83) so that no other j-th thresholds appear in the interval

$$(D_{0,\mathrm{lower}}, D_{0,\mathrm{upper}}) = \left(D^-_{0,K-1}, D^+_{0,K-1}\right)\,,$$

that is

$$D^-_{0,K-1} < D^+_{0,K-1} \le D^-_{0,K-2} < \cdots\,, \tag{3.85}$$

where terms in the ellipsis is of unknown order (though still subject to the restrictions (3.81) and (3.82)), then, it is sufficient to require that $D^+_{0,K-1} \le D^-_{0,K-2}$ holds, and so we apply $j = K-2$ to (3.84). We would then conclude that (3.85) holds if and only if

$$U_0 \le U_{0,\max}\, r_{K-2,K}\,, \tag{3.86}$$

where $r_{j,K}$ is defined in (3.84).

In such a case, one can conclude that there is only one Hopf curve $\tau_u = \mathcal{H}(D_0)$ due to the $K-1$ mode, with the domain

$$D_{0,\mathrm{lower}} = D^-_{0,K-1} < D_0 < D^+_{0,K-1} = D_{0,\mathrm{upper}}\,.$$

There would then be stability with respect to the remaining modes $j = 1, \ldots, K-2$, because

$$D_0 < D^+_{0,K-1} \le D^-_{0,K-2} < D^-_{0,K-3} < \cdots < D^-_{0,1}\,.$$

Although the condition (3.86) on the total amount of police guarantees this ordering, the actual determination of the threshold values $D^+_{0,j}$'s for $j = 1, \ldots, K-2$ would require further work.

From the numerically computed values in Table 3.1, one sees that (3.86) is quite restrictive and actually implies a complete ordering of the thresholds for the given values of K. For

$j \setminus K$	3	4	5	6
1	0.4000	0.4459	0.4660	0.4766
2		0.1907	0.2297	0.2500
3			0.1129	0.1429
4				0.0752

Table 3.1: Values of the constant $r_{j,K}$ defined in (3.84).

example, stability can occur without a complete ordering if

$$\min_j D^-_{0,j} = D^-_{0,K-1}\,.$$

In general, it is possible that there exists a minimal j_0 so that

$$D^-_{0,j_0} < D^+_{0,K-1}\,.$$

A closer examination of this would require a detailed analysis of the $r_{j,K}$ coefficients, which we do not attempt here.

Instead, we only note that $0 < r_{j,K} < 1$ for any $K \geq 3$ and $j = 1, \ldots K-2$, and we leave open the possibility that $D^+_{0,j_1} > D^-_{0,j_2}$, with $j_1 < j_2$, may occur in general. In particular, we recognize the possibility that the adjacent Hopf curves (i.e $j_1 = j_2 - 1$) may have overlapping regions on their domains. See Fig. 3.2 for an illustration of some possible cases where both overlapping and disjoint domains are possible.

Bearing in mind that the domains of the Hopf curves may overlap, our key question now is to determine whether the graphs $\mathcal{H}_j(D_0)$ could intersect in the $\tau_u - D_0$ plane, leading to the possibility of different modes oscillations depending on the location of D_0 in the interval $(D_{0,\text{lower}}, D_{0,\text{upper}})$.

To this end, we first express $\chi_{0,j}$ in terms of $D^-_{0,j}$ as

$$\chi^{-1}_{0,j} = 1 + 2\pi^2(K/\omega)^3 D_{j,2} = 1 + \frac{D_{j,2}}{2}\left(\frac{4\pi^2K^3}{\omega^3}\right)\,.$$

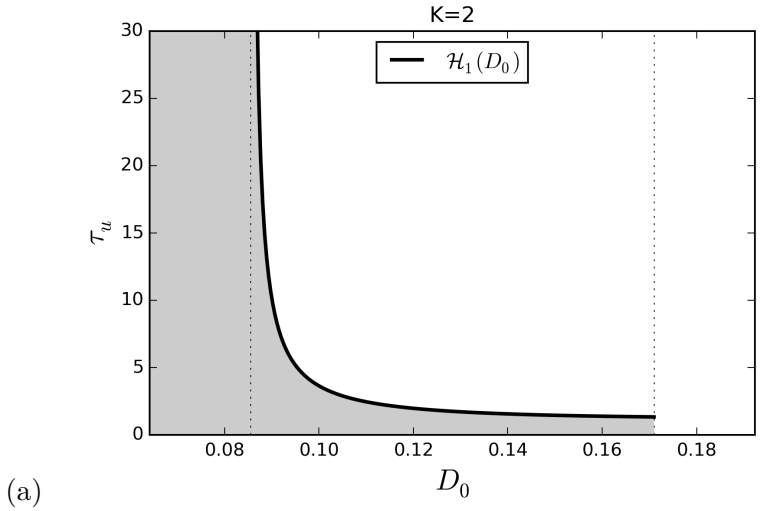

(a)

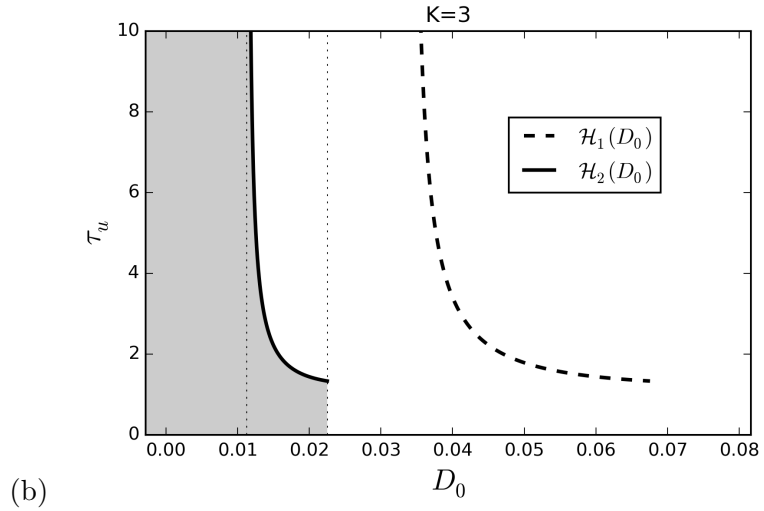

(b)

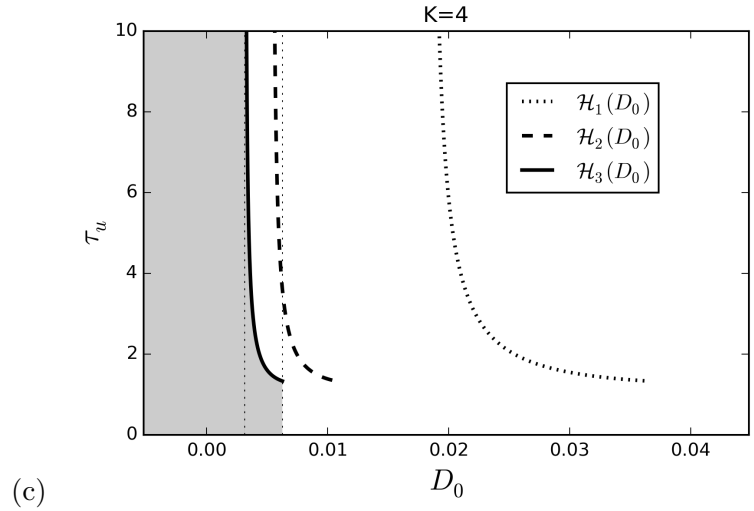

(c)

Figure 3.2: Regions of stability (shaded) and Hopf curves as function of D_0 for $K = 2, 3, 4$ according to (3.92). Model parameters are $S = 4,\ \gamma = 2,\ \alpha = 1,\ U_0 = 1$. The vertical dotted lines denote $D_{0,\text{lower}}$ and $D_{0,\text{upper}}$ respectively.

Then, by using the definition of $D^*_{j,2,\min}$ in (3.76), and recalling (3.81), we get

$$\chi_{0,j}^{-1} = 1 + \frac{D_{j,2}}{2D^*_{j,2,\min}} = 1 + \frac{D_0}{2D^-_{0,j}}\,. \tag{3.87}$$

Then, we can rewrite $\tilde{\tau}_{j,\mathrm{Hopf}}$ as

$$\tilde{\tau}_{j,\mathrm{Hopf}} = \frac{2}{3}\frac{1}{2-3\chi_{0,j}} = \frac{2}{3}\left(\frac{\chi_{0,j}^{-1}}{2\chi_{0,j}^{-1}-3}\right) = \frac{2}{3}\left(\frac{D_0/(2D^-_{0,j})+1}{D_0/D^-_{0,j}-1}\right) = \frac{1}{3} + \left(\frac{D_0}{D^-_{0,j}}-1\right)^{-1}\,. \tag{3.88}$$

Remark 3.15. The simplicity of the final expressions in (3.87) and (3.88) are interesting in their own right, but are not strictly necessary for the following results to hold.

Since we have the ordering $D^-_{0,j+1} < D^-_{0,j}$, we conclude that, for any fixed D_0, it implies that the ordering of the (rescaled) thresholds is

$$\tilde{\tau}_{j+1,\mathrm{Hopf}} < \tilde{\tau}_{j,\mathrm{Hopf}}\,,$$

for all $j = 1, \ldots, K-2$ when $K \geq 3$.

To obtain some qualitative properties for $\tilde{\tau}_{j,\mathrm{Hopf}}$ as a function of $D_{j,2}$, we first observe that for each $j = 1, 2, \ldots K-1$, we have

$$\frac{D_0}{D^-_{0,j}} = \frac{D_{j,2}}{D^*_{j,2,\min}} \to \begin{cases} 1^+ & \text{as } D_{j,2} \to \left(D^*_{j,2,\min}\right)^+\,, \\ 1 + \frac{3U_0}{\omega} & \text{as } D_{j,2} \to D^*_{j,2}\,. \end{cases}$$

This yields the following limiting behaviors for $\tilde{\tau}_{j,\mathrm{Hopf}}$ as $D_{j,2}$ approach the lower and upper thresholds:

$$\tilde{\tau}_{j,\mathrm{Hopf}} \to \begin{cases} +\infty & \text{as } D_{j,2} \to \left(D^*_{j,2,\min}\right)^+\,, \\ \frac{1}{3}\left(1 + \frac{\omega}{U_0}\right) & \text{as } D_{j,2} \to D^*_{j,2}\,. \end{cases} \tag{3.89}$$

Finally, we unpack the definition of $\tilde{\tau}_{j,\mathrm{Hopf}}$ to define the Hopf threshold with respect to the original parameter τ_u. We recall from (3.59) that when $q = 3$ we have $\tau_u = \tilde{\tau}_j D_j \kappa_3$, and so we define

$$\tau_{j,\mathrm{Hopf}} \equiv \tilde{\tau}_{j,\mathrm{Hopf}} D_j \kappa_3\,. \tag{3.90}$$

Therefore, apart from a positive scaling factor $D_j\kappa_3$, the limiting behavior (3.89) still holds qualitatively for $\tau_{j,\text{Hopf}}$.

Finally, according to (3.31), we have $D_{j+1} > D_j$ as well. Therefore, if $D_{0,j}^- < D_{0,j+1}^+$, then for any $D_0 \in \text{Dom}\mathcal{H}_{j+1} \bigcap \text{Dom}\mathcal{H}_j = (D_{0,j}^-, D_{0,j+1}^+)$, we have following majorizing property for the Hopf curves:

$$\tau_{j+1,\text{Hopf}} = \mathcal{H}_{j+1}(D_0) < \mathcal{H}_j(D_0) = \tau_{j,\text{Hopf}}\,, \tag{3.91}$$

with this holding for all $j = 1, \dots K-2$ if $K \geq 3$ whenever there is an intersection of domains. In addition, from (3.89) and (3.90), we also see that the Hopf curves $\tau_{j,\text{Hopf}} = \mathcal{H}_j(D_0)$ tend to $+\infty$ as $D_0 \to D_{0,j}^-$, and to some finite positive limit if $D_0 \to D_{0,j}^+$. This verifies the shape of the numerically computed Hopf bifurcation curves shown in Fig. 3.2.

In conclusion, (3.91) gives a negative answer to the possibility of Hopf curve intersection. More precisely, if $\mathcal{H}_{j_1}$ and $\mathcal{H}_{j_2}$ are any two Hopf curves with $j_1 < j_2$, then their graphs do not intersect even within the overlap of their domains. Instead, the lower mode curve always *majorizes* the higher mode curve wherever they overlap in their domains, according to

$$\mathcal{H}_{j_2}(D_0) < \mathcal{H}_{j_1}(D_0) \quad \text{ for any } \quad D_0 \in \left(D_{0,j_1}^-, D_{0,j_2}^+\right)\,.$$

In other words, for any $D_0 \in (D_{0,\text{lower}}, D_{0,\text{upper}})$, as τ_u increases from 0 to infinity, the first Hopf bifurcation that is triggered is *always* the $K-1$-mode, i.e. the mode associated with the amplitudes of neighboring spikes oscillating in *opposite* directions.

Finally, we would like to determine the formula of $\tau_{j,\text{Hopf}}$ more explicitly in terms of $D_{0,j}^-$. To this end, we first note that

$$\begin{aligned} D_{0,j}^- &= \frac{S}{2K} \cdot \frac{\omega^3}{4\pi^2\alpha^2K^3(1-\cos\frac{j\pi}{K})}\,, \\ &= \frac{\alpha}{2}D_0 \cdot \frac{\ell}{D_0(1-\cos\frac{j\pi}{K})} \cdot \frac{\omega^3}{2\pi^2\alpha^3K^3}\,, \\ &= \frac{\alpha}{2}D_0\,(D_j\kappa_3)^{-1}\,. \end{aligned}$$

By using this expression, we can thus rewrite the scaling factor $\tau_{j,\text{Hopf}}/\tilde{\tau}_{j,\text{Hopf}} = D_j\kappa_3$ (see

(3.90)) as

$$\frac{\tau_{j,\text{Hopf}}}{\tilde{\tau}_{j,\text{Hopf}}} = D_j \kappa_3 = \frac{\alpha}{2} \frac{D_0}{D_{0,j}^-} .$$

With this expression for $\tilde{\tau}_{j,\text{Hopf}}$ in terms of $D_{0,j}^-$ in (3.88), we conclude that

$$\tau_{j,\text{Hopf}} = \mathcal{H}_j(D_0) \equiv \frac{\alpha}{2} \frac{D_0}{D_{0,j}^-} \left[\frac{1}{3} + \left(\frac{D_0}{D_{0,j}^-} - 1 \right)^{-1} \right] , \tag{3.92}$$

which is in agreement with the asymptotic behavior (3.89) as $D_0 \to \left(D_{0,j}^-\right)^-$ derived above, without appealing to this formula. Moreover, we have

$$\mathcal{H}_j(D_{0,j}^+) \quad = \quad \frac{\alpha}{2} \left(\frac{1}{3} + \frac{U_0}{\omega} \right) \left(1 + \frac{\omega}{U_0} \right) .$$

We summarize all these findings in the following main result.

Proposition 3.16. *For $D_{0,\text{lower}} < D_0 < D_{0,\text{upper}}$, a Hopf bifurcation occurs at some unique $\tau_u = \tau_{\text{Hopf}} > 0$ defined as a function of D_0 by*

$$\tau_u = \tau_{\text{Hopf}} = \mathcal{H}_{K-1}(D_0) = \frac{\alpha}{2} \frac{D_0}{D_{0,\text{lower}}} \left[\frac{1}{3} + \left(\frac{D_0}{D_{0,\text{lower}}} - 1 \right)^{-1} \right] , \tag{3.93}$$

where the upper and lower thresholds are defined by

$$D_{0,\text{lower}} \quad \equiv \quad D_{0,K-1}^- = \frac{S\omega^3}{8\pi^2 \alpha^2 K^4 \left(1 + \cos \frac{\pi}{K}\right)} , \tag{3.94a}$$

$$D_{0,\text{upper}} \quad \equiv \quad D_{0,K-1}^+ = D_{0,K-1}^- \left(1 + \frac{3U_0}{\omega} \right) . \tag{3.94b}$$

The oscillation at $\tau_u = \tau_{\text{Hopf}}$ corresponds to the highest mode $j = K-1$, i.e. the amplitudes of neighboring hotspots oscillate in opposite directions (anti-phase oscillatory instability).

If $\tau_u < \tau_{\text{Hopf}}$, we have stability, while if $\tau_u > \tau_{\text{Hopf}}$ we have instability, due to complex eigenvalues with negative and positive real parts respectively.

Moreover, if

$$\tau_u < \tau_{\min} = \lim_{D_0 \to (D_{0,\text{upper}})^-} \mathcal{H}(D_0) = \frac{\alpha}{2} \left(\frac{1}{3} + \frac{U_0}{\omega} \right) \left(1 + \frac{\omega}{U_0} \right) ,$$

the no Hopf bifurcation occurs and the pattern is stable on this interval of D_0.

3.5 General case $q \neq 3$

In this section we analyze the NLEP for the general case where $q \neq 3$.

3.5.1 Determining the Number of Unstable Eigenvalues by the Argument Principle

We will return to the expression given in (3.70) where the discrete eigenvalues of the NLEP are the complex zeros the function $\zeta(\lambda) = \mathcal{C}(\lambda) - \mathcal{F}(\lambda)$. We recall that $\mathcal{C}(\lambda)$ can be written as

$$\mathcal{C}(\lambda) = a(1 + \tilde{\tau}_j \lambda)\left(1 - \frac{b}{3-\lambda}\right), \tag{3.95a}$$

where the coefficients are given by

$$a = \frac{\omega}{qU_0\chi_{0,j}}, \qquad b = \frac{9\chi_{0,j}}{2}, \qquad \chi_{0,j} = (1 + \frac{2\pi^2 K^3}{\omega^3})D_{j,2} = 1 + \alpha\kappa_3 D_j, \tag{3.95b}$$

$$\tilde{\tau}_j = \hat{\tau}_u / \left[\left(\sqrt{2}K\pi/\omega\right)^q D_{j,q} / \int w^q\right] = \frac{\hat{\tau}_u}{\kappa_q D_j}. \tag{3.95c}$$

We observe that $\mathcal{C}(\lambda)$ is a meromorphic function with a simple pole at $\lambda = 3$, and with coefficients defined by all the model parameters.

The latter function $\mathcal{F}(\lambda)$ is also meromorphic with a simple pole at $\lambda = 3$, but is instead defined by integrals involving the local operator L_0 and the ground-state solution w as

$$\mathcal{F}(\lambda) = \frac{\int w^{q-1}(L_0 - \lambda)^{-1} w^3}{\int w^q}. \tag{3.96}$$

It has a closed form given in (3.71) when $q = 3$. Since closed forms for $\mathcal{F}(\lambda)$ are not available for $q \neq 3$, in this section we must appeal to the argument principle to count the number of zeros of the meromorphic function $\mathcal{C}(\lambda) - \mathcal{F}(\lambda)$ in the unstable right half-plane $\mathrm{Re}(\lambda) > 0$.

By using the identity $w^3 = \frac{1}{2} L_0 w$, as given in Lemma A.2, we calculate

$$\begin{aligned} \mathcal{F}(\lambda) &= \frac{1}{2} \frac{\int w^{q-1} \left(L_0 - \lambda\right)^{-1} \left[\left(L_0 - \lambda\right) + \lambda\right] w}{\int w^q} \,, \\ &= \frac{1}{2} + \frac{\lambda}{2 \int w^q} \int w^{q-1} (L_0 - \lambda)^{-1} w \,, \end{aligned} \tag{3.97}$$

which will be in a form more amenable for analysis below. Next, we derive a formula, based on the argument principle, that can be used to determine the number of zeros of $\zeta(\lambda)$ in the right half plane. First we observe that the simple poles of $\mathcal{C}(\lambda)$ and $\mathcal{F}(\lambda)$ do not cancel as $\lambda \to 3^-$, since when restricted to the real line we get

$$\mathcal{F}(\lambda) \to +\infty \quad \text{while} \quad \mathcal{C}(\lambda) \to -\infty \quad \text{as} \quad \lambda \to 3^- \,.$$

We then introduce the anticlockwise "Nyquist" contour that covers the right half plane as $R \to \infty$ consisting of the union of the segments

$$\Gamma_{I_+} = \text{segment from } iR \text{ to } 0, \qquad \Gamma_{I_-} = \text{segment from } 0 \text{ to } -iR,$$
$$C_R = \text{half circle from } -iR \text{ to } iR \,,$$

where $R > 0$. A plot of this contour is shown in Fig. 3.3.

Let N denote the number of roots of $\zeta(\lambda) = 0$ in $\mathrm{Re}(\lambda) > 0$, corresponding to the number of unstable eigenvalues of the NLEP. Then, since the contour encloses the simple pole whenever R is large enough, we have by the argument principle that

$$\lim_{R \to \infty} \Big([\arg \zeta]|_{C_R} + [\arg \zeta]|_{\Gamma_{I_+}} + [\arg \zeta]|_{\Gamma_{I_-}} \Big) = 2\pi(N-1) \,. \tag{3.98}$$

To determine the change in the argument of ζ over the semi-circle, we use the asymptotics of $\mathcal{F}$ and $\mathcal{C}$ as $|\lambda| \to \infty$, given by

$$\mathcal{F}(\lambda) = O(1/|\lambda|) \quad \text{and} \quad \mathcal{C}(\lambda) \sim a\tilde{\tau}\lambda \,,$$

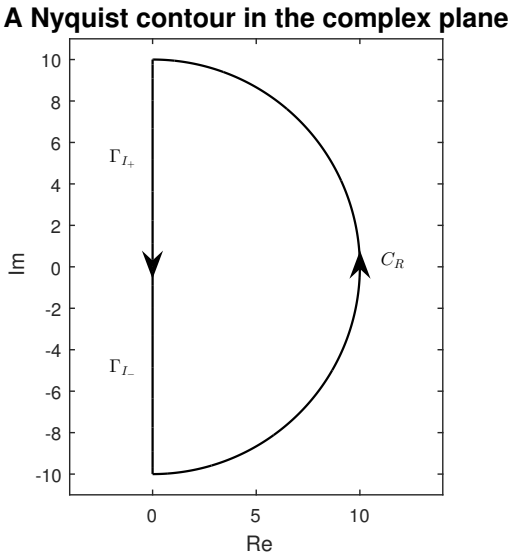

Figure 3.3: Schematic plot of the Nyquist contour used for determining the number of unstable eigenvalues of the NLEP in $\mathrm{Re}(\lambda) > 0$.

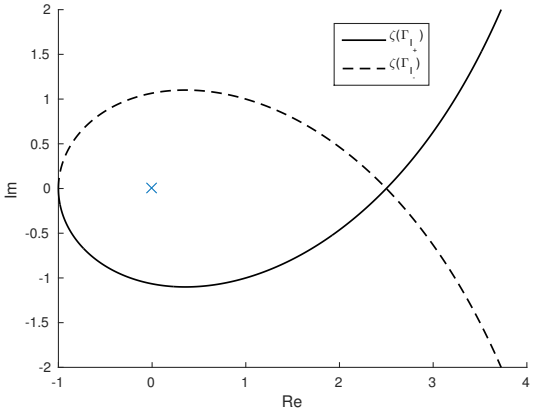

Figure 3.4: An image of the Nyquist contour transformed by ζ. Notice that $\zeta(C_R)$ shrinks to the complex infinity ∞ as $R \to \infty$, and both $\zeta(\Gamma_+)$ and $\zeta(\Gamma_-)$ are asymptotically parallel to the imaginary axis due to (3.101).

to derive that

$$\lim_{R\to\infty} [\arg \zeta]|_{C_R} = \pi, \qquad \text{for any } \tilde{\tau} > 0\,.$$

Therefore the problem of determining the number or unstable eigenvalues is is reduced to computing the change of argument of $\zeta = \mathcal{C} - \mathcal{F}$ as we go down the imaginary axis. In Fig. 3.4 we show a typical picture of how ζ transforms the Nyquist contour. The key question is whether the origin (marked by "x" in the figure) is inside or outside of the fish-shaped loop.

We further observe that since $\overline{\zeta(\lambda)} = \zeta(\overline{\lambda})$, it readily follows that $[\arg\zeta]|_{\Gamma_{I_+}} = [\arg\zeta]|_{\Gamma_{I_-}}$. In this way, we conclude that $2\pi(N-1) = \pi + 2\,[\arg\zeta]|_{\Gamma_{I_+}}$, which determines N as

$$N = \frac{3}{2} + \frac{1}{\pi}\,[\arg\zeta]|_{\Gamma_{I_+}}\,. \tag{3.99}$$

Due to the symmetry, the visual interpretation of whether the "fish loop swallows the origin" (as shown in Fig. (3.4)) then depends crucially on the distinction of whether $\zeta(0) = \mathcal{C}(0) - \mathcal{F}(0)$ is to the left or right of the origin, and then whether the loop is anticlockwise or clockwise with respect to the origin. To this end, we will need to examine the properties of $\mathcal{C}$ and $\mathcal{F}$ on the positive imaginary axis in detail. More explicitly, our strategy in the following sections is to let $\lambda = i\lambda_I$ and let λ_I decrease from ∞ to 0 to determine the behavior of the functions $\mathcal{C}$ and $\mathcal{F}$ in the complex plane.

Before we proceed, we would like to state a typical choice of model parameters, which we will use repeatedly in the subsequent figures for illustrating various stages of the analysis:

$$\alpha = 1,\;\; \gamma = 2,\;\; q = 2,\;\; U_0 = 1,\;\; \ell = 1,\;\; K = 2,\;\; j = 1,\;\; S = 2K\ell = 4\,. \tag{3.100}$$

Our value $q = 2$ corresponds to the "cops on the dots" strategy, whereby the police patrol mimics that of the criminals.

3.5.2 The Starting and Ending Point of the Path and the Two Main Cases

The location of the end of the path at $\lambda_I = 0$ is easily determined. We have $\mathcal{F}(0) = 1/2$ from (3.97), and so

$$\zeta(0) = \zeta_R(0) = \mathcal{C}(0) - \frac{1}{2} = a(1 - \frac{b}{3}) - \frac{1}{2} \in \mathbb{R}\,.$$

Thus, the equation $\zeta(0) = 0$ corresponds to exactly $\mathcal{C}(0) = 1/2$, which we derived in (3.65) in Section 3.3.2 where we studied the competition instability threshold. Moreover, we conclude from (3.95) that

$$\zeta(0) > 0 \quad \text{when} \quad D_{j,2} > D^*_{j,2}\,; \qquad \zeta(0) < 0 \quad \text{when} \quad D_{j,2} < D^*_{j,2}\,.$$

Next, we consider the limiting behavior as $\lambda_I \to +\infty$. We begin by decomposing $\zeta(i\lambda_I)$ into real and imaginary parts as $\zeta(i\lambda_I) \equiv \zeta_R(\lambda_I) + i\zeta_I(\lambda_I)$. Then, we readily have the limiting behavior for $\zeta(i\lambda_I)$ as $\lambda_I \to \infty$, given by

$$\zeta(i\lambda_I) \sim a\,(1 + \tilde{\tau}_j b) + ia\tilde{\tau}_j \lambda_I \quad \text{as} \quad \lambda_I \to +\infty\,,$$

so that

$$\zeta_R(\lambda_I) \sim a(1 + \tilde{\tau}_j b), \qquad \zeta_I(\lambda_I) \sim a\tilde{\tau}_j \lambda_I\,, \quad \text{as} \quad \lambda_I \to \infty\,. \tag{3.101}$$

This means, with respect to the origin, that the path begins asymptotically close to the positive infinity of the imaginary axis.

Therefore, this reduces the problem to determining whether the path crosses the imaginary axis and real axis on the range $0 < \lambda_I < \infty$.

The easiest case to consider is for $D_{j,2} > D_{j,2}^*$ when the end point is on the positive real axis. Then, in order to prove

$$[\arg \zeta]|_{\Gamma_{I_+}} = -\frac{\pi}{2}\,,$$

it suffices to show that the path never crosses the imaginary axis. When this occurs we obtain that $N = 1$, which gives one unique unstable eigenvalue for the NLEP. Fig. 3.5 shows the path $\zeta(\Gamma_{I_+})$ in two distinctive cases.

The next natural step would be to consider $D_{j,2} < D_{j,2}^*$, so that the end point is on the negative real axis. Then, by continuity, the imaginary axis must be crossed. If one can prove monotonicity in the real component it follows that there must be exactly one such crossing, and it would remain to determine whether it occurs on the positive or the negative imaginary axis. If it occurs on the positive imaginary axis, then it is clear that

$$[\arg \zeta]|_{\Gamma_{I_+}} = \frac{\pi}{2}\,,$$

so that $N = 2$, and we have two unstable eigenvalues. Otherwise, if it occurs on the negative imaginary axis, then

$$[\arg \zeta]|_{\Gamma_{I_+}} = -\frac{3\pi}{2}\,.$$

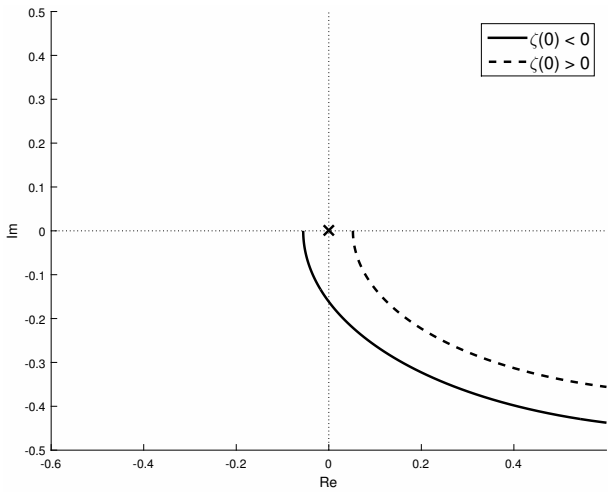

Figure 3.5: Close-up of two distinctive cases of the Nyquist plots for $K = 2$. For the model parameters stated in (3.100), and for $\tau_u = 1$, we show the Nyquist plot for two values of D_0. The upper threshold, corresponding to the competition instability, is given by $D_{0,\text{upper}} = D_{0,1}^{+} \approx 3.103$. The curve with $\zeta(0) < 0$ and $\zeta(0) > 0$ correspond to the choice $D_0 = 3.0$ and $D_0 = 3.2$, respectively. The number of unstable eigenvalues are respectively $N = 0$ and $N = 1$.

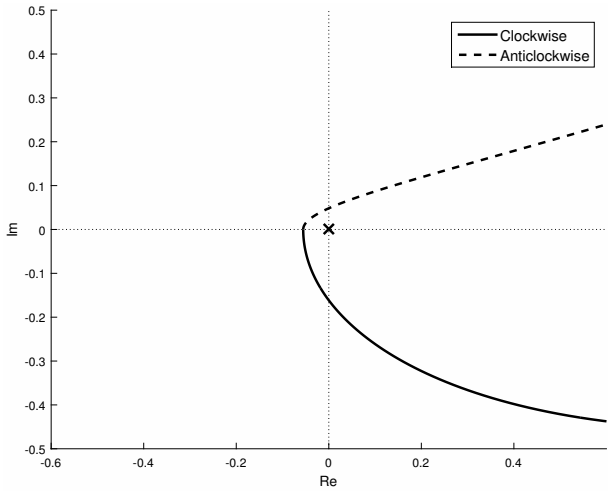

Figure 3.6: Close-up of two distinctive cases of Nyquist plots for $K = 2$. Parameter values common to both are $\alpha = 1$, $\gamma = 2$, $U_0 = 1$, $D_0 = 3$ and $\ell = 1$ (but $S = 2K\ell = 4$). The curves that are clockwise and anticlockwise with respect to the origin correspond to the choices $\tau_u = 1$ and $\tau_u = 4$, respectively. The number of unstable eigenvalues are numerically determined to be $N = 0$ and $N = 2$ for these particular cases.

In this case we would have $N = 0$, and no unstable eigenvalues. See Fig. 3.6 for examples of both paths.

In order to distinguish between these two cases, we must determine detailed properties of the component functions $\mathcal{C}(\lambda)$ and $\mathcal{F}(\lambda)$, and especially for the latter, as it has no closed form

representation.

3.5.3 Key Global and Asymptotic Properties of $\mathcal{C}(\lambda)$ and $\mathcal{F}(\lambda)$

We will analyze the global and asymptotic properties of $\mathcal{C}(\lambda)$ and $\mathcal{F}(\lambda)$ restricted on the positive imaginary axis. We first consider $\mathcal{F}(i\lambda_I) = \mathcal{F}_R(\lambda_I) + i\mathcal{F}_I(\lambda_I)$ where

$$\mathcal{F}(i\lambda_I) = \frac{\int w^{q-1}(L_0 - i\lambda_I)^{-1} w^3}{\int w^q}\,.$$

If we rewrite the operator as

$$\begin{aligned}(L_0 - i\lambda_I)^{-1} &= (L_0 + i\lambda_I)\left[(L_0 + i\lambda_I)^{-1}(L_0 - i\lambda_I)^{-1}\right], \\ &= L_0\left[L_0^2 + \lambda_I^2\right]^{-1} + i\lambda_I\left[L_0^2 + \lambda_I^2\right]^{-1},\end{aligned}$$

we readily obtain upon separating the real and imaginary parts that

$$\mathcal{F}_R(\lambda_I) = \frac{\int w^{q-1} L_0\left[L_0^2 + \lambda_I^2\right]^{-1} w^3}{\int w^q}\,, \qquad \mathcal{F}_I(\lambda_I) = \frac{\lambda_I \int w^{q-1}\left[L_0^2 + \lambda_I^2\right]^{-1} w^3}{\int w^q}\,. \tag{3.102}$$

Now, we call some rigorous results for $\mathcal{F}_R(\lambda_I)$ and $\mathcal{F}_I(\lambda_I)$, as proved in [52].

Fact 3.17.

The real functions $\mathcal{F}_R(\lambda_I)$ and $\mathcal{F}_I(\lambda_I)$ have the following properties:

(i) $\mathcal{F}_R(\lambda_I) = O(\lambda_I^{-2})$ *as* $\lambda_I \to +\infty$, $\quad \mathcal{F}_R(0) = 1/2$.

(ii) $\mathcal{F}_R'(\lambda_I) < 0$ *when* $q = 2$ *[Proposition 3.1 of [52]].*

(iii) $\mathcal{F}_I(\lambda_I) = O(\lambda_I^{-1})$ *as* $\lambda_I \to +\infty$.

(iv) $\mathcal{F}_I(\lambda_I) \sim \frac{\lambda_I}{4}\left(1 - \frac{1}{q}\right) > 0$ *as* $\lambda_I \to 0^+$ *when* $q > 1$ *[Proposition 3.2 of [52]].*

(v) $\mathcal{F}_I(\lambda_I) > 0$ *for* $q = 2$ *and* $q = 4$.

For $q = 3$, we have the explicit formula $\mathcal{F}(\lambda) = \left(\frac{3}{2}\right)\frac{1}{3-\lambda}$ from 3.71, and so for this case it is easy to calculate that

$$\mathcal{F}(i\lambda_I) = \frac{3}{2}\left(\frac{1}{3 - i\lambda_I}\right) = \frac{3}{2}\left(\frac{3 + i\lambda_I}{9 + \lambda_I^2}\right) = \frac{3}{2}\left(\frac{3}{9 + \lambda_I^2} + i\frac{\lambda_I}{9 + \lambda_I^2}\right).$$

Therefore, for $q = 3$, we have the explicit formulas

$$\mathcal{F}_R(\lambda_I) = \frac{3}{2}\frac{3}{9+\lambda_I^2}, \qquad \mathcal{F}_I(\lambda_I) = \frac{3}{2}\frac{\lambda_I}{9+\lambda_I^2}\,, \tag{3.103}$$

which show clearly that property (v) is also true for $q = 3$.

Moreover, we can then further compute

$$\mathcal{F}_R'(\lambda_I) = -\frac{9\lambda_I}{\left(9+\lambda_I^2\right)^2}, \qquad \mathcal{F}_I'(\lambda_I) = \frac{3(3-\lambda)(3+\lambda)}{2\left(9+\lambda_I^2\right)^2}\,, \tag{3.104}$$

and

$$\mathcal{F}_R''(\lambda_I) = \frac{27(\lambda_I^2-3)}{\left(9+\lambda_I^2\right)^3}\,. \tag{3.105}$$

Therefore, it follows that (ii) is true for $q = 3$, and furthermore, we observe that there is a unique maximum of $\mathcal{F}_I$ occurring at the principal eigenvalue of L_0 given by

$$\lambda_I = 3 = \nu_0\,,$$

and that the inflection point of $\mathcal{F}_R$ occurs at

$$\lambda_I = \sqrt{3} = \sqrt{\nu_0}\,.$$

Apart for the asymptotic behaviors (i) , (iii) and (v) which is known to be true for all $q > 1$, we now have some sound reasons to further assume for (ii) and (iv) that the following conjecture should hold:

Conjecture 3.18. *The properties (ii) and (iv) in Fact 3.17 still hold for all* integers $q > 1$*, i.e.*

$$\mathcal{F}_R'(\lambda_I) < 0, \qquad \mathcal{F}_I(\lambda_I) > 0\,. \tag{3.106}$$

We already have rigorous justifications that $\mathcal{F}_R'(\lambda_I) < 0$ when $q = 2, 3$ and that $\mathcal{F}_I(\lambda_I) > 0$ when $q = 2, 3, 4$. In Fig. 3.7 we plot the numerically computed functions $\mathcal{F}_R(\lambda_I)$ and $\mathcal{F}_I(\lambda_I)$ for various values of q.

Next we consider $\mathcal{C}(\lambda)$ restricted to the positive imaginary axis. We first separate $\mathcal{C}(i\lambda_I)$

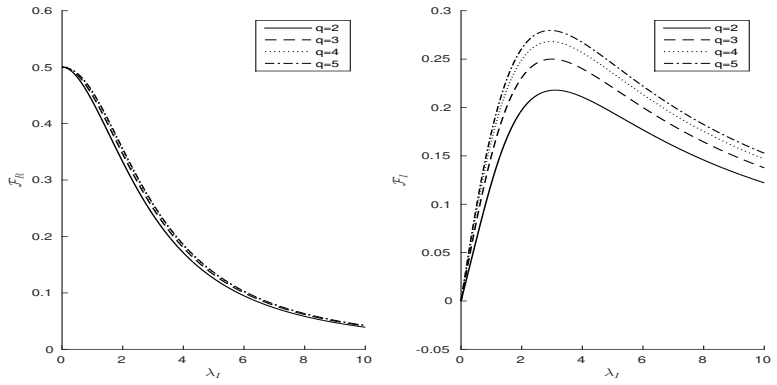

Figure 3.7: Plots of $\mathcal{F}_R$ and $\mathcal{F}_I$ for $q = 2, 3, 4, 5$. Note that $\mathcal{F}_R(0) = 1/2$ and $\mathcal{F}_I(0) = 0$, and that the maximum of $\mathcal{F}_I$ occurs near $\lambda_I = 3$. In fact, the maximum does occur exactly at $\lambda_I = 3$ when $q = 3$.

into its real and imaginary parts as

$$\mathcal{C}(i\lambda_I) = a\,(1 + i\tilde{\tau}_j\lambda_I)\left(1 - \frac{b}{3 - i\lambda_I}\right) = a\,(1 + i\tilde{\tau}_j\lambda_I)\left(1 - \frac{b(3 + i\lambda_I)}{9 + \lambda_I^2}\right)$$

Therefore, if we denote $\mathcal{C}(i\lambda_I) = \mathcal{C}_R(\lambda_I) + i\mathcal{C}_I(\lambda_I)$, we have that

$$\mathcal{C}_R(\lambda_I) = a\left(1 + \tilde{\tau}_j b - \frac{3b}{9 + \lambda_I^2}\,(1 + 3\tilde{\tau}_j)\right), \tag{3.107a}$$

$$\mathcal{C}_I(\lambda_I) = \frac{a\lambda_I}{9 + \lambda_I^2}\left(3\tilde{\tau}_j\,(3 - b) - b + \tilde{\tau}_j\lambda_I^2\right). \tag{3.107b}$$

We now list several elementary properties of $\mathcal{C}_R(\lambda_I)$ and $\mathcal{C}_I(\lambda_I)$.

Properties of $\mathcal{C}_R(\lambda_I)$

(i) $\mathcal{C}_R(0) = a(1 - b/3)$. Therefore, $\mathcal{C}_R(0) > 0$ if and only if $b < 3$ (also, $\mathcal{C}_R(0) < 0$ if and only if $b > 3$).

We also had earlier a similar condition that $\mathcal{C}_R(0) > 1/2$ if and only if $b - 3 + 3/(2a) < 0$, which occurs if and only if $D_{j,2} > D^*_{j,2}$.

(ii) $\mathcal{C}_R'(\lambda_I) > 0$ for $\lambda_I > 0$, and $\mathcal{C}_R(\lambda_I) \to a(1 + \tilde{\tau}_j b) > 0$ as $\lambda_I \to \infty$.

(iii) Suppose $b > 3$, then $\mathcal{C}_R(\lambda_I) < 0$ on the interval

$$0 < \lambda_I < \sqrt{\frac{3(b-3)}{1 + \tilde{\tau}_j b}}.$$

Properties of $\mathcal{C}_I(\lambda_I)$

(iv) $\mathcal{C}_I(\lambda_I) \sim a\lambda_I\left[3\tilde{\tau}_j(3-b)-b\right]$ as $\lambda_I \to 0^+$, and $\mathcal{C}_I(\lambda_I) \sim a\tilde{\tau}_j\lambda_I$ as $\lambda_I \to +\infty$.

(v) $\mathcal{C}_I(\lambda_I) < 0$ on $0 < \lambda_I^2 < 3(b-3) + b/\tilde{\tau}_j$. Otherwise, we have $\mathcal{C}_I(\lambda_I) > 0$.

Therefore, if $b > 3/(1+\frac{1}{3\tilde{\tau}_j})$, it follows that there is a range of λ_I, given by

$$0 < \lambda_I < \sqrt{3(b-3)+\frac{b}{\tilde{\tau}_j}} \equiv \lambda_{I_I}\,,$$

for which $\mathcal{C}_I(\lambda_I) < 0$.

(vi) Alternatively if $b < 3/(1+\frac{1}{3\tilde{\tau}_j})$, we can then show that $\mathcal{C}_I(\lambda_I) > 0$ for all $\lambda_I > 0$.

To establish property (vi) above we begin by calculating

$$\mathcal{C}_I'(\lambda_I) = \frac{a}{(9+\lambda_I^2)^2}\left[\tilde{\tau}_j\lambda_I^4 + \lambda_I^2\left(18\tilde{\tau}_j + b + 3b\tilde{\tau}_j\right) + 9\left(\tilde{\tau}_j(9-3b)-b\right)\right]. \tag{3.108}$$

The expression in the brackets of 3.108 is a quadratic in $x = \lambda_I^2$, and upon setting $\mathcal{C}_I'(\lambda_I) = 0$, we see that the two roots $x_+ \geq x_-$ satisfy

$$x_+ + x_- = -\left[18\tilde{\tau}_j + b + 3b\tilde{\tau}_j\right]/\tilde{\tau}_j, \qquad x_+x_- = 9\left(\tilde{\tau}_j(9-3b)-b\right)/\tilde{\tau}_j\,.$$

Since $x_+ + x_- < 0$ always holds, there is a root $x_+ = \lambda_I^2 > 0$ if and only if $x_+x_- < 0$. It follows that there exists $\lambda_I^2 > 0$ for which $\mathcal{C}_I'(\lambda_I) = 0$ if and only if $\tilde{\tau}_j(9-3b) - b < 0$, which implies that $b > 3/(1+\frac{1}{3\tilde{\tau}_j})$ must hold. Therefore, $\mathcal{C}_I'(\lambda_I) > 0$ for any $\lambda_I > 0$, and with the fact that $\mathcal{C}_I(0) = 0$, we conclude $\mathcal{C}_I(\lambda_I) > 0$ always holds as well. This establishes property (v) for $\mathcal{C}_I(\lambda_I)$.

In Fig. 3.8 we show various plots of $\mathcal{C}_R(\lambda_I)$ and $\mathcal{C}_I(\lambda_I)$ for $\tau_u = 1$ and for the model parameters given in (3.100). These plots illustrate our established properties for $\mathcal{C}_R(\lambda_I)$ and $\mathcal{C}_I(\lambda_I)$.

From property (ii) of $\mathcal{C}_R(\lambda_I)$ we have $\mathcal{C}_R'(\lambda_I) > 0$, while from property (ii) of $\mathcal{F}_R(\lambda_I)$ we

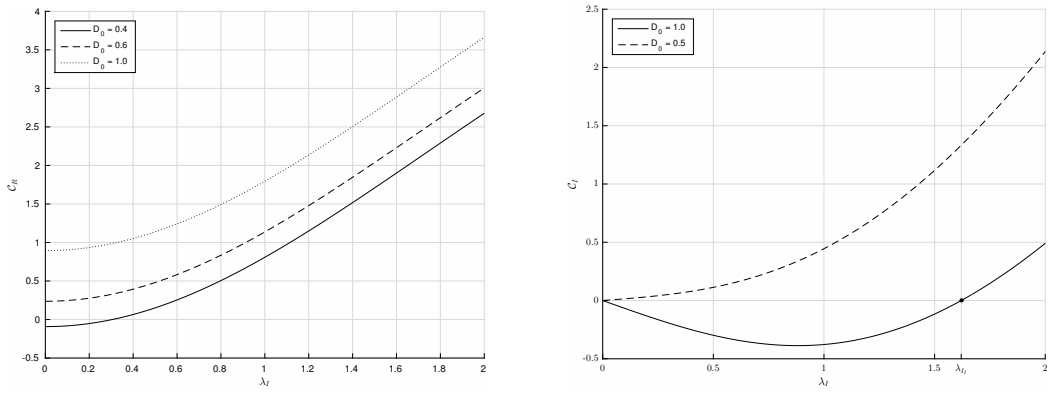

Figure 3.8: Plots of $\mathcal{C}_R$ and $\mathcal{C}_I$ for $\tau_u = 1$ and the model parameters given in (3.100). The value for D_0 was chosen as follows for each curve: Left figure: three cases of $\mathcal{C}_R(\lambda_I)$ are plotted: (i) $b > 3$ ($D_0 = 0.4$), (ii) $3 - 3/(2a) < b < 3$ ($D_0 = 0.6$), (iii) $b < 3 - 3/(2a)$ ($D_0 = 1.0$). Right figure: two cases of $\mathcal{C}_I(\lambda_I)$ are plotted: (i) $b < 3/\left(1 + 1/(3\tilde{\tau}_j)\right)$ ($D_0 = 1.0$), $b > 3/\left(1 + 1/(3\tilde{\tau}_j)\right)$ ($D_0 = 0.5$), and the right end point of the interval of negative values for $\mathcal{C}_I$ is at $\lambda_{I_I} \approx 1.6204$, indicated by a heavy dot.

conclude that $\mathcal{F}_R'(\lambda_I) < 0$. Therefore, we have that $\zeta_R(\lambda_I) = \mathrm{Re}\left[\zeta(i\lambda_I)\right]$ satisfies

$$\zeta_R'(\lambda_I) = \mathcal{C}_R'(\lambda_I) - \mathcal{F}_R'(\lambda_I) > 0 \quad \text{for all} \quad \lambda_I > 0\,. \tag{3.109}$$

This leads to a key result that the path $\zeta(\Gamma_{I_+})$ can only intersect the imaginary axis exactly one or zero times. The only remaining issue will be to determine whether any such intersection point occurs on the positive or negative imaginary axis.

3.5.4 Above Competition Instability Threshold $D_{j,2} > D_{j,2}^*$; A Unique Unstable Real eigenvalue

Suppose that $b < 3 - 3/(2a)$ so that $\mathcal{C}_R(0) = \mathcal{C}(0) > 1/2$. Recall from (3.67) that this implies that $D_{j,2} > D_{j,2}^*$, and so we are above the competition instability threshold.

Since $F_R(0) = 1/2$, it follows that the endpoint of the path is at $\zeta(0) = \mathcal{C}_R(0) - \mathcal{F}_R(0) > 0$. Then, since the path $\zeta(\Gamma_{I_+})$ begins "at positive infinity" in the imaginary axis, stays within the right half-plane and ends at the positive real axis, owing to the key monotonicity property (3.109), it follows that we must have $\left[\arg\zeta\right]|_{\Gamma_{I_+}} = -\frac{\pi}{2}$. Therefore, we conclude from (3.99) that

$$N = 3/2 + \frac{1}{\pi}(-\frac{\pi}{2}) = 1 \quad \text{for all} \quad \tilde{\tau}_j > 0\,.$$

Our main conclusion regarding stability for the regime $D_{j,2} > D^*_{j,2}$ is that for any $j = 1, \ldots, K-1$, a K-hotspot steady-state solution is unstable due to a unique positive real eigenvalue that occurs for any $\tilde{\tau_j} > 0$.

3.5.5 Below Competition Instability Threshold $D_{j,2} < D^*_{j,2}$

Now suppose that $b > 3 - 3/(2a)$, so that $\mathcal{C}_R(0) = \mathcal{C}(0) < 1/2$. From (3.67) this means that $D_{j,2} < D^*_{j,2}$ and so we are below the competition instability threshold.

For this case, since $\zeta(0) = \mathcal{C}_R(0) - \mathcal{F}_R(0) < 0$, while $\mathcal{C}'_R(\lambda_I) > 0$ for any $\lambda_I > 0$ and $\mathcal{F}_R(\lambda_I) = 1/2$ at $\lambda_I = 0$ but decreases monotonically to 0 as $\lambda_I \to \infty$ (by Conjecture 3.18), there must be a unique root λ^*_I to $\zeta_R(\lambda^*_I) = 0$. Since $\zeta_I(0) = 0$, the endpoint is on the negative real axis, with exactly one crossing at $\lambda_I = \lambda^*_I$ when traveling from $\lambda_I = +\infty$. It is then clear that there are two distinctly different cases:

(I) If the crossing occurs on the positive imaginary axis, i.e. $\zeta_I(\lambda^*_I) > 0$, then $[\arg \zeta]\,|_{\Gamma_{I_+}} = \pi/2$, and so $N = 2$.

(II) If the crossing occurs on the negative imaginary axis, i.e. $\zeta_I(\lambda^*_I) < 0$, then $[\arg \zeta]\,|_{\Gamma_{I_+}} = -3\pi/2$, and so $N = 0$.

These two distinguishing cases were presented in Fig. 3.6, where we also noticed that case (I) and (II) implies that the curve approaches $\zeta(0) < 0$ as $\lambda_I \to 0^+$ in an anticlockwise and clockwise direction, respectively, with respect to the origin. Therefore, the final key step in the analysis is to distinguish path (I) from path (II).

We first establish that when $b > 3$ we obtain path (II) if either $\tilde{\tau_j} \gg 1$ or $\tilde{\tau_j} \ll 1$. Recall that $b > 3$ means $9\chi_{0,j}/2 > 3$, or equivalently

$$\frac{1}{\chi_{0,j}} < \frac{3}{2}\,.$$

This is precisely the condition (3.75) which was applied to (3.74) to show that the eigenvalues are stable regardless of $\tilde{\tau_j}$ in the $q = 3$ explicitly solvable case. This condition (3.75) implies a lower threshold

$$D_{j,2} < D^*_{j,2,\min} < D^*_{j,2}, \qquad D_{j,2,\min} = \frac{\omega^3}{4\pi^2 K^3}\,,$$

which for $q = 3$ case guarantees stability regardless of $\tilde{\tau_j}$. However, in the general case $q \neq 3$, the lack of an explicit form for $\mathcal{F}(\lambda)$ prevents us from obtaining the same conclusion as easily. We must then appeal to the local and far-field asymptotic properties of $\mathcal{C}$ and $\mathcal{F}$.

Firstly, if $\tilde{\tau_j} \gg 1$, we obtain from (3.107a) that

$$\mathcal{C}_R(\lambda_I) \sim a\left[\tilde{\tau_j} b - \frac{(3b)(3\tilde{\tau_j})}{9+\lambda_I^2}\right] = \frac{a\tilde{\tau_j} b\lambda_I^2}{9+\lambda_I^2}\,.$$

Then, upon setting $\mathcal{C}_R(\lambda_I) = \mathcal{F}_R(\lambda_I)$ and using $\mathcal{F}_R(0) = 1/2$, we obtain that $\zeta_R(\lambda_I) = 0$ has a root with $\lambda_I = O(\tilde{\tau}^{-1/2})$ when $\tilde{\tau} \gg 1$. In particular, if we write $\lambda_I^* = \lambda_{I,0}^* \tilde{\tau_j}^{-1/2}$ so that $\lambda_{I,0}^* = O(1)$, then we see that $ab\left(\lambda_{I,0}^*\right)^2/9 \sim 1/2$, which yields

$$\lambda_{I,0}^* \sim \frac{1}{\sqrt{ab}}\frac{3}{\sqrt{2}}\,.$$

Therefore, $\zeta_R(\lambda_I^*) = 0$ has a unique root when $\tilde{\tau_j} \gg 1$, and that this root is located near the the origin with asymptotics

$$\lambda_I^* \sim \frac{3}{\sqrt{2ab}}\tilde{\tau_j}^{-1/2}\,. \tag{3.110}$$

Now since $\mathcal{C}_I(\lambda_I) < 0$ on the range $0 < \lambda_I < \sqrt{3(b-3)+b/\tilde{\tau_j}} \sim \sqrt{3(b-3)}$ for $\tilde{\tau_j} \gg 1$, we have $\mathcal{C}_I(\lambda_I^*) < 0$ and so $\zeta_I(\lambda_I^*) < 0$. We then conclude that the crossing occurs on the negative imaginary axis as stipulated, which yields path (II).

Next, if we instead consider $\tilde{\tau_j} \ll 1$, then we have from (3.107a) that

$$\mathcal{C}_R(\lambda_I) \sim a\left[1 - \frac{3b}{9+\lambda_I^2}\right] = a\left[\frac{3(3-b)+\lambda_I^2}{9+\lambda_I^2}\right], \tag{3.111}$$

which is independent of $\tilde{\tau_j}$. Thus, the intersection point where $\mathcal{C}_R = \mathcal{F}_R$ must occur at some $\lambda_I^* = O(1)$. However, since $\mathcal{C}_I(\lambda_I) < 0$ on $0 < \lambda_I < \sqrt{3(b-3)+b/\tilde{\tau_j}} = O(\tilde{\tau_j}^{-1/2})$ as $\tilde{\tau_j} \to 0$, which is now asymptotically large as $\tilde{\tau_j} \to 0$, we conclude that $0 < \lambda_I^* = O(1) \ll \sqrt{3(b-3)+b/\tilde{\tau_j}}$. It follows that $\zeta_I(\lambda_I^*) < 0$, and so the crossing occurs on the negative imaginary axis as well. This again yields path (II).

In both cases, since the point $\zeta_I(\lambda_I^*) < 0$ is the only place the curve $\zeta(\Gamma_{I_+})$ crosses the imaginary axis, we have path (II) so that $N = 0$ by the formula (3.99). As a consequence, there

are no unstable eigenvalues of the NLEP.

The remaining issue is to consider whether the statement above regarding N is still true *for any* $\tilde{\tau}_j > 0$ for the general case $q > 1$. We now consider three possible strategies for exploring this question.

One way to begin an analysis is to observe that $\mathcal{F}_R$ is independent of $\tilde{\tau}_j$ and that

$$\mathcal{C}_R(\lambda_I^*) - \mathcal{F}_R(\lambda_I^*) = 0\,, \tag{3.112}$$

gives us an implicit relation for λ_I^* as a function of $\tilde{\tau}_j$. If we differentiate (3.112) with respect to $\tilde{\tau}_j$ we get

$$\frac{\partial}{\partial \lambda_I^*}\mathcal{C}_R(\lambda_I^*)\frac{d\lambda_I^*}{d\tilde{\tau}_j} + \frac{\partial}{\partial \tilde{\tau}_j}\mathcal{C}_R(\lambda_I^*) - \frac{\partial}{\partial \lambda_I^*}\mathcal{F}_R(\lambda_I^*)\frac{d\lambda_I^*}{d\tilde{\tau}_j} = 0\,.$$

By letting $(\dots)'$ denote derivatives with respect to λ_I^*, and by using (3.107a), we obtain that

$$\left[\mathcal{C}_R'(\lambda_I^*) - \mathcal{F}_R'(\lambda_I^*)\right]\frac{d\lambda_I^*}{d\tilde{\tau}_j} = -\frac{\partial}{\partial \tilde{\tau}_j}\mathcal{C}_R(\lambda_I^*) = -ab\left(1 - \frac{9}{9+\lambda_I^2}\right)\,. \tag{3.113}$$

Since $\mathcal{C}_R'(\lambda_I^*) > 0$ and $\mathcal{F}_R'(\lambda_I^*) < 0$ by (3.107a) and Conjecture (3.18), the expression above yields that

$$\frac{d\lambda_I^*}{d\tilde{\tau}_j} < 0\,, \qquad \text{for all} \quad \tilde{\tau}_j\,.$$

Next, we observe that the upper end point of the interval of negativity of $\mathcal{C}_I(\lambda_I)$ is a function of $\tilde{\tau}_j$ as well. We will denote this endpoint as $h(\tilde{\tau}_j)$. It satisfies

$$\frac{dh}{d\tilde{\tau}_j} \equiv \frac{d}{d\tilde{\tau}_j}\sqrt{3(b-3)+b/\tilde{\tau}_j} = -\frac{b}{2\tilde{\tau}_j^2\sqrt{3(b-3)+b/\tilde{\tau}_j}} < 0\,.$$

In this way, we would conclude that the root λ_I^* stays within the interval $(0, h(\tilde{\tau}_j))$ if we can prove that the following inequality holds for all $\tilde{\tau}_j > 0$:

$$\frac{d\lambda_I^*}{d\tilde{\tau}_j} < \frac{dh}{d\tilde{\tau}_j}\,. \tag{3.114}$$

Then, since $\lambda_I^*(\tilde{\tau}_j) \in (0, h(\tilde{\tau}_j))$ has been shown above to be true for $\tilde{\tau}_j \ll 1$, the inequality above

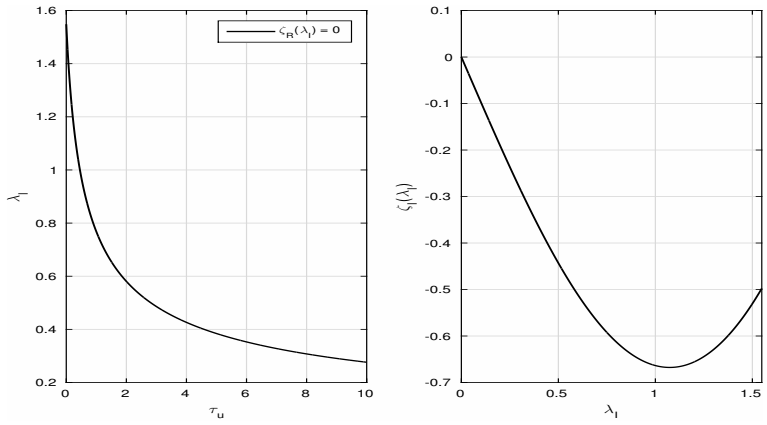

Figure 3.9: Numerical verification of a Nyquist path that predicts stability. Left: a plot of the unique roots to $\zeta_R(\lambda_I) = 0$ as τ_u varies. For very large τ_u, λ_I can be quite close to zero. Right: a plot of the possible range of values of $\zeta_I(\lambda_I)$ when the Nyquist contour hits the imaginary axis, where λ_I was chosen to vary from zero to the maximum value plotted on the left. The model parameters chosen were $D_0 = 0.4$ and the parameters specified in (3.100).

would imply that

$$\lambda_I^*(\tilde{\tau}_j) \in (0, h(\tilde{\tau}_j)) \quad \text{for all} \quad \tilde{\tau}_j > 0\,.$$

However, it seems analytically intractable to prove that (3.114) holds.

A second route of resolution would be to explore this issue numerically. For instance, in Fig. 3.9 we fix $D_0 = 0.4$ so that $b \approx 3.1279 > 3$. Then, we find the unique root to $\zeta_R(\lambda_I) = 0$ for each τ_u from 0 to a large number to determine the range of possible λ_I values so that the eigenvalue is on the imaginary axis. Then, we compute $\zeta_I(\lambda_I)$ for λ_I on this range to determine its sign. For $q = 2$, where the NLEP is not explicitly solvable, we are able to confirm that $\zeta_I(\lambda_I) < 0$. Therefore, since path (II) applies, we conclude that the steady-state spike pattern is linearly stable for this parameter configuration. Nonetheless, it is still desirable to provide an analytical proof to show that the eigenvalues are in $\mathrm{Re}(\lambda) < 0$ for all choices of $q > 1$ and $0 < \tau_u < \infty$.

The final route that we pursue to resolve this final case where $D_{j,2} < D^*_{j,2,\min}$ $(b > 3)$ is to assume an extra condition, as we will derive below. We first observe that $\mathcal{C}_R(\lambda_I) = 0$ at $\lambda_I = \lambda_{I_R} \equiv \sqrt{\frac{3(b-3)}{1+\tilde{\tau}_j b}}$, and we recall that $\mathcal{C}_I(\lambda_I) = 0$ at $\lambda_I = \lambda_{I_I} = \sqrt{(3(b-3) + b/\tilde{\tau}_j}$. Then,

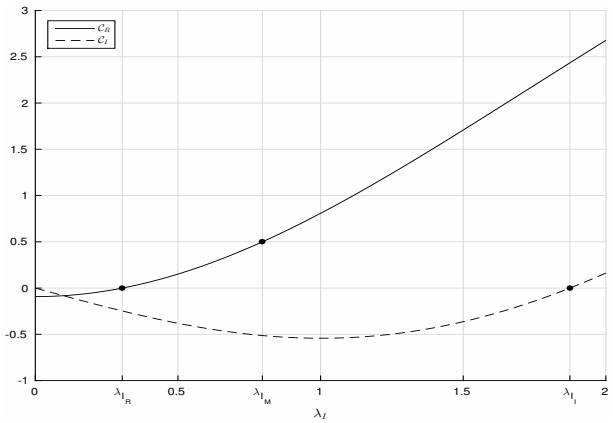

Figure 3.10: Locations of the three special points λ_{I_R}, λ_{I_I} and λ_{I_M} on the graphs of $\mathcal{C}_R$ and $\mathcal{C}_I$ versus λ_I, as discussed in the text. The model parameter values $\tau_u = 1$ and $D_0 = 0.4$, together with those stated in (3.100), were used. The value $b \approx 3.1279 > 3$ was also numerically confirmed.

since $b/\tilde{\tau}_j > 1/(1 + \tilde{\tau}_j b)$ for $b > 1$, it follows that the inequality

$$\lambda_{I_R} < \lambda_{I_I} \, ,$$

holds, because we have $b > 3$. For a typical picture of this scenario, we refer to Fig. 3.10 where we present full numerical computations for a particular parameter set.

We now determine the value λ_{I_M} for which $\mathcal{C}_R(\lambda_{I_M}) = 1/2$. We conclude that the root λ_I^* to $\zeta_R(\lambda_I) = 0$ must occur in $\lambda_{I_R} < \lambda_I^* < \lambda_{I_M}$. If we can further show that $\lambda_{I_M} < \lambda_{I_I}$, so that $\mathcal{C}_I(\lambda_{I_M}) < 0$, it follows also that $\mathcal{C}_I(\lambda_I^*) < 0$. This would imply that $\zeta_I(\lambda_I^*) < 0$ and $N = 0$. Therefore, the desired order of these special values of λ_I, which will guarantee that path (II) holds and so $N = 0$, is that

$$\lambda_{I_R} < \lambda_I^* < \lambda_{I_M} < \lambda_{I_I} \, . \tag{3.115}$$

For a particular set of parameter values this is illustrated in the numerical results shown in Fig. 3.11 .

We now show that the ordering (3.115) does in fact hold under an additional assumption. To show this, we consider the real part of (3.107a), and solve

$$\mathcal{C}_R(\lambda_{I_M}) = \frac{1}{2} = a \left[1 + \tilde{\tau}_j b - \frac{3b}{9 + \lambda_{I_M}^2} \left(1 + 3\tilde{\tau}_j \right) \right] .$$

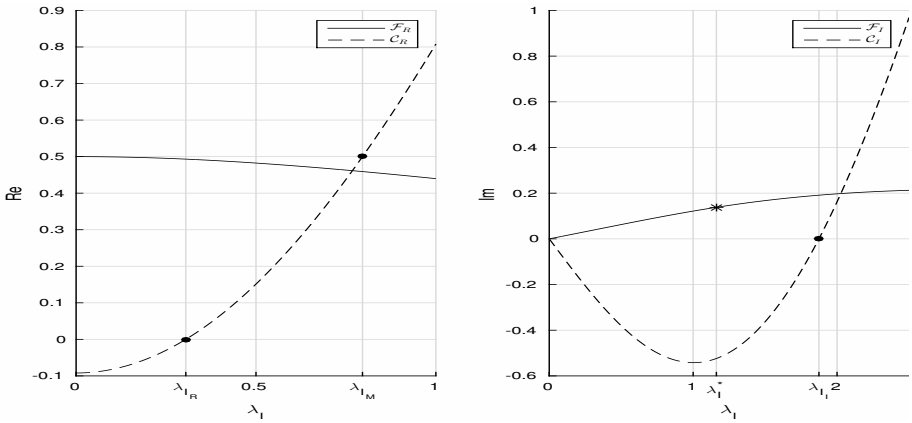

Figure 3.11: Numerical results for the location of λ_I^* (indicated by a star) relative to λ_{I_R}, λ_{I_M}, and λ_{I_I} (indicated by heavy dots), as stated in (3.115). The model parameters, $\tau_u = 1$ and $D_0 = 0.4$, together with the parameter values stated in (3.100), were used.

This readily yields, after a little algebra, that

$$\frac{b(1+3\tilde{\tau}_j)}{9+\lambda_{I_M}^2} = \frac{1}{3}\left(1+\tilde{\tau}_j b - \frac{1}{2a}\right) \quad \text{if} \quad 1+\tilde{\tau}_j b - 1/(2a) > 0\,.$$

Next, we consider the imaginary part of (3.107a). Upon substituting the expression above into it, we calculate that

$$C_I(\lambda_{I_M}) = a\lambda_{I_M}\left[\tilde{\tau}_j - \frac{3b\tilde{\tau}_j + b}{9+\lambda_{I_M}^2}\right] = a\lambda_{I_M}\left[\frac{1}{3}(1+\tilde{\tau}_j b - \frac{1}{2a})\right]\,.$$

This expression can be written as

$$\mathcal{C}_I(\lambda_{I_M}) = -\frac{a}{3}\lambda_{I_M}\left[\tilde{\tau}_j(b-3) + \left(1-\frac{1}{2a}\right)\right]\,.$$

From this last expression, we conclude that if $b > 3$ and the *extra condition* $a > 1/2$ holds, then λ_{I_M} exists and $\mathcal{C}_I(\lambda_{I_M}) < 0$. It follows that $N = 0$ since $\mathcal{C}_I(\lambda_I^*) < \mathcal{C}_I(\lambda_{I_M}) < 0$, and then $\zeta_I(\lambda_I^*) < 0$ because $\mathcal{F}_I > 0$.

We summarize this result in the following statement:

Proposition 3.19. *Suppose that*

$$D_{j,2} < D_{j,2,\min}^* = \frac{\omega^3}{4\pi^2 K^3} \qquad \textit{(i.e. } b > 3\textit{)}\,,$$

and that

$$\frac{\omega}{qU_0\chi_{0,j}} > \frac{1}{2} \quad \textit{(i.e. } a > \tfrac{1}{2}\textit{)},$$

or equivalently,

$$D_{j,2} > \left(\frac{qU_0}{2\omega} - 1\right)\left(\frac{\omega^3}{2\pi^2 K^3}\right). \tag{3.116}$$

Then we have three different possibilities:

(I) If $\frac{qU_0}{2\omega} - 1 < 0$, *i.e.* $qU_0 < 2\omega = 2(U_{0,\max} - U_0)$, *or equivalently*

$$\omega = S(\gamma - \alpha) - U_0(1 + q/2) > U_0 q/2\,, \tag{3.117}$$

then the lower bound is negative and the inequality (3.116) is automatically true. Therefore, (3.117) together with $D_{j,2,} < D^*_{j,2,\min}$ *implies* $N = 0$ *and thus stability, or:*

(II) If $\frac{qU_0}{2\omega} - 1 > 1/2$, *then this conflicts with* $D_{j,2} < D^*_{2,j\,\min}$ *and no conclusion regarding stability can be made, or:*

(III) If $0 < \frac{qU_0}{2\omega} - 1 < 1/2$ *, then if*

$$\left(\frac{qU_0}{2\omega} - 1\right)\left(\frac{\omega^3}{2\pi^2 K^3}\right) < D_{j,2} < D^*_{j,2,\min}\,,$$

we have $N = 0$ *for all* $\tilde{\tau} > 0$. *This gap condition holds with an analogous gap condition in* U_0.

$$U_0 q/3 < \omega = S\left[\gamma - \alpha\right] - U_0 < U_0 q/2\,.$$

It is an open problem to close the gap and drop the condition (3.116), and prove that $N = 0$ for all $\tilde{\tau}_j > 0$ and $0 < D_{j,2} < D^*_{j,2,\min}$, in agreement with what we discovered for the special case $q = 3$. However, Remark 3.12 also suggests that the threshold $D^*_{j,2,\min}$ could possibly be revised, as it may depend on q.

3.5.6 A Gap Between the Lower and Upper Thresholds: $D_{j,2,\min} < D_{j,2} < D^*_{j,2}$, Existence of Hopf Bifurcation

Having considered $D_{j,2}$ above $D^*_{j,2}$, where there is instability due to one unstable eigenvalue, and below $D^*_{j,2,\min}$, where we have stability subject to the extra condition, we now consider the

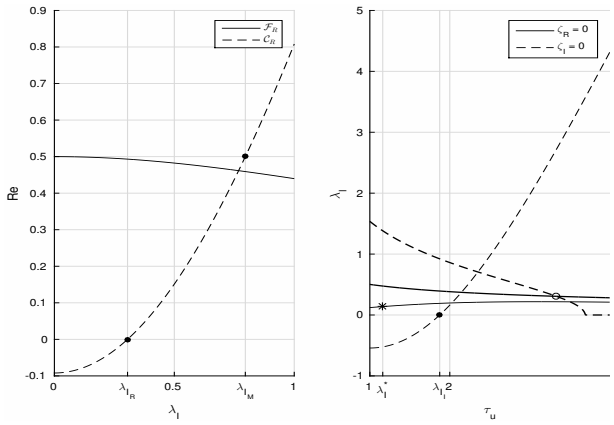

Figure 3.12: Locating the Hopf bifurcation point. The two curves shows the locus of the roots of $\zeta_R(\lambda_I)$ and $\zeta_I(\lambda_I)$ as functions of τ_u. Hopf bifurcation is determined numerically to occur at $\tau_u \approx 3.33$ and $\lambda_I \approx 0.307$, at the intersection of these two curves. The model parameters are $D_0 = 0.6$ and those stated in (3.100). For this parameter set we confirm numerically that $3 - 3/(2a) \approx 2.397 < b \approx 2.714 < 3$, which satisfies (3.118).

gap region defined by

$$D^*_{j,2,\min} < D_{j,2} < D^*_{j,2}\,.$$

In this gap region we will argue that a Hopf bifurcation exists with respect to the parameter $\tilde{\tau}_j$. An example of a such a Hopf bifurcation point is illustrated in Fig. 3.12.

Unlike in the explicitly solvable case, $q = 3$, where a Hopf bifurcation point can be located by a closed-form formula $\tilde{\tau}_j = \tilde{\tau}_{j,\mathrm{Hopf}} = O(1)$ using (3.92) (but only the mode $j = K - 1$ will actually occur), corresponding to the critical case $\zeta_I(\lambda_I^*) = 0$ (and by definition $\zeta_R(\lambda_I^*) = 0$ as well, so $\lambda = \pm i\lambda_I^*$ are a pair of purely imaginary eigenvalues corresponding to Hopf bifurcation), we seek only to confirm that if $\tilde{\tau}_j \ll 1$, we have path (II), i.e. stability, while if $\tilde{\tau}_j \gg 1$, then we have path (I), i.e. instability.

We first observe that when

$$3 - \frac{3}{2a} < b < 3\,, \tag{3.118}$$

then $D_{j,2}$ is on the gap range

$$D^*_{j,2,\min} < D_{j,2} < D^*_{j,2}\,.$$

For the typical model parameter set given in (3.100) with two hotspots, these bounds are

$$0.4559 \approx D^*_{0,\min} < D_0 < D^*_0 \approx 0.7599$$

Since purely imaginary eigenvalue implies $\lambda = \pm i\lambda_I^*$, we still seek to find λ_I^* such that $\zeta_R(\lambda_I^*) = \zeta_I(\lambda_I^*) = 0$ directly. In other words, we are seeking the boundary case where the image of the positive imaginary axis is neither away from nor enclosing the origin, but exactly crosses through the origin.

Now on the range $\tilde{\tau}_j > \frac{b}{3(3-b)} > 0$, we have $\mathcal{C}_I(\lambda_I) > 0$ for all $\lambda_I > 0$. We can again let $\tilde{\tau}_j \to \infty$, as in the derivation of (3.110), to conclude that $\zeta_R(\lambda_I^*) = 0$ when

$$\lambda_I^* \sim \frac{3}{\sqrt{2ab}} \tilde{\tau}_j^{-1/2} \ll 1 \,.$$

Next, by using $\lambda_I^* = O(\tilde{\tau}_j^{-1/2})$, together with $\mathcal{C}_I(\lambda_I^*)$ from (3.107a), we estimate that

$$\mathcal{C}_I(\lambda_I^*) \sim \frac{a\tilde{\tau}_j^{-1/2}}{9} \left[3\tilde{\tau}_j(3-b) + O(1)\right] \sim \frac{a\tilde{\tau}_j^{1/2}}{9}(3-b) > 0 \,,$$

since $b < 3$. Then, since $\mathcal{C}_I(\lambda_I^*) = O(\tilde{\tau}_j^{1/2}) \gg 1$, but $\mathcal{F}_I(\lambda_I^*) = O(\tilde{\tau}_j^{-1/2})$ when $\lambda_I^* = O(\tilde{\tau}_j^{-1/2})$, we conclude that $\zeta_I(\lambda_I^*) > 0$ as $\tilde{\tau}_j \to +\infty$. This implies that path (I) holds and $N = 2$.

On the other hand, when $\tilde{\tau}_j \to 0^+$ we can repeat a previous calculation given in (3.111) to obtain that the intersection of $\mathcal{C}_R(\lambda_I)$ and $\mathcal{F}_R(\lambda_I)$ must occur at some $\lambda_I^* = O(1) > 0$. Then, since for $\tilde{\tau}_j \to 0$ we have from (3.107a) that $\mathcal{C}_I(\lambda_I^*) < 0$ because $b > 0$, we must conclude that $\zeta_I(\lambda_I^*) < 0$ when $\tilde{\tau}_j \ll 1$. This implies that in the limit $\tilde{\tau}_j \ll 1$, path (II) holds and $N = 0$.

We then prove the existence of a Hopf bifurcation by appealing to a continuous path argument, namely that $\lambda_I^* = \lambda_I^*(\tilde{\tau}_j)$ as a continuous function. Since $N = 0$ for $\tilde{\tau}_j \ll 1$, while $N = 2$ for $\tilde{\tau}_j \ll 1$, there must exist a *minimum value* of $\tilde{\tau}_{j,\text{Hopf}} > 0$ such that $\zeta_I(\lambda_I^*(\tilde{\tau}_{j,\text{Hopf}})) = 0$ exactly with $\lambda_I^* > 0$. However, it is not clear whether there are other values of $\tilde{\tau}_j$ at which other Hopf bifurcations occur for $\tilde{\tau}_j > \tilde{\tau}_{j,\text{Hopf}} > 0$.

One way to attempt to prove uniqueness of the Hopf bifurcation value would be to prove a condition of one-way traversality at the onset of a purely imaginary eigenvalue. To do so, we may again let $\lambda = \lambda_R + i\lambda_I$ and consider both real part and imaginary part as a function of $\tilde{\tau}_j$, so that the Hopf bifurcation occurs at $\lambda_I(\tilde{\tau}_j) = \lambda_I^*$ where $\lambda_R = 0$. If one can further show that $d\lambda_R/d\tilde{\tau}_j > 0$ whenever we have a root on the imaginary axis, it would follow that the locus of any eigenvalue in the complex plane can cross the imaginary axis only once, and

in only the direction from left to right. It appears to be analytically rather difficult to prove such a one-way transversal crossing condition.

3.5.7 Conclusions on the Stability of a Symmetric $K-$Hotspot Steady-State

For $q = 2, 3, 4$, suppose that Conjecture 3.18 holds and that $K \geq 2$. Let N denote the number of eigenvalues with positive real part. Then, for any mode of competition instability $j = 1, \ldots, K-1$, we have established the following statement:

(i) If $D_{j,2} > D^*_{j,2}$, then $N = 1$ for all $\tilde{\tau}_j > 0$. The steady-state K-spike pattern is unstable for any q.

(ii) If $D^*_{j,2,\min} < D_{j,2,} < D^*_{j,2}$, then there exists a Hopf bifurcation threshold $\tilde{\tau}_H$ which is possibly non-unique when $q \neq 3$. Moreover, we have $N = 2$ when $\tilde{\tau}_j \gg 1$, and hence instability. Otherwise if $\tilde{\tau}_j \ll 1$, then we have $N = 0$, and hence stability. When $q = 3$, the threshold $\tilde{\tau}_H$ is unique with formula given in (3.88), and we have $N = 0$ and $N = 2$ for $\tilde{\tau}_j$ below and above the threshold $\tilde{\tau}_H$, respectively.

(iii) If $D_{j,2} < D^*_{j,2,\min}$, then for $q \neq 3$ we have $N = 0$ if $\tilde{\tau}_j \gg 1$ and $\tilde{\tau}_j \ll 1$. If we suppose further the additional condition that $\omega = S(\gamma - \alpha) - U_0 > U_0 q/2$, then we have $N = 0$ for any $\tilde{\tau}_j > 0$. For $q = 3$, we have that $N = 0$ for any $\tilde{\tau}_j > 0$ with no extra condition needed.

Remark 3.20.

1. A reason for considering integral values of q only in the range $\{2, 3, 4\}$ is that we assumed in the course of deriving the NLEP 3.36 that $\tau_u \ll O(\epsilon^{-2})$ (see the calculations leading to 3.26). Then, for the parameter

$$\tilde{\tau}_j = \tau_u O(\epsilon^{q-3}) \,,$$

to be $O(1)$, we must have that $\tau_u = O(\epsilon^{3-q})$. This establishes that $q < 5$ is required to satisfy the assumption that $\tau_u \ll O(\epsilon^{-2})$. If $q = 5$, then the ODE for the perturbation η at (3.27) will be changed to

$$D_0 \alpha^q \eta_{xx} = \epsilon^2 \tau_u \lambda \alpha^q \eta \,,$$

where $\tau_u = O(\epsilon^{-2})$. This will result in a different problem to be solved for $\eta(x)$, and consequently a different value for $\eta(0)$. Ultimately, this leads to a different NLEP that requires a separate analysis.

2. Conjecture (3.18) is rigorously established in the literature except for the statement $\mathcal{F}_R'(\lambda_I) < 0$ for $q = 4$. However, this monotonicity condition for $q = 4$ was readily established numerically in Fig. 3.7.

3.5.8 Asymptotic Determination of Hopf Bifurcation Threshold

Finally, we would like to see if we can determine λ_I^* and $\tilde{\tau}_{j,\text{Hopf}}$ asymptotically as $b \to 3$ from below. We recall that for the explicitly solvable case $q = 3$ that we have $\tilde{\tau}_{j,\text{Hopf}} \to \infty$ as $b \to 3^-$ ($D_{j,2} \to \left(D^*_{j,2,\min}\right)^-$) and, correspondingly, that $\lambda_{I,H} \to 0^+$. This motivates us to consider the general case $q \neq 3$ to examine whether only the known local behavior of $\mathcal{C}_R$, $\mathcal{C}_I$, $\mathcal{F}_R$, and $\mathcal{F}_I$ as $\lambda_I \to 0$, is involved in estimate the Hopf bifurcation point.

From [52], it is well known for any $q > 1$ that

$$\mathcal{F}_R(\lambda_I) \sim \frac{1}{2} - k_c\lambda_I^2 + \cdots, \qquad \mathcal{F}_I(\lambda_I) \sim \frac{\lambda_I}{4}(1 - 1/q) \quad \text{as} \quad \lambda_I \to 0\,,$$

where $k_c > 0$ is a constant depending on q. We then recall that $\mathcal{C}_R(\lambda_I)$ can be written as

$$\mathcal{C}_R(\lambda_I) = \frac{a}{9 + \lambda_I^2}\left[3(3 - b) + (1 + \tilde{\tau}_j b)\lambda_I^2\right].$$

To examine the region near $b = 3$, we introducing a detuning parameter δ by $\delta = 3 - b$, where $0 < \delta \ll 1$. We then look for a root to $\mathcal{C}_R(\lambda_I) = \mathcal{F}_R(\lambda_I)$ near $\lambda_I = 0$ when $\tilde{\tau}_j \gg 1$. To this end, we expand $\mathcal{C}_R(\lambda_I)$ near $\lambda_I = 0$ as

$$\mathcal{C}_R(\lambda_I) = \frac{a}{9 + \lambda_I^2}\left[3\delta + (1 + 3\tilde{\tau}_j)\lambda_I^2 + O(\tilde{\tau}_j\delta\lambda_I^2)\right].$$

This suggests that we must have the dominant balance $\tilde{\tau}_j\lambda_I^2 = O(1)$ so that $\mathcal{C}_R \to 1/2 = \mathcal{F}_R(0)$ as $\lambda_I \to 0$. This motivates the introduction of the rescaling

$$\lambda_I \sim \tilde{\tau}_j^{-1/2}\lambda_{I,0}\,,$$

which must be chosen in such a way that

$$\frac{a}{9}\left[3\lambda_{I,0}^2 + O(\delta)\right] \sim \frac{1}{2}\,.$$

This yields that

$$\lambda_{I,0} = \sqrt{\frac{3}{2a}}\,.$$

Therefore, for $\tilde{\tau}_j \gg 1$ and $b = 3 - \delta$ with $0 < \delta \ll 1$, the unique root of $\zeta_R(\lambda_I) = 0$ is located asymptotically at

$$\lambda_I \sim \sqrt{\frac{3}{2a}}\tilde{\tau}_j^{-1/2}\,.$$

Next, we relate $\tilde{\tau}_j$ to δ by enforcing that $\mathcal{C}_I(\lambda_I) \sim \mathcal{F}_I(\lambda_I)$ as $\lambda_I \to 0^+$. This latter condition yields that

$$a\lambda_I\left(\frac{3\tilde{\tau}_j\delta - 3 + O(\delta) + \tilde{\tau}_j\lambda_I^2}{9 + \lambda_I^2}\right) \sim \frac{\lambda_I}{4}\left(1 - 1/q\right)\,.$$

Upon cancelling λ_I from both sides of this expression, and putting $\tilde{\tau}_j\lambda_I^2 = 3/(2a)$, we get

$$\frac{a}{9}\left[3\tilde{\tau}_j\delta - 3 + \frac{3}{2a}\right] = \frac{1}{4}(1 - 1/q)\,.$$

Upon solving this equation for $\tilde{\tau}_j$, we get

$$\tilde{\tau}_j \sim \delta^{-1}\left(1 + \frac{1}{4a} - \frac{3}{4aq}\right)\,.$$

In summary, provided that

$$1 + \frac{1}{4a}(1 - 3/q) > 0, \tag{3.119}$$

we have that as $b \to 3^-$, the Hopf bifurcation occurs at

$$\tilde{\tau}_j = \tilde{\tau}_{j,\mathrm{Hopf}} \sim \frac{1}{\delta}\left(1 + \frac{1}{4a}\left(1 - 3/q\right)\right)\,, \tag{3.120}$$

with corresponding frequency

$$\lambda_I^* \sim \delta^{1/2}\sqrt{\frac{3}{2a}}\left(1 + \frac{1}{4a}\left(1 - 3/q\right)\right)^{-1/2}\,, \tag{3.121}$$

where $\delta = 3 - b \to 0^+$.

Finally, let us compare this result for general q to the explicit result that we obtained earlier for the exactly solvable case $q = 3$.

Firstly, we observe that the quadratic equation (3.73) for λ that occurs when $q = 3$ is equivalent to

$$\lambda^2 + \left(\frac{1 + \tilde{\tau}_j (b-3)}{\tilde{\tau}_j} \right) \lambda + \frac{[b - 3 + 3/(2a)]}{\tilde{\tau}_j} = 0 \,.$$

We conclude that a Hopf bifurcation occurs if the coefficient of λ vanishes, i.e. if $\tilde{\tau}_{j,\mathrm{Hopf}} = (3-b)^{-1} = \delta^{-1}$ in agreement with setting $q = 3$ in (3.120). In addition, since at the Hopf bifurcation we have

$$(\lambda_I^*)^2 = \frac{b - 3 + 3/(2a)}{\tilde{\tau}_j} = \frac{1}{\tilde{\tau}_j} \left(\frac{3}{2a} - \delta \right) ,$$

we conclude that

$$\lambda_I^* \sim \delta^{1/2} \sqrt{\frac{3}{2a}} \,.$$

This expression agrees with (3.121) upon setting $q = 3$.

When $q = 4$, we readily observe that the assumption (3.119) for (3.120) and (3.121) is always satisfied. However for $q = 2$, we have to require that $a > 1/8$ in order for (3.119) to hold. This means for $a = \omega/(U_0 \chi_{0,j})$, $b = 9\chi_{0,j}/2 = 3$, which gives $\chi_{0,j} = 2/3$, that we must have the condition

$$a = \frac{\omega}{\frac{4}{3} U_0} > \frac{1}{8} \,,$$

which is equivalent to the requirement that $\omega > U_0/6$. Therefore, we conclude that a Hopf bifurcation occurs when $D_{j,2} \to (D_{j,2,\min})^+$ with asymptotics given by (3.120) and (3.121) if the condition

$$\omega = S(\gamma - \alpha) - U_0 > U_0/6 \,, \tag{3.122}$$

holds. In other words, the asymptotic conclusions hold provided we are not too close to the existence threshold $\omega = 0$ of the hotspot pattern.

Remark 3.21. The fact that, for $q = 2$, the Hopf bifurcation with the asymptotics (3.120) and (3.121) does not occur for

$$0 < S(\gamma - \alpha) - U_0 < U_0/6 \,,$$

when $b \to 3^-$, i.e. as $D_{j,2} \to \left(D^*_{j,2,\min}\right)^+$ does not contradict the fact that there exists a Hopf bifurcation when

$$D^*_{j,2,\min} < D_{j,2} < D^*_{j,2}\,.$$

It only shows that the limiting asymptotics is not of the form where $\tilde{\tau}_j \to \infty$ and $D_{j,2} \to \left(D^*_{j,2,\min}\right)^+$ simultaneously.

3.6 Stability of a Stripe Pattern, Explicitly Solvable Case.

In this section we extend our 1-D spike stability analysis to study the transverse stability of a homoclinic stripe for our three-component crime model with simple police interaction. A homoclinic stripe occurs when the attractivness concentration A concentrates on a planar curve in the 2-D domain. The simplest type of homoclinic stripe solution is a stripe of zero curvature, which results when a 1-D homoclinic spike solution is trivially extended along the midline of a rectangular domain. The main goal of this section is to analyze the linear stability of this type of stripe solution to transverse perturbations for our three-component model. In our stability analysis we will assume that the patrol focusing parameter is $q = 3$, which will lead to an explicitly solvable NLEP spectral problem, which is then highly tractable analytically. In this way, we are able to explicitly identify a band of unstable transverse wavenumbers, and calculate both the growth rate and most unstable mode within this band. This instability is shown to lead to the breakup of the stripe into a localized hotspot of criminal activity. For two-component reaction-diffusion systems, such as the Gierer-Meinhardt and Gray-Scott models, there have been several prior studies of the stability of homoclinic stripes to transverse perturbations ([16], [25], [26]). As far as we are aware there have been no prior studies for three-component systems.

We formulate our three-component model in the rectangular domain defined by

$$\Omega = \{(x_1, x_2)|\ -\ell < x_1 < \ell,\ 0 < x_2 < d\}\,. \tag{3.123}$$

The three-component RD system (3.3) in 2-D now takes the form

$$A_t = \epsilon^2 \Delta A - A + \rho A + \alpha\,, \quad x \in \Omega\,; \qquad \partial_n A = 0\,, \quad x \equiv (x_1, x_2) \in \partial\Omega\,, \tag{3.124a}$$

$$\rho_t = D\nabla \cdot \left(A^2 \nabla \left(\rho / A^2 \right) \right) - \rho A + \gamma - \alpha - U\,, \quad x \in \Omega\,; \qquad \partial_n \rho = 0\,, \quad x \in \partial\Omega\,, \tag{3.124b}$$

$$\tau_u U_t = D\nabla \cdot \left(A^q \nabla \left(U / A^q \right) \right)\,, \quad x \in \Omega\,; \qquad \partial_n U = 0\,, \quad x \in \partial\Omega\,, \tag{3.124c}$$

where Ω is the rectangular domain of (3.123).

3.6.1 Extension of a 1-D Spike Solution to a 2-D Stripe Solution

In the construction of the steady-state stripe solution below, we will need to assume that $q > 1$. It will be shown that for the case $q = 3$, the NLEP governing the transverse stability of this stripe is explicitly solvable.

We will analyze the transverse stability properties of a steady-state stripe solution for (3.124) for the regime $O(1) \ll D \ll O(\epsilon^{-2})$. As motivated by the scalings in [29], we introduce the new variables v, D_0, and u by

$$\rho = \epsilon^2 v A^2\,, \qquad U = u A^q\,, \qquad D = D_0 / \epsilon^2\,, \tag{3.125}$$

where we will assume that $D_0 \gg O(\epsilon^2)$ so that $D \gg 1$. In terms of these new variables, (3.124) becomes

$$A_t = \epsilon^2 \Delta A - A + \epsilon^2 v A^3 + \alpha\,, \quad x \in \Omega\,; \qquad \partial_n A = 0\,, \quad x \equiv (x_1, x_2) \in \partial\Omega\,, \tag{3.126a}$$

$$\epsilon^2 \left(v A^2 \right)_t = D_0 \nabla \cdot \left(A^2 \nabla v \right) - \epsilon^2 v A^3 + \gamma - \alpha - u A^q\,, \quad x \in \Omega\,; \quad \partial_n v = 0\,, \quad x \in \partial\Omega\,, \tag{3.126b}$$

$$\epsilon^2 \tau_u \left(A^q u \right)_t = D_0 \nabla \cdot \left(A^q \nabla u \right)\,, \quad x \in \Omega\,; \qquad \partial_n u = 0\,, \quad x \in \partial\Omega\,. \tag{3.126c}$$

We now construct a steady-state stripe solution consisting of a localized region of high attractiveness, which we center along the midline $x_1 = 0$ of the rectangle. To do so, we simply construct a steady-state 1-D spike $A = A(x_1)$, $v = v(x_1)$, and $u = u(x_1)$ as in Section 3.1, and extend it trivially in the x_2 direction. Since the total number of police is conserved due

to (3.124c), we have $\int_\Omega U(x,t)\,dx = \mathcal{U}$ for all time, where $\mathcal{U} > 0$ is the initial number of police deployed. As such, we have for the steady-state stripe solution that

$$\int_{-\ell}^{\ell} U(x_1)\,dx_1 = U_0 \equiv \mathcal{U}/d, \tag{3.127}$$

where d is the width of Ω. It follows from (3.126c) that the steady-state 1-D solution $u(x_1)$ is a constant given by

$$u(x_1) = U_0 / \int_{-\ell}^{\ell} [A(x_1)]^q \; dx_1\,, \tag{3.128}$$

and that the steady-state 1-D problem for $A(x_1)$ and $v(x_1)$, from (3.126a) and (3.126b), is

$$\epsilon^2 A_{x_1x_1} - A + \epsilon^2 v A^3 + \alpha = 0\,, \qquad |x_1| \le \ell\,; \qquad A_{x_1}(\pm\ell) = 0\,, \tag{3.129a}$$

$$D_0\left(A^2 v_{x_1}\right)_{x_1} - \epsilon^2 v A^3 + \gamma - \alpha - \frac{U_0 A^q}{\int_{-\ell}^{\ell} A^q\,dx_1} = 0\,, \qquad |x_1| \le \ell\,; \qquad v_{x_1}(\pm\ell) = 0\,. \tag{3.129b}$$

In the inner region $|x_1| \le O(\epsilon)$ near the pulse we set $y = x_1/\epsilon$ and expand

$$A = A_0/\epsilon + \cdots\,, \qquad v = v_0 + \cdots\,,$$

as in [29] and also Section 3.1. Note that we are reusing the notations A_0 and v_0 for the leading order expansions for this context, because the procedures and structures of the asymptotics are very similar.

We readily obtain that v_0 is a constant and $A_{0yy} - A_0 + v_0 A_0^3 = 0$ as before. This yields the leading order inner solution

$$A(x_1) \sim \frac{1}{\epsilon\sqrt{v_0}} w\left(x_1/\epsilon\right)\,, \qquad v \sim v_0\,, \tag{3.130}$$

where $w(y) = \sqrt{2}\,\mathrm{sech}\, y$ satisfies (2.14), and where the constant v_0 is to be determined. To determine the constant v_0, we integrate (3.129b) over $|x_1| \le \ell$ to get $-\epsilon^2 \int_{-\ell}^{\ell} v A^3\,dx_1 + 2\ell(\gamma-\alpha) - U_0 = 0$. Since $A = O(\epsilon^{-1})$ in the inner region, while $A = O(1)$ in the outer region, the integral above can be calculated asymptotically as $\epsilon^2 \int_{-\ell}^{\ell} v A^3\,dx_1 \sim v_0^{-1/2} \int_{-\infty}^{\infty} w^3\,dy = v_0^{-1/2}\sqrt{2}\pi$. In

this way, provided that $0 < U_0 < 2\ell(\gamma - \alpha)$, we calculate v_0 as

$$v_0 = \frac{2\pi^2}{\left[2\ell(\gamma - \alpha) - U_0\right]^2}\,, \tag{3.131}$$

which looks very similar to (3.12) with $K = 1$, except that

$$U_0 = \mathcal{U}/d\,,$$

now carries a different meaning. Therefore a stripe solution exists only if the total police deployment U_0 *per cross-sectional length* satisfies

$$U_0 < 2\ell(\gamma - \alpha).$$

In the inner region, the police concentration $U(x_1)$, given by $U(x_1) = uA^q$, becomes

$$U = \frac{U_0 A^q}{\int_{-\ell}^{\ell} A^q\,dx_1} \sim \frac{U_0}{\epsilon}\frac{w^q}{\int_{-\infty}^{\infty} w^q\,dy}\,, \qquad |x_1| \le O(\epsilon)\,. \tag{3.132}$$

In contrast, in the outer region we have from (3.129a) that $A_{\rm out} = \alpha + O(\epsilon^2)$. To determine the leading-order outer problem for v, we first need to estimate the integral $\int_{-\ell}^{\ell} A^q\,dx_1$ in (3.129b). Since $A = O(\epsilon^{-1})$ in the inner region $|x_1| \le O(\epsilon)$, while $A = O(1)$ in the outer region $O(\epsilon) \ll |x_1| \le 1$, it follows that when $q > 1$ the contribution to the integral $\int_{-\ell}^{\ell} A^q\,dx_1$ from the inner region is dominant, with the estimate $\int_{-\ell}^{\ell} A^q\,dx_1 = O(\epsilon^{1-q}) \gg 1$. We will henceforth assume that $q > 1$, so that the nonlocal term in (3.129b) can be neglected to leading-order in the outer region. Then, from (3.129b) we obtain that the leading-order outer problem for v is $v \sim \tilde{v}_0 + o(1)$, where $\tilde{v}_0$ satisfies

$$\tilde{v}_{0x_1x_1} = -\frac{(\gamma - \alpha)}{D_0\alpha^2}\,, \quad 0 < |x_1| < \ell\,; \quad \tilde{v}_{0x_1}(\pm\ell) = 0\,, \quad \tilde{v}_0(0) = v_0\,. \tag{3.133}$$

This yields the leading-order outer solution for $\tilde{v}_0$ as given below in (3.136).

Finally, we calculate u. Since $q > 1$, we use $A \sim \epsilon^{-1}w/\sqrt{v_0}$ to estimate the integral in

(3.128). This yields that

$$u = \frac{U_0}{\int_{-\ell}^{\ell} A^q \, dx_1} \sim \epsilon^{q-1} \tilde{u}_e \,, \qquad \text{where} \qquad \tilde{u}_e \equiv \frac{U_0 v_0^{q/2}}{\int_{-\infty}^{\infty} w^q \, dy} \,. \tag{3.134}$$

We summarize our result in the following statement.

Proposition 3.22. *For $\epsilon \ll 1$, $D \gg 1$, and $\mathcal{U} < 2d\ell(\gamma - \alpha)$, the steady-state spike solution for (3.126) is given to leading order in the inner region by*

$$A(x_1) \sim \frac{1}{\epsilon\sqrt{v_0}} w\left(x_1/\epsilon\right) \,, \qquad v \sim v_0 \,, \qquad U(x_1) \sim \frac{U_0}{\epsilon} \frac{w^q}{\int_{-\infty}^{\infty} w^q \, dy} \,, \qquad |x_1| \le O(\epsilon) \,, \tag{3.135}$$

where $v_0 \equiv 2\pi^2 \left[2\ell(\gamma - \alpha) - U_0\right]^{-2}$, $U_0 = \mathcal{U}/d$, and $w = \sqrt{2}\,\mathrm{sech}(x_1/\epsilon)$. In the outer region, $O(\epsilon) \ll |x_1| \le \ell$, we have

$$A \sim \alpha \,, \qquad v \sim \frac{(\gamma - \alpha)}{2D_0\alpha^2} \left[\ell^2 - (\ell - |x_1|)^2\right] + v_0 \,, \qquad U \sim \epsilon^{q-1} U_0 \alpha^q \frac{v_0^{q/2}}{\int_{-\infty}^{\infty} w^q \, dy} \,. \tag{3.136}$$

The criminal density in the inner and outer regions, as obtained from (3.125), is

$$\rho(x_1) \sim \left[w\left(x_1/\epsilon\right)\right]^2 \,, \quad |x_1| = O(\epsilon) \,; \tag{3.137a}$$

$$\rho(x_1) \sim \epsilon^2 \alpha^2 \left[v_0 + \frac{(\gamma - \alpha)}{2D_0\alpha^2} \left(\ell^2 - (\ell - |x_1|)^2\right)\right] \,, \quad O(\epsilon) \ll |x_1| \le \ell \,. \tag{3.137b}$$

In Fig. 3.13, we plot the above asymptotic results. We observe that the criminal density ρ is accompanied by a large quantity A, the attractiveness, at the vicinity of the crime hotspot. Moreover, the degree of patrol focus q, can be reflected by the shape of the police concentration. For the larger value of q we observe a more narrow profile near the crime hotspots.

3.6.2 The Stability of a Stripe

Next, we derive an NLEP governing the stability of the stripe solution to transverse perturbations that can lead to the breakup of the stripe into localized hotspots. Let A_e, v_e, and

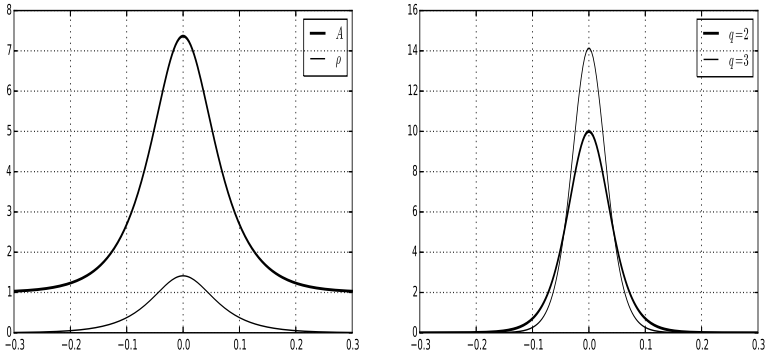

Figure 3.13: Plot of the steady-state spike from Proposition 3.22 in the inner region on the x_1 axis for $\epsilon = 0.05$, $\ell = 1.0$, $\gamma = 2$, and $\alpha = 1$. The x_2 direction is omitted because it extends trivially. Left plot: The attractiveness $A \sim w\left(x_1/\epsilon\right)/(\epsilon\sqrt{v_0}) + \alpha$ (heavy solid curve) and criminal density $\rho \sim w\left(x_1/\epsilon\right)$ (solid curve), these curve do not depend on q. Right plot: The police density U from (3.136) for $q = 2$ (heavy solid curve) and for $q = 3$ (solid curve).

u_e denote the steady-state solution constructed in the previous subsection and summarized in Proposition 3.22. We then extend it trivially in the x_2 direction to make a stripe. To determine the stability of this stripe with respect to transverse perturbations we introduce

$$A = A_e(x_1) + e^{\lambda t + imx_2}\phi(x_1)\,, \qquad v = v_e(x_1) + e^{\lambda t + imx_2}\epsilon\psi(x_1)\,, \qquad u = u_e + e^{\lambda t + imx_2}\epsilon^q\eta(x_1)\,. \tag{3.138}$$

Here $m = k\pi/d$ where d is the width of the rectangle and $k > 0$ is an integer. The relative sizes in ϵ in (3.138) are such that ϕ, ψ, and η are all $O(1)$ in the inner region. Upon substituting (3.138) into (3.126), we obtain on $|x_1| \le l$ that

$$\epsilon^2\phi_{x_1x_1} - (1+\epsilon^2m^2)\phi + 3\epsilon^2v_eA_e^2\phi + \epsilon^3A_e^3\psi = \lambda\phi\,, \tag{3.139a}$$

$$\begin{aligned} D_0\left[\epsilon A_e^2\psi_{x_1} + 2A_ev_{ex_1}\phi\right]_{x_1} - \epsilon m^2D_0A_e^2\psi - 3\epsilon^2v_eA_e^2\phi - \epsilon^3\psi A_e^3 \\ -\epsilon^qA_e^q\eta - qA_e^{q-1}u_e\phi = \lambda\epsilon^2\left(\epsilon A_e^2\psi + 2A_ev_e\phi\right)\,, \end{aligned} \tag{3.139b}$$

$$D_0\left[\epsilon^qA_e^q\eta_{x_1} + qA_e^{q-1}u_{ex_1}\phi\right]_{x_1} - \epsilon^qm^2D_0A_e^q\eta = \epsilon^2\tau_u\lambda\left(\epsilon^qA_e^q\eta + qA_e^{q-1}u_e\phi\right)\,. \tag{3.139c}$$

In the analysis of (3.139), we must allow for spatial perturbations of high frequency as $\epsilon \to 0$ because the hotspot $O(\epsilon)$ width is small relative to the $O(1)$ domain diameter of Ω. As such,

we consider the range $0 < m \leq O(\epsilon^{-1})$. Below, we show that the upper stability threshold occurs when $m = O(\epsilon^{-1})$.

In (3.139b) and (3.139c), we note that $u_{ex_1} = 0$ and $u_e \sim \epsilon^{q-1}\tilde{u}_e$, where $\tilde{u}_e$ is given in (3.134). In the outer region where $A_e \sim \alpha$ we obtain from (3.139b) that $\phi_{\text{out}} = O(\epsilon^3\psi_{\text{out}})$, when $0 < m \leq O(\epsilon^{-1})$. Next, we estimate the terms in (3.139b) in the outer region. We obtain from (3.134), and our estimate of ϕ_{out}, that $qA_e^{q-1}u_e\phi = O(\epsilon^{q+2}\psi_{\text{out}})$. Moreover, since $q > 1$, we have $\epsilon^q A_e^q \eta \ll O(\epsilon)$. In this way, we obtain in the outer region that (3.139b) reduces to

$$\psi_{x_1x_1} - m^2\psi = 0\,, \qquad O(\epsilon) < |x_1| \leq l\,; \qquad \psi_{x_1}(\pm l) = 0\,. \tag{3.140}$$

Similarly, since $\tau_u = O(1)$ and $u_{ex_1} = 0$, we obtain from (3.139c) that to leading order

$$\eta_{x_1x_1} - m^2\eta = 0\,, \qquad O(\epsilon) < |x_1| \leq l\,; \qquad \eta_{x_1}(\pm l) = 0\,. \tag{3.141}$$

In the inner region, we look for a localized eigenfunction for ϕ in the form $\phi = \Phi\,(x_1/\epsilon)$, i.e. which is constant in x_2 direction. Since the equations for ψ and η are not singularly perturbed, we obtain that $\psi \sim \psi(0)$ and $\eta \sim \eta(0)$ to leading order in the inner region. Then, since $A_e \sim \epsilon^{-1}w/\sqrt{v}_0$ and $v_e \sim v_0$ in the inner region, as obtained from (3.135), we find from (3.139b) that $\Phi(y)$ satisfies

$$\Phi'' - \Phi + 3w^2\Phi + \frac{1}{v_0^{3/2}}w^3\psi(0) = \left(\lambda + \epsilon^2 m^2\right)\Phi\,, \qquad -\infty < y < \infty\,. \tag{3.142}$$

Next, we derive the jump conditions for η and ψ across $x = 0$. To do so, we introduce an intermediate length-scale δ with $O(\epsilon) \ll \delta \ll 1$ and integrate (3.139b) from $-\delta < x_1 < \delta$ and use $A_e \sim \alpha$ at $x_1 = \pm\delta$. This yields that

$$e_0\left[\psi_{x_1}\right]_0 = e_1\psi(0) + e_2\eta(0) + e_3\,, \tag{3.143a}$$

where we have defined $[\psi_{x_1}]_0 \equiv \psi_{x_1}(0^+) - \psi_{x_1}(0^-)$. Here e_j for $j = 0, \ldots, 3$ are defined by

$$\begin{aligned} e_0 &= D_0\alpha^2\,, \qquad e_1 = \frac{D_0 m^2}{\epsilon v_0}\int_{-\infty}^{\infty} w^2\,dy + \frac{1}{v_0^{3/2}}\int_{-\infty}^{\infty} w^3\,dy\,, \\ e_2 &= \frac{1}{v_0^{q/2}}\int_{-\infty}^{\infty} w^q\,dy\,, \qquad e_3 = 3\int_{-\infty}^{\infty} w^2\Phi\,dy + \frac{q\tilde{u}_e}{v_0^{(q-1)/2}}\int_{-\infty}^{\infty} w^{q-1}\Phi\,dy\,. \end{aligned} \tag{3.143b}$$

In a similar way, we integrate (3.139c) across $-\delta < x_1 < \delta$ and use $A_e \sim \alpha$ at $x_1 = \pm\delta$. This yields that

$$f_0\,[\eta_{x_1}]_0 = f_1\eta(0) + f_2\,, \tag{3.144a}$$

where f_j for $j = 0, \ldots, 2$ are defined by

$$\begin{aligned} f_0 &= D_0\alpha^q\,, \qquad f_1 = \frac{D_0 m^2\epsilon^{1-q}}{v_0^{q/2}}\int_{-\infty}^{\infty} w^q\,dy + \frac{\epsilon^{3-q}\tau_u\lambda}{v_0^{q/2}}\int_{-\infty}^{\infty} w^q\,dy\,, \\ f_2 &= \frac{\epsilon^{3-q}q\tilde{u}_e\tau_u\lambda}{v_0^{(q-1)/2}}\int_{-\infty}^{\infty} w^{q-1}\Phi\,dy\,. \end{aligned} \tag{3.144b}$$

In (3.143b) and (3.144b), $\tilde{u}_e$ is given in (3.134).

Next, we must solve for $\psi(x_1)$ and $\eta(x_1)$ from the solution to (3.140) and (3.141) subject to the jump conditions (3.143) and (3.144), and the boundary conditions $\psi_{x_1}(\pm\ell) = \eta_{x_1}(\pm\ell) = 0$. From this solution, we calculate $\psi(0)$, which then determines the NLEP for $\Phi(y)$ from (3.142). To solve for η, we introduce the Green's function $G_m(x_1)$ satisfying

$$G_{mx_1x_1} - m^2 G_m = -\delta(x_1)\,, \quad |x_1| \le \ell\,; \qquad G_{mx_1}(\pm\ell) = 0\,. \tag{3.145}$$

The explicit solution to this problem is

$$G_m(x_1) = \frac{\cosh\left[m(\ell - |x_1|)\right]}{2m\sinh(m\ell)}\,, \tag{3.146}$$

for $m > 0$. In terms of $G_m(x_1)$, and using $[G_{mx_1}]_0 = -1$, the solution to (3.141) with (3.144) is

$$\eta(x_1) = \eta(0)\frac{G_m(x_1)}{G_m(0)}\,, \qquad \eta(0) = -\frac{f_2}{f_1 + f_0/G_m(0)}\,. \tag{3.147}$$

Similarly, for $m > 0$, the solution to (3.140) subject to (3.143) is

$$\psi(x_1) = \psi(0)\frac{G_m(x_1)}{G_m(0)}\,, \qquad \psi(0) = -\frac{e_2\eta(0) + e_3}{e_1 + e_0/G_m(0)}\,. \tag{3.148}$$

We estimate the asymptotic order of the terms in (3.144b) as $f_0/G_m(0) = m\tanh(m\ell)\cdot O(1)$, $f_1 = m^2\epsilon^{1-q}\cdot O(1) + \epsilon^{3-q}\tau_u\cdot O(1)$, and $f_2 = \epsilon^{3-q}\tau_u\cdot O(1)$. As such, when $\tau_u = O(1)$ and $q > 1$, we conclude for any $m > 0$ with $m \gg O(\epsilon)$ that

$$f_1 + \frac{f_0}{G_m(0)} \sim \frac{D_0 m^2\epsilon^{1-q}}{v_0^{q/2}}\int_{-\infty}^{\infty} w^q\,dy\,,$$

$$\eta(0) = -\frac{f_2}{f_1 + f_0/G_m(0)} \sim \frac{O(\epsilon^{3-q})}{O(\epsilon^{1-q}m^2)} = O(\epsilon^2/m^2) \ll 1\,.$$

Since $\eta(0) \ll 1$ when $q > 1$, $\tau_u = O(1)$, and $m \gg O(\epsilon)$, we conclude from (3.148) that, in this parameter regime,

$$\psi(0) \sim -\frac{e_3}{e_1 + e_0/G_m(0)}\,. \tag{3.149a}$$

Upon using (3.134) for $\tilde{u}_e$, the coefficients in (3.149a) are

$$\begin{aligned} e_0 = D_0\alpha^2\,, \qquad e_1 &= \frac{D_0 m^2}{\epsilon v_0}\int_{-\infty}^{\infty} w^2\,dy + \frac{1}{v_0^{3/2}}\int_{-\infty}^{\infty} w^3\,dy\,, \\ e_3 &= 3\int_{-\infty}^{\infty} w^2\Phi\,dy + qv_0^{1/2}U_0\frac{\int_{-\infty}^{\infty} w^{q-1}\Phi\,dy}{\int_{-\infty}^{\infty} w^q\,dy}\,, \end{aligned} \tag{3.149b}$$

Upon substituting (3.149a) into (3.142), and by using (3.131) for v_0, together with $\int_{-\infty}^{\infty} w^2\,dy = 4$ and $\int_{-\infty}^{\infty} w^3\,dy = \sqrt{2}\pi$, we obtain the following NLEP with two nonlocal terms:

$$L_0\Phi - \frac{\chi_0 w^3}{\int_{-\infty}^{\infty} w^3\,dy}\left(3\int_{-\infty}^{\infty} w^2\Phi\,dy + qv_0^{1/2}U_0\frac{\int_{-\infty}^{\infty} w^{q-1}\Phi\,dy}{\int_{-\infty}^{\infty} w^q\,dy}\right) = \left(\lambda + \epsilon^2 m^2\right)\Phi\,, \tag{3.150a}$$

$$\chi_0 \equiv \left(1 + \frac{4D_0 m^2\epsilon^{-1}}{[2\ell(\gamma-\alpha) - U_0]} + \frac{4D_0\alpha^2\pi^2 m\tanh(m\ell)}{[2\ell(\gamma-\alpha) - U_0]^3}\right)^{-1}\,. \tag{3.150b}$$

3.6.3 Analysis of the NLEP - Stripe Breakup Instability

The analysis of the spectrum of (3.150) is challenging for general $q > 1$ owing to the presence of the two nonlocal terms. In our analysis below, we will focus on the special case $q = 3$, as we have done before for our 1-D hotspot analysis, for which this NLEP with two nonlocal terms can be transformed to the following NLEP with only one nonlocal term:

$$L_0\Phi - \chi w^3 \frac{\int_{-\infty}^{\infty} w^2\Phi\, dy}{\int_{-\infty}^{\infty} w^3\, dy} = \left(\lambda + \epsilon^2 m^2\right)\Phi\,, \qquad \chi \equiv \chi_0\left[\frac{6\ell(\gamma-\alpha)}{2\ell(\gamma-\alpha)-U_0}\right], \tag{3.151}$$

which is explicitly solvable. Here χ_0 is defined by (3.150b). It is an open problem to analyze (3.150) for arbitrary $q > 1$.

The NLEP (3.151) for $q = 3$ is a special case of the class of explicitly solvable NLEP's of Principal Result 2.2 in [37]. Upon replacing λ, σ, $g(w)$, and $h(w)$ with $\lambda + \epsilon^2 m^2$, 3, $w^2/\int_{-\infty}^{\infty} w^3\, dy$, and w^3 respectively in the formula (2.2) of [37], we get

$$\lambda = \sigma - \chi(\lambda)\int_{-\infty}^{\infty} g(w)h(w)\, dy. \tag{3.152}$$

By using the definition of χ at (3.151), we obtain the following explicit formula for any unstable eigenvalue of (3.151):

Proposition 3.23. *Let $\epsilon \to 0$, $q = 3$, $\tau_u = O(1)$, $U_0 < 2\ell(\gamma-\alpha)$, with $m > 0$ and $m \gg O(\epsilon)$. Then, the transverse stability of a stripe solution for (3.124) on an $O(1)$ time-scale is determined by the sign of the discrete eigenvalue*

$$\lambda = 3 - \epsilon^2 m^2 - \frac{9\ell(\gamma-\alpha)}{[2\ell(\gamma-\alpha)-U_0]}\left[1 + \frac{4D_0 m^2\epsilon^{-1}}{[2\ell(\gamma-\alpha)-U_0]} + \frac{4D_0\alpha^2\pi^2 m\tanh(m\ell)}{[2\ell(\gamma-\alpha)-U_0]^3}\right]^{-1}. \tag{3.153}$$

To determine the edges of the instability band for a stripe, we set $\lambda = 0$ in (3.153) and solve for m. For $\epsilon \ll 1$, the upper edge m_+ of the instability band is $m_+ \sim \sqrt{3}/\epsilon$, with $\lambda < 0$ for $m > m_+$. In contrast, the lower edge m_- of the instability band satisfies $m_- \sim \epsilon^{1/2} m_{0-}$ where m_{0-} satisfies

$$3 \sim \frac{9\ell(\gamma-\alpha)}{[2\ell(\gamma-\alpha)-U_0]}\left(1 + \frac{4D_0 m_0^2}{[2\ell(\gamma-\alpha)-U_0]}\right)^{-1}.$$

Upon solving for m_{0-}, we conclude for $\epsilon \ll 1$ that $\lambda > 0$ when

$$\epsilon^{1/2} m_{0-} < m < \frac{\sqrt{3}}{\epsilon}\,, \qquad m_{0-} \equiv \sqrt{\frac{\ell(\gamma-\alpha)+U_0}{4D_0}}\,. \tag{3.154}$$

We remark that the lower $O(\epsilon^{1/2})$ edge of the band is consistent with the assumption $m \gg O(\epsilon)$ used to derive (3.153). In addition, we note that the lower edge of the band increases with the level U_0 of police effort. This shows that as U_0 increases, less transverse modes become unstable.

Finally, we estimate the mode $m_{\rm dom}$ within the instability band that has the largest growth rate. To do so, we set $d\lambda/dm = 0$ in (3.153), and obtain that $m_{\rm dom}$ is the root of

$$2\epsilon^2 m \sim \frac{9\ell(\gamma-\alpha)}{[2\ell(\gamma-\alpha)-U_0]}\left(\frac{4D_0 m^2\epsilon^{-1}}{[2\ell(\gamma-\alpha)-U_0]}+\cdots\right)^{-2}\left(\frac{8D_0 m}{\epsilon\,[2\ell(\gamma-\alpha)-U_0]}+\cdots\right).$$

For $\epsilon \ll 1$, this reduces to $16D_0 m^4 \sim 36\ell\epsilon^{-1}(\gamma-\alpha)$. For $\epsilon \ll 1$, this yields the most unstable mode as

$$m_{\rm dom} \sim \epsilon^{-1/4}\left[\frac{9}{4D_0}\ell(\gamma-\alpha)\right]^{1/4}, \tag{3.155}$$

which is independent of U_0. We predict that a stripe for the urban crime model (3.124) on a rectangular domain of width d will break up into N localized hot-spots, where N is the closest integer to $m_{\rm dom}d/2\pi$.

In Fig. 3.14 (left plot), we use (3.153) to plot λ versus m for the parameter set $\epsilon = 0.05$, $D_0 = 1$, $\gamma = 2$, $\alpha = 1$, $\ell = 1$, and $U_0 = 1$. In the caption of the figure, the asymptotic predictions for the edges of the instability band, as obtained from (3.154), are compared with results from (3.153). From (3.155), the asymptotic prediction for the most unstable mode is $m_{\rm dom} \sim 2.59$, which compares well with the numerically computed result $m_{\rm dom} \approx 2.44$ as computed from (3.153). In Fig. 3.14 (right plot), we compare λ versus m near the lower threshold m_- for $U_0 = 1$ and for $U_0 = 1.5$.

For the same parameter values as used in Fig. 3.14, we further put $d = 2$ to compute

$$m_{\rm dom}d/2\pi = 2.59/\pi \approx 0.82. \tag{3.156}$$

This suggests that a stripe on a square domain of side-length two should break up into only

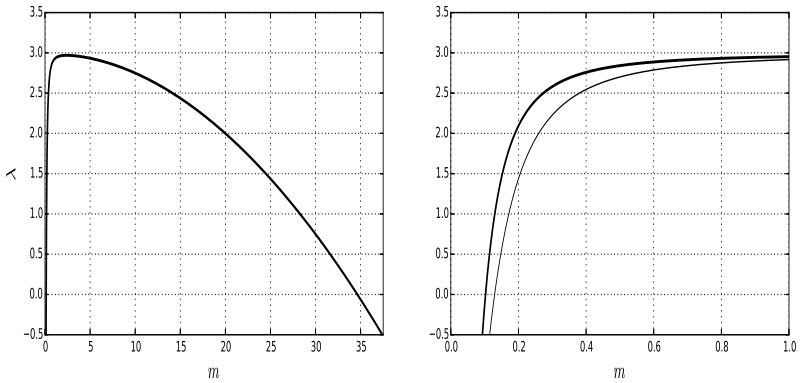

Figure 3.14: Principal eigenvalue λ as a function of frequency m. Left: plot of λ versus m, as given in (3.153), for $\epsilon = 0.05$, $D_0 = 1$, $\gamma = 2$, $\alpha = 1$, $l = 1$, and $U_0 = 1$. The asymptotic prediction as $\epsilon \to 0$ for the instability band from (3.154) is $0.158 < m < 34.64$. The corresponding numerical result is $0.131 < m < 34.56$. Right: plot of λ versus m near the lower threshold m_- for $U_0 = 1$ (solid curve) and $U_0 = 1.5$ (heavy solid curve). The lower edge of the instability band increases as U_0 increases.

one spot, which is relatively few as compared to, say, the case of the Gierer-Meinhardt model studied also in [37] for an explicitly solvable case. To validate this claim we computed full numerical solutions to (3.126) for the parameter set $\epsilon = 0.05$, $D_0 = 1$, $\gamma = 2$, $\alpha = 1$, $U_0 = 1$, on $\Omega = [-1, 1] \times [-1, 1]$, i.e. $\ell = 1$, $d = 2$.

The computations were done using the adaptive grid finite difference solver VLUGR2 [3]. The initial conditions were taken to be the leading order steady-state stripe solution of Proposition 3.22. The results for A at different times, as shown in the gray-scale plot of Fig. 3.15, confirm the theoretical prediction that the stripe breaks up into only one spot.

3.7 Discussions

The modelling aspect of this chapter is relatively preliminary in nature, and we have considered a police-criminal interaction of the simplest type. Nonetheless, what insights can we still draw about how a chief of police should instruct the patrolling policemen?

We discovered that if there are sufficiently many policemen, it would preclude the mathematical existence of crime hotspots. Since this is usually not the case, when crime hotspots do exist, we consider how the policemen should patrol in order to destabilize multiple crime hotspots (single crime hotspot is unconditionally linearly stable). In other words, we want to

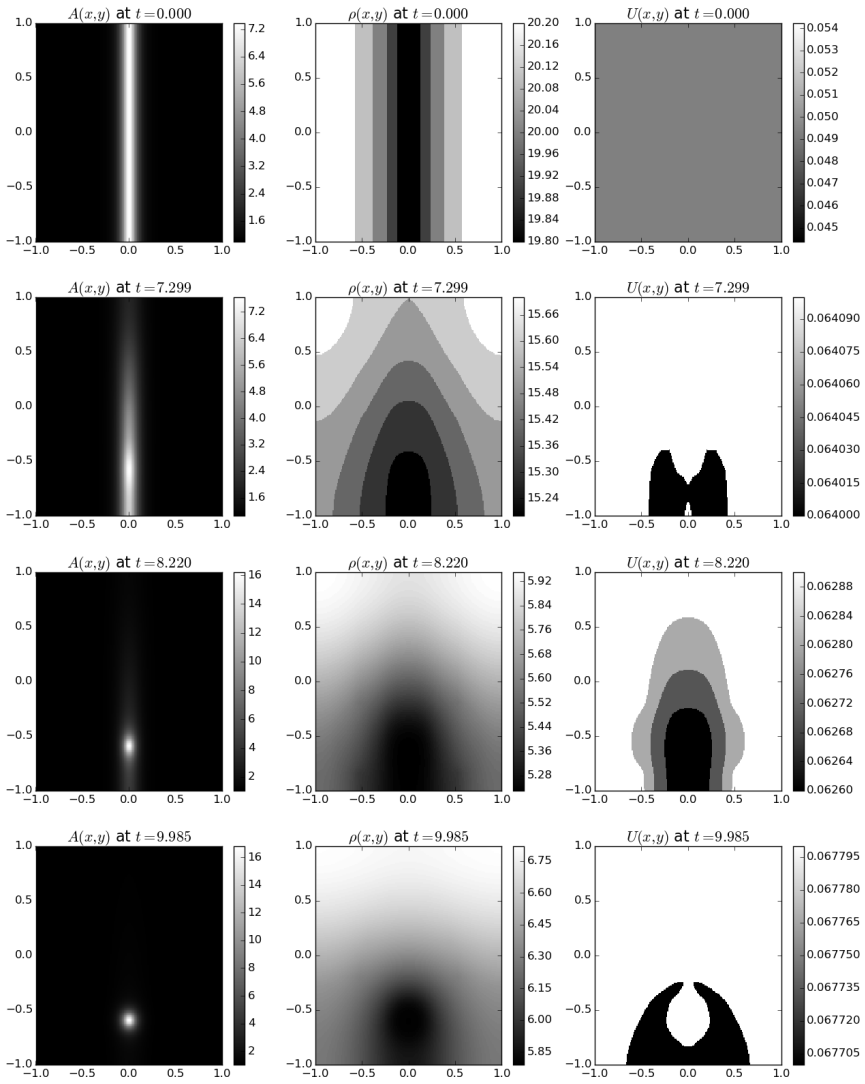

Figure 3.15: Spontaneous breakup of a stripe into one spot, obtained from a full numerical simulations of (3.124) using VLUGR2. The model parameter values were $\epsilon = 0.05$, $D_0 = 1$, $\gamma = 2$, $\alpha = 1$, $U_0 = 1$, $d = 2$ and $\ell = 1$. The time instants chosen were $t = 0.000, 0.7299, 8.220, 9.985$ from top to bottom respectively.

increase the range of criminal diffusivity so that a crime hotspot is unstable (i.e. lowering the competition threshold). This is exactly the main thrust of our mathematical analysis.

Firstly, we found that the competition threshold does not go down necessarily as the number of policemen increase. Paradoxically, if the degree of focus of police patrol is too high, the threshold goes up to a maximum before going down as the number of policemen further increases. This suggests that "hotspot policing" which focuses policemen too much on police hotspots could be counter-productive. The optimal strategy, thus, lie in the middle ground

between "random policing" and "hotspot policing", which suggests some sort of "containment approach".

Secondly, we found that below the competition threshold, the relative speed of policemen also play a role in destabilizing crime hotspots through a novel asynchronous oscillatory instability. The policemen need to travel fast enough relative to criminals so as to trigger instability of crime hotspots through this mechanism. This suggests that upgrades of mobility of patrolling policemen could be potentially valuable to decrease the total number of crime hotspots in a city.

As in many modelling endeavours, both the pros and cons of a model may serve as inspirations for more accurate and applicable models in the future. To this end, here we briefly summarize our main mathematical results, and we suggest a few directions that warrant further investigation, both for the sake of completeness for the analysis of this model, and also for improving it to make it more realistic.

3.7.1 Summary

In this chapter we used the method of matched asymptotic expansions to construct a steady-state hotspot solution to (3.3) having K hotspots of a common amplitude in the limit $\epsilon \to 0$ for the regime $D = O(\epsilon^{-2})$. We then studied the spectrum characterizing the linear stability properties of this steady-state solution by analyzing an NLEP with two nonlocal terms. We studied the NLEP by first considering a special case with patrol focus degree $q = 3$, which results in an explicitly solvable NLEP and, consequently, an explicit formula for the principal eigenvalue. Explicitly solvable NLEP problems also appear in [29, 37, 38]. The general case was then studied using the argument principle to count the number of unstable eigenvalues in the right half plane. This procedure was first developed to study the stability of steady-state spike patterns for the Gierer-Meinhardt model (cf. [52]) and now has a rather large body of literature (see [29] and the references therein). Our conclusions from the explicitly solvable case $q = 3$ are considerably stronger than those for the non-explicitly solvable case $q \neq 3$. In particular, when $q = 3$, two thresholds $D_{0,\text{lower}}$ and $D_{0,\text{upper}}$ given in (3.94) were determined so that the a multiple-hotspot pattern is stable when $D_0 < D_{0,\text{lower}}$ and unstable due to a competition instability when $D_0 > D_{0,\text{upper}}$. Moreover, an explicit formula for the existence of

Hopf bifurcation $\tau_u = \tau_{\text{Hopf}}$ when $D_{0,\text{lower}} < D_0 < D_{0,\text{upper}}$ was given in (3.93). In contrast to the absence of a Hopf bifurcation for the basic crime model with no police intervention, as discovered in [29], the window of existence for a Hopf bifurcation given by $(D_{0,\text{lower}}, D_{0,\text{upper}})$ vanishes exactly when $U_0 = 0$. In other words, the third component of the PDE system, modeling the police interaction, is essential to inducing the possibility of oscillations. Moreover, unlike the case of the Gray-Scott and Gierer-Meinhardt models studied in [9, 52, 50], where synchronous oscillatory instabilities of the spike amplitudes robustly occur and are the dominant instability, our three-component system exhibits asynchronous oscillatory instabilities. These asynchronous, anti-phase, oscillations of the spike amplitudes have the qualitative interpretation that, for a range of police diffusivities, the police presence is only able to mitigate the amplitude of certain hotspots at the expense of the growth of other hotspots in different spatial regions.

However, when $q \neq 3$, we had difficulty in analytically proving results as strong as for the case $q = 3$. In particular, we were not able to prove, without assuming further conditions, that a multiple hotspot pattern is stable when the rescaled criminal diffusivity D_0 is below the same lower threshold defined earlier in the $q = 3$ case. One possibility is that the definition of the lower threshold should be revised and should change with q. When D_0 is between the lower and upper thresholds, we were able to prove the existence of a Hopf bifurcation, but we cannot show uniqueness of the critical Hopf bifurcation value in τ_u. These are interesting open problems that warrant further study. Most importantly, we would like to investigate what are the mathematical relationships between the explicitly solvable case $q = 3$ and the non-explicitly solvable case $q \neq 3$, so that the strong results from the explicitly solvable case can potentially carry over to the general case.

3.7.2 Open Problems and Future Directions

With regards to our police model, with simple police interaction, studied in this chapter, it would be interesting to consider the more challenging $D = O(1)$ regime. One key question would be to investigate whether the police presence can eliminate the peak insertion behaviour that was found for the basic crime model to lead to the nucleation of new spikes of criminal activity. In this direction it would be interesting to determine the influence of the police presence on the global bifurcation of multiple hotspot steady-state solutions.

A second interesting direction would be to study the effect of police presence on crime patterns when the police interaction is modelled by the predator-prey dynamics case $I(U, \rho) = U\rho$ for (1.20). Preliminary results suggest that the NLEP will now have three non-local terms, which makes a detailed stability analysis very challenging. However, the determination of the competition instability threshold, corresponding to the zero eigenvalue crossing, should be readily amenable to analysis.

A third direction would be to consider spatial patterns in more than a simple 1-D spatial context. In Section 3.6 we studied (3.3) on a closed and bounded two-dimensional domain, where we observed that a homoclinic stripe can undergo a breakup into a localized hotspot in two spatial dimensions. An interesting extension of this result would be to study the break-up instability of a ring pattern, which was numerically observed in [48, 49] to lead to 2-D hotspot formation. In this context, it would be interesting to extend the 2-D stability results in [29] for the basic crime model, to study the existence of stability of crime hotspots in 2-D domains in the presence of police. In particular, we would like to investigate the stability and dynamics of 2-D hotspots, allowing for either of our two different models of police intervention.

Bibliography

[1] H. Berestycki and J.-P. Nadal (2010), *Self-organised critical hot spots of criminal activity*, Europ. J. Appl. Math., **21**(4-5), pp. 371–399

[2] H. Berestycki, J. Wei and M. Winter (2014), *Existence of symmetric and asymmetric spikes for a crime hotspot model*, SIAM J. Math. Anal., **46**(1), pp. 691–719

[3] J. G. Blom, R. A. Trompert and J. G. Verwer (1996), *Algorithm 758: VLUGR2: A vectorizable adaptive-grid solver for PDEs in 2D*, ACM Trans. Math. Softw., **22**(3), pp. 302–328.

[4] P. L. Brantingham and P. J. Brantingham (1987), *Crime patterns*, McMillan.

[5] J. Burke and E. Knobloch (2007), *Homoclinic snaking: Structure and stability*, Chaos, **17**, 037102.

[6] V. Brena-Medina and A. Champneys (2014), *Subcritical Turing bifurcation and the morphogenesis of localized patterns*, Phys. Rev. E., **90**, 032923.

[7] R. Cantrell, C. Cosner and R. Manasevich (2012), *Global bifurcation of solutions for crime modeling equations*, SIAM J. Math. Anal., **44**(3), pp. 1340–1358.

[8] L. Chen, N. Goldenfeld and Y. Oono (1994), *Renormalization group theory for global asymptotic analysis*, Phys. Rev. Lett., **73**(10), pp. 1311-1315.

[9] W. Chen and M. J. Ward (2009), *Oscillatory instabilities and dynamics of multi-spike patterns for the one-dimensional Gray-Scott model*, Europ. J. Appl. Math., **20**(2), pp. 187–214.

[10] W. Chen and M. J. Ward (2011), *The stability and dynamics of localized spot patterns in the two-dimensional Gray-Scott model*, SIAM J. Appl. Dyn. Sys., **10**(2), pp. 582–666.

[11] Discover, Science for the Curious (2010), [Fight Crime with Mathematics ranks in Top 100 Stories in 2010]. Retrieved from http://discovermagazine.com/2011/jan-feb/60.

[12] E. J. Doedel and B. Oldeman (2009), *AUTO-07P: continuation and bifurcation software for ordinary differential equations,* Technical report, Concordia University.

[13] A. Doelman, R. A. Gardner and T. J. Kaper (2001), *Large stable pulse solutions in reaction-diffusion equations*, Indiana U. Math. J., **50**(1), pp. 443–507.

[14] A. Doelman and T. J. Kaper (2003), *Semistrong pulse interactions in a class of coupled reaction-diffusion systems*, SIAM J. Appl. Dyn. Sys., **2**(1), pp. 53–96.

[15] A. Doelman, T. J. Kaper and K. Promislow (2007), *Nonlinear asymptotic stability of the semi-strong pulse dynamics in a regularized Gierer-Meinhardt model*, SIAM J. Math. Anal., **38**(6), pp. 1760–1789.

[16] A. Doelman and H. van der Ploeg (2002), *Homoclinic stripe patterns*, SIAM J. Appl. Dyn. Systems, **1**(1), pp. 65-104.

[17] M. R. D'Orsogna and M. Perc (2015), *Statistical physics of crime: A review*, Physics of Life Reviews, **12**, pp. 1-21

[18] Y. Gu, Q. Wang and G. Yi (2014), *Stationary patterns and their selection mechanism of urban crime models with heterogeneous near-repeat victimization effect*, preprint, arXiv:1409.0835.

[19] D. Iron and M. J. Ward (2002), *The dynamics of multi-spike solutions to the one-dimensional Gierer-Meinhardt model*, SIAM J. Appl. Math., **62**(6), pp. 1924–1951.

[20] D. Iron, M. J. Ward and J. Wei (2001), *The stability of spike solutions to the one-dimensional Gierer-Meinhardt model*, Physica D, **150**(1-2), pp. 25–62.

[21] S. Johnson and K. Bower (2005), *Domestic burglary repeats and space-time clusters: The dimensions of risk*, Europ. J. of Criminology, **2**, pp. 67–92.

[22] P. A. Jones, P. J. Brantingham and L. Chayes (2010), *Statistical models of criminal behavior: The effect of law enforcement actions*, Math. Models. Meth. Appl. Sci., **20**, Suppl., pp. 1397–1423.

[23] T. Kolokolnikov and M. J. Ward (2003), *Reduced-wave Green's functions and their effect on the dynamics of a spike for the Gierer-Meinhardt model*, Europ. J. Appl. Math., **14**(5), pp. 513–545.

[24] T. Kolokolnikov, M. J. Ward and J. Wei (2005), *The existence and stability of spike equilibria in the one-dimensional Gray-Scott model: The low feed-rate regime*, Studies in Appl. Math., **115**(1), pp. 21–71.

[25] T. Koloklonikov, W. Sun, M. J. Ward and J. Wei (2006), *The stability of a stripe for the Gierer-Meinhardt model and the effect of saturation*, SIAM J. Appl. Dyn. Sys., **5**(2), pp. 313-363.

[26] T. Kolokolnikov, M. J. Ward and J. Wei (2006), *Zigzag and breakup instabilities of stripes and rings in the two-dimensional Gray-Scott model*, Studies in Appl. Math., **16**(1), pp. 35–95.

[27] T. Kolokolnikov, M. J. Ward and J. Wei (2009), *Spot self-replication and dynamics for the Schnakenburg model in a two-dimensional domain*, J. Nonlinear Sci., **19**(1), pp. 1–56.

[28] T. Kolokolnikov, M. J. Ward, and J. Wei (2007), *Self-replication of mesa patterns in reaction-diffusion models*, Physica D, **236**(2), pp. 104–122.

[29] T. Kolokolnikov, M. J. Ward and J. Wei (2014), *The stability of steady-state hot-spot patterns for a reaction-diffusion model of urban crime*, DCDS-B, **19**(5), p. 1373–1410.

[30] T. Kolokolnikov and J. Wei (2011), *Stability of spiky solutions in a competition model with cross-diffusion*, SIAM J. Appl. Math., **71**, pp. 1428–1457.

[31] P. Lagerstrom (1988), *Matched asymptotic expansions: ideas and techniques*, Applied Mathematical Sciences, **76**, Springer-Verlag, New York.

[32] P. Lagerstrom and D. Reinelt (1984), *Note on logarithmic switchback terms in regular and singular perturbation problems*, SIAM J. Appl. Math., **44**(3), pp. 451–462.

[33] A. Lindsay and M. J. Ward (2010), *Asymptotics of some nonlinear eigevalue problems for a MEMS capacitor: Part II: Multiple solutions and singular asymptotics*, Europ. J. Appl. Math., **22**(2), pp. 83–123.

[34] W. Liu, A. L. Bertozzi, and T. Kolokolnikov (2012), *Diffuse interface surface tension models in an expanding flow*, Comm. Math. Sci., **10**(1), pp. 387–418.

[35] D. J. B. Lloyd and H. O'Farrell (2013), *On localised hotspots of an urban crime model*, Physica D, **253**, pp. 23–29.

[36] R. McKay and T. Kolokolnikov (2012), *Stability transitions and dynamics of localized patterns near the shadow limit of reaction-diffusion systems*, DCDS-B, **17**(1), pp. 191–220.

[37] I. Moyles, W.-H. Tse and M. J. Ward (2016), *Explicitly solvable nonlocal eigenvalue problems and the stability of localized stripes in reaction-diffusion systems*, Studies in Appl. Math., **136**(1), pp. 89–136.

[38] Y. Nec and M. J. Ward (2013), *An explicitly solvable nonlocal eigenvalue problem and the stability of a spike for a class of reaction-diffusion system with sub-diffusion*, Math. Model. of Nat. Phenom., **8**(2), pp. 55–87.

[39] K. Painter and T. Hillen (2011), *Spatio-temporal chaos in a chemotaxis model*, Physica D, **240**, pp. 363–375.

[40] H. van der Ploeg and A. Doelman (2005), *Stability of spatially periodic pulse patterns in a class of singularly perturbed reaction-diffusion equations*, Indiana Univ. Math. J., **54**(5), pp. 1219–1301

[41] A. B. Pitcher (2010), *Adding police to a mathematical model of burglary*, Europ. J. Appl. Math., **21**(4-5), pp. 401–419.

[42] N. Popovic and P. Szymolyan (2004), *A geometric analysis of the Lagerstrom model problem*, J. Diff. Eq., **199**(2), pp. 290–325.

[43] J. D. M. Rademacher (2013), *First and second order semi-strong interaction in reaction-diffusion systems*, SIAM J. Appl. Dyn. Syst., **12**(1), pp. 175–203.

[44] RAIDS Online (2015), *Crime density maps for West Vancouver, B.C., Canada and Santa Clara-Sunnyville, California, US*, BAIR Analytics, Inc. Retrieved from http://raidsonline.com/.

[45] L. Ricketson (2011), *A continuum model of residential burglary incorporating law enforcement*, unpublished. Retrieved from http://cims.nyu.edu/~lfr224/writeup.pdf.

[46] N. Rodriguez and A. Bertozzi (2010), *Local existence and uniqueness of solutions to a PDE model for criminal behavior*, M3AS (special issue on Mathematics and Complexity in Human and Life Sciences), **20**(1), pp. 1425–1457.

[47] M. B. Short, M. R. D'Orsogna, V. B. Pasour, G. E. Tita, P. J. Brantingham, A. L. Bertozzi and L. B. Chayes (2008), *A statistical model of criminal behavior*, Math. Models. Meth. Appl. Sci., **18**, Suppl. pp. 1249–1267.

[48] M. B. Short, A. L. Bertozzi and P. J. Brantingham (2010), *Nonlinear patterns in urban crime - hotspots, bifurcations, and suppression*, SIAM J. Appl. Dyn. Sys., **9**(2), pp. 462–483.

[49] M. B. Short, P. J. Brantingham, A. L. Bertozzi and G. E. Tita (2010), *Dissipation and displacement of hotpsots in reaction-diffusion models of crime*, Proc. Nat. Acad. Sci., **107**(9), pp. 3961-3965.

[50] W. Sun, M. J. Ward and R. Russell (2005), *The slow dynamics of two-spike solutions for the Gray-Scott and Gierer-Meinhardt systems: competition and oscillatory instabilities*, SIAM J. Appl. Dyn. Syst., **4**(4), pp. 904–953.

[51] W.-H. Tse and M. J. Ward (2015), *Hotspot formation and dynamics for a continuum model of urban crime*, Europ. J. Appl. Math., available on CJO2015. doi:10.1017/S0956792515000376.

[52] M. J. Ward and J. Wei (2003), *Hopf bifurcations and oscillatory instabilities of spike solutions for the one-dimensional Gierer-Meinhardt model*, J. Nonlinear Sci., **13**(2), pp. 209–264.

[53] J. Wei (1999), *On single interior spike solutions of the Gierer–Meinhardt system: uniqueness and spectrum estimates*, Europ. J. Appl. Math., **10**(4), pp. 353–378.

[54] J. Wei (2008), *Existence and stability of spikes for the Gierer-Meinhardt system*, book chapter in *Handbook of Differential Equations, Stationary Partial Differential Equations*, Vol. 5 (M. Chipot ed.), Elsevier, pp. 489–581.

[55] J. Q. Wilson and G. L. Kelling (1998), *Broken windows and police and neighborhood safety*, Atlantic Mon., **249**, pp. 29–38.

[56] J. R. Zipkin, M. B. Short and A. L. Bertozzi (2014), *Cops on the dots in a mathematical model of urban crime and police response*, DCDS-B, **19**(5), pp. 1479–1506.

Appendix A

Lemmas and General Formulas

A.1 A Floquet Boundary Condition Approach to Neumann NLEP Problems on a Bounded Interval

When considering the stability of a symmetric, equally-spaced, $K-$spike pattern on a one dimensional interval, we must impose homogeneous Neumann boundary conditions. We observe two special properties for this class of problem. If we denote the spectral problem as $\mathcal{L}\phi = \lambda\phi$, we see that:

1. *Translation-invariance*: If $\phi(x)$ is a Neumann eigenfunction on the interval $[a, b]$, i.e. $\phi_x(a) = \phi_x(b) = 0$, then the translated eigenfunction $\tilde{\phi}(x) = \phi(x - x_0)$ is a Neumann eigenfunction with the translated boundary condition: $\tilde{\phi}_x(a + x_0) = \tilde{\phi}_x(b + x_0) = 0$.

2. *Even symmetry of the linear operator* $\mathcal{L}$: The function $\tilde{\phi}(x) = \phi(-x)$ solves $\mathcal{L}\tilde{\phi} = \lambda\tilde{\phi}$ whenever ϕ solves the same problem. A sufficient condition for this is that $\mathcal{L}$ contains only even derivatives and the nonlocal term is an integral on the whole domain with an even kernel.

The spectral problems on one spatial dimension we considered in this thesis satisfy the above properties. We now show how these simple considerations can be used to reduce a spectral problem with Neumann boundary conditions for a multiple spike pattern to one for a *single* spike with a Floquet-type boundary condition.

The first step is to recognize the Neumann problem as a restriction of a periodic problem.

A.1.1 Converting a Neumann problem to a Periodic Problem with Twice the Domain Length

Because of translation invariance, we may translate our domain to wherever we feel convenient. We describe here a bijective correspondence of Neumann eigenfunctions on a domain of length L to periodic eigenfunctions on a domain of length $2L$.

Suppose $\phi(x)$ is a Neumann eigenfunction on $[0, L]$. Then, if we apply an even extension

$$\tilde{\phi}(x) = \begin{cases} \phi(x) & \text{for } 0 \leq x \leq L \\ \phi(-x) & \text{for } -L \leq x \leq 0\,, \end{cases}$$

it follows that $\tilde{\phi}(x)$ satisfies periodic boundary conditions on $[-L, L]$, i.e. that

$$\tilde{\phi}(L) = \tilde{\phi}(-L), \qquad \tilde{\phi}_x(L) = \tilde{\phi}_x(-L)\,.$$

Conversely, if $\phi(x)$ is a eigenfunction on $[-L, L]$ satisfying periodic boundary conditions, then since the domain is symmetric about the origin, the function

$$\tilde{\phi}(x) = \phi(x) + \phi(-x)\,,$$

restricted to $[0, L]$ solves $\mathcal{L}\phi = \lambda\phi$ and it satisfies $\tilde{\phi}_x(L) = \phi_x(L) - \phi_x(-L) = 0$ by $2L$-periodicity and $\tilde{\phi}_x(0) = \phi_x(0) - \phi_x(0) = 0$ by construction. Thus, $\tilde{\phi}(x)$ is a Neumann eigenfunction.

Therefore, we conclude that the spectrum of the Neumann problem on a domain of length L is exactly the same as the spectrum of the periodic problem on a domain length of $2L$ (whether the domain is actually symmetric is irrelevant, because of translation-invariance)

A.1.2 Converting a Periodic Problem to a Floquet Problem

Now, if we have an eigenvalue problem with periodic boundary conditions on a domain $[a, b]$ with length S, then we can partition the domain into N subintervals of equal length as

$$[a, b] = \bigcup_{j=0}^{N-1} [x_j, x_{j+1}]\,,$$

and consider the following complex-valued problem with the following Floquet-type boundary condition on each subinterval:

$$z \left(\begin{array}{c} \phi \\ \phi_x \end{array} \right) \Bigg|_{x=x_j} = \left(\begin{array}{c} \phi \\ \phi_x \end{array} \right) \Bigg|_{x=x_{j+1}} , \quad \text{for } j = 0, 1, \ldots, N-1 ,$$

where z is a complex number to be determined.

Then, by collapsing the N conditions, we find that

$$z^N \left(\begin{array}{c} \phi \\ \phi_x \end{array} \right) \Bigg|_{x=x_0=a} = \left(\begin{array}{c} \phi \\ \phi_x \end{array} \right) \Bigg|_{x=x_N=b} .$$

Thus, periodicity requires $z^N = 1$, and hence z is determined by the N-th roots of unity as

$$z_j = e^{2\pi i j/N}, \qquad j = 0, 1, \ldots, N-1 ,$$

which yields N possible choices for the multiplier z.

Finally, if the problems restricted on each subinterval are exactly the same (i.e. the functions involved defining $\mathcal{L}$ are identical on each subinterval), which occurs when we consider the stability of a symmetric, equally-spaced multiple spike pattern subject to a S-periodic boundary condition, then we only need consider the Floquet eigenfunction that satisfies

$$\mathcal{L}\phi = \lambda\phi , \quad -\ell < x < \ell ; \qquad \phi(l) = z_j \phi(-l), \quad \phi_x(l) = z_j \phi_x(-l) ,$$

where $2lN = S$, so that $l = S/(2N)$.

A.1.3 The Floquet Eigenvalue Problem for the Stability of a K-spike Symmetric Pattern with Neumann Boundary Conditions

For our problem defined on the domain $[-L, L]$ with length $2L$ with K spikes, we first apply an even reflection as described above, which yields the periodic problem with $S = 4L$ having

$N = 2K$ spikes. Therefore, we look for eigenfunctions that satisfy

$$\mathcal{L}\phi = \lambda\phi\,, \quad -\ell < x < \ell\,; \qquad \phi(l) = z_j\phi(-l), \quad \phi_x(l) = z_j\phi_x(-l)\,,$$

with $l = S/(2N) = 4L/(4K) = L/K$, and

$$z_j = e^{2\pi ij/N} = e^{\pi ij/K}\,, \quad j = 0, \ldots, N-1\,,$$

which when solved, gives N different modes depending on j to the original problem.

We end this discussion with a lemma which we use frequently to solve a BVP problem resulting from imposing Floquet boundary conditions.

Lemma A.1. *The following BVP with a jump condition at $x = 0$ and, subject to Floquet boundary conditions on the interval $[-\ell, \ell]$, formulated as*

$$\eta_{xx} = 0\,, \quad -\ell < x < \ell\,; \qquad d_0\left[\eta_x\right]_0 = d_1\eta(0) + d_2\,,$$
$$\eta(\ell) = z\eta(-\ell), \quad \eta_x(\ell) = z\eta_x(-\ell)\,,$$

is solvable with the central value $\eta_0 = \eta(0)$ given by

$$\eta_0 = d_2\left[\frac{d_0}{2\ell}\frac{(z-1)^2}{z} - d_1\right]^{-1}\,.$$

In particular, if $z = z_j = e^{\pi ij/K}$, where $0 \le j < K$ is an integer, then

$$\eta_0 = -\frac{d_2}{d_0\left(1 - \cos(\pi j/K)\right)/\ell + d_1}\,.$$

Proof: Let $\eta_0 = \eta(0)$. The solution of the ODE is continuous but not differentiable at $x = 0$, with the general form

$$\eta(x) = \begin{cases} \eta_0 + A_+ x & \text{if } 0 < x < \ell\,, \\ \eta_0 + A_- x & \text{if } -\ell < x < 0\,. \end{cases}$$

Upon imposing the Floquet boundary conditions we obtain

$$A_+ = zA_-\,, \qquad \eta_0 + A_+\ell = z\,(\eta_0 - A_-\ell) = z\eta_0 - A_+\ell\,,$$

so that $A_+ = \frac{(z-1)}{2\ell}\eta_0$. Then, upon imposing the jump condition we get

$$d_1\eta_0 + d_2 = d_0\,[\eta_x]_0 = d_0\,(A_+ - A_-) = \frac{d_0\eta_0}{2\ell}\,(z-1)\left(1 - \frac{1}{z}\right)\,,$$

which determines $\eta(0) = \eta_0$ as

$$\eta_0 = d_2\left[\frac{d_0}{2\ell}\frac{(z-1)^2}{z} - d_1\right]^{-1}\,, \tag{A.1}$$

as was claimed. If we set $z = e^{\pi ij/K}$, we obtain

$$\frac{(z-1)^2}{z} = (z-1)\left(1 - \frac{1}{z}\right) = -(1-z)(1-\bar{z}) = -2 - (z+\bar{z}) = -2\,(1 - \cos(\pi j/K))\,.$$

■

A.2 Properties of the Local Operator L_0 in One Spatial Dimension

Consider positive solutions on $-\infty < y < \infty$ to

$$w'' - w + w^p = 0\,, \tag{A.2}$$

which vanish as $y \to \pm\infty$. It is well-known that the unique positive solution to this problem is

$$w(y) = \left(\frac{(p+1)}{2}\mathrm{sech}^2\left[\frac{(p-1)y}{2}\right]\right)^{1/(p-1)}\,. \tag{A.3}$$

In particular, for $p = 2$ we have

$$w(y) = \frac{3}{2}\mathrm{sech}^2\left(\frac{y}{2}\right)\,, \tag{A.4}$$

while for $p = 3$, we get

$$w(y) = \sqrt{2}\mathrm{sech}(y)\,. \tag{A.5}$$

We define the linear operator obtained from linearizing around this solution by

$$L_0[\phi] := \phi'' - \phi + pw^{p-1}\phi\,. \tag{A.6}$$

We refer to L_0 as the *local operator* in the context of our NLEP stability analysis.

First, we recall a few well-known results for the discrete spectrum of L_0. By converting the differential operator to a hypergeometric equation, a more precise statement for the local eigenvalue problem $L_0\psi = \nu\psi$ is that it has exactly two discrete eigenvalues when $p \geq 3$ is an integer, given by

$$\nu_0 = \left(\frac{1+p}{2}\right)^2 - 1, \qquad \psi_0 = w^2 > 0\,; \qquad \nu_1 = 0, \qquad \psi_1 = w'\,, \tag{A.7}$$

and there are no other discrete eigenvalues in $-1 < \nu < 0$. When $p = 2$, then $\nu_2 = -3/4$ is also an eigenvalue. The proof of these results is given in Proposition 5.6 of [13].

Secondly, we list several algebraic properties when L_0 acts on functions of w.

Lemma A.2. *The local operator L_0 satisfies the following identities*

(i) $\quad L_0[w] = (p-1)w^p, \qquad so \quad L_0^{-1}[w^p] = \frac{w}{p-1},$

(ii) $\quad L_0[yw'] = 2(w - w^p), \qquad so \quad L_0^{-1}[w] = \frac{1}{2}yw' + \frac{1}{p-1}w^p,$

(iii) $\quad L_0[w^s] = (s^2-1)w^s\,, \qquad iff \quad s = \frac{p+1}{2},$

(iv) $\quad L_0[w^s] = \left(s^2-1\right)w^s + (p+s)\left(1 - \frac{2s}{p+1}\right)w^{s+p-1}\,, \qquad for\ any\ \ s > 1.$

(v) $\quad$ *For $s > p-1$ and $s \neq p - 1 + \frac{p+1}{2}$, we have the reduction formula*

$$L_0^{-1}[w^s] = \frac{p+1}{(s+1)(2s-3p+1)}\left[(s-p)(s-p+2)L_0^{-1}[w^{s-p+1}] - w^{s-p+1}\right]\,.$$

Proof: (i) and (ii) can be verified readily by calculating

$$L_0[w] = w'' - w + pw^p = (p-1)w^p\,,$$

as well as

$$\begin{aligned} L_0[yw'] &= 2w'' + yw''' - yw' + y(pw^{p-1}w')\,, \\ &= 2(w - w^p) + y(w'' - w + w^p)'\,, \\ &= 2(w - w^p)\,. \end{aligned}$$

Now we show (iii). We multiply A.2 by w' and integrate to get

$$\frac{w'^2}{2} - \frac{w^2}{2} + \frac{w^{p+1}}{p+1} = 0\,,$$

which yields that

$$(w')^2 = w^2 - \frac{2}{p+1}w^{p+1}\,.$$

Thus, we obtain that

$$\begin{aligned} L_0[w^s] &= \left(sw^{s-1}w'\right)' - w^s + pw^{p+s-1}\,, \\ &= s(s-1)w^{s-2}(w')^2 + sw^{s-1}w'' - w^s + pw^{p+s-1}\,, \\ &= w^{s-2}\left(s(s-1)(w')^2 + sww'' - w^2 + pw^{p+1}\right)\,, \\ &\triangleq w^{s-2}T_{p,s}[w]\,. \end{aligned} \tag{A.8}$$

Then, using $w'' = w - w^p$ and $(w')^2 = w^2 - \frac{2}{p+1}w^{p+1}$, we get

$$\begin{aligned} T_{p,s}[w] &= [s(s-1) + s - 1]\,w^2 + [-2s(s-1)/(p+1) - s + p]\,w^{p+1}\,, \\ &= \left(s^2 - 1\right)w^2 + \frac{1}{p+1}\left(p^2 - (s-1)\,p - 2s^2 + s\right)w^{p+1}\,, \\ &= \left(s^2 - 1\right)w^2 + (p+s)\left(1 - \frac{2s}{p+1}\right)w^{p+1}\,. \end{aligned} \tag{A.9}$$

This shows (iv), and it is now obvious that the second term in (A.9) vanishes iff $s = (p+1)/2$, which establishes (iii) as claimed.

Finally for (v), we proceed by a direct computation to get

$$L_0[w^{s-p+1}] = \left[(s-p+1)^2 - 1\right]w^{s-p+1} - \frac{s+1}{p+1}(2s - 3p + 1)w^s\,.$$

So taking L_0^{-1} on both sides and rearranging yields the desired result. Observe that $2s - 3p + 1 = 0$ exactly when $s = p - 1 + (p+1)/2$. Moreover, when $s = p$, we recover (i), given by $L_0[w] = (p-1)w^p$. ■

In other words, (iii) means that for $s > 1$, the principal eigenvalue for L_0 is

$$\nu_0 = s^2 - 1 > 0\,,$$

with w^s being the corresponding eigenfunction. Since we have neither assumed p and q to be integers, in fact, for any $p > 1$, we have $s = (p+1)/2$ and $w^{(p+1)/2}$ is an eigenfunction corresponding to the principal eigenvalue $\nu_0 = \left(\frac{1+p}{2}\right)^2 - 1 > 0$. In particular, for the cases $p = 2$ and $p = 3$ we get $\nu_0 = \frac{5}{4}$ and $\nu_0 = 3$, respectively.

The identities (i) and (ii) are useful in the analysis of a class of nonlinear function defined implicitly by L_0, given by

$$\mathcal{F}(\lambda) = \frac{\int w^{m-1}(L_0 - \lambda)^{-1} w^p}{\int w^m}\,,$$

when $m - 1 = s$. This function appears frequently in the NLEP analysis of spike stability where the eigenvalues can be found to satisfy the equation

$$g(\lambda) = \mathcal{C}(\lambda) - \mathcal{F}(\lambda) = 0\,,$$

where $\mathcal{C}(\lambda)$ is usually some rational or transcendental function of λ defined in terms of the model parameters of the reaction-diffusion system.

The identity (iii) turns out to be very powerful and gives tremendous simplifications to the NLEP analysis, which effectively allows $\mathcal{F}(\lambda)$ to be rewritten explicitly in a closed form. In this way the study of the roots of $g(\lambda) = 0$ will only require finding roots of some explicit transcendental equation in the eigenvalue parameter.

A.2.1 Applications to Explicitly Solvable NLEP

Proposition A.3. *Consider the NLEP*

$$L_0[\Phi] - \chi w^r \int_{-\infty}^{\infty} w^s \Phi dy = \lambda \Phi\,, \qquad -\infty < y < \infty\,, \qquad \Phi \to 0 \quad as \quad |y| \to \infty\,,$$

where $s = (p+1)/2$ and $r > -s$ is arbitrary. Then, any unstable eigenvalue must be root of

$$\lambda = \nu_0 - \chi \int_{-\infty}^{\infty} w^{s+r} dy = \left[\left(\frac{p+1}{2} \right)^2 - 1 \right] - \chi \int_{-\infty}^{\infty} w^{\frac{p+1}{2}+r} dy\,. \tag{A.10}$$

Proof: We apply Green's identity to w^s and Φ, using decay properties of w^s and Φ as $|y| \to \infty$ together with integration by parts. This yields

$$\begin{aligned} 0 &= \int_{-\infty}^{\infty} w^s L_0[\Phi] - \Phi L_0[w^s] dy\,, \\ &= \int_{-\infty}^{\infty} \left(w^s \left[\lambda \Phi + \chi w^r \int_{-\infty}^{\infty} w^s \Phi dy \right] - \Phi \nu_0 w^s \right) dy\,, \\ &= \left(\int_{-\infty}^{\infty} w^s \Phi dy \right) \left(\lambda - \nu_0 + \chi \int_{-\infty}^{\infty} w^{s+r} dy \right)\,. \end{aligned}$$

Therefore, when $\int_{-\infty}^{\infty} w^s \Phi dy \neq 0$, we obtain $\lambda = \nu_0 - \chi \int_{-\infty}^{\infty} w^{s+r} dy$ as claimed.

Moreover, the condition $\int_{-\infty}^{\infty} w^s \Phi dy \neq 0$ fails only if the NLEP was in fact the local eigenvalue problem, given by $L_0[\Phi] = \lambda \Phi$. Hence $\int_{-\infty}^{\infty} w^s \Phi dy = 0$ implies that Φ is an eigenfunction of L_0. However, since the principal eigenfunction of L_0 is one-signed, the only eigenpairs of L_0 that satisfy $\int_{-\infty}^{\infty} w^s \Phi dy = 0$ are either the translation mode $\lambda = 0$ where $\Phi = w'$ or possibly an eigenfunction whose eigenvalue is in $-1 < \lambda < 0$. Therefore, the transcendental equation for the eigenvalue given above will characterize any unstable eigenvalue of the NLEP. ■

A.3 Miscellaneous Formulas

A.3.1 Formulas for the L^q-Norm of the Ground State $w(y)$: $p = 3$ Case

Lemma A.4. For $p = 3$, $w(y) = \sqrt{2}\mathrm{sech}y$. We have the general formula for its q-th integral:

$$I_q = \int_{-\infty}^{\infty} w^q(y)dy = 2^{3q/2-1}B(\frac{q}{2},\frac{q}{2}) = 2^{3q/2-1}\frac{\Gamma^2(q/2)}{\Gamma(q)}\,, \tag{A.11}$$

where $B(s,t)$ is a beta function. In addition, we have the reduction formula

$$I_{q+2} = \frac{2q}{q+1}I_q\,. \tag{A.12}$$

Proof: $I_q/2^{q/2} = 2^q\int_{-\infty}^{\infty}\frac{dy}{(e^{-y}+e^y)^q} = 2^q\int_{-\infty}^{\infty}\frac{\left(e^{-2y}\right)^{q/2}}{(e^{-2y}+1)^q}dy$. So we substitute $t = e^{-2y}$ to obtain

$$I_q/2^{q/2} = 2^{q-1}\int_0^{\infty}\frac{t^{q/2-1}}{(1+t)^q}dt = 2^{q-1}B(\frac{q}{2},\frac{q}{2})\,,$$

where the last identity for the Beta function can by shown from the definition by the substitution $s = \frac{1}{1-t} - 1 = \frac{t}{1-t}$, $ds = \frac{1}{(1-t)^2}dt = (s+1)^2\,dt$. In this way, we calculate that

$$\begin{aligned} B(x,y) &= \int_0^1 t^{x-1}\,(1-t)^{y-1}\,dt\,, \\ &= \int_0^1 \left(\frac{t}{1-t}\right)^{x-1}(1-t)^{x+y-2}\,dt\,, \\ &= \int_0^{\infty} s^{x-1}\,(s+1)^{-(x+y-2)}\,(s+1)^{-2}\,ds\,, \\ &= \int_0^{\infty}\frac{s^{x-1}}{(1+s)^{x+y}}ds\,. \end{aligned}$$

The reduction formula can then be seen as a result of the general formula, but can also be easily obtained from a simple integration by parts. ■

The general formula is most useful for real numbers $0 < q < 2$ and for general q we can apply the reduction formula first. For integers $q = 1, 2, 3, 4$, one can readily recover the following values, which were frequently used in this thesis: $I_1 = \sqrt{2}\pi$, $I_2 = 4$, $I_3 = \sqrt{2}\pi$, $I_4 = 16/3$.

A.3.2 Formulas for the L^q-Norm of the Ground State $w(y)$: General Case

For general p, the formula of the ground state is:

$$w(y) = \left(\frac{(p+1)}{2}\mathrm{sech}^2\left[\frac{(p-1)y}{2}\right]\right)^{1/(p-1)}\,.$$

Therefore, we compute

$$I_{p,q} \equiv \int_{-\infty}^{\infty} w^q(y)dy = \left(\frac{p+1}{2}\right)^{q/(p-1)} \int_{-\infty}^{\infty} \left(\mathrm{sech}^2\left[\frac{(p-1)y}{2}\right]\right)^{q/(p-1)} dy\,.$$

Let $u = \tanh\frac{(p-1)y}{2}$, then $du = \frac{p-1}{2}\mathrm{sech}^2\left[\frac{(p-1)y}{2}\right]dy$. We calculate that

$$I_{p,q} = \left(\frac{p+1}{2}\right)^{q/(p-1)} \left(\frac{p-1}{2}\right)^{-1} \int_{-1}^{1} \left(1-u^2\right)^{q/(p-1)-1} du\,.$$

With the substitution $t = (1+u)/2$, we further obtain that

$$\begin{aligned} I_{p,q} &= \frac{(p^2-1)}{2}\left(\frac{p+1}{2}\right)^{\frac{q}{p-1}-1} \int_0^1 [4t(1-t)]^{\frac{q}{p-1}-1}\,dt\,, \\ &= \frac{(p^2-1)}{2}(2p+2)^{\frac{q}{p-1}-1} \int_0^1 t^{\frac{q}{p-1}-1}(1-t)^{\frac{q}{p-1}-1}dt\,, \\ &= \frac{(p^2-1)}{2}(2p+2)^{\frac{q}{p-1}-1}\, B(\frac{q}{p-1},\frac{q}{p-1})\,, \\ &= \frac{(p^2-1)}{2}(2p+2)^{\frac{q}{p-1}-1}\,\frac{\Gamma^2(\frac{q}{p-1})}{\Gamma\left(\frac{2q}{p-1}\right)}\,. \end{aligned} \tag{A.13}$$

This expression also implies a reduction formula:

$$\begin{aligned} I_{p,q} &= \frac{p^2-1}{2}(2p+2)^{(\frac{q-(p-1)}{p-1}-1)+1}\,\frac{\Gamma^2(\frac{q-(p-1)}{p-1}+1)}{\Gamma\left(\frac{2(q-(p-1))}{p-1}+2\right)}\,, \\ &= I_{q-(p-1)}(2p+2)\frac{\left(\frac{q-(p-1)}{p-1}\right)^2}{\left(\frac{2(q-(p-1))}{p-1}+1\right)\left(\frac{2(q-(p-1))}{p-1}\right)}\,, \\ &= I_{q-(p-1)}(p+1)\frac{q-p+1}{2q-p+1}\,. \end{aligned} \tag{A.14}$$

For $p = 3$, the expression (A.13) simplifies to

$$I_{3,q} = 4\cdot 8^{q/2-1}\frac{\Gamma^2(\frac{q}{2})}{\Gamma(q)} = 2^{3q/2-1}\frac{\Gamma^2(\frac{q}{2})}{\Gamma(q)}\,,$$

while (A.14) yields

$$I_{3,q} = I_{3,q-2}\frac{4(q-2)}{2q-2} = \frac{2(q-2)}{q-1}I_{3,q-2}\,.$$

in full agreement to (A.11) and (A.12).

We remark that the integral $I_{p,q}$ has a closed form with simple surds and factorials when $\frac{q}{p-1}$ is an integer, and also when $\frac{q}{p-1} = n + 1/2$ for some integer n, but with an extra factor of π (because $\Gamma(\frac{1}{2}) = \sqrt{\pi}$). In all cases, $I_{p,q}$ can be reduced to a formula of surds and factorials except for a factor of $\Gamma(q_c)$ where $q_c = \mod (q, 1)$ is the non-integral part of the number q.